Novel Tandem Mass Spectrometry (MS/MS) Approaches for Structural Characterization of Glycans

by

Di Gao

A dissertation submitted in partial fulfillment
of the requirements for the degree of
Doctor of Philosophy
(Chemistry)
in The University of Michigan
2013

Doctoral Committee:

Professor Kristina Håkansson, Chair
Professor Mark E. Meyerhoff
Associate Professor Alexey I. Nesvizhskii
Assistant Professor Brandon Ruotolo

Acknowledgements

After almost five years working on my Ph.D. degree in the Department of Chemistry at the University of Michigan, I would like to express my most sincere appreciation to those who offered me tremendous help.

First and foremost I would like to thank my Ph.D. advisor Prof. Kristina Håkansson for her dedicated mentorship during my graduate study and continuous support about my personal development. Her excellent expertise in analytical chemistry and rigorous working attitude are extremely helpful for me to finish my degree. Her great personality has encouraged me to overcome difficulties. She is not only an excellent scientist, but also the best mentor I can think of. It is my fortune and honor to have worked with her during the past few years.

I would like to thank the other dissertation committee members for their help as well. I was very fortunate to work with Prof. Meyerhoff as his teaching assistant for analytical chemistry lab course. He sets a perfect model example as an instructor. I am always inspired by his passion for science and education. Prof. Nesvizhskii is an exact scholar and asked great questions during the committee meetings. Prof. Ruotolo gave me many valuable suggestions. I also want to thank him, together with Russell Bornschein and Shuai Niu in Ruotolo group for their generous help about the ion mobility experiments.

Thirdly, I would like to express my thanks to the former and present colleagues in the Håkansson lab: Hangtian, Wen, Bo, Hyun Ju, Chris, Katie, Ashley, Ning, Wendi, Tao,

and Jordan. I am so fortunate to have such nice and helpful colleagues! I also want to thank my classmates and friends in the university for their help and friendship.

Financial support from National Institutes of Health (NIH) and the University of Michigan also needs to be acknowledged.

Last but not the least, I want to thank my family for their eternal love. My parents Dengkuan Gao and Ni Deng, have given me so much support and guidance during these years. I can keep moving forward because I know they are always standing by me. I would not have achieved so much without their encouragement and understanding.

Di Gao

April 2nd, 2013

Ann Arbor, MI

Table of Contents

List of Figures

List of Tables

List of Abbreviations

2-AA	2-aminobenzoic acid
2-AB	2-aminobenzamide
CAD	Collision activated dissociation
CI	Chemical ionization
CRM	Charge residue model
DMSO	Dimethyl sulfoxide
ECD	Electron capture dissociation
EDD	Electron detachment dissociation
EID	Electron induced dissociation
Endo-H	Endoglycosidase-H
ESI	Electrospray ionization
ETD	Electron transfer dissociation
FTICR-MS	Fourier transform ion cyclotron resonance mass spectrometry
GC	Gas chromatography
GlcNAc	*N*-acetyl glucosamine
heCAD	High-energy collision activated dissociation
HILIC	Hydrophilic interaction chromatography
IEM	Ion evaporation model
IMMS	Ion-mobility mass spectrometry
IMS	Ion-mobility spectrometry
IRMPD	Infrared multiphoton dissociation
LC	Liquid chromatography
MALDI	Matrix-assisted laser desorption/ionization
MS	Mass spectrometry
MS/MS or MS^n	Tandem mass spectrometry
m/z	Mass-to-charge ratio
NeuAc	*N*-acetyl neuraminic acid
NMR	Nuclear magnetic resonance
PGC	Porous graphitized carbon
PNGase F	Peptide-*N*-glycosidase F
PTM	Posttranslational modification
Q	Quadrupole

S/N	Signal to noise
SORI	Sustained off-resonance irradiation
TOF	Time of flight
TW IMS	Traveling wave ion-mobility spectrometry
UVPD	Ultraviolet photodissociation
υUVPD	Vacuum ultraviolet photodissociation

Abstract

Glycosylation is a prevalent post-translational modification playing significant roles in cellular interactions and changing with the onset of cancer. Detailed glycan structural information is crucial to further understand disease and to find vaccine candidates. Although several analytical techniques are used for glycan structural analysis, mass spectrometry occupies an important position due to its high sensitivity and selectivity. Tandem mass spectrometry (MS/MS) cleaves chemical bonds and structural information is elucidated from unique molecular fragments and specific fragmentation pathways.

In this dissertation, novel MS/MS approaches involving ion-electron and ion-ion reactions are presented for improved glycan structural characterization compared with conventional collision activated dissociation (CAD). Divalent metal-assisted electron capture dissociation (ECD) and electron transfer dissociation (ETD) are directly compared. Metal adduction increases charge to enable ECD/ETD which require multiply charged precursor ions and also influences fragmentation. For magnesium adduction, extensive glycosidic and cross-ring cleavages, many unique to either ECD or ETD of underivatized glycans compared with CAD of the same precursor ions, or with ETD of permethylated glycans, are generated in both ECD and ETD. However, the number of structurally informative fragments and fragmentation efficiency are both higher in ECD. This discrepancy between ECD and ETD, likely related to the different pressures during

these reactions, is even more significant for cobalt and calcium adduction. Trivalent metals are also used for the first time in glycan structural analysis, producing higher charge states and inducing enhanced ECD/ETD fragmentation compared with divalent metal adduction. Electron induced dissociation (EID), which is compatible with singly charged ions, is applied to both glycan cations and anions. Positive and negative ion EID yield complementary fragmentation patterns for singly protonated or deprotonated glycans compared with CAD. Reducing end derivatization with aromatic tags facilitates electronic excitation and improves EID fragmentation. Fucose migration in derivatized glycans is significantly reduced in positive ion EID compared with CAD and completely avoided in negative ion EID and CAD. Both metal-assisted ECD/ETD and aromatic tagging/negative ion EID are demonstrated to allow glycan isomer differentiation.

The newly developed techniques can be used for structural characterization of, e.g., surface glycans on cancer stem cells.

Chapter 1 Introduction

1.1 Glycosylation

1.1.1 Biological Roles of Carbohydrates

Glycosylation refers to the attachment of carbohydrates, or glycans, to proteins. It is one of the most ubiquitous forms of post-translational modification (PTM).[1-3] Carbohydrates are major components of the cell membrane and perform key functions in various biological processes such as protein folding, self/nonself recognition, metastasis, cell adhesion, receptor activation, signal transmission, molecular trafficking and clearance.[4] In biological systems, glycans are typically conjugated to other biomolecules and presented in the form of glycoproteins, glycolipids, and glycosaminoglycans. Glycan chains are often significantly changed with the onset of diseases such as cancer and inflammation in various ways, including increased glycan branching, increased or decreased levels of glycosylation, elevated levels of sialic acids, or altered sulfonation.[4-8] Although the underlying causes are not well understood, these disease-related alterations are thought to affect growth, adhesion, differentiation, transformation, progression, metastasis, and immune surveillance of cancer cells.[3, 9, 10] Therefore, detailed and correct glycan structural information would facilitate improved understanding of their roles in cellular function and disease. For example, glycosylation is being recognized as an important biomarker and therapeutic target in cancer.[6, 11, 12]

Specifically, the work presented in this thesis is funded through a collaboration with Prof. Simeone's group in the University of Michigan Medical School. They have recently identified pancreatic cancer stem cells on the basis of three glycoprotein surface markers: CD44, CD24, and epithelial-specific antigen (ESA) using a xenograft model in which primary human pancreatic tumors were grown in immunocompromised mice (see Figure 1.1).[13] The CD44+CD24+ESA+ subpopulation (0.2-0.8% of pancreatic cancer cells) showed 100-fold increased tumorigenic potential compared to "non-stem" cancer cells and also displayed stem cell properties such as self-renewal and differentiation. An improved understanding of the nature of these cancer stem cells, including structural information of related glycans, may not only improve the understanding of the disease but may also provide a means for cancer early detection, or identification of cancer vaccine candidates.

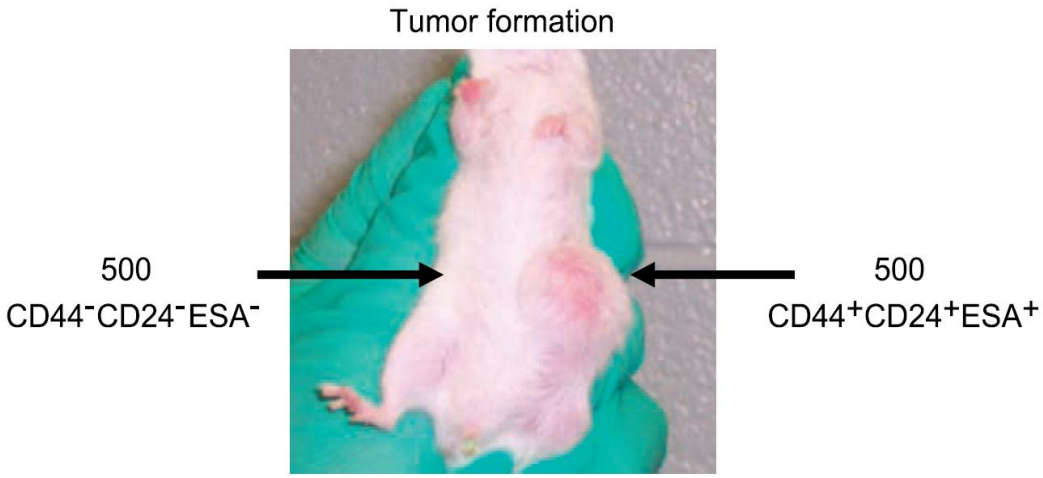

Figure 1.1 Identification of pancreatic cancer stem cells.[13]

1.1.2 Glycan Structural Complexities

Glycans are more diverse in terms of chemical structure and information density than are DNA and proteins. Variable composition, linkage, branching, and anomericity of the constituent monosaccharides in combination with the general structural heterogeneity due to the indirect, non-template based biosynthesis constitute the basis of the structural complexity of glycans. In addition, glycans are typically conjugated to other biomolecules such as proteins. All these challenges make carbohydrates the least explored among three major classes of biomolecules (carbohydrates, proteins and nucleic acids).

Symbolic representation of monosaccharides is well established in Glycobiology.[14] Figure 1.2 displays some examples of the most common monosaccharides in biological systems.

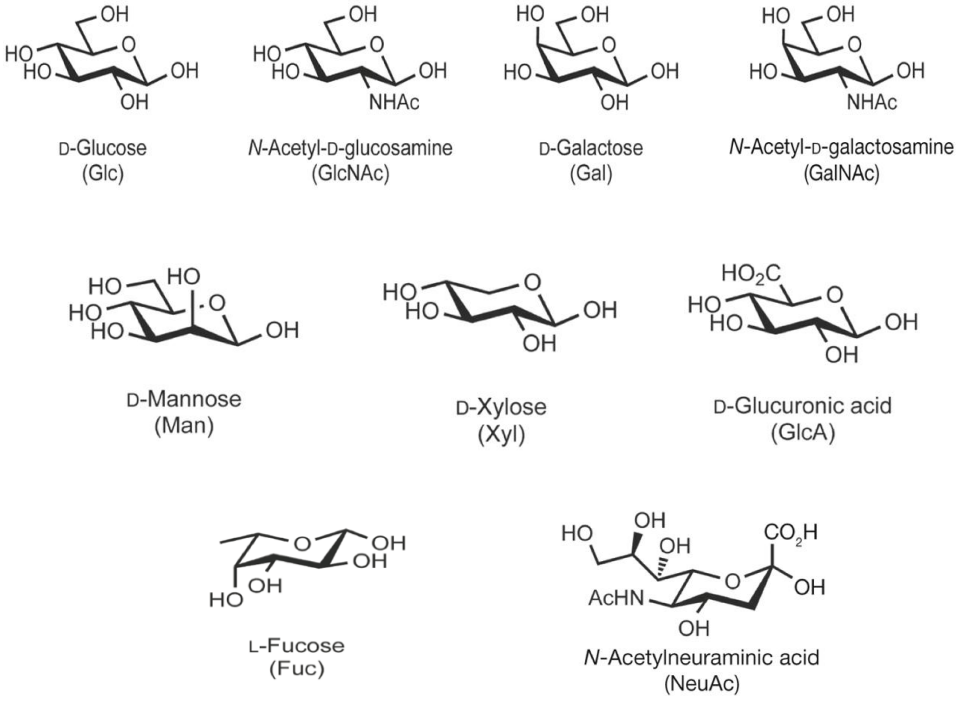

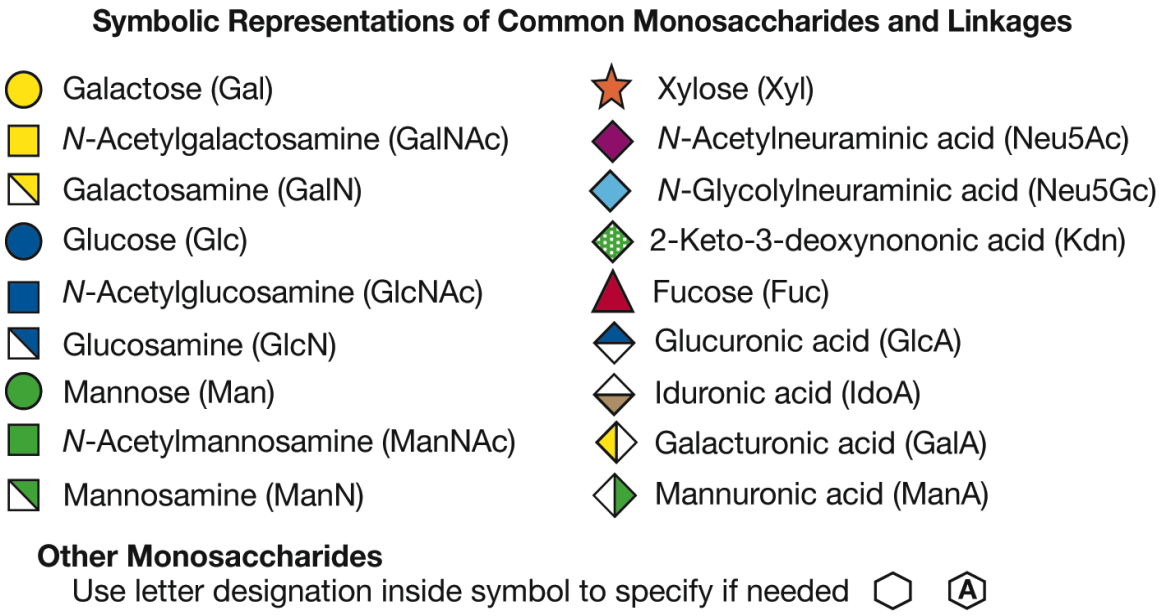

Figure 1.2 Structures and standard representations of common monosaccharides in Glycobiology.[14]

Protein glycosylation in biological systems includes N-linked glycans, O-linked glycans, and the glycosaminoglycan (GAG) family of polysaccharides (see Figure 1.3). In N-linked glycans (see Figure 1.4 (a)), carbohydrate chains are covalently attached to proteins at asparagine (Asn) residues via a GlcNAc (or in much more rare cases via GalNAc such as in Archaea[14]) saccharide in the consensus protein sequence Asn-X-Ser/Thr (X may be any amino acid residue other than proline). Three general types of *N*-glycans in mature glycoproteins are oligomannose, complex, and hybrid types, as shown in Figure 1.3. Five different *N*-glycan linkages have been reported, of which *N*-acetylglucosamine to asparagine (GlcNAcβ1-Asn) is the most common.[14] All *N*-glycans share a common core sugar sequence, Manα1–6(Manα1–3)Manβ1–4GlcNAcβ1–4GlcNAcβ1 with the terminal GlcNAc linked to the consensus protein sequence Asn-X-Ser/Thr. *N*-glycans can be classified into three types: (1) High mannose, in which only mannose residues are attached to the core; (2) complex, in which "antennae" initiated by

N-acetylglucosaminyltransferases (GlcNAcTs) are attached to the core; and (3) hybrid, in which only mannose residues are attached to the Manα1–6 arm of the core and one or two antennae are on the Manα1–3 arm.[14]

O-glycosylation is the other common covalent attachment of carbohydrates to proteins. Different from *N*-glycosylation, *O*-glycosylation occurs on serine and threonine residues of mammalian glycoproteins (see Figure 1.4 (b)). In mucins, *O*-glycans are covalently α-linked via an GalNAc moiety to the -OH of serine or threonine via an *O*-glycosidic bond and the corresponding structures are thus named mucin *O*-glycans or *O*-GalNAc glycans. There are also several types of nonmucin *O*-glycans, including α-linked *O*-fucose, β-linked *O*-xylose, α-linked *O*-mannose, β-linked *O*-GlcNAc, α- or β-linked *O*-galactose, and α- or β-linked *O*-glucose glycans.[14] O-linked glycans have highly diverse sizes but are typically smaller and less branched than most *N*-glycans. It is more challenging to characterize O-linked glycans because, in contrast to N-linked glycans, O-linked glycans do not have a specific glycan core structure, and they lack a consensus protein sequence.[14]

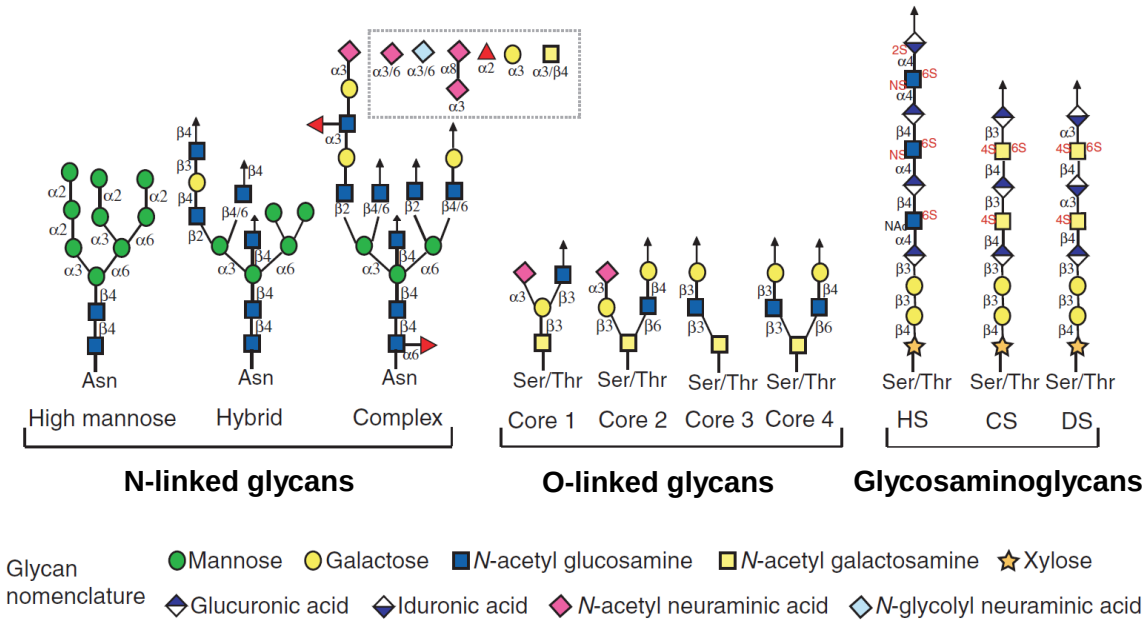

Figure 1.3 Representative structures of typical N-linked glycans, O-linked glycans, and glycosaminoglycans (GAGs).[15]

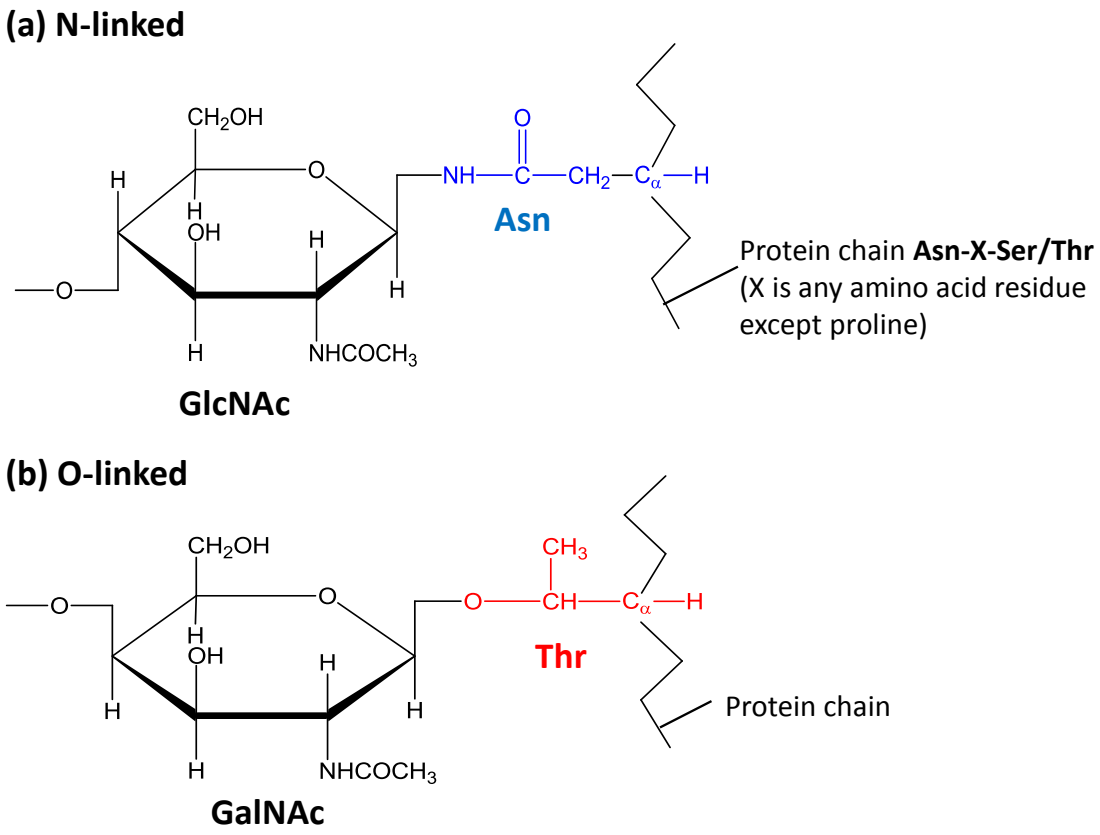

Figure 1.4 Representations of typical structures of N-linked and O-linked glycosylation. (a) N-linked; (b) O-linked.

Glycosaminoglycans (GAGs) are long and linear polysaccharides consisting of a repeating disaccharide unit. Their high heterogeneity, high molecular weight, variation in disaccharide composition and linkage, and degrees of sulfonation makes characterization of these molecules highly challenging.[16, 17]

1.1.3 Current Analytical Techniques for Glycan Structural Characterization

The importance of glycosylation in biological events and the critical roles they play in the specific function and structure of glycoconjugates such as glycoproteins, have made Glycomics an area of growing interest. However, due to the high structural complexity and branched nature of glycans, the advancement of Glycomics has faced

unique challenges in comparison with Genomics and Proteomics and pursuit of suitable analytical tools for obtaining detailed glycan structures, and for learning about glycan structure-function relationships, is ongoing. Current available analytical methods for structural characterization of glycans include ^{1}H- and ^{13}C- nuclear magnetic resonance (NMR) spectroscopy,[18-21] X-ray crystallography,[22, 23] and chromatography.[24] Mass spectrometry (MS) is more sensitive than NMR spectroscopy and X-ray crystallography and more selective than chromatography,[24, 25] and therefore plays an increasingly important role in glycan structural characterization.

1.2 Structural Characterization of Glycans by Mass Spectrometry

1.2.1 Introduction to Mass Spectrometry and Tandem Mass Spectrometry (MS/MS)

Mass spectrometers measure mass-to-charge (*m/z*) ratios of charged analytes (ions). A mass spectrometer consists of at least three components: an ion source, which converts neutral molecules to ions, a mass analyzer, which separates ions based on their *m/z* ratio, and an ion detector, which detects and outputs the signals of the separated ions. In the early years of the technique, the use of MS was limited to small and/or volatile molecules. More recent and ongoing improvements in ionization are due to increasing demands for biopolymer analysis.

MS alone, employing modern "soft" ionization, only provides molecular weight of analyte ions. In order to elucidate structure, tandem mass spectrometry (MS/MS) is needed. MS/MS involves multiple stages of MS in which a particular ion is selected at a specific *m/z* ratio, activated and dissociated into fragments under different conditions (e.g., multiple collisions with inert gas molecules, electron irradiation, interaction with

photons). Valuable structural information is generated through specific bond cleavages and unique fragmentation pathways.

For glycan structural characterization, carbohydrate MS/MS nomenclature is well established. As displayed in Figure 1.5, carbohydrate fragments include glycosidic cleavages (B, C, Y, and Z ions) and cross-ring cleavages (A and X ions). Glycosidic cleavages can provide information about sequence and composition, and some information about branching and linkage. In order to obtain more detailed structural information, A- and X-type cross-ring cleavages are highly needed. However, the most widely used MS/MS technique, collision activated dissociation (CAD), typically yields mainly glycosidic cleavages and very few cross-ring cleavages.[26-30] One aim of this dissertation is to develop and systematically study alternative MS/MS activation methods and compare them with CAD, including gas-phase ion-electron and ion-ion reactions for more detailed structural characterization of glycans.

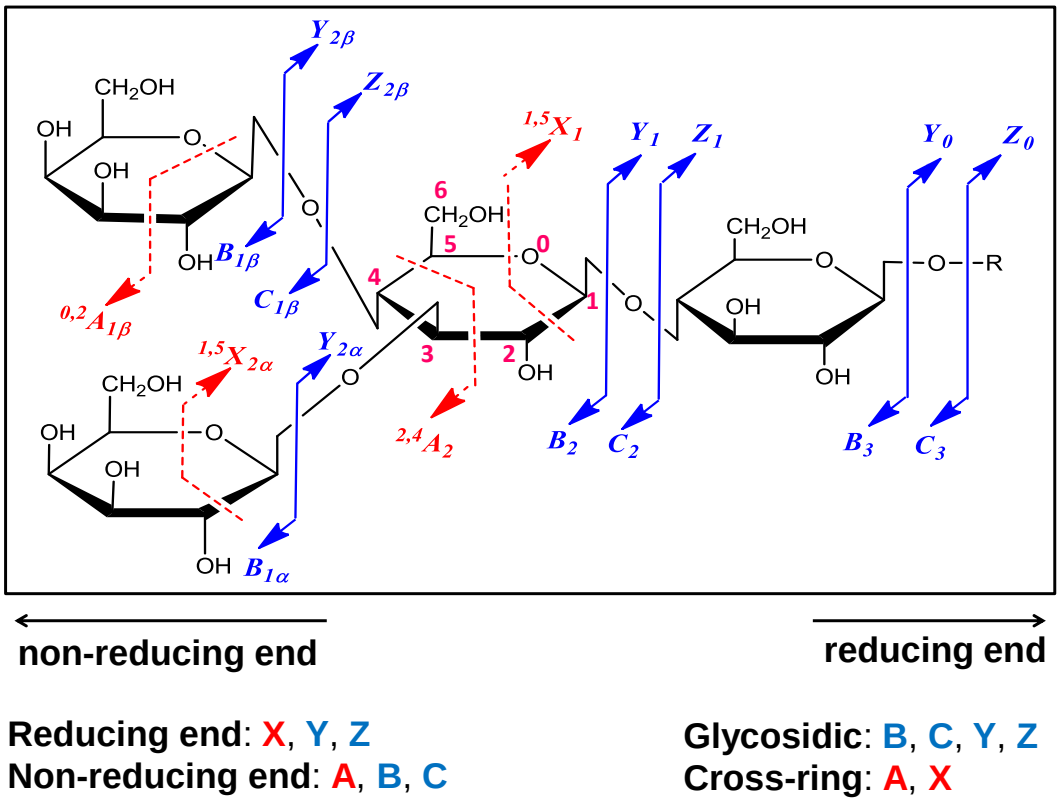

Figure 1.5 Nomenclature for carbohydrate fragments as defined by Domon and Costello.[31]

1.2.2 MS Ionization Methods

MS ionization methods for biomolecules include fast atom bombardment (FAB), matrix-assisted laser desorption/ionization (MALDI), and electrospray ionization (ESI).

In FAB, the analyte is protected by a liquid matrix and impacted by a high energy (typically a few keV) atomic beam. The kinetic energy is absorbed by the matrix and the non-volatile analyte is ionized by energy transfer from the matrix. Compared with MALDI and ESI, FAB is much more energetic and less sensitive and thus is now used very infrequently for glycan analysis.[32]

At present, MALDI is the most widely used ionization method for MS analysis of glycans. MALDI involves two steps. The first step is absorption of UV laser light and

generation of a hot plume. The second step is ionization of analyte molecules in the hot plume. Although the mechanism of MALDI is still under debate, it has been well demonstrated that a good choice of matrix aids the generation of abundant MS signals for carbohydrates.[33] Advantages of MALDI include convenience, high sensitivity, and tolerance to buffers and detergents. Although a large number of matrices have been investigated, only a few have general acceptance, such as 2,5-dihydroxybenzoic acid (2,5-DHB), 2',4',6'-trihydroxyacetophenone monohydrate (THAP), arabinosazone, and 2,5-DHB combined with either 1-hydroxyisoquinoline (1-HIQ) or 2-hydroxy-5-methoxybenzoic acid.[33] Furthermore, to allow generation of intact sialylated and sulfonated glycan ions, specific matrix and additives are needed to avoid loss of these labile substituents.[25] Sialic acid stabilization is an important problem and can be solved by chemical derivatization, such as permethylation.[25] However, this approach is challenging for low sample amounts (such as cell subpopulations, e.g., cancer stem cells) due to incomplete reactions, side reactions, and losses in the derivatization and the following clean-up process. Although improved characterization of sialylated glycans can be achieved by lectin affinity chromatography prior to MS detection, these lectins only select specific carbohydrate linkage types and are therefore not compatible with general analysis.[15, 34]

On the other hand, ESI is a softer ionization method in which sample solution is sprayed through a needle supplied with an appropriate electric potential (3-6 kV) and singly or multiply charged gas-phase ions are produced (see Figure 1.6). In addition, because of its liquid-based nature, ESI is much more compatible with on-line liquid chromatography than MALDI. ESI was first successfully introduced as a mass

spectrometric ionization technique by Yamashita and Fenn in 1984[35, 36] and by Alexandrov et al in 1985[37, 38]. In a typical ESI experiment, the liquid containing the analytes of interest is dispersed by electrospray and formed into an aerosol. Ion formation involves solvent evaporation and thus electrospray solutions typically contain volatile organic solvents. Assisted nebulization by an inert gas such as nitrogen is often added for a wider flow rate allowance. The aerosol is directed into the first vacuum stage of a mass spectrometer, typically through a capillary. The capillary is often heated to further aid solvent evaporation. As droplets evaporate and decrease in size, the electric charge density on the surface increases. The mutual repulsion between charges on the surface becomes strong enough to exceed the forces of surface tension (known as the "Rayleigh limit"). After reaching the Rayleigh limit, droplets divide into smaller droplets (i.e., "Coulomb fission"). The smaller droplets continue to undergo evaporation and Coulomb fission, creating many even smaller, more stable droplets. Regarding the final production of gas-phase ions, there are currently two major theories; the ion evaporation model (IEM)[39, 40] and the charge residue model (CRM).[41] IEM suggests the mechanism as field desorption of ions from the droplets when they have reached the right size, whereas in CRM electrospray droplets continue the evaporation and fissions cycles until progeny droplets containing one or less analyte ions are generated. In CRM, gas-phase ions form following evaporation of the remaining solvent molecules from these ultimate droplets. Experimental observations suggest IEM for small ions[40, 42] and CRM for large ions.[43] Large molecules with several ionizable (i.e., basic or acidic) sites typically carry a great number of charges after ESI. ESI can also be used to ionize molecules without acid/base properties through the formation of sodium, ammonium, chloride, acetate or

other charged adducts. Because ESI produces multiply charged ions it allows detection of large molecules with conventional mass spectrometers, such as quadrupoles, and also is compatible with a wide variety of MS/MS techniques.

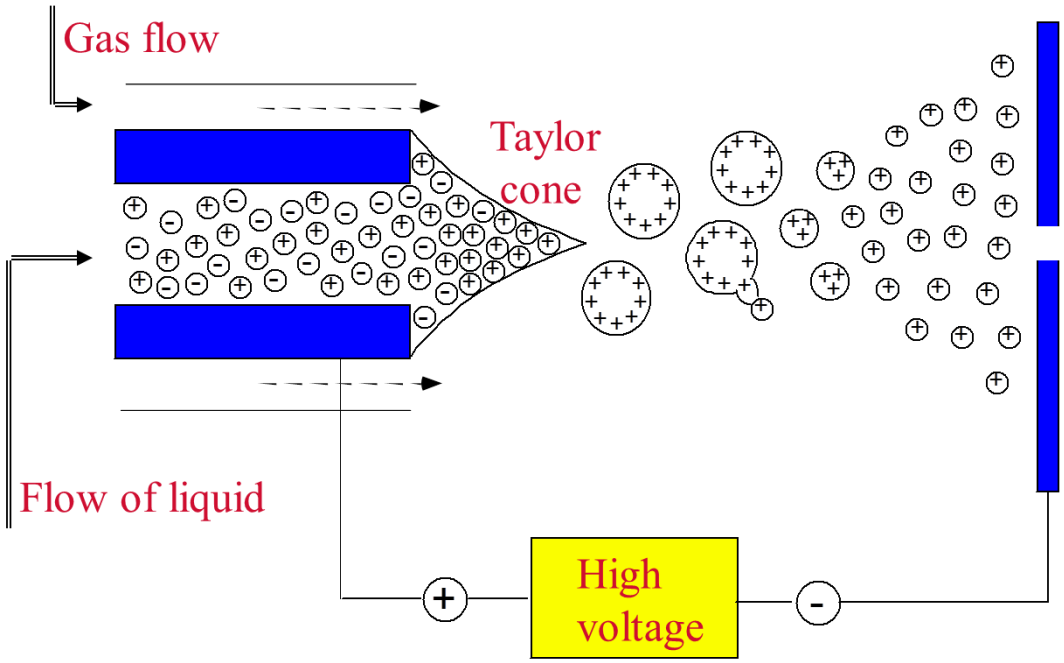

Figure 1.6 Mechanism of ESI (positive ion mode as an example) in MS.

1.2.3 Mass Analyzers

1.2.3.1 General Overview of Different Types of Mass Analyzers

Once ionized, the gas-phase charged analytes need to be separated according to their m/z ratios. Different types of mass analyzers separate and measure *m/z* ratios based on different principles (see Table 1.1). For example, the quadrupole, a common mass analyzer, is constructed out of four rods of circular or hyperbolic cross section and separates ions based on the stability of their trajectories in oscillating electric fields (see Figure 1.7). Potentials are adjusted so that only ions with a particular *m/z* ratio will be able to pass between the rods.

Table 1.1 Types of analyzers used in mass spectrometry.[44]

Type of analyzer	Symbol	Principle of separation
Quadrupole	Q	trajectory stability
Ion trap	IT	resonance frequency /trajectory stability
Time-of-flight	TOF	velocity (flight time)
Fourier transform ion cyclotron resonance	FT-ICR	resonance frequency
Fourier transform orbitrap	FT-OT	resonance frequency

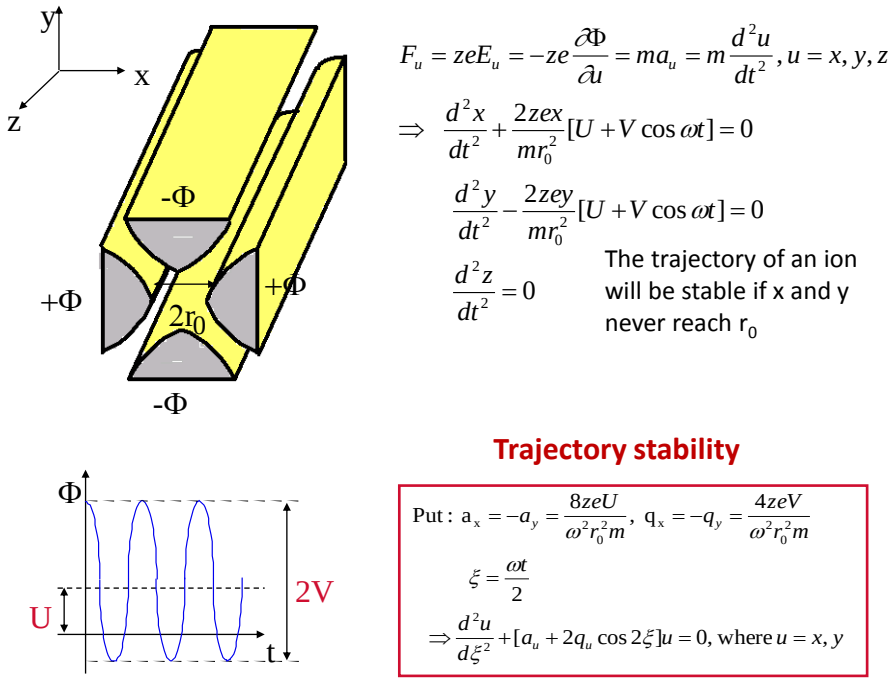

Figure 1.7 Principle of a quadrupole mass analyzer. The applied voltages affect the trajectory of ions traveling down the flight path centered between the four rods. For given DC and AC voltages, only ions of a certain mass-to-charge ratio pass through the quadrupole filter and all other ions are ejected radially.

1.2.3.2 Fourier Transform Ion Cyclotron Resonance (FT-ICR) Mass Spectrometry

1.2.3.2.1 General Principles of FT-ICR MS

The FT-ICR mass analyzer is powerful based on its ultrahigh mass accuracy, ultrahigh resolution, and a wide capability of performing various MS/MS dissociation techniques.[45] FT-ICR MS was invented by Melvin B. Comisarow and Alan G. Marshall and described for the first time in 1974.[46] A typical FT-ICR mass analyzer has two major components with the first being a superconducting magnet. Higher performance is obtained with higher-field magnets. Current commercial instruments provide magnets ranging from 4.7 to 15 T but the Pacific Northwest National Laboratory (PNNL) and the National High Magnetic Field Laboratory (NHMFL) are currently constructing 21 T FT-ICR MS instruments. The second major component is an ICR cell (see Figure 1.8) in which ions are analyzed and detected. Typically, an ICR cell contains two trapping plates, two excitation plates, and two detection plates as illustrated in Figure 1.8. The two trapping plates are perpendicular to the magnetic field whereas the two excitation plates and the two detector plates are parallel to the direction of the magnetic field. Incoming ions are trapped radially by the magnetic field and axially by trapping voltages on the two trapping plates. In the xy plane (perpendicular to the magnet field), ions rotate around the z axis in a cyclotron motion at a specific frequency dependent on their *m/z* ratio and the strength of the fixed magnetic field because of the balance between the Lorentz Force and the centripetal force due to the ions' cyclotron motion (following the cyclotron equation shown in Figure 1.8). At the same time, ions oscillate along the z axis between the electrostatic trapping plates.

Exposure to an alternating current voltage (applied to the excitation plates) with the same frequency as the ion cyclotron frequency allows resonance absorption. Ions thus increase their kinetic energy, resulting in an increased radius of their cyclotron motion. Image current is induced in the detection plates by the coherent circulation of ions close to the cell wall. Such a time-domain signal is converted to the frequency domain through Fourier transformation and then further converted into an *m/z* spectrum following the cyclotron equation.

Maintaining phase coherence during detection of ions is critical in FT-ICR mass analysis. If ions of a given *m/z* ratio are located randomly on the ICR orbit, their image currents will cancel each other out. Therefore, upon arrival in the ICR cell, ions should be well focused and excitation should occur in a very short time (typically microseconds).

As for any time-domain technique, the longer the observation time, the higher the resolution. The observation time in an ICR is related to the disappearance of the detected signal, which mainly results from ion-molecule collisions and ion dephasing. In order to achieve high resolution, collisions should be prevented to the highest possible extent and thus ultrahigh vacuum is required (usually $<10^{-9}$ mbar).

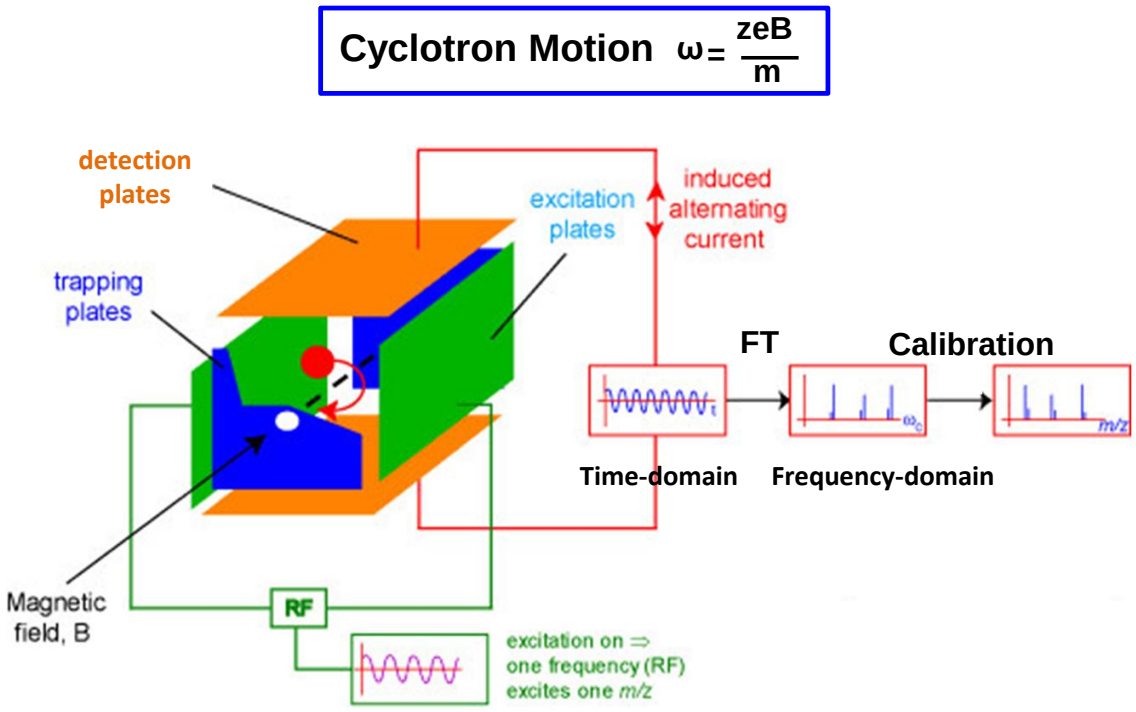

Figure 1.8 Schematic illustration of Fourier transform ion cyclotron resonance mass spectrometry (FT-ICR MS). Figure modified from http://www.chm.bris.ac.uk/ms/theory/fticr-massspec.html). In the equation, ω is the angular cyclotron frequency (related to frequency (f) in Hz via $f = \omega/2\pi$), z = ion charge, e = the numerical value of the charge of a body (or space) in atomic units, B = magnetic field strength and m = ion mass.

Each mass analyzer has advantages and disadvantages and, therefore, should be used based on specific requirements. The FT-ICR mass spectrometer is able to provide ultrahigh mass accuracy, high mass resolution, and wide versatility of MS/MS techniques. These advantages are critical for glycan structural characterization and thus exploited in this dissertation.

1.2.3.2.2 FT-ICR Instruments Used in This Thesis

The work in this thesis was performed with two different 7 T ESI quadrupole-FT-ICR mass spectrometers (Apex and SolariX, Bruker Daltonics, Billerica, MA). Schematics of both instruments are shown in Figure 1.9. Dual ion funnels provide improved ion transmission efficiency and ion sensitivity.[47] Ion transfer optics (on Apex) and the transfer hexapole (on SolariX) accelerate and focus the ions exiting the collision cell and thus overcome the magnetic mirror effect.[48] The mass analyzer of either Apex or SolariX is an infinity cell, which has a cylindrical geometry.[49] Hollow cathodes are located at the back of the instruments to enable ion-electron reactions. SolariX is a more recent design than Apex, equipped with a longer entrance capillary and optimized ion optics (hexapole in SolariX vs. a series of lenses in Apex). Therefore, SolariX provides more effective focusing and transmission than Apex. SolariX also provides softer ionization because of the higher pressure in the first vacuum stage.

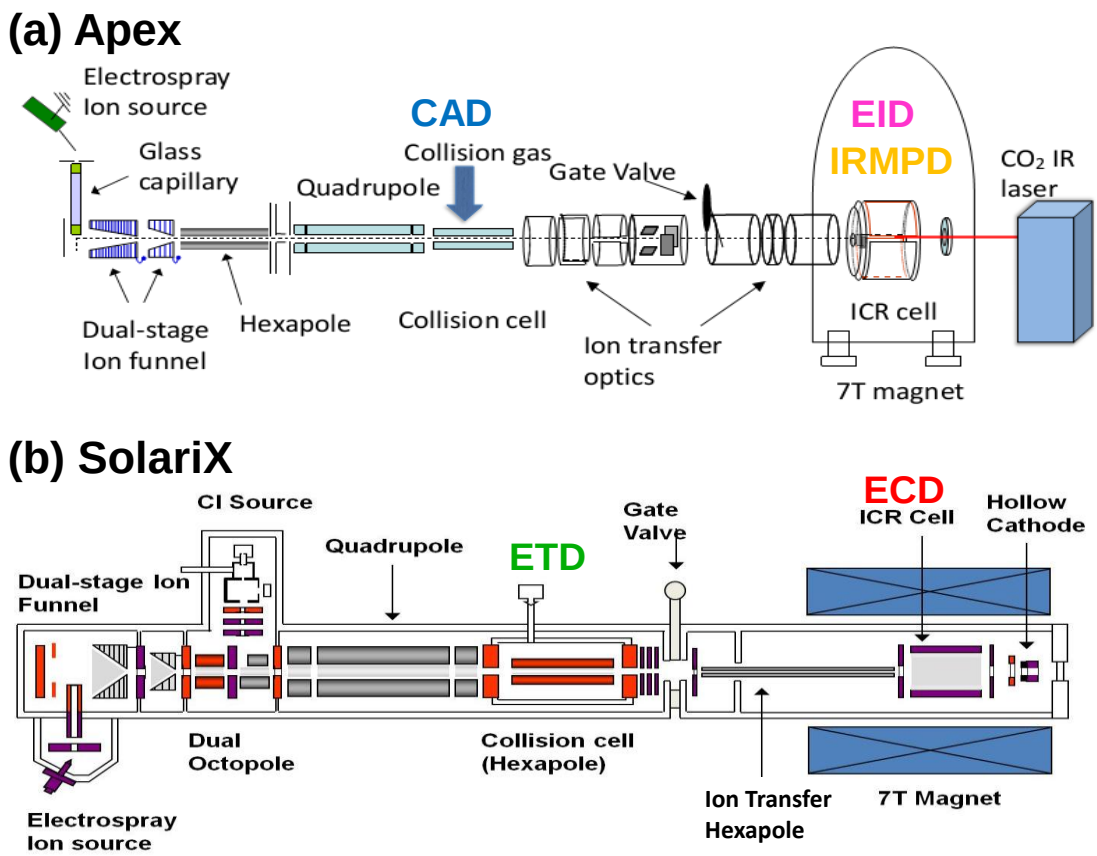

Figure 1.9 Two 7T ESI-Q-FT-ICR mass spectrometers used in this thesis. (a) Apex; (b) SolariX.

1.2.4 Ion-Mobility-Mass Spectrometry (IMMS)

Mass spectrometry can be coupled with ion mobility spectrometry (IMS), i.e., ion mobility-mass spectrometry (IMMS), to generate a powerful analytical tool for rapid separation (by IMS) and identification (by MS) of components in complex samples. In IMS, ions travel through a drift tube in the presence of a static or time dependent electric field that pushes ions forward, while a carrier buffer gas that opposes the ion motion. At the end of the drift tube is the mass spectrometer as a detector. The migration time through the tube (the "drift time") is based on an ion's mass, charge, size, and shape, thus allowing differentiation of different structures with identical mass-to-charge ratios.

McDaniel is considered the father of IMS-MS. Together with his co-workers he coupled an ion mobility drift cell to a sector mass spectrometer in the early 1960s.[50] However, since the demonstration of protein conformer separation by Clemmer et al in 1995,[51] applications and instrumental designs of IMMS have become one of the most rapidly growing areas of mass spectrometry.[52] For example, IMMS has been applied to semiconductor materials,[53] saccharides,[54, 55] peptides,[56] proteins,[57, 58] nucleic acids,[59] drugs,[60] and metabolites.[61]

An IMMS instrument involves five basic processes, sample introduction, compound ionization, ion mobility separation, mass separation, and ion detection. Gas and liquid samples can be easily introduced into IMMS and solid samples may be deposited on plates and then inserted into the instrument as well. For liquid samples, ESI is a common ionization method. Four types of ion mobility spectrometers have been described based on drift time in a static electric field,[62] aspiration,[63, 64] differential,[65] and travelling wave separation.[66] Various mass analyzers may be coupled to IMS, such as time-of-flight (TOF), quadrupole, ion-trap, ion-cyclotron, and sector mass spectrometers.[52] TOF, in particular, is appropriate for IMMS because of its high accuracy and wide dynamic range. A schematic diagram of Synapt G2 HDMS (Waters, Milford MA, USA), the IMS-MS instrument used in this dissertation is shown in Figure 1.10.

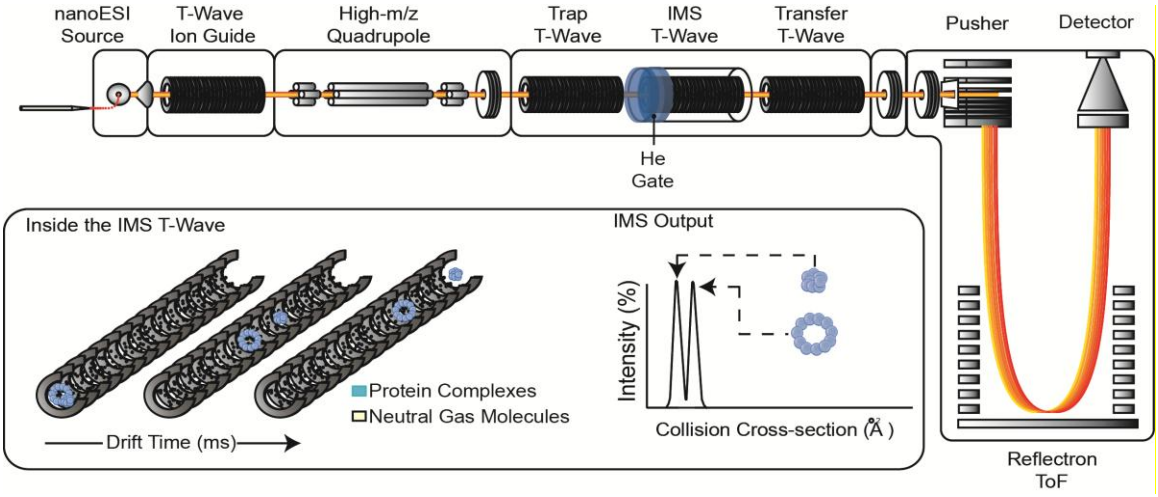

Figure 1.10 Synapt G2 HDMS (Waters, Milford MA, USA).

1.2.5 Glycan Sample Preparation

1.2.5.1 Enzymatic and Chemical Release of Glycans from Glycoproteins

To release *N*-glycans from glycoproteins, an enzymatic release method using peptide-*N*-glycosidase F (PNGase F) or peptide-*N*-glycosidase A (PNGase A) is most widely applied. PNGase F cleaves the amide bond between asparagine residues and glycan residues. This enzyme is able to release most N-linked glycans, except those containing an α1→3 fucose linkage at the reducing end GlcNAc.[67] In such situations, PNGase A should be used. Another reported enzyme is endoglycosidase-H (Endo-H), which cleaves the glycosidic bond between the two GlcNAcs at the chitobiose core. [68]

Release of *O*-glycans is more challenging than that of *N*-glycans because there is currently no universal enzyme for releasing *O*-glycans. Endo-*O*-glycosidase cleaves exclusively at serine/threonine-glycan bonds but is only active for core-1 type *O*-glycans.[69] Several options for chemical release of *O*-glycans have been reported such as reductive and non-reductive β-elimination and hydrazinolysis.[34, 70-73] For such chemical

release, which employs high concentration of salts, a subsequent desalting procedure is critical to enable the following MS analysis.

1.2.5.2 Glycan Derivatization Methods

Various derivatization methods are used for MS-based glycan analysis (see Figure 1.11). Fluorescence tags are used for simultaneous UV detection in LC/MS and have also been shown to improve MS ionization yield due to the increased glycan hydrophobicity.[8] Such tags are introduced via reaction of free amine groups on the tag with the glycan reducing end through reduction amination. The reaction involves a Schiff base intermediate, which undergoes reduction to yield a stable linkage between the fluorophore and the oligosaccharide.

In addition to reductive amination, permethylation is another widely used derivatization method prior to MS analysis. Advantages of permethylation include an even higher increase in glycan hydrophobicity compared with fluorescent tagging (and therefore even higher increase in ionization), stabilization of labile groups such as sialic acids, as well as prevention of possible migration/rearrangement in carbohydrate MS/MS.[74, 75] Traditionally, permethylation is performed with iodomethane and sodium hydroxide prepared in dimethyl sulfoxide (DMSO).[76] More recently, Novotny and co-workers reported a rapid and efficient solid-phase permethylation procedure involving sodium hydroxide powder in microspin columns or fused-silica capillaries prior to MS analysis. [77, 78]

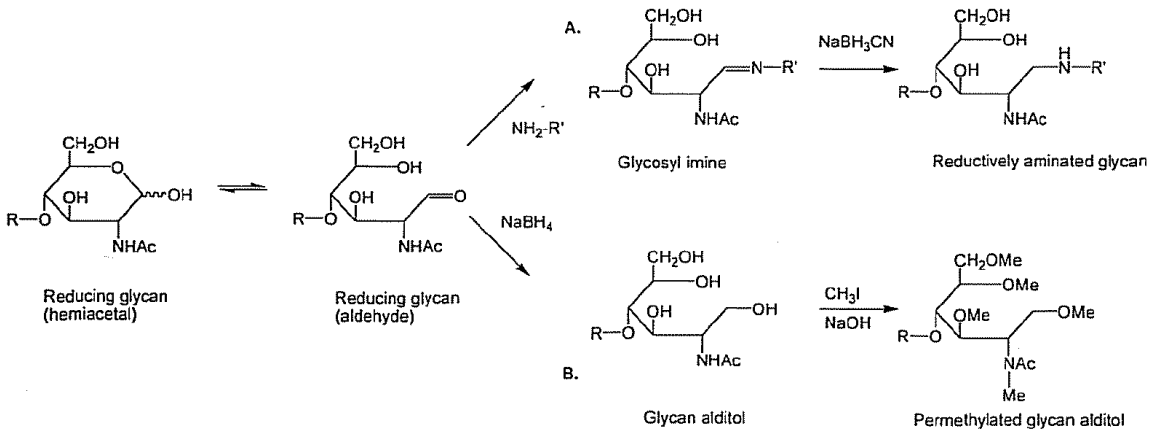

Figure 1.11 Representative scheme of common derivatization methods for glycan analysis in MS: A. Reductive amination; B. permethylation. [32]

1.2.6 Overview of Tandem Mass Spectrometry (MS/MS) for Glycan Analysis

Once ionized, gas-phase fragmentation of glycans from tandem mass spectrometry can generate abundant structural information through specific bond cleavages and unique fragmentation pathways. The use of MS/MS is driven by the need for structural analysis of glycans expressed in serum/plasma or tissue relevant to disease processes and biomarker discovery.[79] Because glycoconjugates are expressed as a distribution of glycosylation variants relative to a core structure, a glycan composition indicated by mass is often a mixture of positional isomers. Isomer separation prior to MS analysis is a possible approach, but often cannot be achieved due to the minor chemical differences of isomers. Another possible option is to analyze the mixture of positional isomers directly by MS/MS.

Most glycan tandem mass spectra are produced by CAD,[26-30] in which selected precursor ions are activated by collisions with inert gas in a collision cell. Vibrational energy is increased and cleavages tend to occur at the weakest bonds. Infrared multiphoton dissociation (IRMPD) is also used in this field because of its ability to

readily yield secondary fragmentation and higher fragmentation efficiency compared with CAD, and also because a collision gas is not required.[26, 80-83] These two "slow heating" techniques generally result in predominant glycosidic bond cleavages (B, Y, C, and Z-type fragments in Figure. 1.2) for protonated glycans.[31, 84] However, in order to gain more detailed structural information such as glycan branch positions and specific linkages, cross-ring cleavages (A and X-type fragments in Figure 1.2), which are typically of low abundance, are highly needed. Two available strategies to increase cross-ring cleavages are high energy CAD (heCAD)[85-89] at keV collision energies and metal ligation of oligosaccharides combined with CAD.[90, 91] However, heCAD involves extensive ion scattering (causing signal loss) and generally produces complex spectra in which glycosidic cleavages can be much more prevalent than cross-ring cleavages.[92] Adamson and Hakansson have shown that electron capture dissociation (ECD, see Scheme 1.1) of metal-adducted oligosaccharides produces complementary fragmentation patterns compared with CAD and IRMPD of the same species, thus making ECD a potentially useful tool for glycan structural characterization.[93] Other activation methods, including electron detachment dissociation (EDD),[94] electron transfer dissociation (ETD),[95, 96] and ultraviolet photodissociation (UVPD) at 157 nm (vacuum ultraviolet photodissociation (υUVPD))[97, 98] or 355 nm,[99] have all been reported for structural determination of glycans and glycopeptides (see Scheme 1.1).

Vibrational Activation Methods

CAD: Collision Activated Dissociation

$[M +/- nH/metal]^{m+/-} + collision \rightarrow [M +/- nH/metal]^{m+/-*} \rightarrow fragments$

IRMPD: Infrared Multiphoton Dissociation

$[M +/- H]^{+/-} + nh\upsilon \rightarrow [M +/- H]^{+/-*} \rightarrow fragments$

Ion-Electron and Ion-Ion Reactions

ECD: Electron Capture Dissociation

$[M + nH/metal]^{m+} + e^-_{<1\ eV} \rightarrow [M + nH/metal]^{(m-1)+\bullet} \rightarrow fragments$

ETD: Electron Transfer Dissociation

$[M + nH/metal]^{m+} + A^{-\bullet} \rightarrow [M + nH/metal]^{(m-1)+\bullet} + A \rightarrow fragments$

EDD: Electron Detachment Dissociation

$[M - nH]^{n-} + e^-_{>10\ eV} \rightarrow [M - nH]^{(n-1)-\bullet *} + 2e^- \rightarrow fragments$

EID: Electron Induced Dissociation

$[M +/- H]^{+/-} + e^-_{>10\ eV} \rightarrow [M +/- H]^{+/-*} + e^- \rightarrow fragments$

υUVPD: Vacuum Ultraviolet Photodissociation

$[M + H]^+ + h\upsilon_{157\ nm} \rightarrow [M + H]^{+*} \rightarrow fragments$

Scheme 1.1 MS/MS techniques utilized for glycan structural analysis.

1.2.6.1 Vibrational Excitation Reactions

1.2.6.1.1 Collision Activated Dissociation (CAD)

Cross-ring cleavages are not abundant in low energy CAD, because higher energy is required to break two chemical bonds. Low energy CAD (1-100 eV) involves multiple collisions between the precursor ions and inert gas molecules. Such activation favors breakage of weaker bonds and results in loss of labile groups. The glycosidic cleavages dominating in CAD are useful for identifying glycan composition and sequence.[100] Negative ion mode CAD typically generates more cross-ring cleavages than positive ion mode CAD.[101, 102] Positive ion heCAD at keV collision energies, on the other hand, provides extensive cross-ring cleavages, such as ^{1,5}X- and ^{3,5}A-type ions in both positive

and negative ion mode.[89, 103-105] However, heCAD is not widely used due to its limited compatibility with modern mass spectrometry instruments. Currently, heCAD is only practical in MALDI TOF instruments.[8]

1.2.6.1.2 Infrared Multiphoton Dissociation (IRMPD)

Another vibrational excitation reaction is infrared multiphoton dissociation, which involves absorption of multiple infrared photons by the precursor ions. The precursor ions thus become excited into more energetic vibrational states until a bond(s) is cleaved, resulting in gas-phase fragments. IRMPD is most often used in FT-ICR mass spectrometry but[106, 107] is also compatible with ion trap instruments. The typical set-up for IRMPD includes a 10.6 μm CO_2 laser with a power of 25-50 W, positioned behind the ICR cell. IRMPD can also be performed with tunable lasers.

1.2.6.2 Ion-Electron and Ion-Ion Reactions

1.2.6.2.1 Electron Capture Dissociation (ECD)

ECD is traditionally a positive ion mode MS/MS technique (with the recent invention of negative ion ECD (niECD) being an exception[108]) applied to multiply charged cations. ECD involves interaction between precursor ions and a beam of low energy electrons generated from a cathode. Such low energy electrons (typically <1 eV) are required to promote electron capture. Following electron capture by precursor ions, the 5-7 eV recombination energy assists radical driven dissociation. ECD is much faster (assumed to occur within 10^{-14} s) than CAD or IRMPD. The charge state of product ions is at least one less than that of precursor ions. ECD is complementary to CAD/IRMPD due to its distinctive dissociation mechanism. Although the mechanism is still under

debate, this technique provides valuable features such as unique backbone cleavages and retention of post-translational modifications in analysis of peptides/proteins.[109]

The utility of ECD has been widely documented for, e.g., peptide and protein analysis,[81, 110-112] but it has not been widely applied to carbohydrate analysis. Zubarev and colleagues reported the first application of ECD to carbohydrate analysis in 2003.[113] However, no cross-ring cleavages were observed in their experiments, and their report was limited to aminoglycans due to the requirement of multiply-charged precursor ions. Hakansson and other groups have demonstrated the utility of divalent metal ions as charge carriers in ECD for analysis of peptides,[114-116] and O-sulfonated peptides without basic amino acid residues.[117] Adamson and Hakansson applied this strategy to both linear and branched oligosaccharides in ECD by use of Ca (II), Ba (II), Mg (II), Mn (II), Co (II), and Zn (II) as charge carriers,[93] showing that ECD provides complementary bond cleavages compared with IRMPD, including greatly enhanced cross-ring fragments. Although the presence of some metal ions, such as sodium and potassium, is well known for the possibility of reducing ESI sensitivity, carefully controlled metal concentrations can be beneficial.[118, 119] The same group also successfully applied ECD to sulfonated oligosaccharides[120] and sulfonated *N*-glycans released from standard glycoprotein[121] by using divalent metal adduction.

1.2.6.2.2 Electron Transfer Dissociation (ETD)

ETD has emerged as another MS/MS technique complementary to CAD and IRMPD[122, 123] and was recently shown to have promise for structural characterization of glycans. Similar to ECD, ETD induces fragmentation of multiply charged cations by electron transfer to precursor ions. However, in ETD, the electron is delivered by anions

with low electron affinities, instead of originating as free near-thermal electrons in ECD. The latter strategy remains a technical challenge for mass spectrometers involving alternating currents due to rapid radio frequency heating of electrons. Although ETD was invented as an analog of ECD (to expand instrument compatibility), studies have already suggested differences between ECD and ETD: in spite of similarities in many respects, the two approaches may not lead to identical products.[96] ETD has been reported for structural characterization of glycopeptides, providing complementary structural information to CAD.[84, 96, 124] The McLuckey group elucidated both glycan structure and peptide sequence for an *N*-glycosylated peptide by combining CAD and ETD: CAD yields almost exclusively cleavages at glycosidic bonds and ETD yields cleavages of the peptide backbone with no loss of the glycan structure.[96] More recently, the Costello group investigated ETD fragmentation of permethylated glycans, demonstrating that ETD can be a valuable complementary MS/MS technique compared with CAD.[125]

1.2.6.2.3 Electron Induced Dissociation (EID)

EID involves irradiation of singly charged cations or anions with >10 eV electrons to generate vibrational and electronic excitation without ionization (which would form neutrals for anions).[113, 126] EID has been shown to generate complementary fragmentation patterns compared with CAD for, e.g., metabolite anions.[126]

1.2.6.2.4 Electron Detachment Dissociation (EDD)

EDD involves electron irradiation of multiply charged anions to yield electron ejection from precursor ions, and subsequent dissociation. Although EDD typically has lower fragmentation efficiency than ECD/ETD, unique structural information is

generated for structural characterization of oligosaccharides,[94, 127] oligodeoxynucleotides,[128] and proteins.[129] Anion attachment[130] and fluorescent tags[131] affect EDD fragmentation.

1.2.6.3 Ion-Photon Reactions

1.2.6.3.1 Vacuum Ultraviolet Photodissociation (υUVPD)

The Reilly group first implemented 157 nm υUVPD for fragmentation of singly charged peptide ions.[132, 133] Since then, υUVPD has been extended to the analysis of glycan cations and glycopeptides, providing valuable structural information.[97-99, 134] This relatively new dissociation method potentially can become a powerful tool for glycan structural analysis. For implementation on FT-ICR instruments, an ultrahigh vacuum compatible υUV transparent window, such as a CaF_2 window, is required for transmission of 157 nm photons. For peptides, research has already shown that both photodissociation wavelength and mass analyzer can have an effect.[135] Compared with peptides, glycans are particularly challenging due to difficulties with ionization and more complex structures. The application of UVPD for glycan structural characterization has recently emerged. Devakumar et al applied different MS/MS techniques to Girard's T-derivatized carbohydrates and observed unique fragmentation patterns in 157 nm υUVPD. The tag provided a fixed charge and thus improved ion signal.[97] The same group further extended 157 nm υUVPD to *N*-glycans in 2008.[134] Other work applying UVPD to carbohydrates includes, for example, 193 nm UVPD of deprotonated sialylated oligosaccharides.[136]

1.2.6.4 Remaining Challenges in MS-Based Glycan Structural Characterization

In spite of all the diverse MS/MS activation methods discussed above, challenges still remain in the area of mass spectrometry-based structural characterization of glycans. Migration/rearrangement of monosaccharide residues has been reported in CAD MS/MS of glycans, thus yielding false structural information.[137-141] ECD and ETD have only been applied towards certain glycans or glycoconjugates due to the requirement for higher precursor ion charge states. Some potentially useful techniques had not previously been used in glycan analysis (e.g., EID). Furthermore, limitations still exist among dissociation methods that have been applied to glycans. For example, desirable cross-ring cleavages are elusive with most MS/MS techniques and low fragmentation efficiency can pose a problem. Considering the complex structures of glycans and the high sensitivity requirement, mass spectrometric structural analysis of small sample sizes, such as cancer stem cell glycans, is expected to be particularly challenging.

1.3 Dissertation Overview

The most widely used MS/MS technique for carbohydrate analysis, CAD, is not sufficient for detailed structural characterization due to lack of cross-ring cleavages. ECD and ETD can be alternative MS/MS techniques but both techniques require multiply charged precursor ions. Metal adduction can be an effective means to increase charge states. Metal-assisted ECD and ETD are directly compared for the first time in Chapter 2. This work is being submitted to *Analytical Chemistry*.

In Chapter 3, triply charged metal-glycan complexes are generated via ESI for the first time by using specific trivalent metal salts. Human milk oligosaccharides, an *N*-glycan, and glycan isomers are investigated in this Chapter. Ion mobility mass

spectrometry experiments are also conducted to examine the effect of glycan-metal complex gas-phase structures on ECD/ETD outcome.

In many cases, the most abundant ions observed for glycans in MS are singly charged. Therefore, MS/MS techniques that are compatible with singly charged precursor ions are of major interest. In Chapter 4, positive ion mode EID is applied towards singly protonated glycans for structural characterization. Three aromatic reducing end tags, including 9-aminofluorene (9FL), 2-amino benzamide (2AB), and 2-anthranilic acid (2AA), are used for glycan derivatization, in order to study the EID mechanism. This work has been accepted for publication in the *Journal of the American Society for Mass Spectrometry*.

Many cancer related glycans contain sialic acids, which ionize more easily in negative ion mode.[142, 143] In addition, negative ion mode MS/MS has advantages such as lack of structural rearrangement and more cross-ring cleavages. Chapter 5 explores negative ion EID for glycan structural analysis. The overall conclusions from all projects in this dissertation are summarized in Chapter 6. Chapters 2-5 are all written in manuscript format.

1.4 Bibliography

(1) Bertozzi, C. R.; Kiessling, L. L. Chemical Glycobiology. *Science* **2001**, *291*, 2357-2364.

(2) Ohtsubo, K.; Marth, J. D. Glycosylation in Cellular Mechanisms of Health and Disease. *Cell* **2006**, *126*, 855-867.

(3) Dennis, J. W.; Granovsky, M.; Warren, C. E. Glycoprotein Glycosylation and Cancer Progression. *BBA - Gen. Subjects* **1999**, *1473*, 21-34.

(4) Li, M.; Song, L. J.; Qin, X. Y. Glycan Changes: Cancer Metastasis and Anti-Cancer Vaccines. *J. Bioscience.* **2010**, *35*, 665-673.

(5) Adamczyk, B.; Tharmalingam, T.; Rudd, P. M. Glycans as Cancer Biomarkers. *BBA - Gen. Subjects* **2012**, *1820*, 1347-1353.

(6) Brooks, S. A.; Carter, T. M.; Royle, L.; Harvey, D. J.; Fry, S. A.; Kinch, C.; Dwek, R. A.; Rudd, P. M. Altered Glycosylation of Proteins in Cancer: What is the Potential for New Anti-Tumour Strategies. *Anti-Cancer Agent. Me.* **2008**, *8*, 2-21.

(7) Gerber-Lemaire, S.; Juillerat-Jeanneret, L. Glycosylation Pathways as Drug Targets for Cancer: Glycosidase Inhibitors. *Mini-Rev. Med. Chem.* **2006**, *6*, 1043-1052.

(8) Zhou, W.; Hakansson, K. Structural Characterization of Carbohydrates by Fourier Transform Tandem Mass Spectrometry. *Curr. Proteomics* **2011**, *8*, 297-308.

(9) Wu, Y. M.; Nowack, D. D.; Omenn, G. S.; Haab, B. B. Mucin Glycosylation Is Altered by Pro-Inflammatory Signaling in Pancreatic-Cancer Cells. *J. Proteome Res.* **2009**, *8*, 1876-1886.

(10) Laidler, P.; Lityńska, A. Tumor Cell *N*-Glycans in Metastasis. *Acta Biochim. Pol.* **1997**, *44*, 343-357.

(11) Dwek, M. V.; Brooks, S. A. Harnessing Changes in Cellular Glycosylation in New Cancer Treatment Strategies. *Curr. Cancer Drug Tar.* **2004**, *4*, 425-442.

(12) Kang, J. G.; Ko, J. H.; Kim, Y. S. Pros and Cons of Using Aberrant Glycosylation as Companion Biomarkers for Therapeutics in Cancer. *Bmb Reports* **2011**, *44*, 765-771.

(13) Li, C. W.; Heidt, D. G.; Dalerba, P.; Burant, C. F.; Zhang, L. J.; Adsay, V.; Wicha, M.; Clarke, M. F.; Simeone, D. M. Identification of Pancreatic Cancer Stem Cells. *Cancer Res.* **2007**, *67*, 1030-1037.

(14) Varki, A.; Cummings, R. D.; Esko, J. D.; Freeze, H. H.; Stanley, P.; Bertozzi, C. R.; Hart, G. W.; Etzler, M. E. *Essentials of Glycobiology, 2nd edition*; Cold Spring Harbor Laboratory Press: New York, 2009.

(15) Raman, R.; Raguram, S.; Venkataraman, G.; Paulson, J. C.; Sasisekharan, R. Glycomics: An Integrated Systems Approach to Structure-Function Relationships of Glycans. *Nat. Methods* **2005**, *2*, 817-824.

(16) Zaia, J.; Costello, C. E. Tandem Mass Spectrometry of Sulfated Heparin-Like Glycosaminoglycan Oligosaccharides. *Anal. Chem.* **2003**, *75*, 2445-2455.

(17) Auray-Blais, C.; Lavoie, P.; Zhang, H. Y.; Gagnon, R.; Clarke, J. T. R.; Maranda, B.; Young, S. P.; An, Y.; Millington, D. S. An Improved Method for Glycosaminoglycan Analysis by LC-MS/MS of Urine Samples Collected on Filter Paper. *Clin. Chim. Acta* **2012**, *413*, 771-778.

(18) Kajihara, Y.; Sato, H. Structural Analysis of Oligosaccharides by Nuclear Magnetic Resonance Method. *Trends Glycosci. Glyc.* **2003**, *15*, 197-220.

(19) Kogelberg, H.; Solis, D.; Jimenez-Barbero, J. New Structural Insights into Carbohydrate-Protein Interactions from NMR Spectroscopy. *Curr. Opin. Struc. Biol.* **2003**, *13*, 646-653.

(20) Vanhalbeek, H. NMR Developments in Structural Studies of Carbohydrates and Their Complexes. *Curr. Opin. Struc. Biol.* **1994**, *4*, 697-709.

(21) Duus, J. O.; Gotfredsen, C. H.; Bock, K. Carbohydrate Structural Determination by NMR Spectroscopy: Modern Methods and Limitations. *Chem. Rev.* **2000**, *100*, 4589-4614.

(22) Lutteke, T. Analysis and Validation of Carbohydrate Three-Dimensional Structures. *Acta Crystallogr. D* **2009**, *65*, 156-168.

(23) Lobsanov, Y. D.; Pletnev, V. Z.; Mokulskii, M. A. X-Ray Study of the Pea Lectin-Carbohydrate Complex at 2.4 A Resolution .2. Metal and Carbohydrate Binding-Sites-A Model of Lectin-Carbohydrate Interaction. *Bioorg. Khim* **1990**, *16*, 1599-1606.

(24) Davies, M. J.; Hounsell, E. F. Carbohydrate Chromatography: Towards Yoctomole Sensitivity. *Biomed. Chromatogr.* **1996**, *10*, 285-289.

(25) Zaia, J. Mass Spectrometry and the Emerging Field of Glycomics. *Chem. Biol.* **2008**, *15*, 881-892.

(26) Park, Y.; Lebrilla, C. B. Application of Fourier Transform Ion Cyclotron Resonance Mass Spectrometry to Oligosaccharides. *Mass Spectrom. Rev.* **2005**, *24*, 232-264.

(27) Harvey, D. J. Analysis of Carbohydrates and Glycoconjugates by Matrix-Assisted Laser Desorption/Ionization Mass Spectrometry: An Update For 2003-2004. *Mass Spectrom. Rev.* **2009**, *28*, 273-361.

(28) Penn, S. G.; Cancilla, M. T.; Lebrilla, C. B. Collision-Induced Dissociation of Branched Oligosaccharide Ions with Analysis and Calculation of Relative Dissociation Thresholds. *Anal. Chem.* **1996**, *68*, 2331-2339.

(29) Maslen, S.; Sadowski, P.; Adam, A.; Lilley, K.; Stephens, E. Differentiation of Isomeric *N*-Glycan Structures by Normal-Phase Liquid Chromatography-MALDI-TOF/TOF Tandem Mass Spectrometry. *Anal. Chem.* **2006**, *78*, 8491-8498.

(30) Es-Safi, N. E.; Kerhoas, L.; Einhorn, J.; Ducrot, P. H. Application of ESI/MS, CID/MS and Tandem MS/MS to the Fragmentation Study of Eriodictyol 7-*O*-

Glucosyl-(1 -> 2)-Glucoside and Luteolin 7-*O*-Glucosyl-(1 -> 2)-Glucoside. *Int. J. Mass spectrom.* **2005**, *247*, 93-100.

(31) Domon, B.; Costello, C. E. A Systematic Nomenclature for Carbohydrate Fragmentations in FAB-MS/MS Spectra of Glycoconjugates. *Glycoconjugate J.* **1988**, *5*, 397-409.

(32) Bielik, A. M.; Zaia, J. Historical Overview of Glycoanalysis. *MIMB* **2010**, *600*, 9-30.

(33) Harvey, D. J. Matrix-Assisted Laser Desorption/Ionization Mass Spectrometry of Carbohydrates. *Mass Spectrom. Rev.* **1999**, *18*, 349-450.

(34) Mechref, Y.; Novotny, M. V. Structural Investigations of Glycoconjugates at High Sensitivity. *Chem. Rev.* **2002**, *102*, 321-370.

(35) Fenn, J. B.; Mann, M.; Meng, C. K.; Wong, S. F.; Whitehouse, C. M. Electrospray Ionization for Mass-Spectrometry of Large Biomolecules. *Science* **1989**, *246*, 64-71.

(36) Yamashita, M.; Fenn, J. B. Electrospray Ion Source. Another Variation on the Free-Jet Theme. *J. Phys. Chem.* **1984**, *88*, 4451-4459.

(37) Aleksandrov, M. L.; Gall, L. N.; Krasnov, N. V.; Nikolaev, V. I.; Shkurov, V. A. Mass-Spectrometric Analysis of Thermally Unstable Compounds of Low Volatility by the Extraction of Ions from Solution at Atmospheric-Pressure. *Journal of Analytical Chemistry of the Ussr* **1985**, *40*, 1227-1236.

(38) Alexandrov, M. L.; Gall, L. N.; Krasnov, N. V.; Nikolaev, V. I.; Pavlenko, V. A.; Shkurov, V. A. Ion Extraction from Solutions at Atmospheric-Pressure- A Method of Mass-Spectrometric Analysis of Bioorganic Substances. *Dokl. Akad. Nauk. Sssr* **1984**, *277*, 379-383.

(39) Iribarne, J. V.; Thomson, B. A. On the Evaporation of Small Ions from Charged Droplets. *J. Chem. Phys.* **1976**, *64*, 2287-2294.

(40) Nguyen, S.; Fenn, J. B. Gas-Phase Ions of Solute Species from Charged Droplets of Solutions. *Proc. Natl. Acad. Sci. U.S.A* **2007**, *104*, 1111-1117.

(41) Dole, M.; Mack, L. L.; Hines, R. L. Molecular Beams of Macroions. *J. Chem. Phys.* **1968**, *49*, 2240-&.

(42) Gamero-Castano, M.; de la Mora, J. F. Direct Measurement of Ion Evaporation Kinetics from Electrified Liquid Surfaces. *J. Chem. Phys.* **2000**, *113*, 815-832.

(43) de la Mora, J. F. Electrospray Ionization of Large Multiply Charged Species Proceeds via Dole's Charged Residue Mechanism. *Anal. Chim. Acta* **2000**, *406*, 93-104.

(44) Hoffmann, E. d.; Stroobant, V. *Mass spectrometry: principles and applications*, Third ed.; Wiley: Chichester ; New York, 2007.

(45) Marshall, A. G.; Hendrickson, C. L.; Jackson, G. S. Fourier Transform Ion Cyclotron Resonance Mass Spectrometry: A Primer. *Mass Spectrom. Rev.* **1998**, *17*, 1-35.

(46) Comisarow, M. B.; Marshall, A. G. Fourier Transform Ion Cyclotron Resonance Spectroscopy. *Chem. Phys. Lett.* **1974**, *25*, 282-283.

(47) Tang, K. Q.; Tolmachev, A. V.; Nikolaev, E.; Zhang, R.; Belov, M. E.; Udseth, H. R.; Smith, R. D. Independent Control of Ion Transmission in a Jet Disrupter Dual-Channel Ion Funnel Electrospray Ionization MS Interface. *Anal. Chem.* **2002**, *74*, 5431-5437.

(48) Guan, S. H.; Pasatolic, L.; Marshall, A. G.; Xiang, X. Z. Off-Axis Injection into an ICR Ion-Trap - A Means For Efficient Capture of a Continuous Beam of Externally Generated Ions. *Int. J. Mass spectrom.* **1994**, *139*, 75-86.

(49) Caravatti, P.; Allemann, M. The "Infinity Cell": A New Trapped-Ion Cell with Radiofrequency Covered Trapping Electrodes for Fourier Transform Ion Cyclotron Resonance Mass Spectrometry. *Org. Mass Spectrom.* **1991**, *26*, 514-518.

(50) McDaniel, E. W.; Martin, D. W.; Barnes, W. S. Drift Tube-Mass Spectrometer for Studies of Low-Energy Ion-Molecule Reactions *Rev. Sci. Instrum.* **1962**, *33*, 2-7.

(51) Clemmer, D. E.; Hudgins, R. R.; Jarrold, M. F. Naked Protein Conformations - Cytochrome-C in the Gas-Phase. *J. Am. Chem. Soc.* **1995**, *117*, 10141-10142.

(52) Kanu, A. B.; Dwivedi, P.; Tam, M.; Matz, L.; Hill, H. H., Jr. Ion Mobility-Mass Spectrometry. *J. Mass Spectrom.* **2008**, *43*, 1-22.

(53) Hunter, J. M.; Fye, J. L.; Jarrold, M. F.; Bower, J. E. Structural Transitions In Size-Selected Germanium Cluster Ions. *Phys. Rev. Lett.* **1994**, *73*, 2063-2066.

(54) Balaguer, E.; Neususs, C. Glycoprotein Characterization Combining Intact Protein and Glycan Analysis by Capillary Electrophoresis-Electrospray Ionization-Mass Spectrometry. *Anal. Chem.* **2006**, *78*, 5384-5393.

(55) Plasencia, M. D.; Isailovic, D.; Merenbloom, S. I.; Mechref, Y.; Clemmer, D. E. Resolving and Assigning *N*-Linked Glycan Structural Isomers from Ovalbumin by IMS-MS. *J. Am. Soc. Mass. Spectrom.* **2008**, *19*, 1706-1715.

(56) Pringle, S. D.; Giles, K.; Wildgoose, J. L.; Williams, J. P.; Slade, S. E.; Thalassinos, K.; Bateman, R. H.; Bowers, M. T.; Scrivens, J. H. An Investigation of the Mobility Separation of Some Peptide and Protein Ions Using A New

Hybrid Quadrupole/Travelling Wave IMS/oa-TOF Instrument. *Int. J. Mass spectrom.* **2007**, *261*, 1-12.

(57) Ruotolo, B. T.; Benesch, J. L. P.; Sandercock, A. M.; Hyung, S. J.; Robinson, C. V. Ion Mobility-Mass Spectrometry Analysis of Large Protein Complexes. *Nat Protoc* **2008**, *3*, 1139-1152.

(58) Saikusa, K.; Fuchigami, S.; Takahashi, K.; Asano, Y.; Nagadoi, A.; Tachiwana, H.; Kurumizaka, H.; Ikeguchi, M.; Nishimura, Y.; Akashi, S. Gas-Phase Structure of the Histone Multimers Characterized by Ion Mobility Mass Spectrometry and Molecular Dynamics Simulation. *Anal. Chem.* **2013**, *85*, 4165-4171.

(59) Gidden, J.; Bowers, M. T. Gas-Phase Conformations of Deprotonated and Protonated Mononucleotides Determined by Ion mobility and Theoretical Modeling. *J. Phys. Chem. B* **2003**, *107*, 12829-12837.

(60) Gryniewicz, C. M.; Reepmeyer, J. C.; Kauffman, J. F.; Buhse, L. F. Detection of Undeclared Erectile Dysfunction Drugs and Analogues in Dietary Supplements by Ion Mobility Spectrometry. *J. Pharm. Biomed. Anal.* **2009**, *49*, 601-606.

(61) Dwivedi, P.; Wu, P.; Klopsch, S. J.; Puzon, G. J.; Xun, L.; Hill, H. H. Metabolic Profiling by Ion Mobility Mass Spectrometry (IMMS). *Metabolomics* **2008**, *4*, 63-80.

(62) Cohen, M. J.; Karasek, F. W. Plasma Chromatography - A New Dimension for Gas Chromatography and Mass Spectrometry. *J. Chromatogr. Sci.* **1970**, *8*, 330-&.

(63) Sacristan, E.; Solis, A. A. A Swept-Field Aspiration Condenser As An Ion-Mobility Spectrometer. *IEEE T. Instrum. Meas.* **1998**, *47*, 769-775.

(64) Solis, A. A.; Sacristan, E. Designing the Measurement Cell of A Swept-Field Differential Aspiration Condenser. *Rev. Mex. Fis.* **2006**, *52*, 322-328.

(65) Buryakov, I. A.; Krylov, E. V.; Nazarov, E. G.; Rasulev, U. K. A New Method of Separation of Multi-Atomic Ions by Mobility at Atmospheric-Pressure Using a High-Frequency Amplitude-Asymmetric Strong Electric-Field. *Int. J. Mass Spectrom. Ion Processes* **1993**, *128*, 143-148.

(66) Giles, K.; Pringle, S. D.; Worthington, K. R.; Little, D.; Wildgoose, J. L.; Bateman, R. H. Applications of A Travelling Wave-Based Radio-Frequencyonly Stacked Ring Ion Guide. *Rapid Commun. Mass Spectrom.* **2004**, *18*, 2401-2414.

(67) Tretter, V.; Altmann, F.; Marz, L. Peptide-N4-(N-Acetyl-Beta-Glucosaminyl) Asparagine Amidase-F Cannot Release Glycans with Fucose Attached Alpha-1- 3 to the Asparagine-Linked N-Acetylglucosamine Residue. *Eur. J. Biochem.* **1991**, *199*, 647-652.

(68) Tarentin.Al; Plummer, T. H.; Maley, F. Release of Intact Oligosaccharides From Specific Glycoproteins by Endo-Beta-N-Acetylglucosaminidase H. *J. Biol. Chem.* **1974**, *249*, 818-824.

(69) Adolf, G. R.; Kalsner, I.; Ahorn, H.; Maurerfogy, I.; Cantell, K. Natural Human in Terferon-Alpha-2 is *O*-Glycosylated. *Biochem. J* **1991**, *276*, 511-518.

(70) Harvey, D. J. Matrix-Assisted Laser Desorption/Ionization Mass Spectrometry of Carbohydrates and Glycoconjugates. *Int. J. Mass spectrom.* **2003**, *226*, 1-35.

(71) Zauner, G.; Koeleman, C. A. M.; Deelder, A. M.; Wuhrer, M. Mass Spectrometric O-Glycan Analysis after Combined *O*-Glycan Release by Beta-Elimination and 1-Phenyl-3-Methyl-5-Pyrazolone Labeling. *BBA - Gen. Subjects* **2012**, *1820*, 1420-1428.

(72) An, H. J.; Miyamoto, S.; Lancaster, K. S.; Kirmiz, C.; Li, B.; Lam, K. S.; Leiserowitz, G. S.; Lebrilla, C. B. Profiling of Glycans in Serum for the Discovery of Potential Biomarkers for Ovarian Cancer. *J. Proteome Res.* **2006**, *5*, 1626-1635.

(73) Geyer, H.; Geyer, R. Strategies for Analysis of Glycoprotein Glycosylation. *BBA - Proteins. Proteom.* **2006**, *1764*, 1853-1869.

(74) Price, N. P. J. Permethylation Linkage Analysis Techniques for Residual Carbohydrates. *Appl. Biochem. Biotechnol.* **2008**, *148*, 271-276.

(75) Ruhaak, L. R.; Zauner, G.; Huhn, C.; Bruggink, C.; Deelder, A. M.; Wuhrer, M. Glycan Labeling Strategies and Their Use in Identification and Quantification. *Anal. Bioanal. Chem.* **2010**, *397*, 3457-3481.

(76) Ciucanu, I.; Kerek, F. A Simple and Rapid Method for the Permethylation of Carbohydrates. *Carbohydr. Res.* **1984**, *131*, 209-217.

(77) Kang, P.; Mechref, Y.; Klouckova, I.; Novotny, M. V. Solid-Phase Permethylation of Glycans for Mass Spectrometric Analysis. *Rapid Commun. Mass Spectrom.* **2005**, *19*, 3421-3428.

(78) Kang, P.; Mechref, Y.; Novotny, M. V. High-Throughput Solid-Phase Permethylation of Glycans Prior to Mass Spectrometry. *Rapid Commun. Mass Spectrom.* **2008**, *22*, 721-734.

(79) Packer, N. H.; Lieth, C.-W. v. d.; Aoki-Kinoshita, K. F.; Lebrilla, C. B.; Paulson, J. C.; Raman, R.; Rudd, P.; Sasisekharan, R.; Taniguchi, N.; York, W. S. Frontiers in Glycomics: Bioinformatics and Biomarkers in Disease An NIH White Paper Prepared from Discussions by the Focus Groups at a Workshop on the NIH Campus, Bethesda MD (September 11-13, 2006). *Proteomics* **2008**, *8*, 8-20.

(80) Seipert, R. R.; Dodds, E. D.; Clowers, B. H.; Beecroft, S. M.; German, J. B.; Lebrilla, C. B. Factors that Influence Fragmentation Behavior of N-Linked Glycopeptide Ions. *Anal. Chem.* **2008**, *80*, 3684-3692.

(81) Håkansson, K.; Cooper, H. J.; Emmett, M. R.; Costello, C. E.; Marshall, A. G.; Nilsson, C. L. Electron Capture Dissociation and Infrared Multiphoton Dissociation MS/MS of an *N*-Glycosylated Tryptic Peptide To Yield Complementary Sequence Information. *Anal. Chem.* **2001**, *73*, 4530-4536.

(82) Wolff, J. J.; Laremore, T. N.; Leach, F. E.; Linhardt, R. J.; Amster, I. J. Electron Capture Dissociation, Electron Detachment Dissociation and Infrared Multiphoton Dissociation of Sucrose Octasulfate. *Eur. J. Mass Spectrom.* **2009**, *15*, 275-281.

(83) Adamson, J. T.; Hakansson, K. Infrared Multiphoton Dissociation and Electron Capture Dissociation of High-Mannose Type Glycopeptides. *J. Proteome Res.* **2006**, *5*, 493-501.

(84) Wuhrer, M.; Catalina, M. I.; Deelder, A. M.; Hokke, C. H. Glycoproteomics Based on Tandem Mass Spectrometry of Glycopeptides. *J. Chromatogr. B* **2007**, *849*, 115-128.

(85) Gillece-Castro, B. L.; Burlingame, A. L. In *Mass Spectrometry*; Academic Press, 1990; Vol. Volume 193, pp 689-712.

(86) Küster, B.; Naven, T. J. P.; Harvey, D. J. Effect of the Reducing-Terminal Substituents on the High Energy Collision-Induced Dissociation Matrix-Assisted Laser Desorption/Ionization Mass Spectra of Oligosaccharides. *Rapid Commun. Mass Spectrom.* **1996**, *10*, 1645-1651.

(87) Lewandrowski, U.; Resemann, A.; Sickmann, A. Laser-Induced Dissociation/High-Energy Collision-Induced Dissociation Fragmentation Using MALDI-TOF/TOF-MS Instrumentation for the Analysis of Neutral and Acidic Oligosaccharides. *Anal. Chem.* **2005**, *77*, 3274-3283.

(88) Pittenauer, E.; Allmaier, G. High-Energy Collision Induced Dissociation of Biomolecules: MALDI-TOF/RTOF Mass Spectrometry in Comparison to Tandem Sector Mass Spectrometry. *Comb. Chem. High T. Scr.* **2009**, *12*, 137-155.

(89) Yu, S. Y.; Wu, S. W.; Khoo, K. H. Distinctive Characteristics of MALDI-Q/TOF and TOF/TOF Tandem Mass Spectrometry for Sequencing of Permethylated Complex Type N-Glycans. *Glycoconjugate J.* **2006**, *23*, 355-369.

(90) Srikanth, R.; Reddy, P. N.; Srinivas, R.; Sharma, G. V. M.; Reddy, K. R.; Krishna, P. R. Mass Spectral Study of Alkali-Cationized Boc-Carbo-B3-Peptides by Electrospray Tandem Mass Spectrometry. *Rapid Commun. Mass Spectrom.* **2004**, *18*, 3041-3050.

(91) Kohler, M.; Leary, J. A. Gas Phase Reactions of Doubly Charged Alkaline Earth and Transition Metal(II)-Ligand Complexes Generated by Electrospray Ionization. *Int. J. Mass Spectrom. Ion Processes* **1997**, *162*, 17-34.

(92) Morelle, W.; Slomianny, M. C.; Diemer, H.; Schaeffer, C.; Dorsselaer, A. v.; Michalski, J. C. Fragmentation Characteristics of Permethylated Oligosaccharides Using a Matrix-Assisted Laser Desorption/Ionization Two-Stage Time-of-Flight (TOF/TOF) Tandem Mass Spectrometer. *Rapid Commun. Mass Spectrom.* **2004**, *18*, 2637-2649.

(93) Adamson, J. T.; Håkansson, K. Electron Capture Dissociation of Oligosaccharides Ionized with Alkali, Alkaline Earth, and Transition Metals. *Anal. Chem.* **2007**, *79*, 2901-2910.

(94) Adamson, J. T.; Håkansson, K. Electron Detachment Dissociation of Neutral and Sialylated Oligosaccharides. *J. Am. Soc. Mass. Spectrom.* **2007**, *18*, 2162-2172.

(95) Zhang, Q.; Frolov, A.; Tang, N.; Hoffmann, R.; Goor, T. v. d.; Metz, T. O.; Smith, R. D. Application of Electron Transfer Dissociation Mass Spectrometry in Analyses of Non-Enzymatically Glycated Peptides. *Rapid Commun. Mass Spectrom.* **2007**, *21*, 661-666.

(96) Hogan, J. M.; Pitteri, S. J.; Chrisman, P. A.; McLuckey, S. A. Complementary Structural Information from a Tryptic *N*-Linked Glycopeptide via Electron Transfer Ion/Ion Reactions and Collision-Induced Dissociation. *J. Proteome Res.* **2005**, *4*, 628-632.

(97) Devakumar, A.; Thompson, M. S.; Reilly, J. P. Fragmentation of Oligosaccharide Ions with 157 nm Vacuum Ultraviolet Light. *Rapid Commun. Mass Spectrom.* **2005**, *19*, 2313-2320.

(98) Zhang, L.; Reilly, J. P. Extracting Both Peptide Sequence and Glycan Structural Information by 157 nm Photodissociation of N-Linked Glycopeptides. *J. Proteome Res.* **2009**, *8*, 734-742.

(99) Wilson, J. J.; Brodbelt, J. S. Ultraviolet Photodissociation at 355 nm of Fluorescently Labeled Oligosaccharides. *Anal. Chem.* **2008**, *80*, 5186-5196.

(100) Zaia, J. Mass Spectrometry of Oligosaccharides. *Mass Spectrom. Rev.* **2004**, *23*, 161-227.

(101) Ricci, A.; Fiorentino, A.; Piccolella, S.; D'Abrosca, B.; Pacifico, S.; Monaco, P. Structural Discrimination of Isomeric Tetrahydrofuran Lignan Glucosides by Tandem Mass Spectrometry. *Rapid Commun. Mass Spectrom.* **2010**, *24*, 979-985.

(102) Yoon, E. Y. Comparison between Positive and Negative Ion Mode FAB CAD MS/MS Spectra of Linkage-Isomeric Oligosaccharides. *J. Biochem. Mol. Biol.* **1997**, *30*, 253-257.

(103) Harvey, D. J.; Bateman, R. H.; Green, M. R. High-Energy Collision-Induced Fragmentation of Complex Oligosaccharides Ionized by Matrix-assisted Laser Desorption/Ionization Mass Spectrometry. *J. Mass Spectrom.* **1997**, *32*, 167-187.

(104) Suzuki, K.; Dalkoku, S.; Ako, T.; Shioiri, Y.; Kurimoto, A.; Ohtake, A.; Sarkar, S. K.; Kanie, O. High-Yielding and Controlled Dissociation of Glycosides Producing B- and C-ion Species under Collision-Induced Dissociation MS/MS Conditions and Use in Structural Determination. *Anal. Chem.* **2007**, *79*, 9022-9029.

(105) Scrivens, J. H.; Jackson, A. T.; Jennings, K. R.; Jennings, R. C. K.; Everall, N. J. High Energy Collision-Induced Dissociation (CID) Product Ion Spectra of Isomeric Polyhydroxy Sugars. *Int. J. Mass spectrom.* **2003**, *230*, 201-208.

(106) Li, B.; An, H. J.; Hedrick, J. L.; Lebrilla, C. B. In *Glycomics: Methods and Protocols*; Packer, N. H., Karlsson, N. G., Eds.; Humana Press Inc, 999 Riverview Dr, Ste 208, Totowa, Nj 07512-1165 USA, 2009; Vol. 534, pp 23-35.

(107) Lancaster, K. S.; An, H. J.; Li, B. S.; Lebrilla, C. B. Interrogation of N-Linked Oligosaccharides Using Infrared Multiphoton Dissociation in FT-ICR Mass Spectrometry. *Anal. Chem.* **2006**, *78*, 4990-4997.

(108) Yoo, H. J.; Wang, N.; Zhuang, S.; Song, H.; Håkansson, K. Negative-Ion Electron Capture Dissociation: Radical-Driven Fragmentation of Charge-Increased Gaseous Peptide Anions. *J. Am. Chem. Soc.* **2011**, *133*, 16790-16793.

(109) Cooper, H. J.; Hakansson, K.; Marshall, A. G. The Role of Electron Capture Dissociation in Biomolecular Analysis. *Mass Spectrom. Rev.* **2005**, *24*, 201-222.

(110) Clarke, D. J.; Murray, E.; Hupp, T.; Mackay, C. L.; Langridge-Smith, P. R. R. Mapping a Noncovalent Protein-Peptide Interface by Top-Down FTICR Mass Spectrometry Using Electron Capture Dissociation. *J. Am. Soc. Mass. Spectrom.* **2011**, *22*, 1432-1440.

(111) Pan, J.; Borchers, C. H. Top-Down Structural Analysis of Posttranslationally Modified Proteins by Fourier Transform Ion Cyclotron Resonance-MS with Hydrogen/Deuterium Exchange and Electron Capture Dissociation. *Proteomics* **2013**, *13*, 974-981.

(112) Robb, D. B.; Rogalski, J. C.; Kast, J.; Blades, M. W. Liquid Chromatography-Atmospheric Pressure Electron Capture Dissociation Mass Spectrometry for the Structural Analysis of Peptides and Proteins. *Anal. Chem.* **2012**, *84*, 4221-4226.

(113) Budnik, B. A.; Haselmann, K. F.; Elkin, Y. N.; Gorbach, V. I.; Zubarev, R. A. Applications of Electron−Ion Dissociation Reactions for Analysis of Polycationic Chitooligosaccharides in Fourier Transform Mass Spectrometry. *Anal. Chem.* **2003**, *75*, 5994-6001.

(114) Eva Fung, Y. M.; Liu, H.; Chan, T. W. D. Electron Capture Dissociation of Peptides Metalated with Alkaline-Earth Metal Ions. *J. Am. Soc. Mass. Spectrom.* **2006**, *17*, 757-771.

(115) Liu, H.; Håkansson, K. Divalent Metal Ion-Peptide Interactions Probed by Electron Capture Dissociation of Trications. *J. Am. Soc. Mass. Spectrom.* **2006**, *17*, 1731-1741.

(116) Kleinnijenhuis, A. J.; Mihalca, R.; Heeren, R. M. A.; Heck, A. J. R. Atypical Behavior in the Electron Capture Induced Dissociation of Biologically Relevant Transition Metal Ion Complexes of the Peptide Hormone Oxytocin. *Int. J. Mass spectrom.* **2006**, *253*, 217-224.

(117) Liu, H.; Håkansson, K. Electron Capture Dissociation of Tyrosine *O*-Sulfated Peptides Complexed with Divalent Metal Cations. *Anal. Chem.* **2006**, *78*, 7570-7576.

(118) Kohler, M.; Leary, J. A. LC/MS/MS of Carbohydrates with Postcolumn Addition of Metal Chlorides Using Triaxial Electrospray Probe. *Anal. Chem.* **1995**, *67*, 3501-3508.

(119) Karlsson, K. E. Cationization in Electrospray Microcolumn Liquid Chromatography-Mass Spectrometry. *J. Chromatogr. A* **1998**, *794*, 359-366.

(120) Liu, H.; Håkansson, K. Electron Capture Dissociation of Divalent Metal-Adducted Sulfated Oligosaccharides. *Int. J. Mass spectrom.* **2011**, *305*, 170-177.

(121) Zhou, W.; Hakansson, K. Electron Capture Dissociation of Divalent Metal-adducted Sulfonated N-Glycans Released from Bovine Thyroid Stimulating Hormone. *J. Am. Soc. Mass. Spectrom.* **2013**, Accepted.

(122) Syka, J. E. P.; Coon, J. J.; Schroeder, M. J.; Shabanowitz, J.; Hunt, D. F. Peptide and Protein Sequence Analysis by Electron Transfer Dissociation Mass Spectrometry. *Proc. Natl. Acad. Sci. U.S.A* **2004**, *101*, 9528-9533.

(123) Pitteri, S. J.; Chrisman, P. A.; Hogan, J. M.; McLuckey, S. A. Electron Transfer Ion/Ion Reactions in a Three-Dimensional Quadrupole Ion Trap: Reactions of Doubly and Triply Protonated Peptides with $SO_2^{\bullet-}$. *Anal. Chem.* **2005**, *77*, 1831-1839.

(124) Catalina, M. I.; Koeleman, C. A. M.; Deelder, A. M.; Wuhrer, M. Electron Transfer Dissociation of *N*-Glycopeptides: Loss of the Entire N-Glycosylated Asparagine Side Chain. *Rapid Commun. Mass Spectrom.* **2007**, *21*, 1053-1061.

(125) Han, L.; Costello, C. Electron Transfer Dissociation of Milk Oligosaccharides. *J. Am. Soc. Mass. Spectrom.* **2011**, *22*, 997-1013.

(126) Yoo, H. J.; Liu, H.; Håkansson, K. Infrared Multiphoton Dissociation and Electron-Induced Dissociation as Alternative MS/MS Strategies for Metabolite Identification. *Anal. Chem.* **2007**, *79*, 7858-7866.

(127) Leach, F. E.; Ly, M.; Laremore, T. N.; Wolff, J. J.; Perlow, J.; Linhardt, R. J.; Amster, I. J. Hexuronic Acid Stereochemistry Determination in Chondroitin Sulfate Glycosaminoglycan Oligosaccharides by Electron Detachment Dissociation. *J. Am. Soc. Mass. Spectrom.* **2012**, *23*, 1488-1497.

(128) Yang, J.; Mo, J.; Adamson, J. T.; Hakansson, K. Characterization of Oligodeoxynucleotides by Electron Detachment Dissociation Fourier Transform Ion Cyclotron Resonance Mass Spectrometry. *Anal. Chem.* **2005**, *77*, 1876-1882.

(129) Ganisl, B.; Valovka, T.; Hartl, M.; Taucher, M.; Bister, K.; Breuker, K. Electron Detachment Dissociation for Top-Down Mass Spectrometry of Acidic Proteins. *Chem - Eur. J.* **2011**, *17*, 4460-4469.

(130) Kornacki, J. R.; Adamson, J. T.; Hakansson, K. Electron Detachment Dissociation of Underivatized Chloride-Adducted Oligosaccharides. *J. Am. Soc. Mass. Spectrom.* **2012**, *23*, 2031-2042.

(131) Zhou, W.; Hakansson, K. Electron Detachment Dissociation of Fluorescently Labeled Sialylated Oligosaccharides. *Electrophoresis* **2011**, *32*, 3526-3535.

(132) Thompson, M. S.; Cui, W.; Reilly, J. P. Fragmentation of Singly Charged Peptide Ions by Photodissociation at λ=157 nm. *Angew. Chem. Int. Ed.* **2004**, *43*, 4791-4794.

(133) Reilly, J. P. Ultraviolet Photofragmentation of Biomolecular Ions. *Mass Spectrom. Rev.* **2009**, *28*, 425-447.

(134) Devakumar, A.; Mechref, Y.; Kang, P.; Novotny, M. V.; Reilly, J. P. Identification of Isomeric *N*-Glycan Structures by Mass Spectrometry With 157 nm Laser-Induced Photofragmentation. *J. Am. Soc. Mass. Spectrom.* **2008**, *19*, 1027-1040.

(135) Thompson, M. S.; Cui, W.; Reilly, J. P. Factors That Impact the Vacuum Ultraviolet Photofragmentation of Peptide Ions. *J. Am. Soc. Mass. Spectrom.* **2007**, *18*, 1439-1452.

(136) Ko, B. J.; Brodbelt, J. S. 193 nm Ultraviolet Photodissociation of Deprotonated Sialylated Oligosaccharides. *Anal. Chem.* **2011**, *83*, 8192-8200.

(137) Wuhrer, M.; Koeleman, C. A. M.; Deelder, A. M. Hexose Rearrangements upon Fragmentation of *N*-Glycopeptides and Reductively Aminated *N*-Glycans. *Anal. Chem.* **2009**, *81*, 4422-4432.

(138) Hashii, N.; Kawasaki, N.; Itoh, S.; Nakajima, Y.; Harazono, A.; Kawanishi, T.; Yamaguchi, T. Identification of Glycoproteins Carrying a Target Glycan-Motif by Liquid Chromatography/Multiple-Stage Mass Spectrometry: Identification of Lewis x-Conjugated Glycoproteins in Mouse Kidney. *J. Proteome Res.* **2009**, *8*, 3415-3429.

(139) Broberg, A. High-Performance Liquid Chromatography/Electrospray Ionization Ion-Trap Mass Spectrometry for Analysis of Oligosaccharides Derivatized by Reductive Amination and N,N-Dimethylation. *Carbohydr. Res.* **2007**, *342*, 1462-1469.

(140) Hsu, F.-F.; Turk, J. Studies on Sulfatides by Quadrupole Ion-Trap Mass Spectrometry with Electrospray Ionization: Structural Characterization and the Fragmentation Processes that Include an Unusual Internal Galactose Residue Loss and the Classical Charge-Remote Fragmentation. *J. Am. Soc. Mass. Spectrom.* **2004**, *15*, 536-546.

(141) Kovacik, V.; Hirsch, J.; Kovac, P.; Heerma, W.; Thomasoates, J.; Haverkamp, J. Oligosaccharide Characterization Using Collision-Induced Dissociation Fast-Atom-Bombardment Mass-Spectrometry- Evidence for Internal Monosaccharide Residue Loss. *J. Mass Spectrom.* **1995**, *30*, 949-958.

(142) Narayanan, S. Sialic-Acid as a Tumor-Marker. *Ann. Clin. Lab. Sci.* **1994**, *24*, 376-384.

(143) Varki, A. Glycan-Based Interactions Involving Vertebrate Sialic-Acid-Recognizing Proteins. *Nature* **2007**, *446*, 1023-1029.

Chapter 2 Electron Capture Dissociation vs. Electron Transfer Dissociation of Divalent Metal-Adducted Underivatized Oligosaccharides

2.1 Introduction

Glycans modulate and mediate a variety of cell-cell and cell-molecule interactions. More than 50% of proteins in mammalian cells are glycosylated and glycan structures change with the onset of diseases such as cancer.[1-6] Correct and detailed structural information for disease-associated glycans is strongly desired for improved understanding of the molecular mechanisms of disease, and for identification of drug candidates, including cancer vaccines.[7-10] However, such structural characterization is highly challenging due to the complex and branched nature of glycans, arising from their synthesis by a variety of glycosyltransferases in a non-template driven manner. Complete structural characterization of glycans includes not only the nature and order of constituent monosaccharides and position of glycosidic linkages, but also the degree of branching and stereochemistry. In addition, glycan isomers with identical composition but, e.g., different linkages are present in biological systems.[11, 12] Glycans with minor structural differences can dramatically alter biological function.[1] For example, maltose (Glcα4Glc) and gentiobiose (Glcβ6Glc) have very different three-dimensional structures and biological activities.[1] As another example, Reinhold and co-workers recently reported cell-line specific presences of multiple structural isomers of the composition $Hex_6HexNAc_3Fuc_1$ (at *m/z* 1121.1 (2+)) released from tumor cells.[13] Various

modifications, such as sulfonation, phosphorylation, and acylation, are associated with glycans. In addition, glycans are typically conjugated to other biomolecules (e.g., proteins). All of these complexities contribute to the higher difficulty in characterizing glycans compared with other linear biomolecules.[1,14]

Current available glycan structural characterization methods include NMR spectroscopy, X-ray crystallography, chromatography, and mass spectrometry (MS). NMR is a powerful tool for determination of anomeric configuration, linkage and sequence. It is also a powerful tool for identifying isomers. However, NMR requires a large amount of pure sample, typically 1 mg or more. Further, tedious data interpretation poses a challenge to the unique assignment of protons and carbon atoms.[15-19] X-ray crystallography can generate detailed 3D structures of glycans but, in addition to a large amount of pure sample, X-ray crystallography requires the formation of crystals.[20-23] Chromatography is well-known for its superior reproducibility and sensitivity (particularly by use of fluorescence detection), but this method requires standards and, accordingly, it is difficult to identify unknown and new structures.[24] Mass spectrometry does not require large amounts of pure sample, nor does it require formation of crystals. Instead, mass spectrometry has advantages such as high sensitivity and high selectivity. Because of these advantages, MS is a highly useful analytical tool in glycan structural analysis.[25-28] Fourier transform ion cyclotron resonance (FT-ICR) MS is particularly powerful based on its ultrahigh mass accuracy, ultrahigh resolution, and wide capability of performing various tandem mass spectrometry (MS/MS) techniques.

MS/MS involves mass selection, ion activation, and mass separation of resulting molecular ion fragments. Structure is elucidated through these unique fragments and

specific dissociation pathways. In carbohydrate MS/MS, bond cleavage occurs either between two monosaccharides (defined as "glycosidic cleavages"), or within one monosaccharide (defined as "cross-ring cleavages").[29] Glycosidic cleavages are useful for identifying constituent monosaccharides, but are not useful for identifying linkage and branching. By contrast, cross-ring cleavages can provide information about linkage and branching and are thus highly needed for detailed structural characterization of glycans. However, cross-ring cleavages are typically less prevalent because higher energy is required to cleave two covalent bonds. Conventional MS/MS activation techniques, such as positive ion mode collision activated dissociation (CAD), are very successful for producing glycosidic B- and Y-type cleavages.[30-33] In order to generate more cross-ring cleavages for improved structural detail of glycan cations, alternative MS/MS activation techniques have been developed, such as electron capture dissociation (ECD)[34, 35] and electron transfer dissociation (ETD).[36]

In ECD, multiply charged (≥ 2) precursor cations capture low energy (usually <1 eV) electrons to generate charge-reduced species and several fragments from radical-driven processes.[37] One limitation of ECD is that this ion-electron dissociation method requires a magnetic field to confine low energy electrons. In order to extend the utility of ECD, the ion-ion analog ETD was introduced. ETD was first demonstrated in a linear radio-frequency quadruple ion trap,[38] and later implemented on other mass spectrometers such as orbitrap and FT-ICR instruments.[39, 40] ECD and ETD are widely applied to proteins and peptides for structural determination. These activation techniques are particularly powerful for characterization of post-translational modifications (PTMs), such as phosphorylation, glycosylation, methylation, acetylation, and disulfide bonds.[41-45]

ECD and ETD have relatively recently been applied towards glycan structural characterization.[31, 34-36, 46-48] ECD was first applied to aminoglycans because such glycans can readily form multiply charged cations.[48] However, the requirement of multiply charged precursor ions can limit the applicability of ECD/ETD towards glycans, because they do not generally contain basic sites.

Metal adduction can be an effective approach to increase glycan charge states and has also been shown to stabilize labile groups.[34, 49] Our group demonstrated that ECD of oligosaccharides adducted with alkali, alkaline earth, and transition metals generates complementary structural information compared with slow-heating techniques such as CAD and infrared multiphoton dissociation (IRMPD). We also showed that calcium adduction allows structural characterization of highly acidic sulfonated oligosaccharides.[49, 50] Recently, magnesium adduction was shown to yield informative ETD fragmentation for permethylated glycans.[36]

Previous literature has suggested differences between the mechanisms and fragmentation behaviors of ECD and ETD for peptides.[51, 52] In this chapter, these two MS/MS techniques for divalent metal-adducted carbohydrates are directly compared on the same FT-ICR mass spectrometer. We also explored whether glycan isomer differentiation is feasible with ECD and/or ETD.

2.2 Experimental Section

2.2.1 Reagents

Lacto-N-difucohexaose I (LNDFH I), LS-tetrasaccharide A (LSTa), LS-tetrasaccharide B (LSTb), LS-tetrasaccharide C (LSTc), and an asialo, biantennary N-glycan (NA2) were purchased from V-Labs Inc (Covington, LA), Prozyme (Hayward,

CA) or Carbosynth (Compton, Berkshire, UK). $MgCl_2$, $CaCl_2$, and $CoBr_2$ were obtained from Fisher (Fair Lawn, NJ) or Sigma-Aldrich.

2.2.2 Sample Preparation

Five μM solutions of oligosaccharides were mixed with 20 μM salt ($MgCl_2$, $CaCl_2$, and $CoBr_2$) in 50% methanol (v/v) for positive ion mode analysis.

2.2.3 Mass Spectrometry

All mass spectra were acquired on a SolariX 7T electrospray ionization (ESI)-quadrupole-FT-ICR mass spectrometer (Bruker Daltonics, Billerica, MA). Samples were infused via an Apollo II electrospray source (Bruker Daltonics, Billerica, MA) at 70 to 100 μL/h and ionized with the assistance of N2 nebulizing gas. Precursor ions for MS/MS were selected by the quadrupole and accumulated externally in the collision cell (hexapole). ECD experiments were conducted by irradiating precursor ions in the ICR cell by an electron beam from an indirectly heated cathode. The cathode heating current was 1.6 A and the cathode bias voltage was pulsed to -0.9 to -1.3 V for 180 to 300 ms. ETD experiments were conducted in the collision cell. ETD reagent (fluoranthene anions, Sigma-Aldrich, St. Louis, MO) were produced externally in the chemical ionization source, trapped in the collision cell for 350–2000 ms, and then allowed to react with mass-selected precursor ions for 100 ms. All mass spectra were acquired with SolarixControl software (Bruker Daltonics, Billerica, MA) with 256 data points from *m/z* 200 to 2000 and averaged over 64 - 100 scans.

2.2.4 Data Analysis

Data processing was performed with Data Analysis software (Bruker Daltonics, Billerica, MA). Preliminary calibration was performed externally with the calibration function in Data Analysis software followed by internal calibration based on four known *m/z* ratios (the precursor ion, charge reduced/proton stripped species, and two expected product ions (typically glycosidic fragments). Data were analyzed manually with the aid of GlycoWorkbench software.[53] Product ions were not assigned unless the S/N ratio was at least 3. ECD and ETD fragmentation efficiencies were calculated based on equation 1, excluding the charge-reduced but non-dissociated products.

Fragmentation efficiency = $\frac{\sum \boldsymbol{I}\,(\boldsymbol{fi})}{\boldsymbol{Pi}\,(\boldsymbol{before})}$ (1) in which I (f_i) is the summed product ion abundance (charge state normalization is unnecessary as all fragments are singly charged) and P_i (before) is the precursor ion abundance in a separate spectrum prior to dissociation.

2.3 Results and Discussion

2.3.1 ECD and ETD of Divalent Metal-Adducted Underivatized LNDFH

LNDFH is a common human milk oligosaccharide with the composition Fucα2Galβ3(Fucα4)GlcNAcβ3Galβ4Glc.

Figure 2.1 shows a positive ion ESI-FT-ICR mass spectrum of 5 μM LNDFH in the presence of 20 μM $MgCl_2$. Several molecular ion species are detected, such as singly protonated LNDFH and its fragments, however doubly charged $[LNDFH + Mg]^{2+}$ is the most abundant ion. Following quadrupole isolation of this precursor ion at *m/z* 511.7, ECD and ETD were performed in order to compare the resulting fragmentation patterns.

Experimental conditions were optimized to obtain the highest variety of fragments in each technique, starting with identical precursor ion abundance prior to MS/MS.

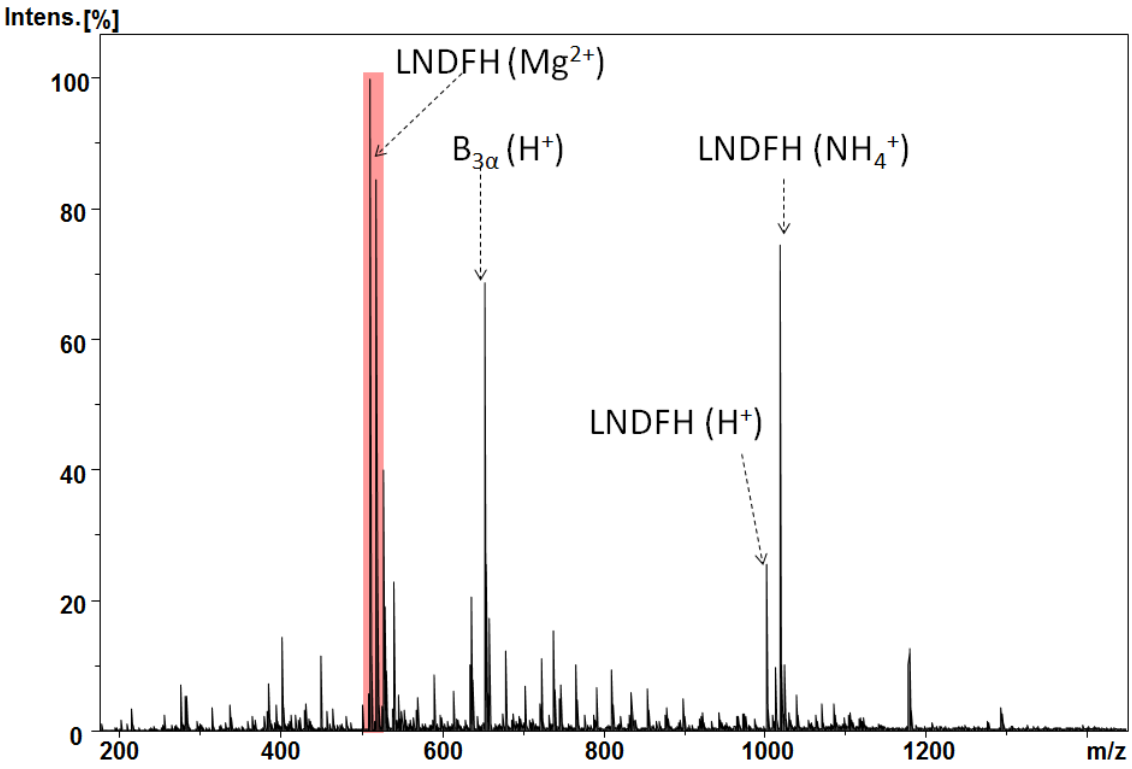

Figure 2.1 ESI FT-ICR mass spectrum of 5 μM LNDFH in the presence of 20 μM $MgCl_2$.

Figure 2.2 displays ECD and ETD spectra for Mg-adducted LNDFH. This precursor ion ($[M + Mg]^{2+}$) fragmented extensively at optimized ECD and ETD conditions, generating a plentitude of glycosidic, cross-ring, and internal cleavages. Both ECD and ETD generated sufficient glycosidic cleavages to cover the entire oligosaccharide sequence. ECD of Mg-adducted LNDFH generated four glycosidic cleavages, including $Z_{3\alpha}$, $C_{3\alpha}$, $Y_{3\alpha}$, and C_4, as well as seven cross-ring cleavages, including $^{1,3}A_3$, $^{1,4}X_2$, $^{2,4}A_3$, $^{2,5}A_3$, $^{0,2}A_3$, $^{1,3}A_{4\alpha}(^{2,4}A_{4\alpha})$, and $^{2,4}A_5(^{0,2}X_{3\alpha})$ (see Table 2.1). Fragments indicated within parentheses are alternative assignments with identical mass.

All fragments were deprotonated with a magnesium ion as positive charge carrier for an overall charge of one. Compared with ECD of Co-adducted LNDFH (Figure 2.3 (top)), the $Z_{3\alpha}$, $^{2,4}A_3$, $^{2,5}A_3$, and $^{0,2}A_3$ fragments are unique to ECD of Mg-adducted LNDFH. Among these unique fragments, $^{2,4}A_3$, $^{2,5}A_3$, and $^{0,2}A_3$ identify the branching site at the GlcNAc residue. ETD of Mg-adducted LNDFH generated four glycosidic cleavages, including $Z_{3\alpha}$, $Y_{3\alpha}$, C_4, and $Y_{3\beta}$ (Y_4), and two cross-ring cleavages: $^{0,3}X_2$ ($^{1,4}X_{3\alpha}$) and $^{2,4}A_5$ ($^{0,2}X_{3\alpha}$). Similar to ECD, unique fragments ($Z_{3\alpha}$) were observed compared with ETD of Co-adducted LNDFH (Fig. 2.3 (bottom)).

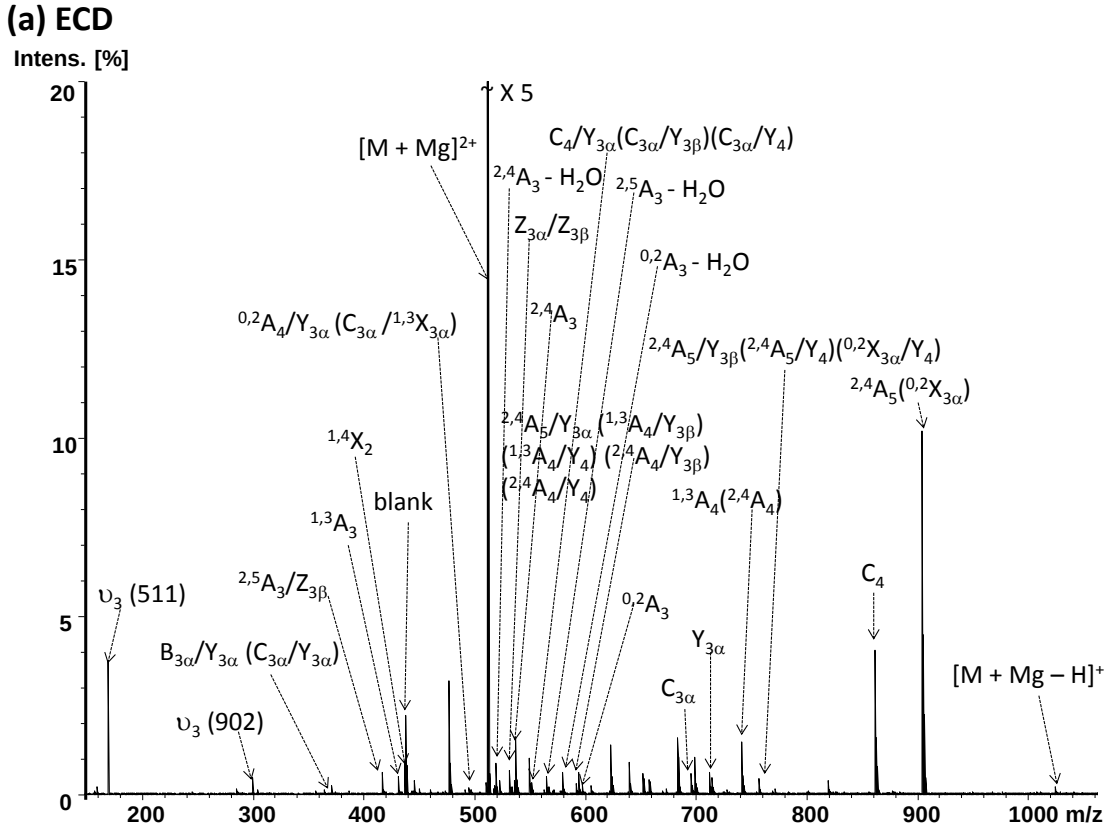

(b) ETD

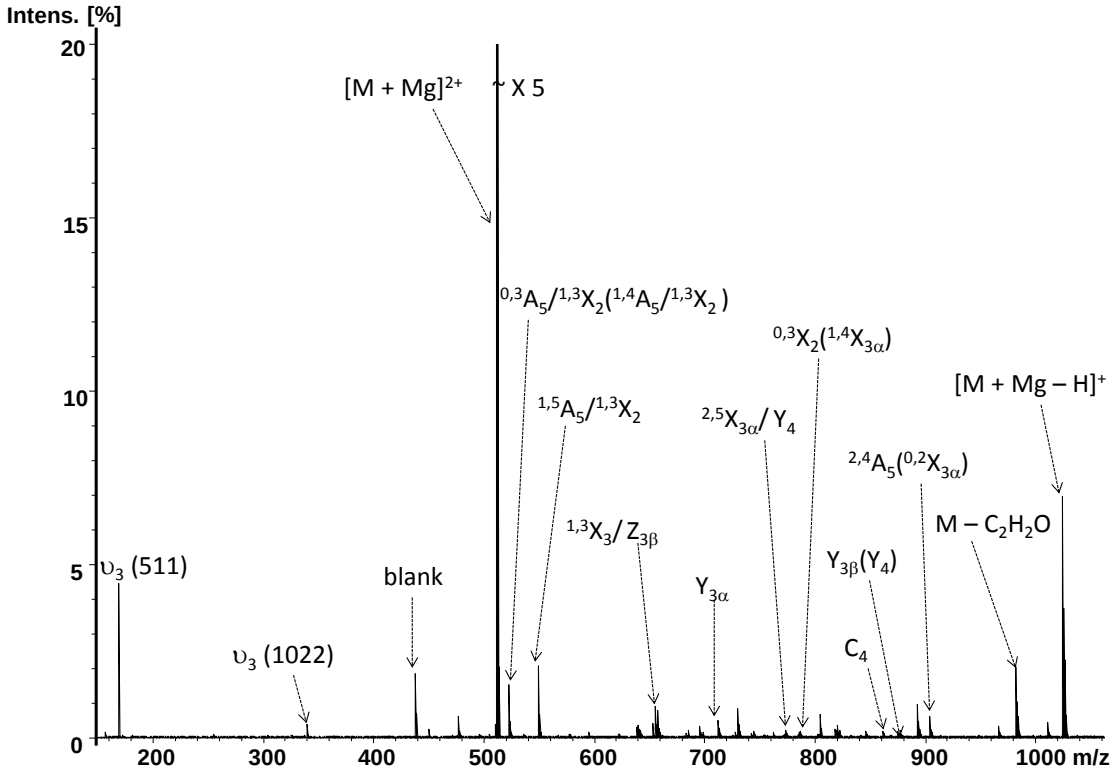
Intens. [%]
20
15
10
5
0
200
300
400
500
600
700
800
900
1000 m/z
[M + Mg]2+
~ X 5
0,3A5/1,3X2(1,4A5/1,3X2)
0,3X2(1,4X3α)
[M + Mg – H]+
1,5A5/1,3X2
2,5X3α/ Y4
2,4A5(0,2X3α)
M – C2H2O
1,3X3/ Z3β
Y3β(Y4)
υ3 (511)
blank
Y3α
υ3 (1022)
C4

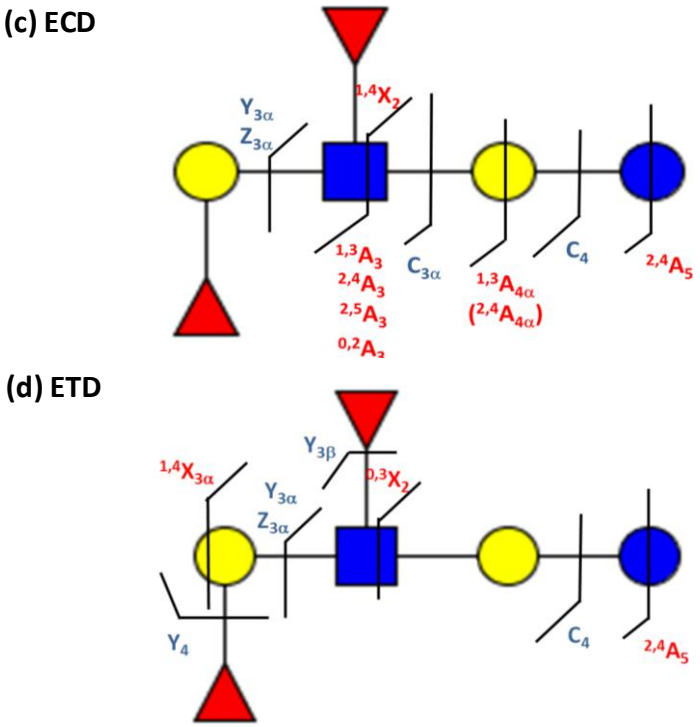

Figure 2.2 FT-ICR MS/MS of Mg-adducted LNDFH. (a) ECD (64 scans, 200 ms electron irradiation with a bias voltage of – 1.0 V); (b) ETD (64 scans, 300 ms reagent accumulation time and 100 ms reaction time). Fragmentation patterns from ECD (c) and ETD (d).

Table 2.1 Summary of product ions observed for Mg-adducted LNDFH following positive-ion mode ECD and ETD. Fragments in bold are those unique to either ECD or ETD of $[LNDFH + Mg]^{2+}$. Underlined fragments are radical ions containing one additional, or one less, hydrogen atom than the corresponding even-electron fragment.

$[LNDFH + Mg]^{2+}$			
ECD		**ETD**	
Glycosidic (4)	**Cross-ring (7)**	**Glycosidic (4)**	**Cross-ring (2)**
$Z_{3\alpha}$ **$C_{3\alpha}$** $Y_{3\alpha}$ C_4	**$^{1,3}A_3$** **$^{1,4}X_2$** **$^{2,4}A_3$** **$^{2,5}A_3$** **$^{0,2}A_3$** **$^{1,3}A_{4\alpha}$ $(^{2,4}A_{4\alpha})$** $^{2,4}A_5$ $(^{0,2}X_{3\alpha})$	$Z_{3\alpha}$ $Y_{3\alpha}$ C_4 **$Y_{3\beta}$ (Y_4)**	**$^{0,3}X_2$ $(^{1,4}X_{3\alpha})$** $^{2,4}A_5$ $(^{0,2}X_{3\alpha})$

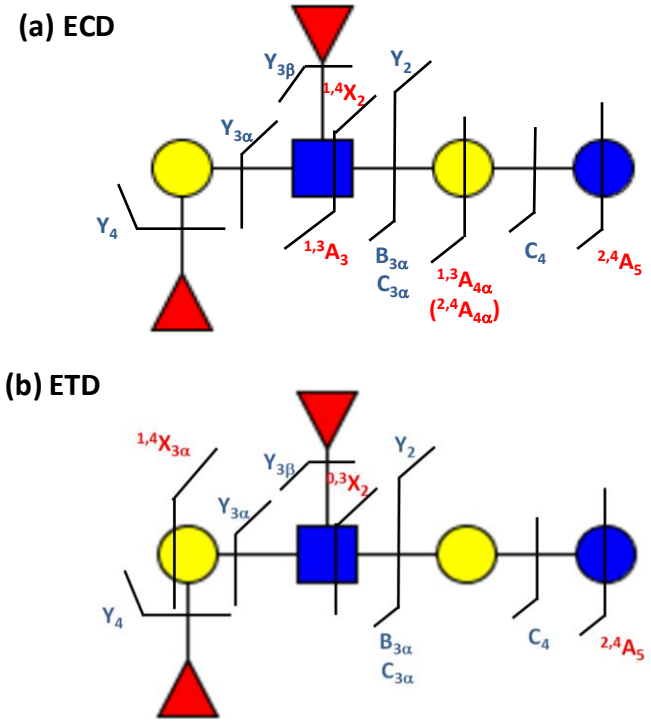

Figure 2.3 FT-ICR MS/MS fragmentation patterns for Co-adducted LNDFH. (a) ECD (50 scans, 200 ms electron irradiation with a bias voltage of – 1.0 V); (b) ETD (50 scans, 500 ms reagent accumulation time and 500 ms reaction time).

LNDFH was also mixed with $CaCl_2$ and found to form Ca adducts more readily than Mg or Co adducts, generating highly abundant $[LNDFH + Ca]^{2+}$ doubly charged cations in positive ion mode. ECD of $[LNDFH + Ca]^{2+}$ showed extensive fragmentation (Figure 2.4a), including three glycosidic cleavages and seven cross-ring cleavages. Similar to Mg- and Co-adducted LNDFH, all fragments were singly charged with one Ca(II) adduct and one deprotonated site. The $^{2,4}A_3$ and $^{0,2}A_3$ cross-ring fragments provide branching information for the fucose residue.

ETD (Figure 2.4b) of the same Ca-adducted precursor ion only generated one glycosidic cleavage (corresponding to fucose loss and thus not providing additional structural information compared with CAD) and one cross-ring cleavage. This level of

fragmentation is much lower than that in ETD of $[LNDFH + Mg]^{2+}$ and $[LNDFH + Co]^{2+}$.

Metal-electron recombination energy has previously been suggested to have a significant effect on ECD outcome.[49, 54-57] Mg has a higher IE2 (15.04 eV) than Ca (11.87 eV) and, thus, more energy may be released upon electron capture, contributing to further excitation and fragmentation. However, Co has an even higher IE2 (17.08 eV) than Mg, but Co adduction resulted in inferior ECD/ETD, indicating a more complex mechanism. Gas-phase structures of precursor ions have also been previously proposed to greatly influence ECD outcome[58] and the metal coordination sphere/binding site has been recently proposed to affect ETD outcome[59]. Williams and co-workers successfully separated multiple gas-phase conformers by a combination of high-filed asymmetric waveform ion mobility spectrometry (FAIMS) and FT-ICR MS.[60, 61] Extensive work by Leary et al.[62] and Lebrilla et al.[63] has shown that metal adduction does change gas-phase structures of oligosaccharides.

(a) ECD

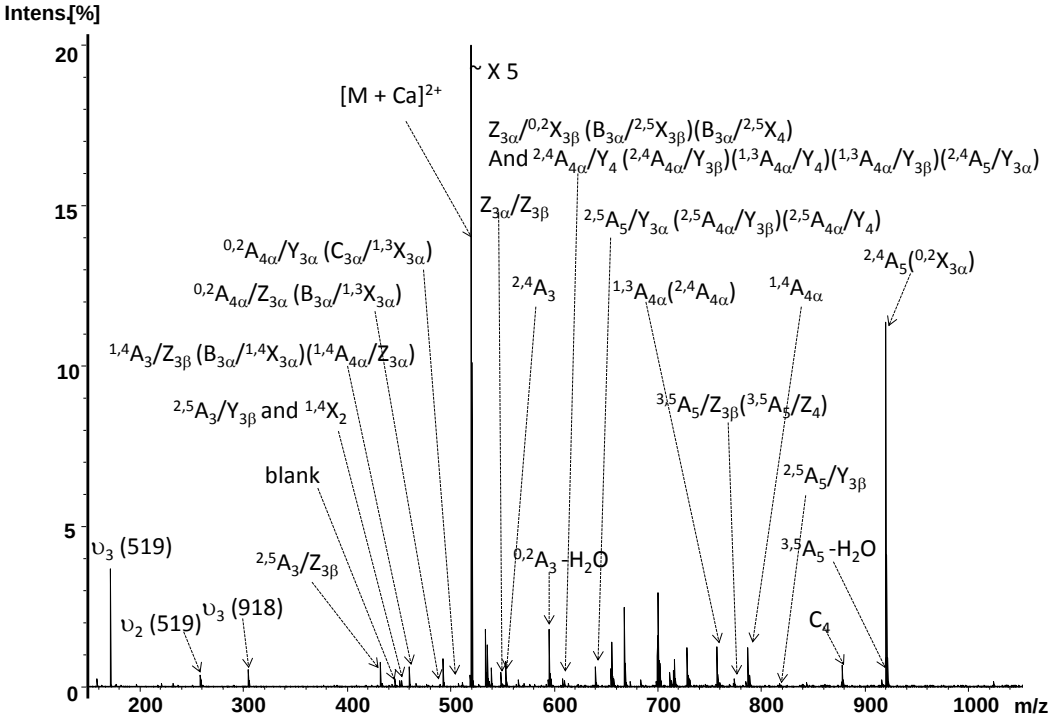
Intens.[%]
20
15
10
5
0
~ X 5
[M + Ca]2+
Z3α/0,2X3β (B3α/2,5X3β)(B3α/2,5X4)
And 2,4A4α/Y4 (2,4A4α/Y3β)(1,3A4α/Y4)(1,3A4α/Y3β)(2,4A5/Y3α)
Z3α/Z3β
2,5A5/Y3α (2,5A4α/Y3β)(2,5A4α/Y4)
0,2A4α/Y3α (C3α/1,3X3α)
2,4A5(0,2X3α)
0,2A4α/Z3α (B3α/1,3X3α)
2,4A3
1,3A4α(2,4A4α)
1,4A4α
1,4A3/Z3β (B3α/1,4X3α)(1,4A4α/Z3α)
3,5A5/Z3β(3,5A5/Z4)
2,5A3/Y3β and 1,4X2
blank
2,5A5/Y3β
υ3 (519)
2,5A3/Z3β
0,2A3 -H2O
3,5A5 -H2O
υ2 (519)
υ3 (918)
C4
200
300
400
500
600
700
800
900
1000
m/z

(b) ETD

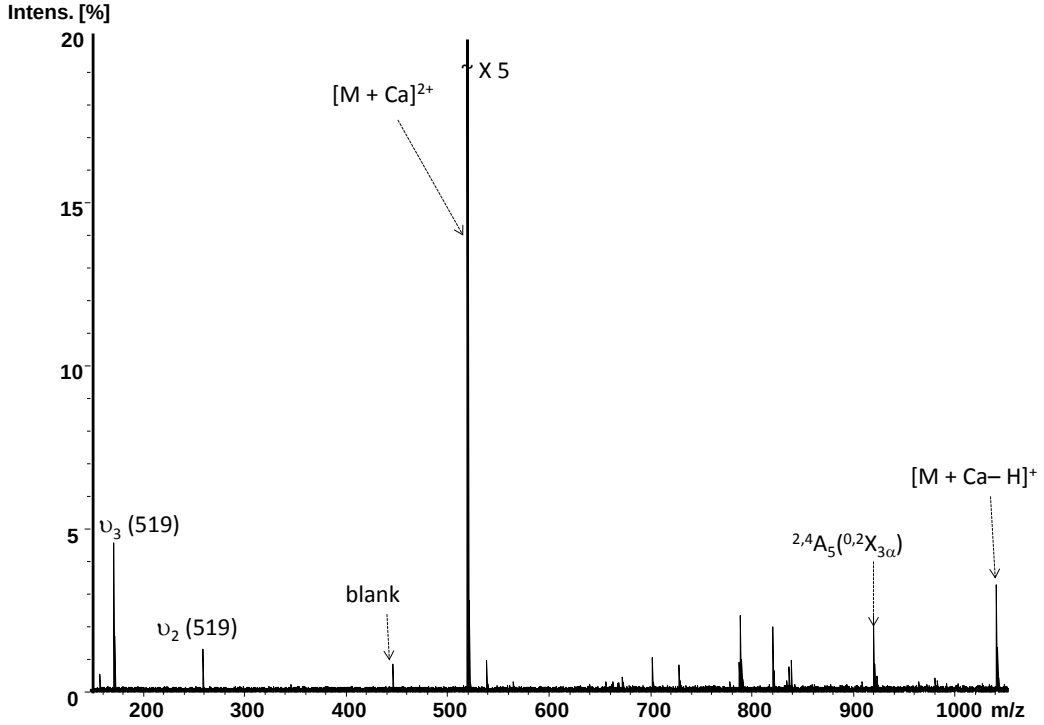
Intens. [%]
20
15
10
5
0
~ X 5
[M + Ca]2+
[M + Ca– H]+
υ3 (519)
2,4A5(0,2X3α)
blank
υ2 (519)
200
300
400
500
600
700
800
900
1000
m/z

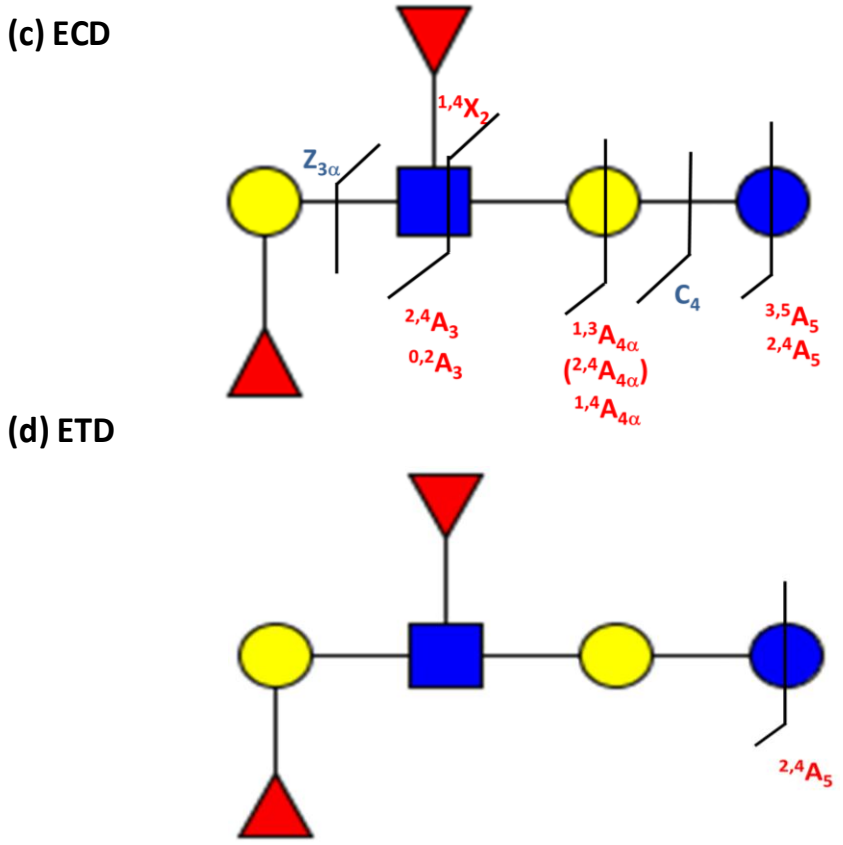

Figure 2.4 FT-ICR MS/MS of Ca-adducted LNDFH. (a) ECD (64 scans, 180 ms electron irradiation with a bias voltage of – 1.0 V); (b) ETD (64 scans, 300 ms reagent accumulation time and 100 ms reaction time). Fragmentation patterns from ECD (c) and ETD (d).

Comparing ECD with ETD for the same divalent metal adduct, charge reduced radical species were not observed in either technique. Instead, proton stripped species were generated following electron capture or transfer. Overall, ECD showed higher fragmentation efficiency than ETD of the same precursor ions. For example, for Mg adduction, ECD showed 16% fragmentation efficiency, while the fragmentation efficiency of ETD was 1.7%. This distinct difference may be explained by the very different pressures during ECD and ETD: ECD occurs in the high vacuum inside the ICR cell ($<10^{-9}$ mbar) and, thus, no effective cooling mechanism is in operation for the

precursor ions. By contrast, the pressure in the collision cell where ETD occurs is around 10^{-3} mbar, resulting in effective cooling of precursor ions and thus a higher energy requirement for dissociation.

2.3.2 ECD and ETD of Divalent Metal-Adducted Underivatized NA2

NA2 is a biantennary oligosaccharide found on glycoproteins, including asialo serum transferrin and fibrin. It is the simplest *N*-glycan in nature.

Mg-adducted NA2 underwent extensive fragmentation in ECD and ETD. Mg adduction (Figure 2.5) resulted in superior fragmentation behavior compared with Co (Figure 2.6) and Ca (Figure 2.7) adduction, including the unique fragments $\underline{^{3,5}X_{4\alpha}}$, $Z_{4\alpha}$, $^{1,5}X_{3\alpha}$, $\underline{^{3,5}X_2}$, $^{2,5}A_4$, $(\underline{^{1,5}A_4 - H_2O})$, $\underline{^{1,5}A_4}$, $^{0,4}X_1$, $(^{1,5}A_5 - H_2O)$, $(^{0,3}A_5 - H_2O)$, $^{0,3}A_5$, and $^{0,3}A_6$ (underlined fragments are radical ions containing one additional, or one less, hydrogen atom than the corresponding even-electron fragment). Such hydrogen transfer has been previously observed in ETD of Mg-adducted permethylated glycans.[36] The additional A- and X-type cross-ring cleavages observed for the Mg-adducted glycan are highly valuable for identification of linkage and branching. The advantage of Mg adduction appears even higher for NA2 compared with LNDFH. For example, ETD of Co-adducted NA2 only generated one glycosidic cleavage, $Y_{4\alpha}$, while ETD of Mg-adducted NA2 generated a variety of fragments, including three glycosidic cleavages and six cross-ring cleavages.

ECD and ETD of the same precursor ions, Mg-, or Co-, or Ca-adducted NA2, demonstrated distinctive fragmentation behavior. For example, ECD of Mg-adducted NA2 generated six glycosidic fragments and 13 cross-ring cleavages, whereas ETD of the same precursor ions generated three glycosidic cleavages and six cross-ring cleavages.

Three glycosidic cleavages, $B_{2\alpha}(H^+)$, B_5, and C_5, and nine cross-ring cleavages, $^{1,5}X_{3\alpha}$, $^{2,5}A_4$, ($^{1,5}A_4 - H_2O$), $^{1,5}A_4$, ($^{1,5}A_5 - H_2O$), ($^{0,3}A_5 - H_2O$), $^{0,3}A_5$, $^{2,4}A_6$, and $^{0,2}A_6$ were only observed in ECD.

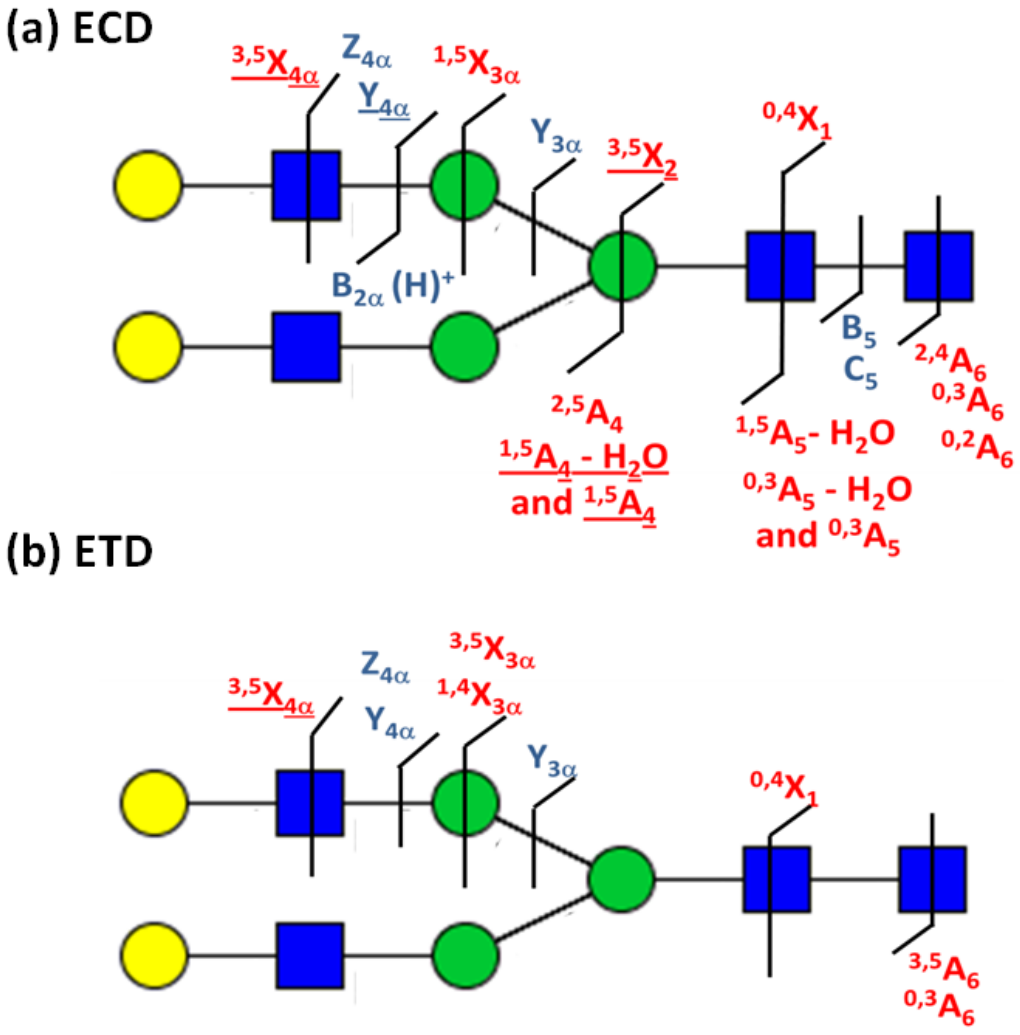

Figure 2.5 FT-ICR MS/MS fragmentation patterns of Mg-adducted NA2. (a) ECD (64 scans, 180 ms electron irradiation with a bias voltage of – 1.0 V); (b) ETD (64 scans, 500 ms reagent accumulation time and 100 ms reaction time). Underlined fragments are radical ions containing one additional, or one less, hydrogen atom than the corresponding even-electron fragment.

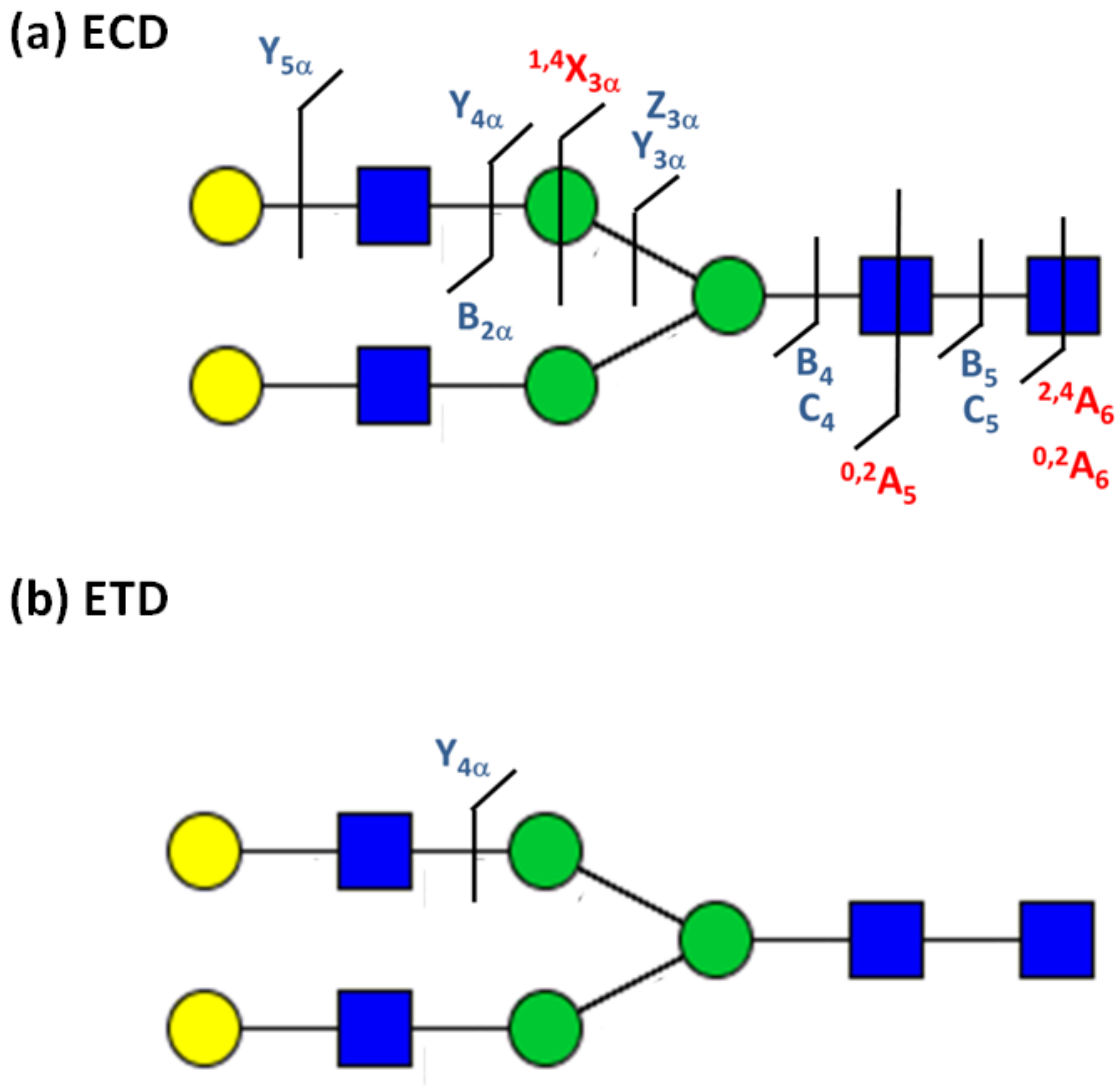

Figure 2.6 FT-ICR MS/MS fragmentation patterns of Co-adducted NA2. (a) ECD (80 scans, 300 ms electron irradiation with a bias voltage of – 1.0 V); (b) ETD (80 scans, 500 ms reagent accumulation time and 100 ms reaction time).

Similar to LNDFH, Ca formed NA2-metal complexes more readily than either Co or Mg. However, the five cross-ring cleavages generated by ECD of Ca-adducted NA2 did not occur at the critical GlcNAc branching site and ETD of the same species only generated one glycosidic cleavage (C_5) and one cross-ring cleavage ($^{3,5}A_6$), although this cross-ring fragment was not observed in ECD of the same precursor ions thus providing complementary structural information. Overall, Ca adduction produced less fragments

than the other metals in both ECD and ETD. The more pronounced difference between ECD and ETD (with particularly poor ETD performance for the calcium adduct) observed for NA2 compared with LNDFH may be due to the larger size of this particular oligosaccharide, allowing more interactions with the metal ions and thus requiring more energy for dissociation.

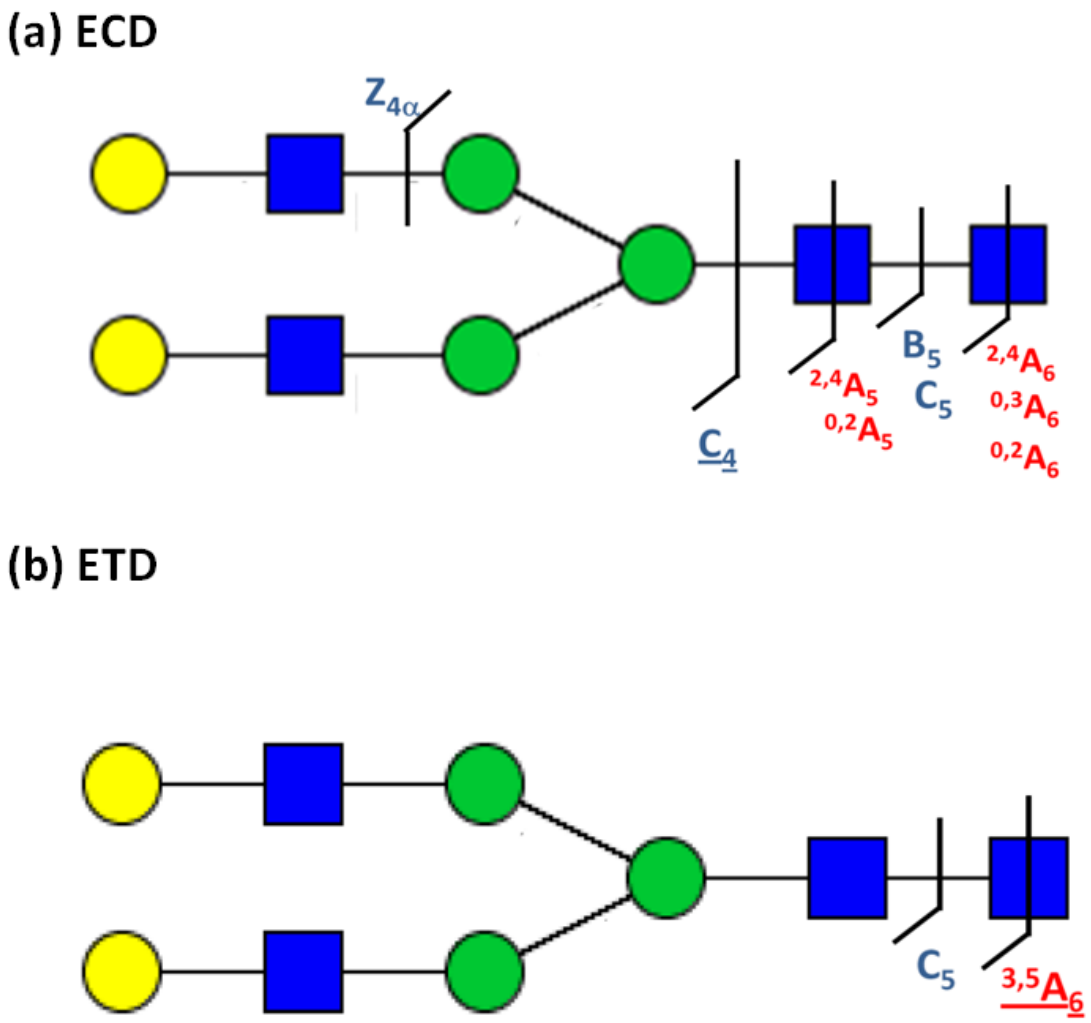

Figure 2.7 FT-ICR MS/MS fragmentation patterns of Ca-adducted NA2. (a) ECD (64 scans, 300 ms electron irradiation with a bias voltage of – 0.8 V); (b) ETD (64 scans, 500 ms reagent accumulation time and 100 ms reaction time). Underlined fragments are radical ions containing one additional, or one less, hydrogen atom than the corresponding even-electron fragment.

2.3.3 Isomer Differentiation by Divalent Metal-Assisted ECD/ETD: The Case of LSTa, LSTb, and LSTc

Isomer differentiation is one of the biggest challenges in mass spectrometry-based structural characterization of glycans. LSTa, LSTb, and LSTc are three common oligosaccharides from human milk, all composed of five monosaccharides (see Figure 2.8). LSTb is a branched glycan with linkages at the 3 and 6 positions on the GlcNAc residue. For this glycan, the cross-ring cleavages A_2 and X_2 would provide valuable structural information differentiating it from the linear isomers LSTa and LSTc. It is more challenging to differentiate LSTa and LSTc due to their identical composition and sequence. The only differences between these two glycans are the linkage between the sialic acid and the Gal residue, and the linkage between the Gal and the GlcNAc (see Figure 2.8). To differentiate LSTa and LSTc, the cross-ring cleavages A_2, A_3, X_3, and X_2 are desired.

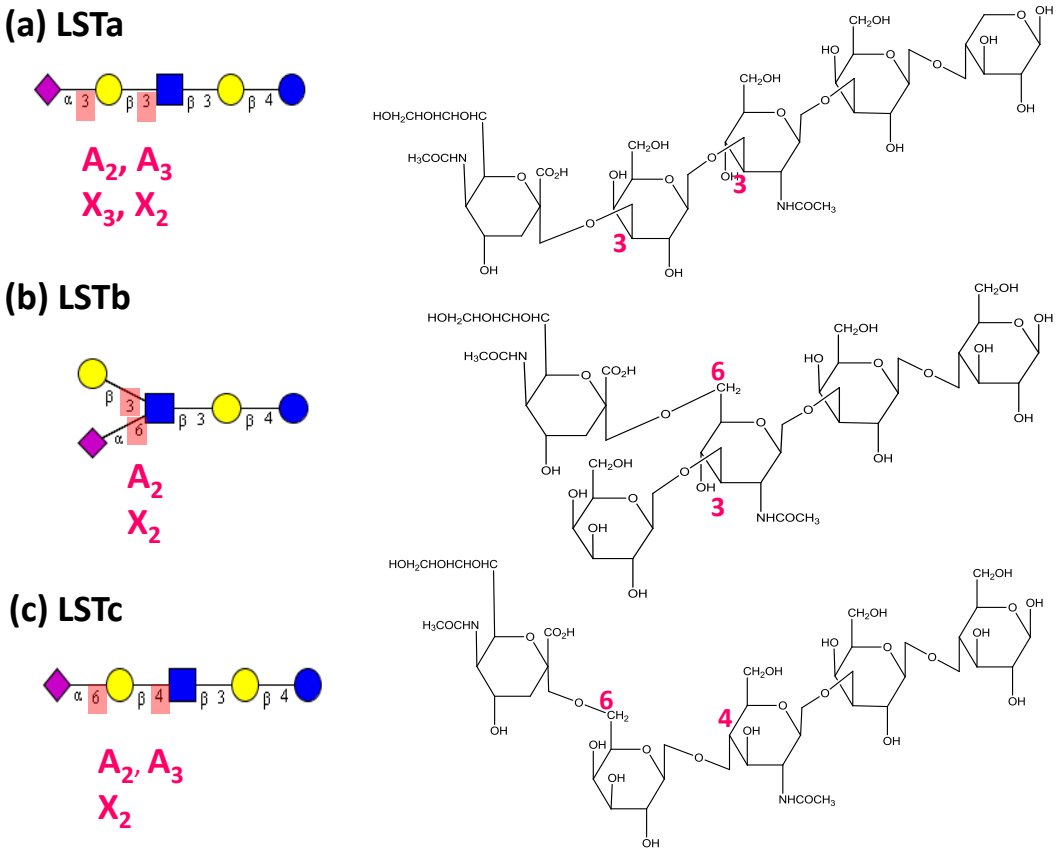

Figure 2.8 Structures of the isomers LSTa, LSTb, and LSTc. (a) LSTa; (b) LSTb; (c) LSTc. The specific differences in branching or linkage are highlighted in pink. Desired cross-ring cleavages are listed in pink on the left.

The data presented above on LNDFH and NA2 as well as previous literature[34, 49] have shown that ECD and ETD of divalent metal-adducted underivatized glycans generate extensive cross-ring cleavages. Therefore, divalent metal-assisted ECD and ETD were examined for differentiation of LSTa-c. For all three glycans, Co, Mg, and Ca were used to generate multiply charged glycan-metal complexes of the form [glycan + metal(II)]$^{2+}$.

For divalent metal-adducted underivatized LSTa both ECD and ETD generated critical cross-ring cleavages that can be used for isomer differentiation. These critical cleavages, $^{1,5}A_2$, ($^{2,4}A_3$ – H_2O), $^{2,4}A_3$, and $^{0,4}X_2$ for the Mg adducted species, ($^{0,4}X_2$ –

H_2O), $^{0,4}X_2$, $^{1,5}A_2$, and $\underline{^{2,4}A_3}$ for the Co-adducted species, and ($^{0,4}X_2 - H_2O$), $^{0,4}X_2$, and $^{1,5}A_2$ for the Ca-adducted species, are highlighted in pink in Figure 2.9.

(a) ECD of [LSTa + Co]$^{2+}$

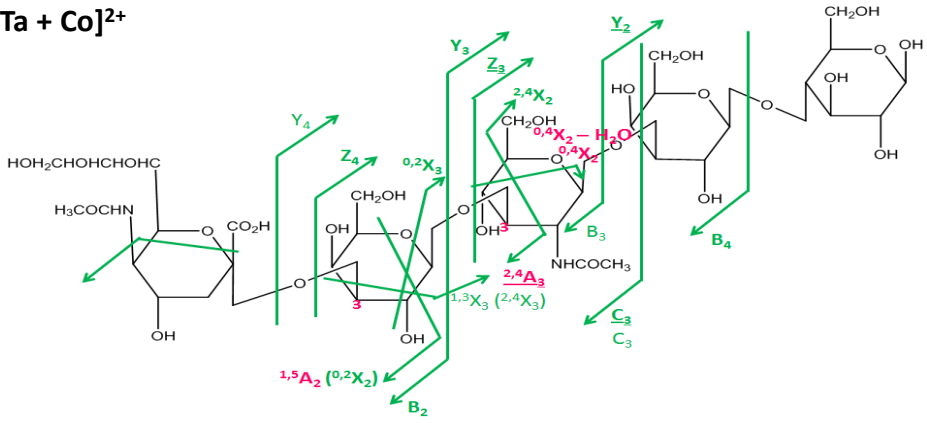

(b) ETD of [LSTa + Co]$^{2+}$

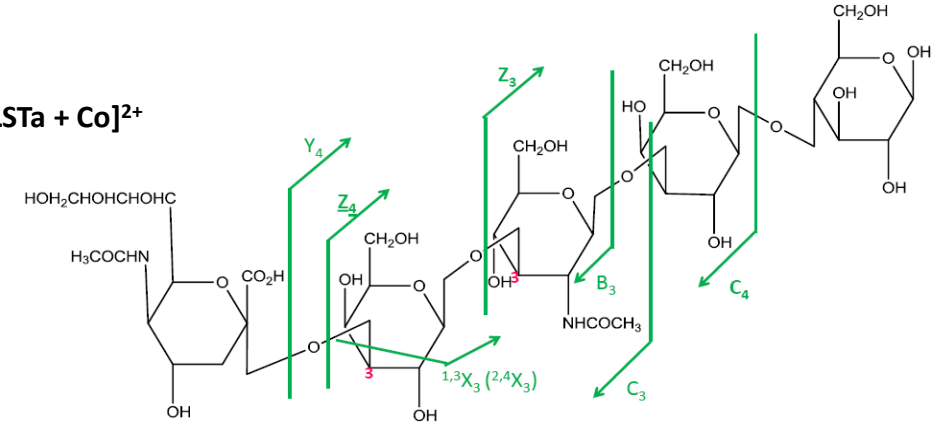

(c) ECD of [LSTa + Mg]$^{2+}$

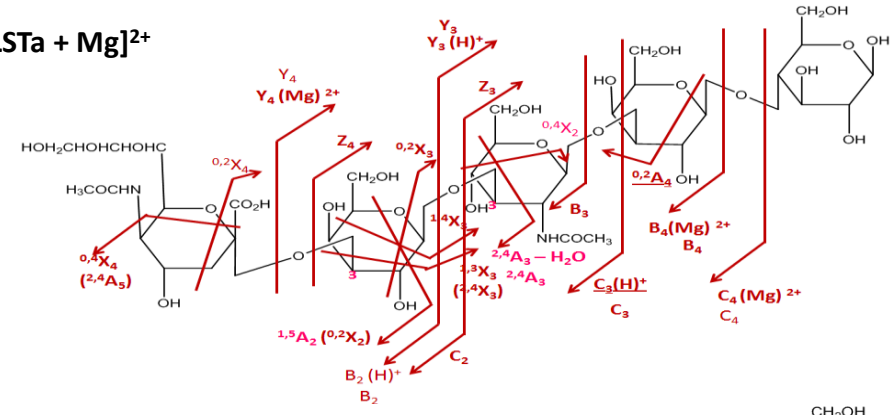

(d) ETD of [LSTa + Mg]$^{2+}$

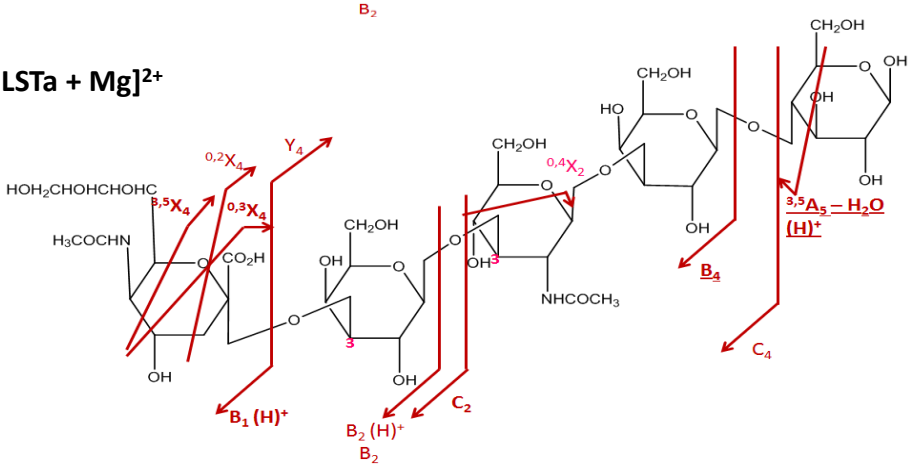

(e) ECD of [LSTa + Ca]$^{2+}$

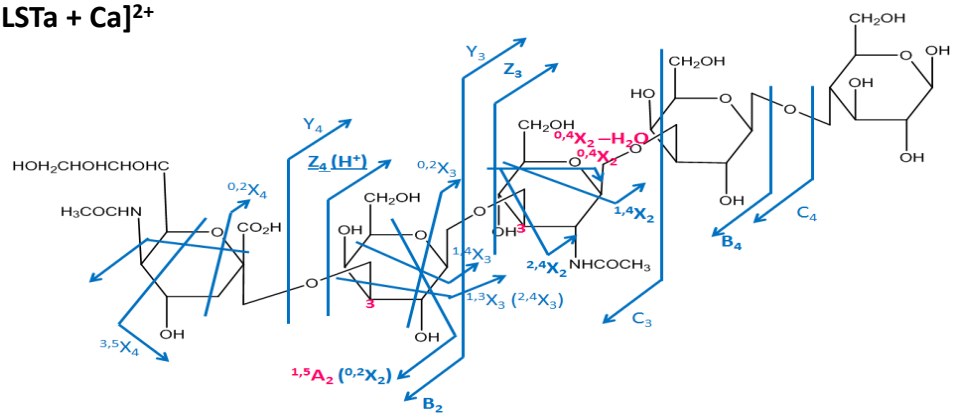

(f) ETD of [LSTa + Ca]$^{2+}$

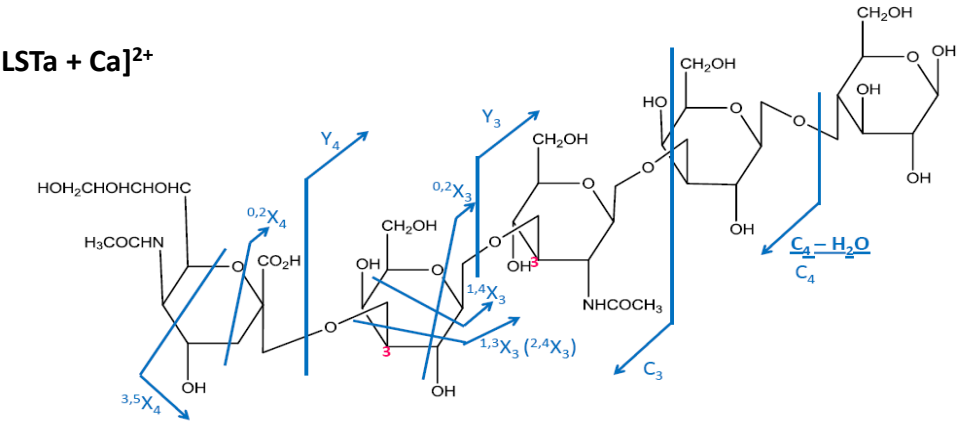

Figure 2.9 Fragmentation pattern summary for divalent metal-assisted ECD and ETD of LSTa. (a) ECD of [LSTa + Co]$^{2+}$; (b) ETD of [LSTa + Co]$^{2+}$; (c) ECD of [LSTa + Mg]$^{2+}$; (d) ETD of [LSTa + Mg]$^{2+}$; (e) ECD of [LSTa + Ca]$^{2+}$; (f) ETD of [LSTa + Ca]$^{2+}$.

Similar to LSTa, many valuable cross-ring cleavages were identified from ECD and ETD of divalent metal-adducted LSTb. In particular, Mg adduction generated $^{0,2}X_{3\beta}$, $^{2,4}X_2$, $^{3,5}X_2$, $^{0,3}X_2$, $^{0,4}X_2$, ($^{1,4}A_2 - H_2O$), $^{1,4}A_2$, $^{0,3}A_2$, $^{3,5}A_2$, ($^{1,4}X_2 - H_2O\ (H)^+$), $^{2,5}X_{3\beta}$, and ($^{0,2}X_{3\beta} - H_2O\ (H)^+$). Co adduction generated $^{3,5}X_2$, $^{0,4}X_2$, $^{3,5}A_2$, $\underline{^{3,5}A_2}$, and $^{1,4}A_2$, whereas Ca adduction only resulted in detection of $^{0,4}X_2$, $^{0,3}X_2$, and ($^{1,4}X_2 - H_2O$) in ECD and no structurally differentiating cleavages in ETD.

(a) ECD of [LSTb + Co]$^{2+}$

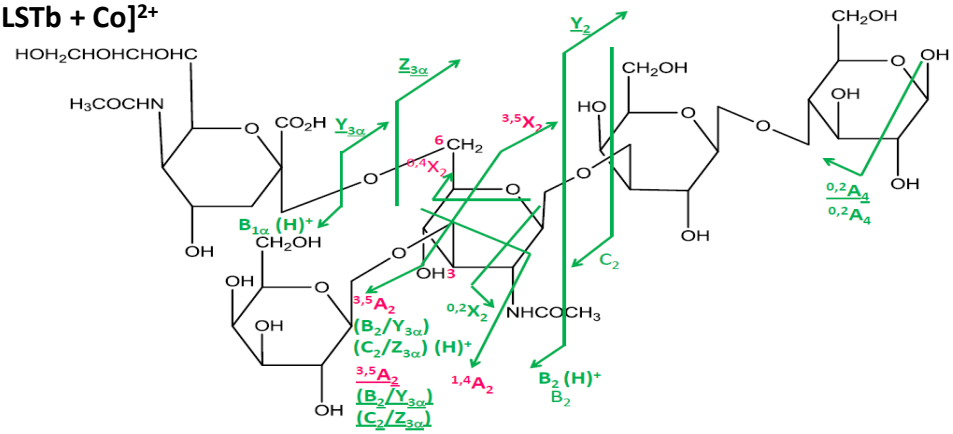

(b) ETD of [LSTb + Co]$^{2+}$

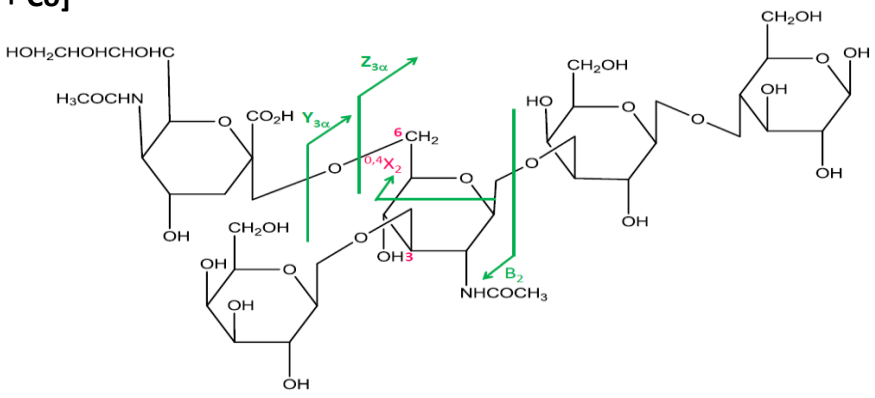

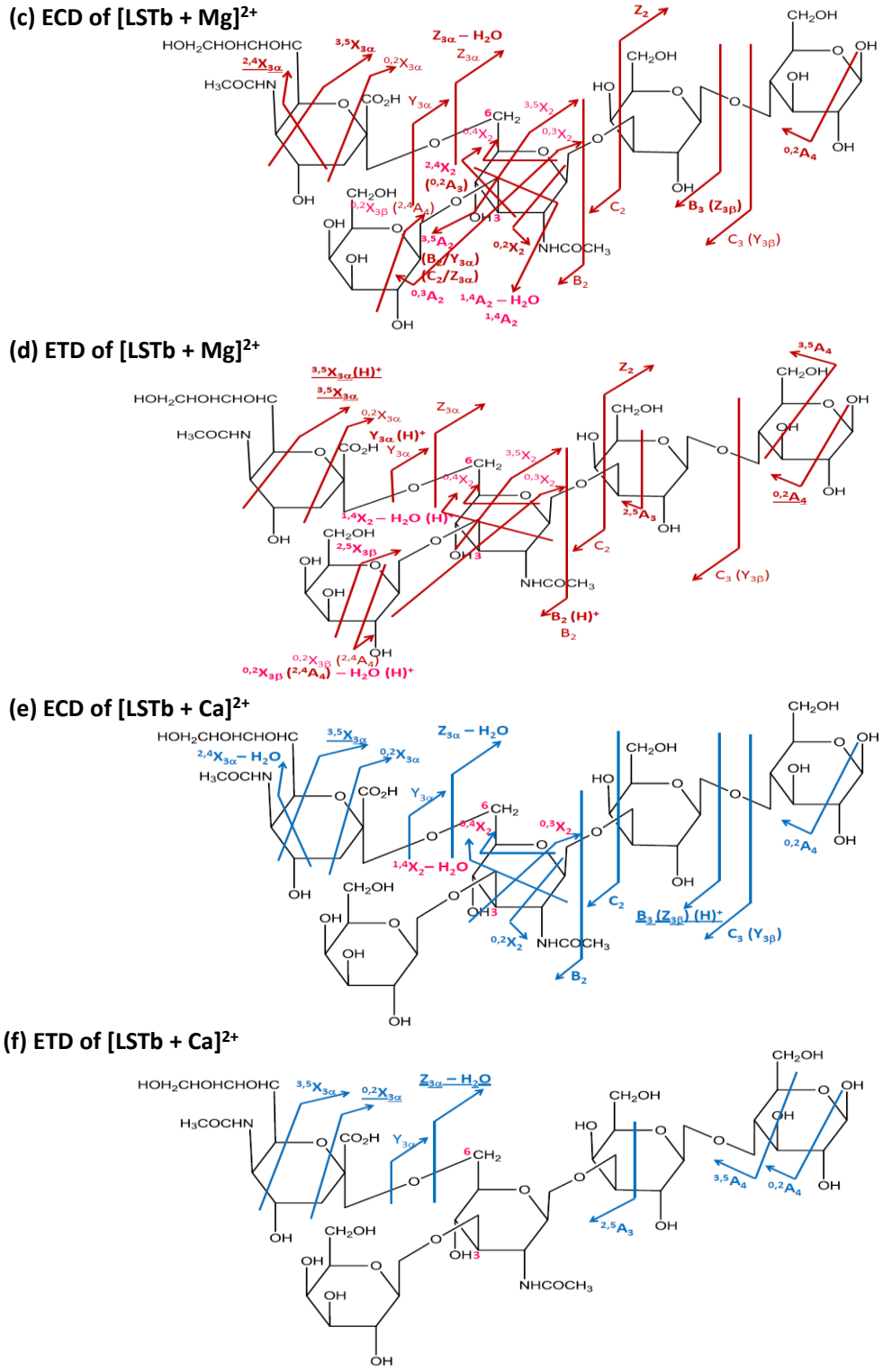

Figure 2.10 Fragmentation pattern summary for divalent metal-assisted ECD and ETD of LSTb. (a) ECD of $[LSTb + Co]^{2+}$; (b) ETD of $[LSTb + Co]^{2+}$; (c) ECD of $[LSTb + Mg]^{2+}$; (d) ETD of $[LSTb + Mg]^{2+}$; (e) ECD of $[LSTb + Ca]^{2+}$; (f) ETD of $[LSTb + Ca]^{2+}$.

Divalent metal-adducted LSTc also demonstrated efficient fragmentation in ECD and ETD (see Figure 2.11). Mg adduction yielded $\underline{^{2,4}A_3 - H_2O}$, $^{3,5}A_2$, $^{0,2}A_2$, $^{2,4}A_3$, ($^{2,5}A_3 - H_2O$), $\underline{^{1,3}X_2}$, $^{0,3}A_3$, $^{0,4}X_2$, and $^{0,2}A_3$ in both ECD and ETD. Co adduction generated $\underline{^{3,5}A_2}$, $^{0,2}A_3$, $^{0,2}A_2$, $^{0,4}X_2$, $^{2,4}A_3$, ($\underline{^{2,4}A_3 - H_2O}$), and $^{1,4}A_3$ in ECD, and ($^{1,3}X_2 - H_2O$), $^{3,5}A_2(H)^+$, and $^{3,5}A_2$ in ETD, whereas Ca adduction generated $^{3,5}A_3$, $\underline{^{0,2}A_3}$, $^{0,2}A_3$, $\underline{^{1,3}X_2}$, $^{1,5}A_3$, (^{0,3}A3 – H_2O), $^{0,3}A_3$, $^{0,4}X_2$, $^{2,4}A_3$, and $^{2,5}A_3$ in ECD but no such critical cross-ring cleavages in ETD.

(a) ECD of [LSTc + Co]$^{2+}$

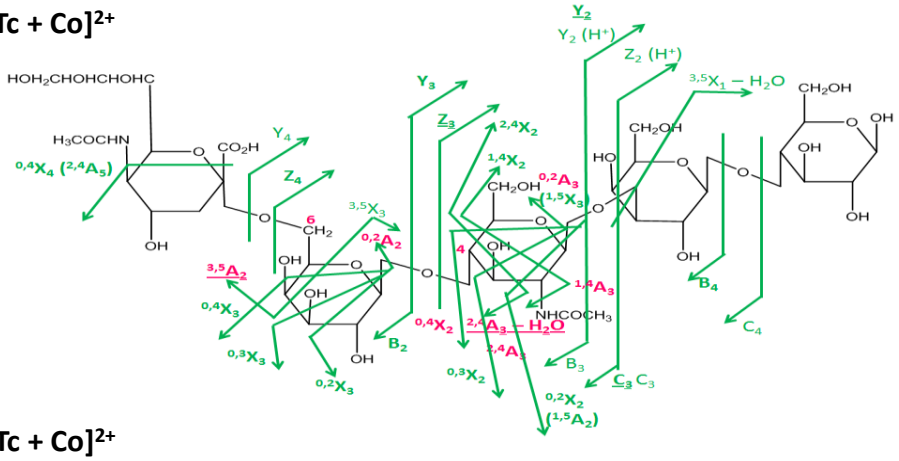

(b) ETD of [LSTc + Co]$^{2+}$

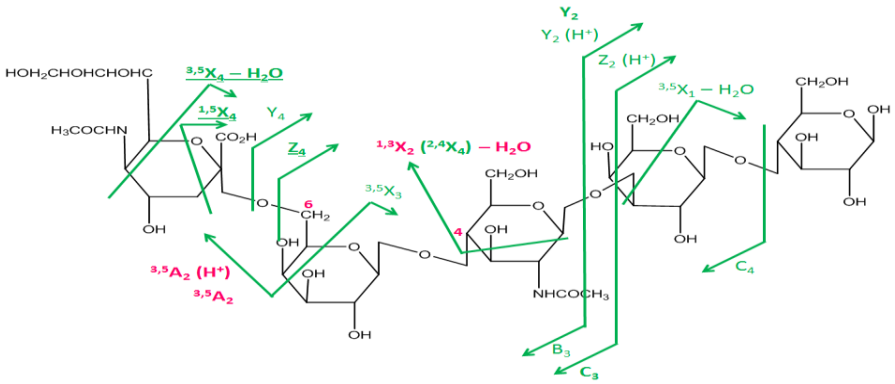

(c) ECD of [LSTc + Mg]$^{2+}$

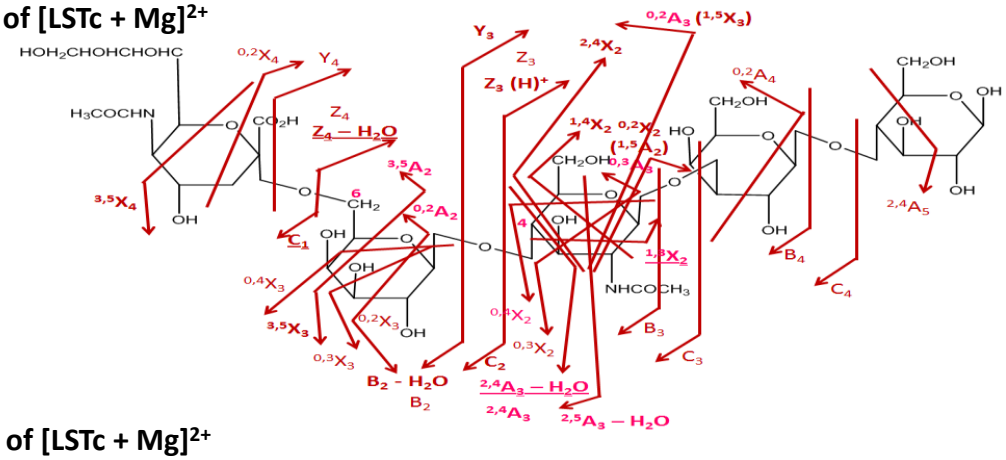

(d) ETD of [LSTc + Mg]$^{2+}$

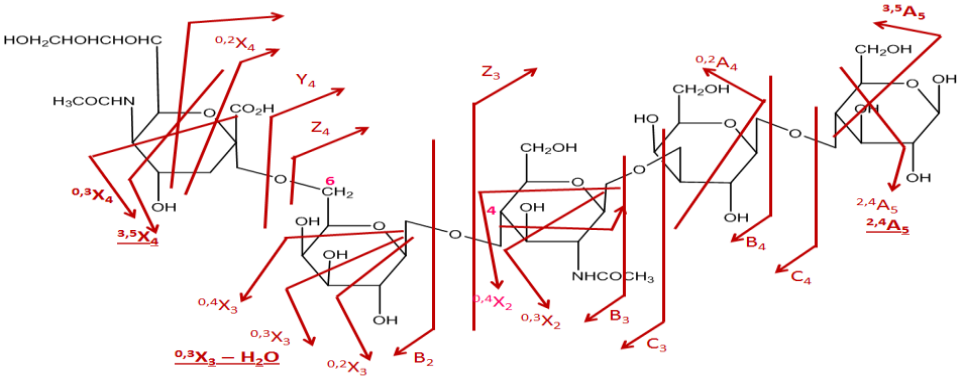

(e) ECD of [LSTc + Ca]$^{2+}$

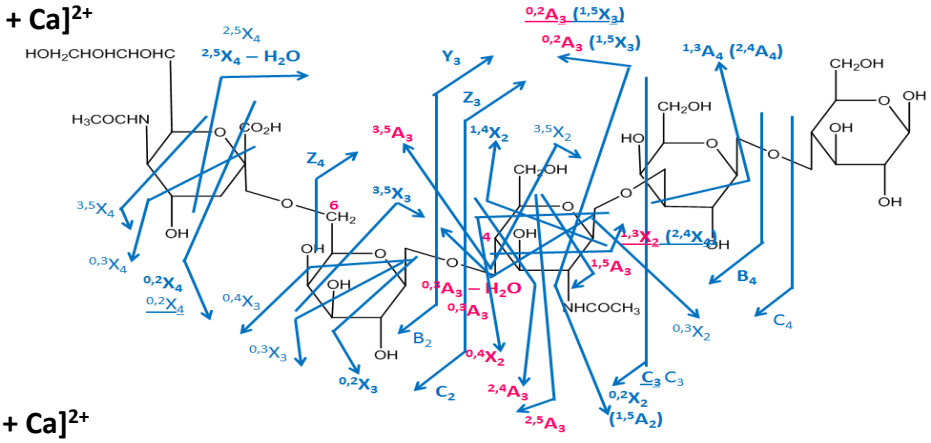

(f) ETD of [LSTc + Ca]$^{2+}$

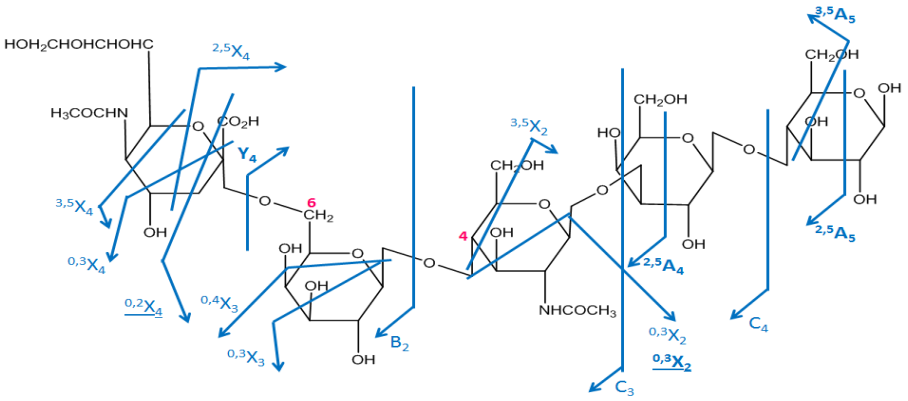

Figure 2.11 Fragmentation pattern summary for divalent metal-assisted ECD and ETD of LSTc. (a) ECD of [LSTc + Co]$^{2+}$; (b) ETD of [LSTc + Co]$^{2+}$; (c) ECD of [LSTc + Mg]$^{2+}$; (d) ETD of [LSTc + Mg]$^{2+}$; (e) ECD of [LSTc + Ca]$^{2+}$; (f) ETD of [LSTc + Ca]$^{2+}$.

All three divalent metals (Co, Mg, Ca) could be used for isomer differentiation although Mg adduction produced the most informative cleavages. In general, ECD generated more critical cross-ring cleavages than ETD for differentiation of LSTa, LSTb, and LSTc.

2.4 Conclusions

In this chapter, three divalent metal ions were examined as charge carriers in ECD and ETD. ECD and ETD fragmentation patterns of divalent metals Co (II)-, Mg (II)-, Ca (II)-adducted glycans were directly compared and summarized in Table 1.2. For both two

glycans and three divalent metals we studied in this chapter, ECD always generated more fragments than ETD and generally resulted in higher fragmentation efficiency. Such distinction is likely attributed to the different pressures during ECD ($<10^{-9}$ mbar) and ETD (around 10^{-3} mbar), which resulted in a more effective cooling of precursor ions and a higher energy requirement for dissociation in ETD. Ca formed metal-glycan complexes most readily, while Mg complexes generated superior ECD and ETD fragmentation. In particular, Mg adduction showed superior application towards isomer differentiation compared with Co or Ca by generating the highest variety of informative cross-ring cleavages. The mechanism of divalent metal-assisted ECD/ETD is likely related to both metal ionization energy and the gas-phase structures of metal-glycan complexes. Metals with a higher IE2 may contribute more energy to fragmentation and thus assist in generating a higher variety of fragments and more diverse structural populations of glycan-metal complexes presumably also enable more fragmentation channels.

Table 2.2 Direct comparison of ECD and ETD of divalent Metals Co (II)-, Mg (II)-, and Ca (II)-adducted LNDFH and NA2.

Glycan	Metal	ECD	ETD
LNDFH	Co (2+)	6 glycosidic, 4 cross-ring	7 glycosidic, 2 cross-ring
	Mg (2+)	4 glycosidic, 7 cross-ring	4 glycosidic, 2 cross-ring
	Ca (2+)	2 glycosidic, 7 cross-ring	0 glycosidic, 1 cross-ring
NA2	Co (2+)	9 glycosidic, 4 cross-ring	0 glycosidic, 1 cross-ring
	Mg (2+)	6 glycosidic, 13 cross-ring	3 glycosidic, 6 cross-ring
	Ca (2+)	4 glycosidic, 5 cross-ring	1 glycosidic, 1 cross-ring

2.5 Bibliography

(1) Varki, A.; Cummings, R. D.; Esko, J. D.; Freeze, H. H.; Stanley, P.; Bertozzi, C. R.; Hart, G. W.; Etzler, M. E. *Essentials of Glycobiology, 2nd edition*; Cold Spring Harbor Laboratory Press: New York, 2009.

(2) Varki, A. Glycan-Based Interactions Involving Vertebrate Sialic-Acid-Recognizing Proteins. *Nature* **2007**, *446*, 1023-1029.

(3) Chen, X.; Varki, A. Advances in the Biology and Chemistry of Sialic Acids. *ACS Chem. Biol.* **2010**, *5*, 163-176.

(4) Kiessling, L. L.; Splain, R. A. In *Annu. Rev. Biochem*; Kornberg, R. D., Raetz, C. R. H., Rothman, J. E., Thorner, J. W., Eds.; Annual Reviews: Palo Alto, 2010; Vol. 79, pp 619-653.

(5) Miyamoto, S. Clinical Applications of Glycomic Approaches for the Detection of Cancer and Other Diseases. *Curr. Opin. Mol. Ther.* **2006**, *8*, 507-513.

(6) An, H. J.; Kronewitter, S. R.; de Leoz, M. L. A.; Lebrilla, C. B. Glycomics and Disease Markers. *Curr. Opin. Chem. Biol.* **2009**, *13*, 601-607.

(7) Li, M.; Song, L. J.; Qin, X. Y. Glycan Changes: Cancer Metastasis and Anti-Cancer Vaccines. *J. Bioscience.* **2010**, *35*, 665-673.

(8) Sirois, S.; Touaibia, M.; Chou, K. C.; Roy, R. Glycosylation of HIV-1 Gp120 V3 Loop: Towards the Rational Design of a Synthetic Carbohydrate Vaccine. *Curr. Med. Chem.* **2007**, *14*, 3232-3242.

(9) del Campo, J. Glicopatology, Glycotherapeutic and Glycan Tumor Markers. *An. Real. Acad. Nac. F* **2012**, *78*, 168-191.

(10) Cipolla, L.; Araujo, A. C.; Bini, D.; Gabrielli, L.; Russo, L.; Shaikh, N. Discovery and Design of Carbohydrate-Based Therapeutics. *Expert Opin. Drug Dis.* **2010**, *5*, 721-737.

(11) Nakagawa, H. The Use of 2-Dimensional Mapping in Medical Research. *Trends Glycosci. Glyc.* **2009**, *21*, 87-94.

(12) Hua, S.; An, H. J.; Ozcan, S.; Ro, G. S.; Soares, S.; DeVere-White, R.; Lebrilla, C. B. Comprehensive Native Glycan Profiling with Isomer Separation and Quantitation for the Discovery of Cancer Biomarkers. *Analyst* **2011**, *136*, 3663-3671.

(13) Prien, J. M.; Huysentruyt, L. C.; Ashline, D. J.; Lapadula, A. J.; Seyfried, T. N.; Reinhold, V. N. Differentiating N-linked Glycan Structural Isomers in Metastatic and Nonmetastatic Tumor Cells Using Sequential Mass Spectrometry. *Glycobiology* **2008**, *18*, 353-366.

(14) Park, Y.; Lebrilla, C. B. Application of Fourier Transform Ion Cyclotron Resonance Mass Spectrometry to Oligosaccharides. *Mass Spectrom. Rev.* **2005**, *24*, 232-264.

(15) Cheng, H. N.; Neiss, T. G. Solution NMR Spectroscopy of Food Polysaccharides. *Polym. Rev.* **2012**, *52*, 81-114.

(16) Barb, A. W.; Prestegard, J. H. NMR Analysis Demonstrates Immunoglobulin G *N*-glycans Are Accessible and Dynamic. *Nat. Chem. Biol.* **2011**, *7*, 147-153.

(17) Duus, J. O.; Gotfredsen, C. H.; Bock, K. Carbohydrate Structural Determination by NMR Spectroscopy: Modern Methods and Limitations. *Chem. Rev.* **2000**, *100*, 4589-4614.

(18) Barb, A. W.; Meng, L.; Gao, Z. W.; Johnson, R. W.; Moremen, K. W.; Prestegard, J. H. NMR Characterization of Immunoglobulin G Fc Glycan Motion on Enzymatic Sialylation. *Biochemistry* **2012**, *51*, 4618-4626.

(19) Shaw, G. S.; Sun, Y.; Barber, K. R.; van Huystee, R. B. Sequence Specific Analysis of the Heterogeneous Glycan Chain From Peanut Peroxidase by H-1-NMR Spectroscopy. *Phytochemistry* **2000**, *53*, 135-144.

(20) Nagae, M.; Yamaguchi, Y. Function and 3D Structure of the *N*-Glycans on Glycoproteins. *Int. J. Mol. Sci.* **2012**, *13*, 8398-8429.

(21) Colgrave, M. L.; Snelling, H. J.; Shiell, B. J.; Feng, Y. R.; Chan, Y. P.; Bossart, K. N.; Xu, K.; Nikolov, D. B.; Broder, C. C.; Michalski, W. P. Site Occupancy and Glycan Compositional Analysis of Two Soluble Recombinant Forms of the Attachment Glycoprotein of Hendra Virus. *Glycobiology* **2012**, *22*, 572-584.

(22) Vallee, F.; Lipari, F.; Yip, P.; Sleno, B.; Herscovics, A.; Howell, P. L. Crystal Structure of A Class I Alpha 1,2-Mannosidase Involved in N-Glycan Processing and Endoplasmic Reticulum Quality Control. *EMBO J.* **2000**, *19*, 581-588.

(23) Huang, J. W.; Xu, Z.; Wang, D.; Ogata, C. M.; Palczewski, K.; Lee, X.; Young, N. M. Characterization of The Secondary Binding Sites of Maclura Pomifera Agglutinin by Glycan Array and Crystallographic Analyses. *Glycobiology* **2010**, *20*, 1643-1653.

(24) Bielik, A. M.; Zaia, J. In *Functional Glycomics: Methods and Protocols*; Li, J., Ed.; Humana Press Inc: Totowa, 2010; Vol. 600, pp 9-30.

(25) Pompach, P.; Chandler, K. B.; Lan, R.; Edwards, N.; Goldman, R. Semi-Automated Identification of N-Glycopeptides by Hydrophilic Interaction Chromatography, Nano-Reverse-Phase LC-MS/MS, and Glycan Database Search. *J. Proteome Res.* **2012**, *11*, 1728-1740.

(26) Wuhrer, M.; Koeleman, C. A. M.; Deelder, A. M. In *Glycomics: Methods and Protocols*; Packer, N. H., Karlsson, N. G., Eds.; Humana Press Inc, 999 Riverview Dr, Ste 208, Totowa, NJ 07512-1165 USA, 2009; Vol. 534, pp 79-91.

(27) Tryfona, T.; Stephens, E. In *LC-MS/MS in Proteomics: Methods and Applications*; Cutillas, P. R., Timms, J. F., Eds.; Humana Press Inc: Totowa, 2010; Vol. 658, pp 137-151.

(28) Peltoniemi, H.; Joenvaara, S.; Renkonen, R. De Novo Glycan Structure Search with the CID MS/MS Spectra of Native *N*-Glycopeptides. *Glycobiology* **2009**, *19*, 707-714.

(29) Domon, B.; Costello, C. E. A Systematic Nomenclature for Carbohydrate Fragmentations in FAB-MS/MS Spectra of Glycoconjugates. *Glycoconjugate J.* **1988**, *5*, 397-409.

(30) Zaia, J. Mass Spectrometry of Oligosaccharides. *Mass Spectrom. Rev.* **2004**, *23*, 161-227.

(31) Zhou, W.; Hakansson, K. Structural Characterization of Carbohydrates by Fourier Transform Tandem Mass Spectrometry. *Curr. Proteomics* **2011**, *8*, 297-308.

(32) Li, B.; An, H. J.; Hedrick, J. L.; Lebrilla, C. B. In *Glycomics: Methods and Protocols*; Packer, N. H., Karlsson, N. G., Eds.; Humana Press Inc, 999 Riverview Dr, Ste 208, Totowa, NJ 07512-1165 USA, 2009; Vol. 534, pp 133-145.

(33) Harvey, D. J. Matrix-Assisted Laser Desorption/Ionization Mass Spectrometry of Carbohydrates. *Mass Spectrom. Rev.* **1999**, *18*, 349-450.

(34) Adamson, J. T.; Håkansson, K. Electron Capture Dissociation of Oligosaccharides Ionized with Alkali, Alkaline Earth, and Transition Metals. *Anal. Chem.* **2007**, *79*, 2901-2910.

(35) Zhao, C.; Xie, B.; Chan, S. Y.; Costello, C. E.; O'Connor, P. B. Collisionally Activated Dissociation and Electron Capture Dissociation Provide Complementary Structural Information for Branched Permethylated Oligosaccharides. *J. Am. Soc. Mass. Spectrom.* **2008**, *19*, 138-150.

(36) Han, L.; Costello, C. Electron Transfer Dissociation of Milk Oligosaccharides. *J. Am. Soc. Mass. Spectrom.* **2011**, *22*, 997-1013.

(37) Zubarev, R. A.; Kelleher, N. L.; McLafferty, F. W. Electron Capture Dissociation of Multiply Charged Protein Cations. A Nonergodic Process. *J. Am. Chem. Soc.* **1998**, *120*, 3265-3266.

(38) Syka, J. E. P.; Coon, J. J.; Schroeder, M. J.; Shabanowitz, J.; Hunt, D. F. Peptide and Protein Sequence Analysis by Electron Transfer Dissociation Mass Spectrometry. *Proc. Natl. Acad. Sci. U.S.A* **2004**, *101*, 9528-9533.

(39) McAlister, G. C.; Phanstiel, D.; Good, D. M.; Berggren, W. T.; Coon, J. J. Implementation of Electron-Transfer Dissociation on a Hybrid Linear Ion Trap-Orbitrap Mass Spectrometer. *Anal. Chem.* **2007**, *79*, 3525-3534.

(40) Kaplan, D. A.; Hartmer, R.; Speir, J. P.; Stoermer, C.; Gumerov, D.; Easterling, M. L.; Brekenfeld, A.; Kim, T.; Laukien, F.; Park, M. A. Electron Transfer Dissociation in the Hexapole Collision Cell of a Hybrid Quadrupole-Hexapole Fourier Transform Ion Cyclotron Resonance Mass Spectrometer. *Rapid Commun. Mass Spectrom.* **2008**, *22*, 271-278.

(41) Cooper, H. J.; Hakansson, K.; Marshall, A. G. The Role of Electron Capture Dissociation in Biomolecular Analysis. *Mass Spectrom. Rev.* **2005**, *24*, 201-222.

(42) Bakhtiar, R.; Guan, Z. Q. Electron Capture Dissociation Mass Spectrometry in Characterization of Post-Translational Modifications. *Biochem. Biophys. Res. Commun.* **2005**, *334*, 1-8.

(43) Wiesner, J.; Premsler, T.; Sickmann, A. Application of Electron Transfer Dissociation (ETD) for the Analysis of Posttranslational Modifications. *Proteomics* **2008**, *8*, 4466-4483.

(44) Zhou, Y. P.; Dong, J.; Vachet, R. W. Electron Transfer Dissociation of Modified Peptides and Proteins. *Curr. Pharm. Biotechnol.* **2011**, *12*, 1558-1567.

(45) Jones, A. W.; Cooper, H. J. Dissociation Techniques in Mass Spectrometry-Based Proteomics. *Analyst* **2011**, *136*, 3419-3429.

(46) Wuhrer, M.; Catalina, M. I.; Deelder, A. M.; Hokke, C. H. Glycoproteomics Based on Tandem Mass Spectrometry of Glycopeptides. *J. Chromatogr. B* **2007**, *849*, 115-128.

(47) Zauner, G.; Kozak, R. P.; Gardner, R. A.; Fernandes, D. L.; Deelder, A. M.; Wuhrer, M. Protein O-Glycosylation Analysis. *Biol. Chem.* **2012**, *393*, 687-708.

(48) Budnik, B. A.; Haselmann, K. F.; Elkin, Y. N.; Gorbach, V. I.; Zubarev, R. A. Applications of Electron−Ion Dissociation Reactions for Analysis of Polycationic Chitooligosaccharides in Fourier Transform Mass Spectrometry. *Anal. Chem.* **2003**, *75*, 5994-6001.

(49) Liu, H.; Håkansson, K. Electron Capture Dissociation of Divalent Metal-Adducted Sulfated Oligosaccharides. *Int. J. Mass spectrom.* **2011**, *305*, 170-177.

(50) Zhou, W.; Hakansson, K. Electron Capture Dissociation of Divalent Metal-adducted Sulfonated *N*-Glycans Released from Bovine Thyroid Stimulating Hormone. *J. Am. Soc. Mass. Spectrom.* **2013**, Accepted.

(51) Sohn, C. H.; Chung, C. K.; Yin, S.; Ramachandran, P.; Loo, J. A.; Beauchamp, J. L. Probing the Mechanism of Electron Capture and Electron Transfer Dissociation Using Tags with Variable Electron Affinity. *J. Am. Chem. Soc.* **2009**, *131*, 5444-5459.

(52) Li, X. J.; Lin, C.; Han, L.; Costello, C. E.; O'Connor, P. B. Charge Remote Fragmentation in Electron Capture and Electron Transfer Dissociation. *J. Am. Soc. Mass. Spectrom.* **2010**, *21*, 646-656.

(53) Ceroni, A.; Maass, K.; Geyer, H.; Geyer, R.; Dell, A.; Haslam, S. M. GlycoWorkbench: A Tool for the Computer-Assisted Annotation of Mass Spectra of Glycans. *J. Proteome Res.* **2008**, *7*, 1650-1659.

(54) Chen, X.; Chan, W. Y. K.; Wong, P. S.; Yeung, H. S.; Chan, T. W. D. Formation of Peptide Radical Cations ($M^{+\cdot}$) in Electron Capture Dissociation of Peptides Adducted with Group IIB Metal Ions. *J. Am. Soc. Mass. Spectrom.* **2011**, *22*, 233-244.

(55) Iavarone, A. T.; Paech, K.; Williams, E. R. Effects of Charge State and Cationizing Agent on the Electron Capture Dissociation of a Peptide. *Anal. Chem.* **2004**, *76*, 2231-2238.

(56) Chen, X.; Fung, Y.; Chan, W.; Wong, P.; Yeung, H.; Chan, T. W. Transition Metal Ions: Charge Carriers that Mediate the Electron Capture Dissociation Pathways of Peptides. *J. Am. Soc. Mass. Spectrom.* **2011**, *22*, 2232-2245.

(57) Liu, H.; Håkansson, K. Divalent Metal Ion-Peptide Interactions Probed by Electron Capture Dissociation of Trications. *J. Am. Soc. Mass. Spectrom.* **2006**, *17*, 1731-1741.

(58) Mihalca, R.; Kleinnijenhuis, A. J.; McDonnell, L. A.; Heck, A. J. R.; Heeren, R. M. A. Electron Capture Dissociation at Low Temperatures Reveals Selective Dissociations. *J. Am. Soc. Mass. Spectrom.* **2004**, *15*, 1869-1873.

(59) Dong, J.; Vachet, R. W. Coordination Sphere Tuning of the Electron Transfer Dissociation Behavior of Cu(II)-Peptide Complexes. *J. Am. Soc. Mass. Spectrom.* **2012**, *23*, 321-329.

(60) Robinson, E. W.; Leib, R. D.; Williams, E. R. The Role of Conformation on Electron Capture Dissociation of Ubiquitin. *J. Am. Soc. Mass. Spectrom.* **2006**, *17*, 1470-1480.

(61) Robinson, E. W.; Garcia, D. E.; Leib, R. D.; Williams, E. R. Enhanced Mixture Analysis of Poly(Ethylene Glycol) Using High-Field Asymmetric Waveform Ion

Mobility Spectrometry Combined With Fourier Transform Ion Cyclotron Resonance Mass Spectrometry. *Anal. Chem.* **2006**, *78*, 2190-2198.

(62) Seo, Y. J.; Schenauer, M. R.; Leary, J. A. Biologically Relevant Metal-Cation Binding Induces Conformational Changes in Heparin Oligosaccharides as Measured by Ion Mobility Mass Spectrometry. *Int. J. Mass spectrom.* **2011**, *303*, 191-198.

(63) Cancilla, M. T.; Penn, S. G.; Carroll, J. A.; Lebrilla, C. B. Coordination of Alkali Metals to Oligosaccharides Dictates Fragmentation Behavior in Matrix Assisted Laser Desorption Ionization/Fourier Transform Mass Spectrometry. *J. Am. Chem. Soc.* **1996**, *118*, 6736-6745.

Chapter 3 Electron Capture Dissociation and Electron Transfer Dissociation of Trivalent Metal-Adducted Underivatized Oligosaccharides

3.1 Introduction

Glycosylation is a common post-translational modification to cell surfaces. Cells respond to the surrounding environment via structural alterations of the surface glycans.[1-4] Some glycans are recognized as critical mediators of tumor progression.[5-7] The structural diversity and complexity of carbohydrates are impediments to an in-depth understanding of their biological functions and to the development of carbohydrate-based drugs and vaccine candidates.[8, 9] The development of tandem mass spectrometry (MS/MS)-based techniques for carbohydrate structural analysis is driven by these biomedical needs. MS/MS is able to provide detailed structural information at high sensitivity. [10] The latter characteristic is particularly valuable for biomedical applications given the limited sample amounts in many applications.

Electrospray ionization (ESI) is one of the most widely used ionization methods for modern mass spectrometers. ESI is softer than many other ionization methods and directly compatible with liquid chromatography (LC). Another valuable aspect of ESI is its tendency to generate multiply charged ions for macromolecular analytes. Increased charge is advantageous in most MS/MS activation methods.

Currently, collision activated dissociation (CAD) is the most widely used MS/MS technique for carbohydrate analysis. Low energy CAD typically generates glycosidic

cleavages which are not sufficient for detailed structural analysis.[11, 12] Electron capture dissociation (ECD) and electron transfer dissociation (ETD) are two emerging MS/MS fragmentation techniques that can be valuable for generating complementary fragments compared with CAD and thus adding structural information.[11, 13-15] However, ECD and ETD require multiply charged precursor cations. This requirement can be highly challenging for carbohydrates, because they lack preferred protonation sites. Moreover, the extent of fragmentation, electron capture/transfer efficiency, and recombination energy all increase with increasing ion charge state in ECD/ETD.[16-20] Thus, charge states higher than two are preferred although they are even more challenging to generate than doubly charged ions.

Metal adduction can be an effective way to manipulate charge states prior to ECD/ETD. Alkali metals and divalent metals have been utilized towards peptides and oligosaccharides.[14, 21-26] Chapter 2 of this dissertation presented a direct comparison of ECD and ETD for such precursor ion species. Trivalent metals were recently reported as charge carriers for supercharging of proteins to yield extensive ECD fragmentation.[27] The same group also explored the effect of a range of trivalent metal adducts in ECD of peptides.[28] Our group has previously examined Fe^{3+} and Ga^{3+} binding of a *B. anthracis* siderophore and found that ECD generated more structural information compared with sustained off-resonance irradiation (SORI) CAD or infrared multiphoton dissociation (IRMPD).[29] In this chapter, the formation of trivalent metal, including La, Al, Ga, Eu, Ce, and Sm, ion-glycan complexes, including isomeric oligosaccharides is compared. Their ECD/ETD fragmentation behavior is inverstigated. Traveling wave ion mobility spectrometry (TW IMS) was also employed to assess gas-phase structures of metal-

glycan complexes in order to gain further insight into the metal influence on ECD/ETD behavior.

3.2 Experimental Section

3.2.1 Reagents

Lacto-N-difucohexaose I (LNDFH I), LS-tetrasaccharide A (LSTa), LS-tetrasaccharide B (LSTb), LS-tetrasaccharide C (LSTc), and an asialo, biantennary N-glycan (NA2) were purchased from V-Labs Inc (Covington, LA), Prozyme (Hayward, CA) or Carbosynth (Compton, Berkshire, UK). $La(OAc)_3$, $AlCl_3$, $GaCl_3$, $Eu(OAc)_3$, $Ce(OAc)_3$, and $Sm(OAc)_3$ were obtained from Fisher (Fair Lawn, NJ) or Sigma-Aldrich (St. Louis, MO).

3.2.2 Sample Preparation

Five μM solutions of oligosaccharides were mixed with 20 μM salt ($LaCl_3$, $La(OAc)_3$, $AlCl_3$, $GaCl_3$, $Eu(OAc)_3$, $Ce(OAc)_3$, or $Sm(OAc)_3$) in 50% methanol (v/v) for positive ion mode analysis.

3.2.3 Mass Spectrometry

All mass spectra were acquired on a SolariX 7T ESI-quadrupole-Fourier transform ion cyclotron resonance (FT-ICR) mass spectrometer (Bruker Daltonics, Billerica, MA). Samples were infused via an Apollo II electrospray source (Bruker Daltonics) at 70 to 100 μL/h and ionized with the assistance of N_2 nebulizing gas. Precursor ions for MS/MS were selected by the quadrupole and accumulated externally in the collision cell (hexapole). ECD experiments were conducted by irradiating precursor

ions in the ICR cell by an electron beam from an indirectly heated cathode. The cathode heating current was 1.6 A and the cathode bias voltage was pulsed to -0.9 to -1.3 V for 180 to 300 ms. ETD experiments were conducted in the collision cell. ETD reagent (fluoranthene, Sigma-Aldrich) anions were produced externally in the chemical ionization source, trapped in the collision cell for 350–2000 ms, and then allowed to react with mass-selected precursor ions for 100 ms. All mass spectra were acquired with SolarixControl software (Bruker Daltonics) with 256 data points from *m/z* 200 to 2000 and averaged over 64-100 scans.

TW IMS experiments were performed on a Synapt G2 HDMS quadrapole ion mobility-time-of-flight mass spectrometer (Waters, Milford, MA). For each measurement, 5 μM oligosaccharide was mixed with 20 μM metal salt. The travelling-wave ion mobility cell was operated with a nitrogen gas pressure of 3.2-3.7 mbar and employed a series of DC voltage waves (wave heights: 23-27 V, wave velocities: 650-900 m/s) to generate ion mobility separations. The TOF-MS was operated over an m/z range of 200-3000 with a pressure of 1.2×10^{-6} mbar. Drift time values of a species with various metal ligands were compared under identical ion mobility conditions and charge states. Reported drift times are associated with the value at a peak's maximum intensity.

3.2.4 Data Analysis

Data were analyzed manually with the aid of GlycoWorkbench software.[30] Product ions were not assigned unless the S/N ratio was at least 3.

Fragmentation efficiency = $\frac{\sum \boldsymbol{I}\,(\boldsymbol{fi})}{\boldsymbol{Pi}\,(\boldsymbol{before})}$ (1) in which I (f_i) is the summed product ion abundance (charge state normalization is unnecessary as all fragments are singly

charged) and P_i (before) is the precursor ion abundance in a separate spectrum prior to dissociation.

3.3 Results

3.3.1 ECD and ETD of Triple and Doubly Charged La-Adducted NA2

A triply charged La-glycan complex was generated via ESI for the *N*-glycan NA2 (see glycan structure in Figure 3.2) when using acetate counter ions (see Figure 3.1). By contrast, $LaCl_3$ only generated an overall doubly charged, singly deprotonated La-NA2 complex with HCl adducts. Triply charged $[NA2 + La]^{3+}$ ions were the most abundant species from ESI of a 5 μM NA2 solution with 20 μM $La(OAc)_3$.

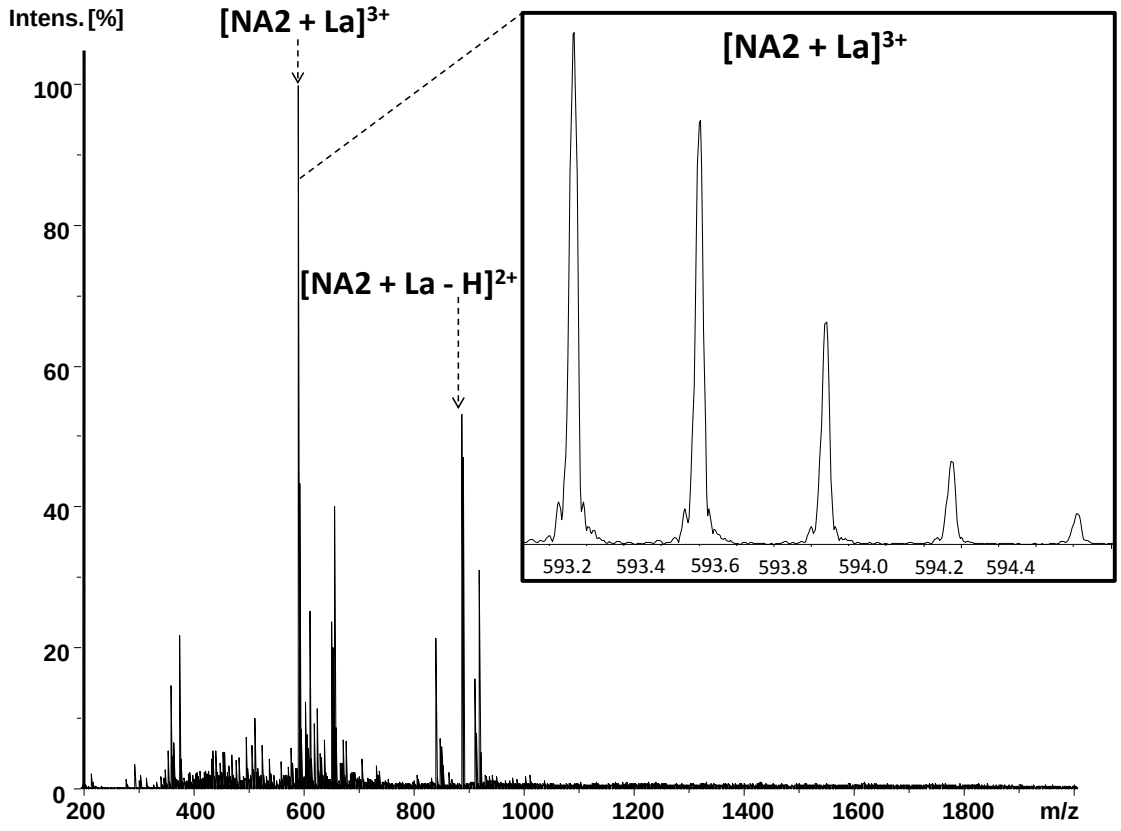

Figure 3.1 ESI-FT-ICR mass spectrum of 5 μM NA2 solution with 20 μM $La(OAc)_3$ (32 scans). The most abundant ions correspond to $[NA2 + La]^{3+}$ at *m/z* = 593.1656. The inset displays the corresponding isotopic distribution of this triply charged cation.

ECD and ETD spectra of La-adducted triply charged NA2 are shown in Figure 3.2. Fragmentation is significantly enhanced compared with previous data on doubly charged divalent metal-adducted NA2 (Chapter 2). In addition to extensive internal fragments, 16 glycosidic and 13 cross-ring cleavages were observed in ECD and 12 glycosidic and 18 cross-ring cleavages were observed in ETD. Twenty three of these products were shared by ECD and ETD, including 10 glycosidic cleavages ($B_{2\alpha}(H)^+$, $Y_2(H)^+$, $B_{3\alpha}(H)^+$, B_4, C_4 (or $\underline{C_4}$), $Z_{4\alpha}$, $Y_{4\alpha}$, B_5, C_5, and $Y_{5\alpha}$ and eight cross-ring cleavages: $^{0,2}A_4$, ($^{0,3}A_5$ - H_2O) (or $\underline{^{0,3}A_5 - H_2O}$), $^{0,3}A_5$, $^{0,2}A_5$, $^{1,5}A_5$- H_2O (or $\underline{^{1,5}A_5 - H_2O}$ and $\underline{^{1,5}A_5}$), $^{2,4}A_6$ (or $\underline{^{2,4}A_6 - H_2O}$), $^{0,2}A_6$ ($^{1,3}X_1$) ($^{1,3}X_0$) ($^{1,3}X_{4\alpha}$) (or $\underline{^{0,2}A_6}$ ($\underline{^{1,3}X_1}$) ($\underline{^{1,3}X_0}$) ($\underline{^{1,3}X_{4\alpha}}$)), $^{0,4}X_1$

($^{0,4}X_0$) ($^{0,4}X_{4\alpha}$) ($^{0,4}X_{5\alpha}$) ($^{1,3}X_{5\alpha}$) ($^{2,4}X_{5\alpha}$) ($^{0,4}X_{3\alpha}$) ($^{2,4}X_{3\alpha}$) (underlined fragments are radical ions containing one additional, or one less, hydrogen atom than the corresponding even-electron fragment, "$(H)^+$" indicate protonated singly charged fragments, all other fragments carry a lanthanum adduct.). Twenty seven product ions were unique to ECD, and twenty two fragments were only observed in ETD. These fragments are highlighted in bold in Figure 3.2 (a) and (b). Both ECD and ETD generated a series of glycosidic cleavages that fully cover the glycan sequence.

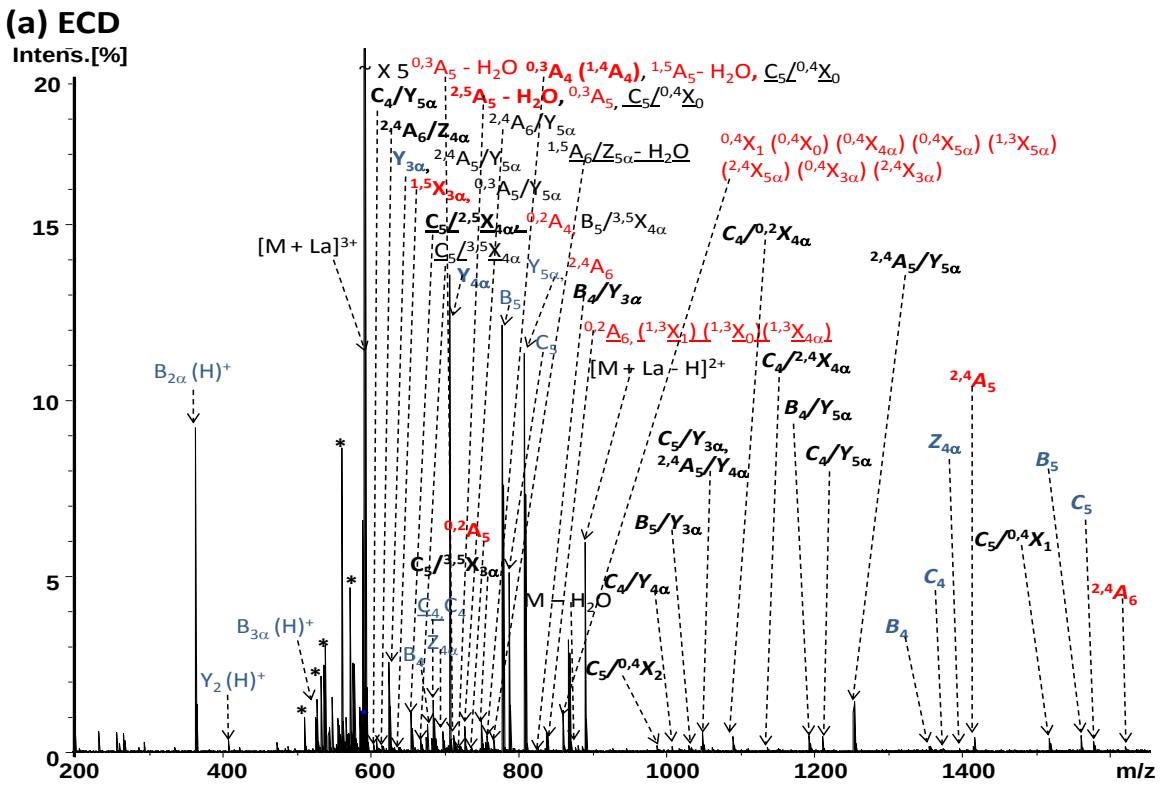
(a) ECD
Intens.[%]
m/z

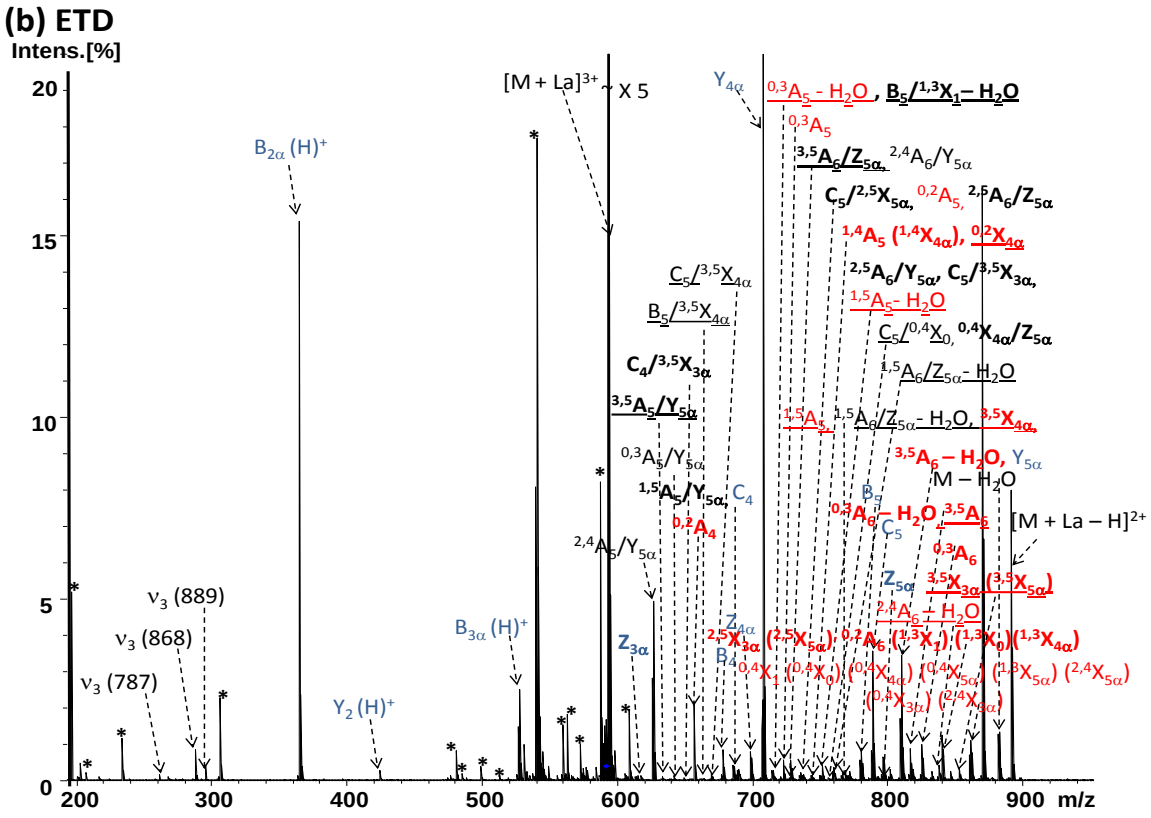
(b) ETD
Intens.[%]
m/z

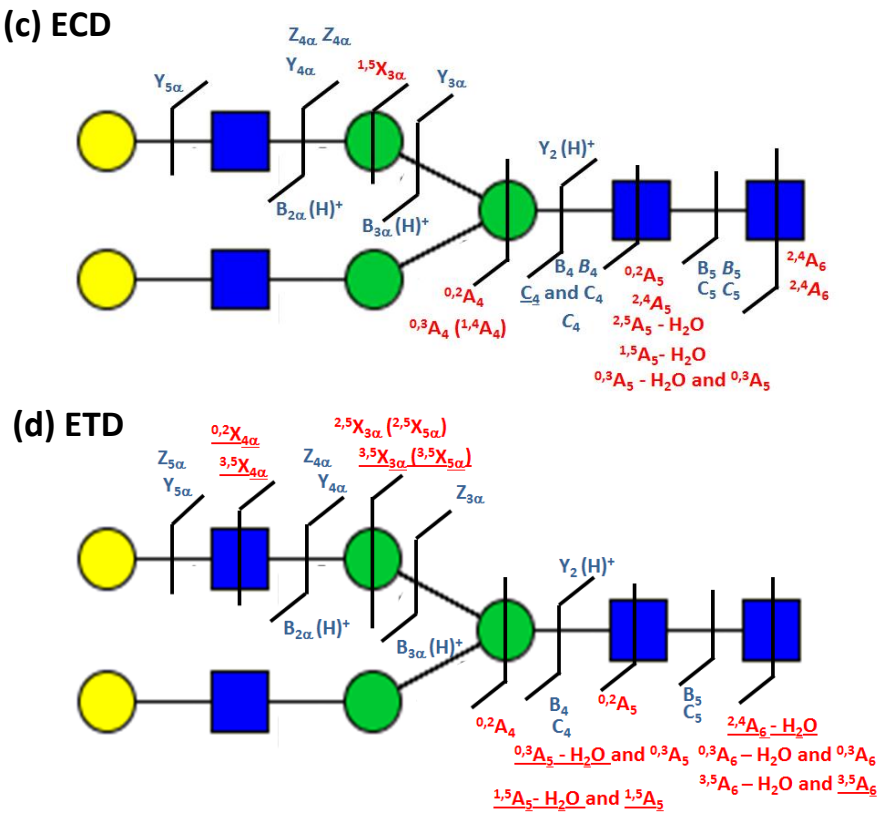

Figure 3.2 FT-ICR tandem mass spectra of La-adducted NA2, $[NA2 + La]^{3+}$. (a) ECD of $[NA2 + La]^{3+}$ (64 scans, 100 ms electron irradiation with a bias voltage of – 0.7 V). (b) ETD of $[NA2 + La]^{3+}$ (64 scans, 100 ms electron irradiation with a bias voltage of – 0.7 V). Underlined fragments are radical ions containing one additional, or one less, hydrogen atom than the corresponding even-electron fragment; Italics: singly charged $[La - 2H]^+$ fragments. Fragmentation patterns from ECD (c) and ETD (d). ν_3 = third harmonics. Glycosidic cleavages are highlighted in blue, and cross-ring cleavages are highlighted in red.

ESI of the NA2/$La(OAc)_3$ solution (as well as an NA2/$LaCl_3$ solution) also yielded abundant doubly charged La-glycan complexes of the form $[NA2 + La – H]^{2+}$ (see Fig. 3.1 for the acetate salt). These doubly charged precursor ions also showed dramatically different fragmentation behavior compared with divalent metal (M)-adducted NA2 ($[NA2 + M(II)]^{2+}$, see Chapter 2). ECD and ETD spectra of $[NA2 + La – H]^{2+}$ are shown in Figure 3.3 and Table 3.1 summarizes all the glycosidic and cross-ring cleavages observed from ECD and ETD of these precursor ions. Fragments highlighted

in pink in Table 3.1 were not observed in ECD/ETD of divalent metal (Mg, Co, and Ca)-adducted doubly charged NA2.

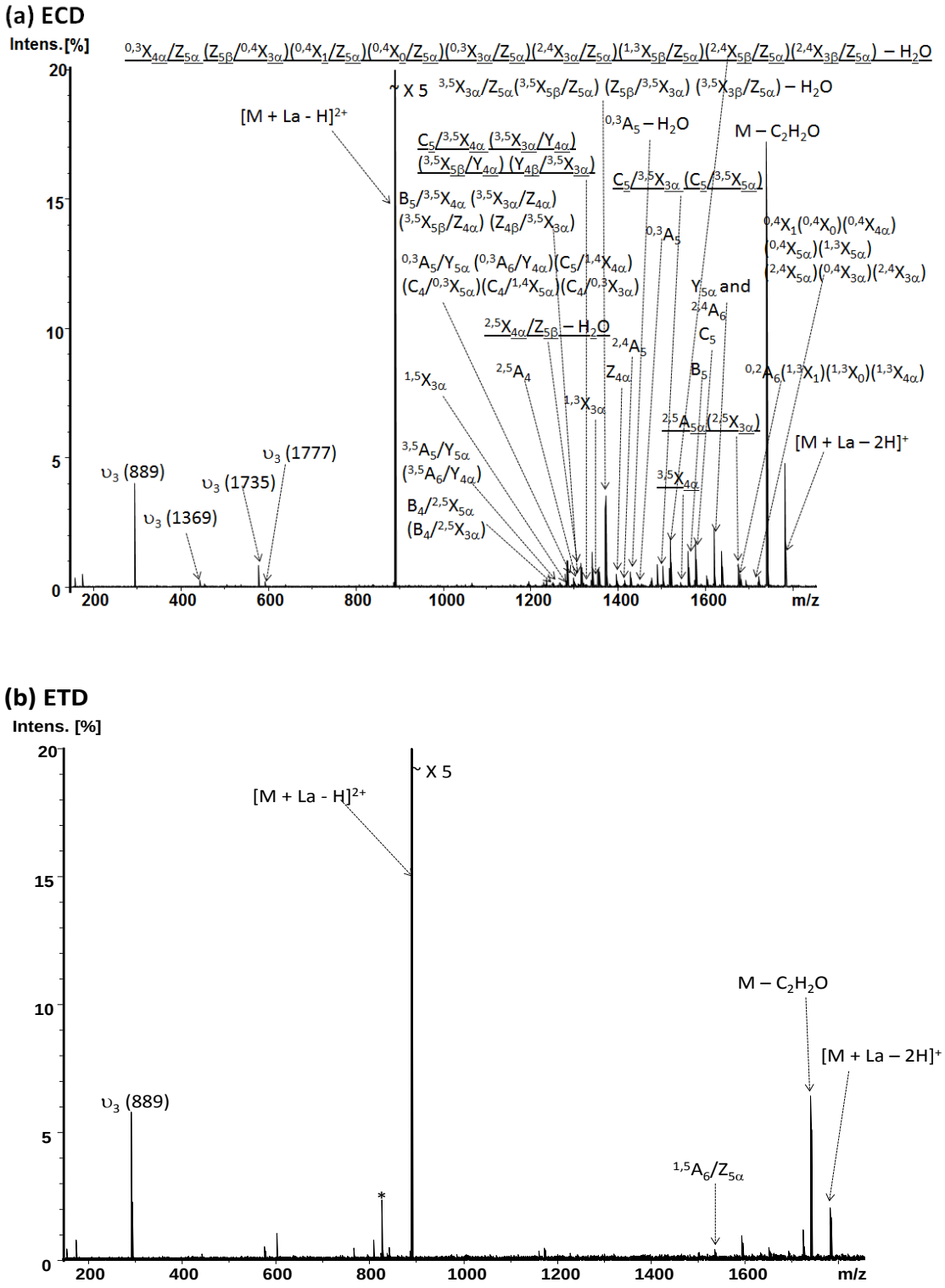

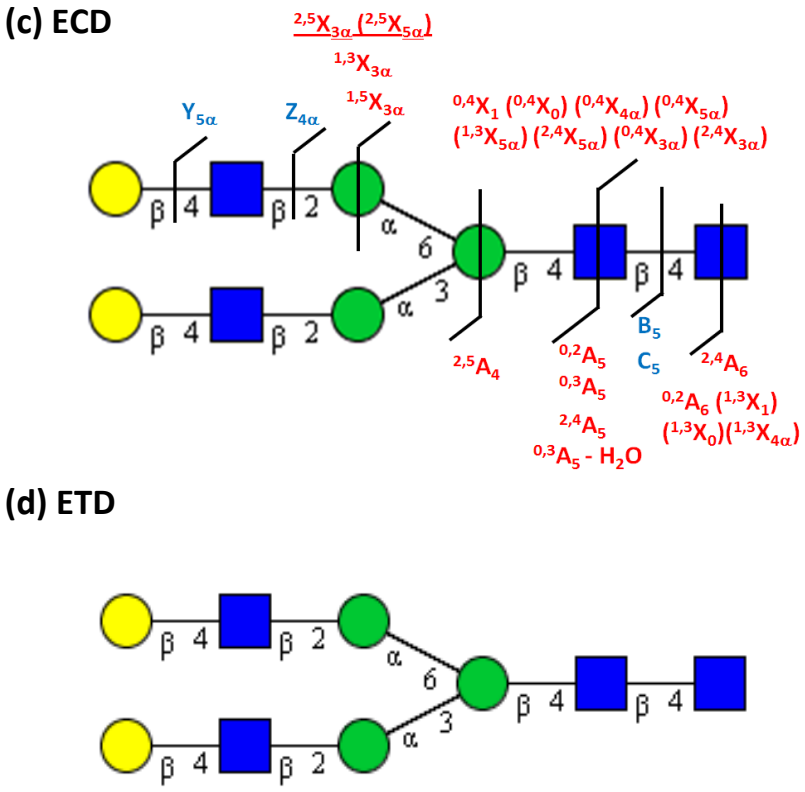

Figure 3.3 FT-ICR tandem mass spectra of La-adducted deprotonated NA2, $[NA2 + La - H]^{2+}$. (a) ECD (64 scans, 180 ms electron irradiation with a bias voltage of – 1.0 V); (b) ETD (100 scans, 240 ms reagent accumulation time and 100 ms reaction time). Fragmentation patterns from ECD (c) and ETD (d). * = signal present prior to ETD; ν_3 = third harmonics.

Table 3.1 Product ions observed for La-adducted deprotonated NA2, $[NA2 + La - H]^{2+}$, following ECD (left) and ETD (right). Fragments highlighted in pink are unique to this trivalent metal-adducted doubly charged species compared with previous divalent metal-adducted NA2 (Chapter 2). Underlined fragments are radical ions containing one additional, or one less, hydrogen atom than the corresponding even-electron fragment.

$[NA2 + La - H]^{2+}$			
ECD		ETD	
Glycosidic (4)	Cross-ring (11)	Glycosidic (0)	Cross-ring (0)
$Z_{4\alpha}$ B_5 C_5 $Y_{5\alpha}$	$^{2,4}A_6$ $^{1,5}X_{3\alpha}$ $^{2,5}A_4$ $^{1,3}X_{3\alpha}$ $^{2,4}A_5$ $^{0,3}A_5 - H_2O$ $^{0,3}A_5$ $^{0,2}A_5$ $\underline{^{2,5}X_{3\alpha}}$ $(\underline{^{2,5}X_{5\alpha}})$ $^{0,2}A_6$ $(^{1,3}X_1)$ $(^{1,3}X_0)$ $(^{1,3}X_{4\alpha})$ $^{0,4}X_1$ $(^{0,4}X_0)$ $(^{0,4}X_{4\alpha})$ $(^{0,4}X_{5\alpha})$ $(^{1,3}X_{5\alpha})$ $(^{2,4}X_{5\alpha})$ $(^{0,4}X_{3\alpha})$ $(^{2,4}X_{3\alpha})$		

3.3.2 ECD and ETD of Doubly Charged La-Adducted LNDFH

A smaller, branched oligosaccharide, LNDFH, was also subjected to ESI in the presence of lanthanum. For this smaller glycan (mononisotopic mass 999.3641 vs. 1640.5919 for NA2) only doubly charged, deprotonated La complexes, $[LNDFH + La - H]^{2+}$ were observed, even with acetate counter ions. Fragmentation patterns and product ion identities from ECD and ETD of this doubly charged species are shown in Figure 3.4 and Table 3.2. Fragments highlighted in pink in Table 3.2 were not observed in previous ECD/ETD of divalent metal-adducted LNDFH (Chapter 2).

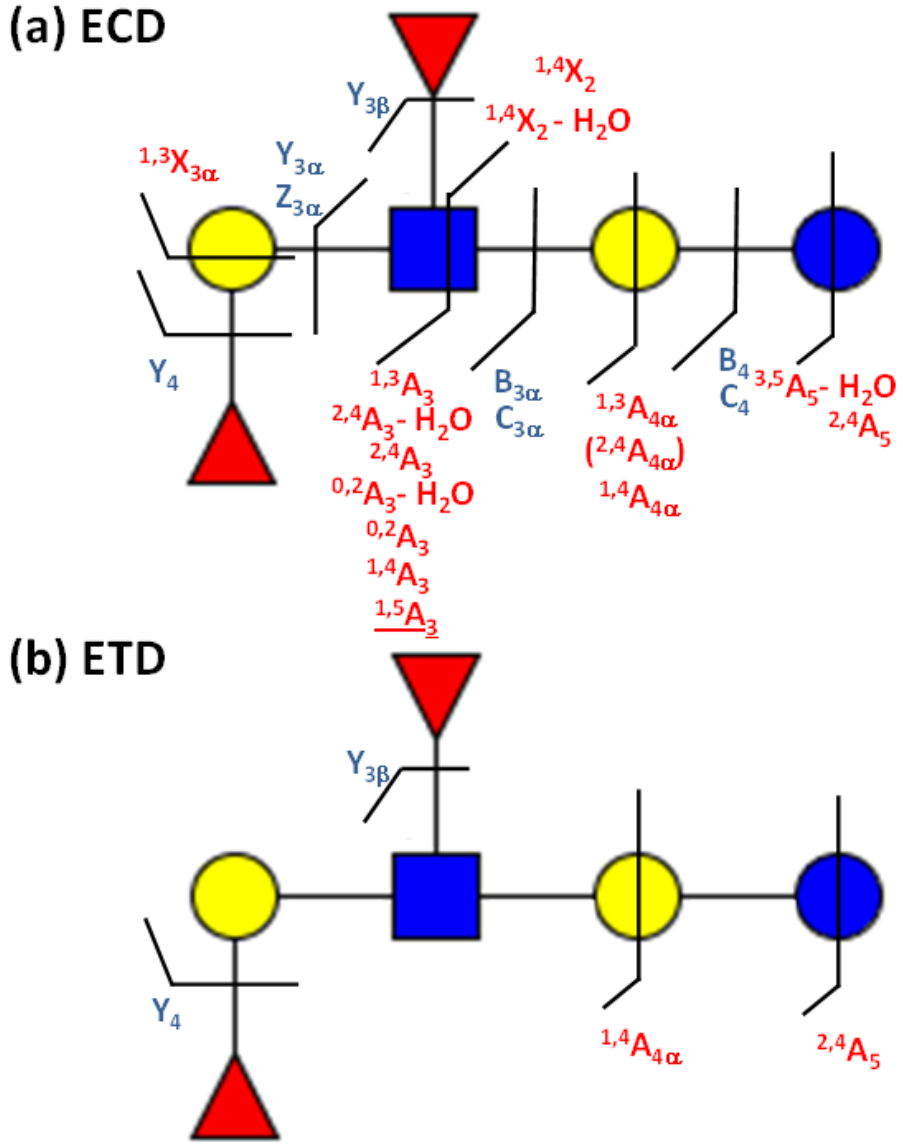

Figure 3.4 FT-ICR MS/MS fragmentation patterns for La-adducted deprotonated LNDFH $[LNDFH + La - H]^{2+}$. (a) ECD (64 scans, 300 ms electron irradiation with a bias voltage of – 0.8 V); (b) ETD (64 scans, 250 ms reagent accumulation time and 100 ms reaction time).

Table 3.2 Summary of product ions observed for La-adducted deprotonated LNDFH $[LNDFH + La - H]^{2+}$ following ECD and ETD. Fragments in bold are unique to ECD of $[LNDFH + La - H]^{+}$. Fragments highlighted in pink are unique to this trivalent metal-adducted species compared with previous ECD/ETD of divalent metal-adducted LNDFH. Underlined fragments are radical ions containing one additional, or one less, hydrogen atom than the corresponding even-electron fragment.

$[LNDFH + La - H]^{2+}$			
ECD		ETD	
Glycosidic (6)	Cross-ring (14)	Glycosidic (1)	Cross-ring (2)
$\mathbf{B_{3\alpha}}$ $\mathbf{C_{3\alpha}}$ $\mathbf{Y_{3\alpha}}$ $\mathbf{B_4}$ $\mathbf{C_4}$ $Y_{3\beta}$ (Y_4)	$\mathbf{^{1,4}X_2 - H_2O}$ $\mathbf{^{1,3}A_3}$ $\mathbf{^{1,4}X_2}$ $\mathbf{^{2,4}A_3 - H_2O}$ $\mathbf{^{2,4}A_3}$ $\mathbf{^{0,2}A_3 - H_2O}$ $\mathbf{^{0,2}A_3}$ $\mathbf{^{1,4}A_3}$ $\underline{\mathbf{^{1,5}A_3}}$ $\mathbf{^{1,3}A_{4\alpha}}$ ($\mathbf{^{2,4}A_{4\alpha}}$) $^{1,4}A_{4\alpha}$ $\mathbf{^{1,3}X_{3\alpha}}$ $\mathbf{^{3,5}A_5 - H_2O}$ $^{2,4}A_5$ ($^{0,2}X_{3\alpha}$)	$Y_{3\beta}$ (Y_4)	$^{1,4}A_{4\alpha}$ $^{2,4}A_5$ ($^{0,2}X_{3\alpha}$)

3.3.3 ECD and ETD of Triply Charged Al-Adducted NA2

Triply charged trivalent metal-glycan complexes were also generated via ESI of NA2 in the presence of $AlCl_3$ as shown in Figure 3.5. Doubly charged, deprotonated ions were also observed (Figure 3.5). At the same 5 μM carbohydrate and 20 μM metal salts concentration, La produced more abundant triply and doubly charged ions (about 1.5-2.5-fold). ECD and ETD of $[NA2 + Al]^{3+}$ generated a variety of glycosidic, cross-ring, and internal fragments, as shown in Figure 3.6 and summarized in Table 3.3. Twenty

fragments were shared between both techniques but 38 products were unique to ECD and 25 were unique to ETD.

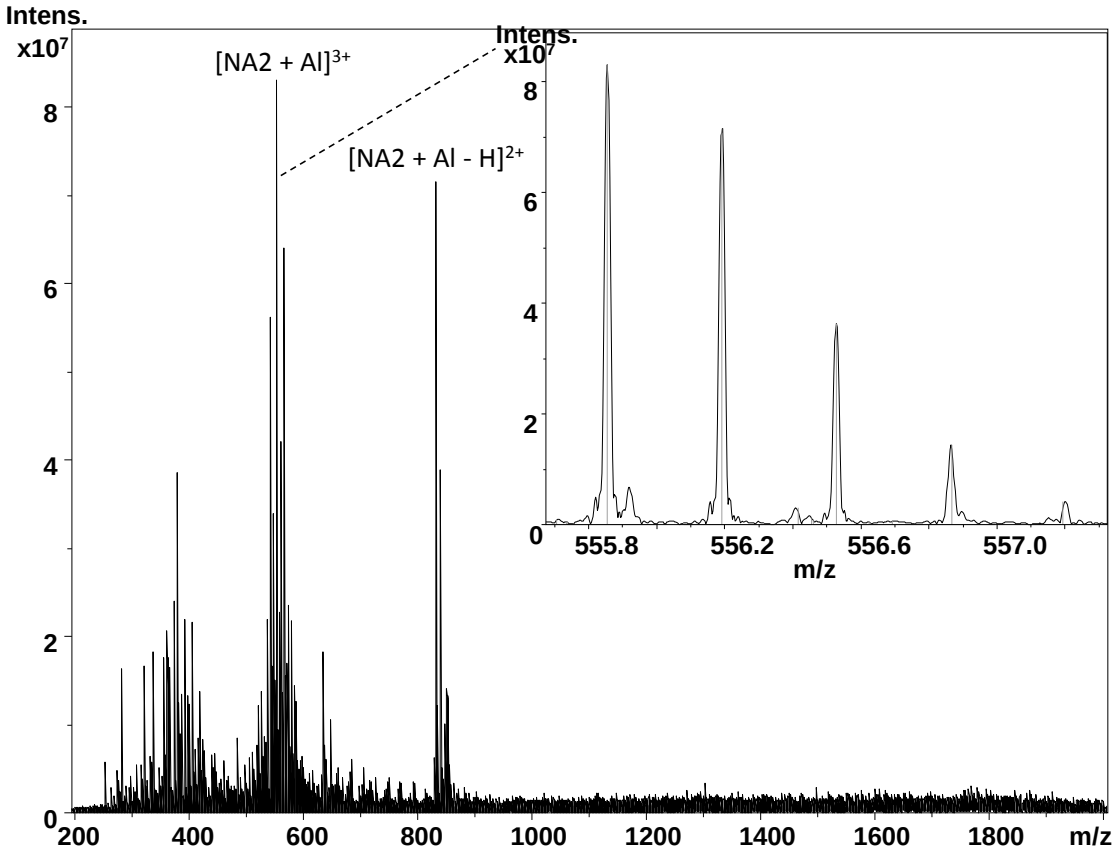

Figure 3.5 FT-ICR mass spectrum of a mixed solution of NA2 (5 μM) and $AlCl_3$ (20 μM) (20 scans). $[NA2 + Al]^{3+}$ (calculated *m/z* monoisotopic = 555.86, average = 556.16), and $[NA2 + Al – H]^{2+}$ (calculated *m/z* monoisotopic = 833.28, average = 833.74) are observed. $[NA2 + Al – 2H]^{+}$ (calculated *m/z* monoisotopic = 1665.56, average = 1666.47) was not observed. $[NA2 + Al]^{3+}$ is enlarged in the inset figure.

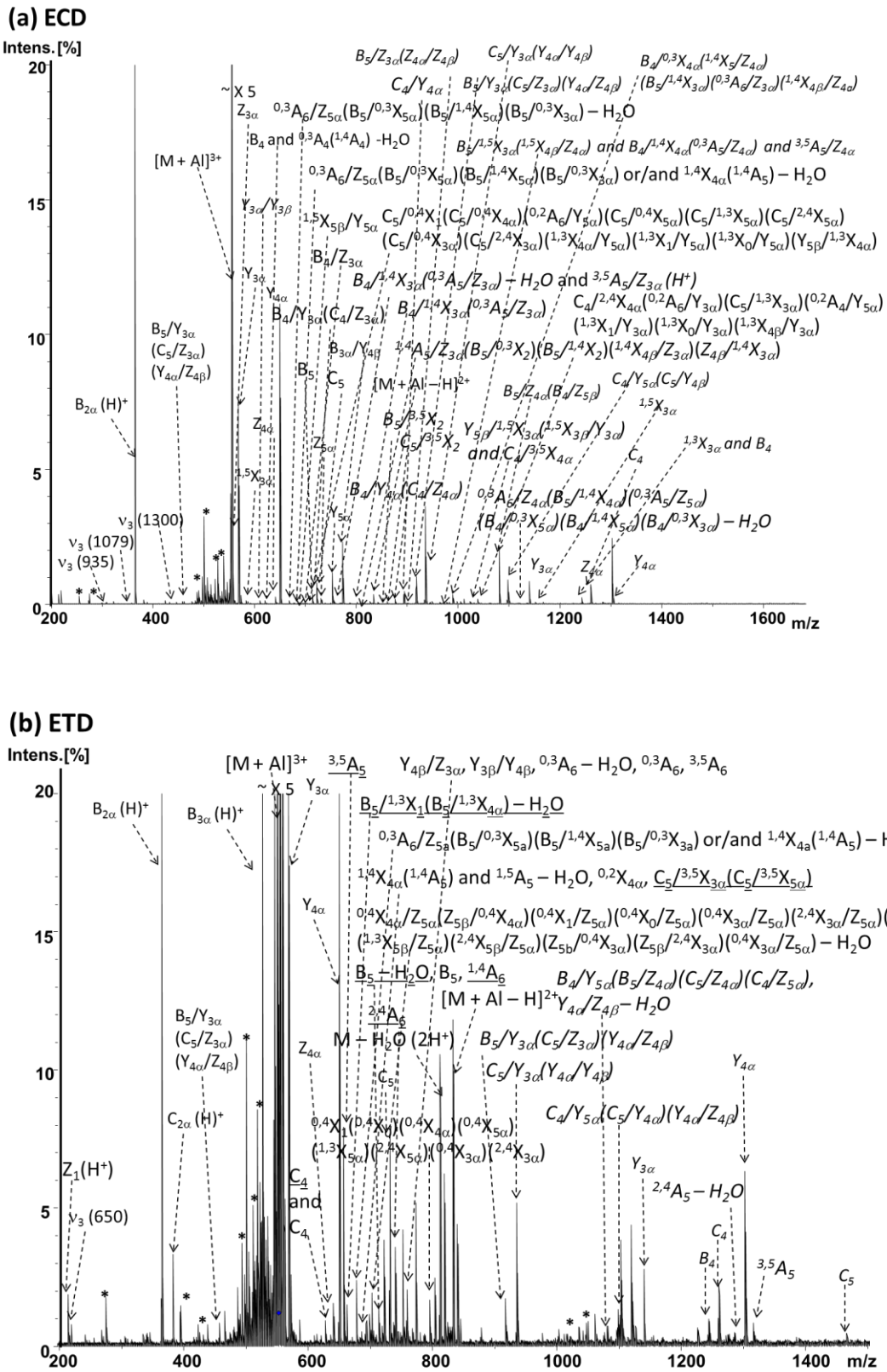
(a) ECD
Intens.[%]
m/z
(b) ETD
Intens.[%]
m/z

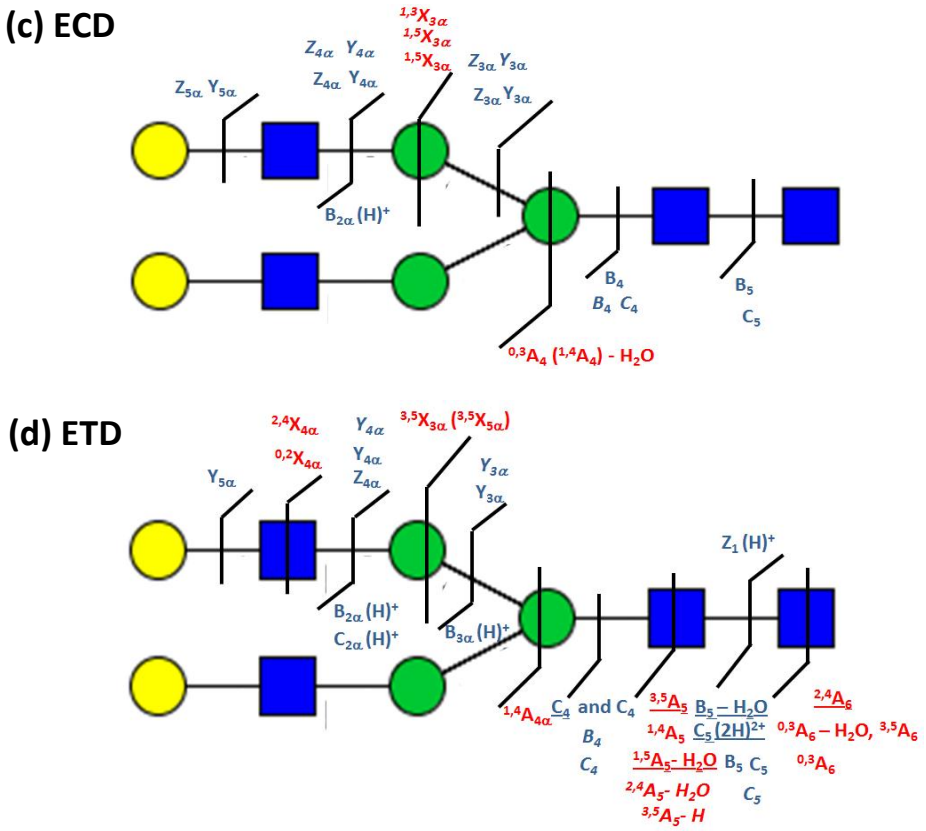

Figure 3.6 FT-ICR tandem mass spectra of Al-adducted NA2, $[NA2 + Al]^{3+}$. (a) ECD (64 scans, 280 ms electron irradiation with a bias voltage of – 0.55 V); (b) ETD (100 scans, 280 ms reagent accumulation time and 100 ms reaction time). Underlined fragments are radical ions containing one additional, or one less, hydrogen atom than the corresponding even-electron fragment; Italics: singly charged $[Al - 2H]^+$ fragments; *: in blank or noise. Fragmentation patterns from ECD (c) and ETD (d).

Table 3.3 Product ions from ECD (left) and ETD (right) of triply charged Al-adducted NA2, $[NA2 + Al]^{3+}$. For both ECD and ETD, the left columns contain fragments shared between both techniques whereas the right columns contain fragments unique to either ECD or ETD. Underlined fragments are radical ions containing one additional, or one less, hydrogen atom than the corresponding even-electron fragment; Italics: singly charged $[Al - 2H]^{+}$ fragments.

$[NA2 + Al]^{3+}$			
ECD		ETD	
20	38	20	25
$B_{2\alpha}(H)^+$ $B_5/Y_{3\alpha}$ $(C_5/Z_{3\alpha})$ $(Y_{4\alpha}/Z_{4\beta})$ $Y_{3\alpha}$ $Z_{4\alpha}$ $Y_{4\alpha}$ $^{0,3}A_6/Z_{5\alpha}$ $(B_5/^{0,3}X_{5\alpha})$ $(B_5/^{1,4}X_{5\alpha})$ $(B_5/^{0,3}X_{3\alpha})$ or/and $^{1,4}X_{4\alpha}$ $(^{1,4}A_5) - H_2O$ B_5 C_5 $Z_{5\alpha}$ $Y_{5\alpha}$ $Y_{4\beta}/Z_{3\alpha}$ $Y_{3\alpha}/Y_{4\beta}$ $B_5/Y_{3\alpha}(C_5/Z_{3\alpha})(Y_{4\alpha}/Z_{4\beta})$ $C_5/Y_{3\alpha}(Y_{4\alpha}/Y_{4\beta})$ $B_4/Y_{5\alpha}$ $(B_5/Y_{4\alpha})$ $(C_5/Z_{4\alpha})$ $(C_4/Z_{5\alpha})$ and/or $Z_{4\alpha}/Z_{5\alpha} - H_2O$ $C_4/Y_{5\alpha}$ $(C_5/Y_{4\alpha})$ $(Z_{4\alpha}/Z_{5\alpha})$ $Y_{3\alpha}$ B_4 C_4 $Y_{4\alpha}$	$Z_{3\alpha}$ $^{1,5}X_{3\alpha}$ $Y_{3\alpha}/Y_{3\beta}$ B_4 $^{0,3}A_4$ $(^{1,4}A_4) - H_2O$ $^{0,3}A_6/Z_{5\alpha}$ $(B_5/^{0,3}X_{5\alpha})$ $(B_5/^{1,4}X_{5\alpha})$ $(B_5/^{0,3}X_{3\alpha}) - H_2O$ $^{1,5}X_{3\beta}/Y_{5\alpha}$ $B_4/Z_{3\alpha}$ $C_5/^{0,4}X_1$ $(C_5/^{0,4}X_{4\alpha})$ $(^{0,2}A_6/Y_{5\alpha})$ $(C_5/^{0,4}X_{5\alpha})$ $(C_5/^{1,3}X_{5\alpha})$ $(C_5/^{2,4}X_{5\alpha})$ $(C_5/^{0,4}X_{3\alpha})$ $(C_5/^{2,4}X_{3\alpha})$ $(^{1,3}X_{4\alpha}/Y_{5\alpha})(^{1,3}X_1/Y_{5\alpha})$ $(^{1,3}x_0/Y_{5\alpha})(Y_{5\beta}/^{1,3}X_{4\alpha})$ $B_4/Y_{3\alpha}$ $(C_4/Z_{3\alpha})$ $B_4/^{1,4}X_{3\alpha}$ $(^{0,3}A_5/Z_{3\alpha}) - H_2O$ $\underline{^{3,5}A_5/Z_{3\alpha}}$ $B_4/^{1,4}X_{3\alpha}$ $(^{0,3}A_5/Z_{3\alpha})$ $^{1,5}X_{4\beta}/Y_{3\alpha}$ $(Y_{4\beta}/^{1,5}X_{3\alpha})$ $^{1,4}A_5/Z_{3\alpha}(B_5/^{0,3}X_2)$ $(B_5/^{1,4}X_2)$ $(^{1,3}X_{4\beta}/Z_{3\alpha})(Z_{4\beta}/^{1,4}X_{3\alpha})$ $\underline{B_5/^{3,5}X_2}$ $\underline{C_5/^{3,5}X_2}$ $B_4/Y_{4\alpha}$ $(C_5/Z_{4\alpha})$ $C_4/Y_{4\alpha}$ $B_5/Z_{3\alpha}(Z_{4\alpha}/Z_{4\beta})$ $\underline{^{3,5}A_5/Z_{4\alpha}}$ $B_5/^{1,5}X_{3\alpha}$ $(^{1,5}X_{4\beta}/Z_{4\alpha})$ $B_4/^{1,4}X_{4\alpha}$ $(^{0,3}A_5/Z_{4\alpha})$ $C_5/^{1,5}X_{3\alpha}$ $(^{1,5}X_{4\beta}/Y_{4\alpha})$ $Y_{3\alpha}/Y_{5\beta}$ $B_4/^{0,3}X_{4\alpha}$ $(^{1,4}A_5/Z_{4\alpha})(B_5/^{1,4}X_{3\alpha})$ $(^{0,3}A_6/Z_{3\alpha})(^{1,4}X_{4\beta}/Z_{4\alpha})$ $Y_{5\beta}/^{1,5}X_{3\alpha}$ $(^{1,5}X_{3\beta}/Y_{3\alpha})$ $\underline{C_4/^{3,5}X_{4\alpha}}$ $C_4/^{2,4}X_{4\alpha}$ $(^{0,2}A_6/Y_{3\alpha})$ $(C_5/^{1,3}X_{3\alpha})$ $(^{0,2}A_4/Y_{5\alpha})$ $(^{1,3}X_1/Y_{3\alpha})$ $(^{1,3}X_0/Y_{3\alpha})$ $(^{1,3}X_{4\beta}/Y_{3\alpha})$ $B_5/Z_{4\alpha}(B_4/Z_{5\alpha})$ $Z_{3\alpha}$ $^{0,3}A_6/Z_{4\alpha}(B_5/^{1,4}X_{4\alpha})(^{0,3}A_5/Z_{5\alpha})(B_4/^{0,3}X_{5\alpha})$ $(B_4/^{1,4}X_{5\alpha})$ $(B_4/^{0,3}X_{3\alpha}) - H_2O$ $^{0,3}A_6/Z_{4\alpha}(B_5/^{1,4}X_{4\alpha})(^{0,3}A_5/Z_{5\alpha})(B_4/^{0,3}X_{5\alpha})$ $(B_4/^{1,4}X_{5\alpha})$ $(B_4/^{0,3}X_{3\alpha})$ $^{1,5}X_{3\alpha}$ $^{1,3}X_{3\alpha}$ $Z_{4\alpha}$ $B_5/^{1,5}X_{5\alpha}$ $^{3,5}A_6/Z_{5\alpha}$	$B_{2\alpha}(H)^+$ $B_5/Y_{3\alpha}$ $(C_5/Z_{3\alpha})$ $(Y_{4\alpha}/Z_{4\beta})$ $Y_{3\alpha}$ $Z_{4\alpha}$ $Y_{4\alpha}$ $^{0,3}A_6/Z_{5\alpha}$ $(B_5/^{0,3}X_{5\alpha})$ $(B_5/^{1,4}X_{5\alpha})$ $(B_5/^{0,3}X_{3\alpha})$ or/and $^{1,4}X_{4\alpha}$ $(^{1,4}A_5) - H_2O$ B_5 C_5 $Y_{5\alpha}$ $Y_{4\beta}/Z_{3\alpha}$ $Y_{3\alpha}/Y_{4\beta}$ $B_5/Y_{3\alpha}(C_5/Z_{3\alpha})(Y_{4\alpha}/Z_{4\beta})$ $C_5/Y_{3\alpha}(Y_{4\alpha}/Y_{4\beta})$ $B_4/Y_{5\alpha}$ $(B_5/Y_{4\alpha})$ $(C_5/Z_{4\alpha})$ $(C_4/Z_{5\alpha})$ and/or $Z_{4\alpha}/Z_{5\alpha} - H_2O$ $C_4/Y_{5\alpha}$ $(C_5/Y_{4\alpha})$ $(Z_{4\alpha}/Z_{5\alpha})$ $Y_{3\alpha}$ $\underline{B_4}$ C_4 $Y_{4\alpha}$	$Z_1(H)^+$ $C_{2\alpha}(H)^+$ $Y_{3\alpha}/Y_{5\beta}$ $B_{3\alpha}(H)^+$ $\underline{C_3}$ and C_4 $\underline{^{3,5}A_5}$ $\underline{B_5/^{1,3}X_1\ (B_5/^{1,3}X_{4\alpha}) - H_2O}$ $B_5 - H_2O$ $\underline{C_5(2H)^{2+}}$ $^{1,4}X_{4\alpha}$ $(^{1,4}A_5)$ $\underline{^{0,2}X_{4\alpha}}$ $\underline{C_5/^{3,5}X_{3\alpha}\ (C_5/^{3,5}X_{5\alpha})}$ $\underline{^{1,5}A_5 - H_2O}$ $^{0,4}X_{4\alpha}/Z_{5\alpha}$ $(Z_{5\beta}/^{0,4}X_{4\alpha})$ $(^{0,4}X_1/Z_{5\alpha})$ $(^{0,4}X_0/Z_{5\alpha})$ $(^{0,4}X_{3\alpha}/Z_{5\alpha})$ $(^{2,4}X_{3\alpha}/Z_{5\alpha})$ $(^{0,4}X_{5\beta}/Z_{5\alpha})$ $(^{1,3}X_{5\beta}/Z_{5\alpha})$ $(^{2,4}X_{5\beta}/Z_{5\alpha})$ $(Z_{5\beta}/^{0,4}X_{3\alpha})$ $(Z_{5\beta}/^{2,4}X_{3\alpha})$ $(^{0,4}X_{3\beta}/Z_{5\alpha}) - H_2O$ $^{2,4}X_{4\alpha}$ $^{2,4}A_6$ $^{0,3}A_6 - H_2O$ and/or $^{3,5}A_6$ $^{0,3}A_6$ $^{3,5}X_{3\alpha}$ $(^{3,5}X_{5\alpha})$ $^{0,4}X_1$ $(^{0,4}X_0)$ $(^{0,4}X_{4\alpha})$ $(^{0,4}X_{5\alpha})$ $(^{1,3}X_{5\alpha})$ $(^{2,4}X_{5\alpha})$ $(^{0,4}X_{3\alpha})$ $(^{2,4}X_{3\alpha})$ $M - H_2O\ (2H)^{2+}$ $M - H_2O$ $^{2,4}A_5 - H_2O$ $^{3,5}A_5 - H$ C_5

3.3.4 ESI of NA2 in the Presence of Ce, Sm, Eu, and Ga

Other trivalent metals, including Ce, Sm, Eu, and Ga, were also investigated for generation of metal-glycan complexes. Neither one of these metals resulted in detection of triply charged metal-glycan complexes, however, the presence of Ce, Sm, and Eu

generated [NA2 + metal(III) – H]$^{2+}$ cations, as demonstrated in Figures 3.7-3.9 For all these four metals (and for Al), the mass spectra of glycan/metal salt mixtures contained more unassigned peaks than for La, probably due to salt impurities. Addition of Ga to the ESI solution did not result in any 3+, 2+, or 1+ ions containing the metal.

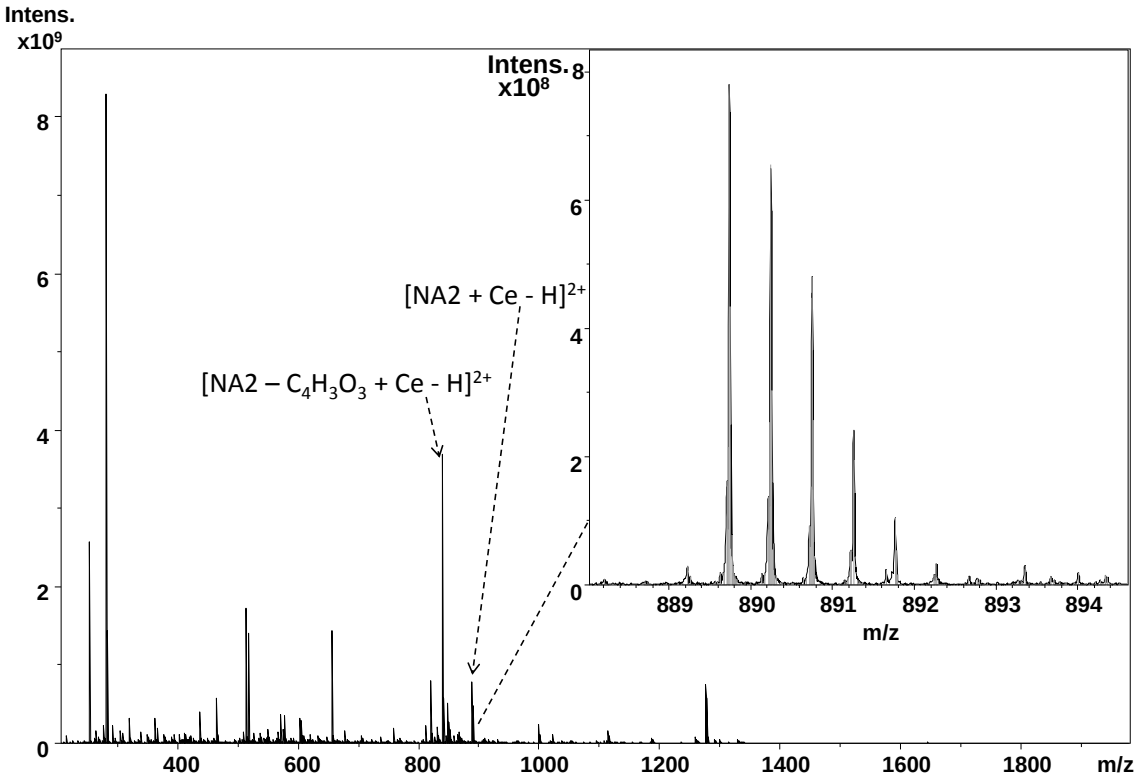

Figure 3.7 ESI-FT-ICR mass spectrum of 5 μM NA2 solution with 20 μM $Ce(OAc)_3$ (64 scans). [NA2 + Ce]$^{3+}$ (calculated average *m/z* = 593.87) was not observed but [NA2 + Ce – H]$^{2+}$ (calculated average *m/z* = 890.31) was detected as shown in the inset.

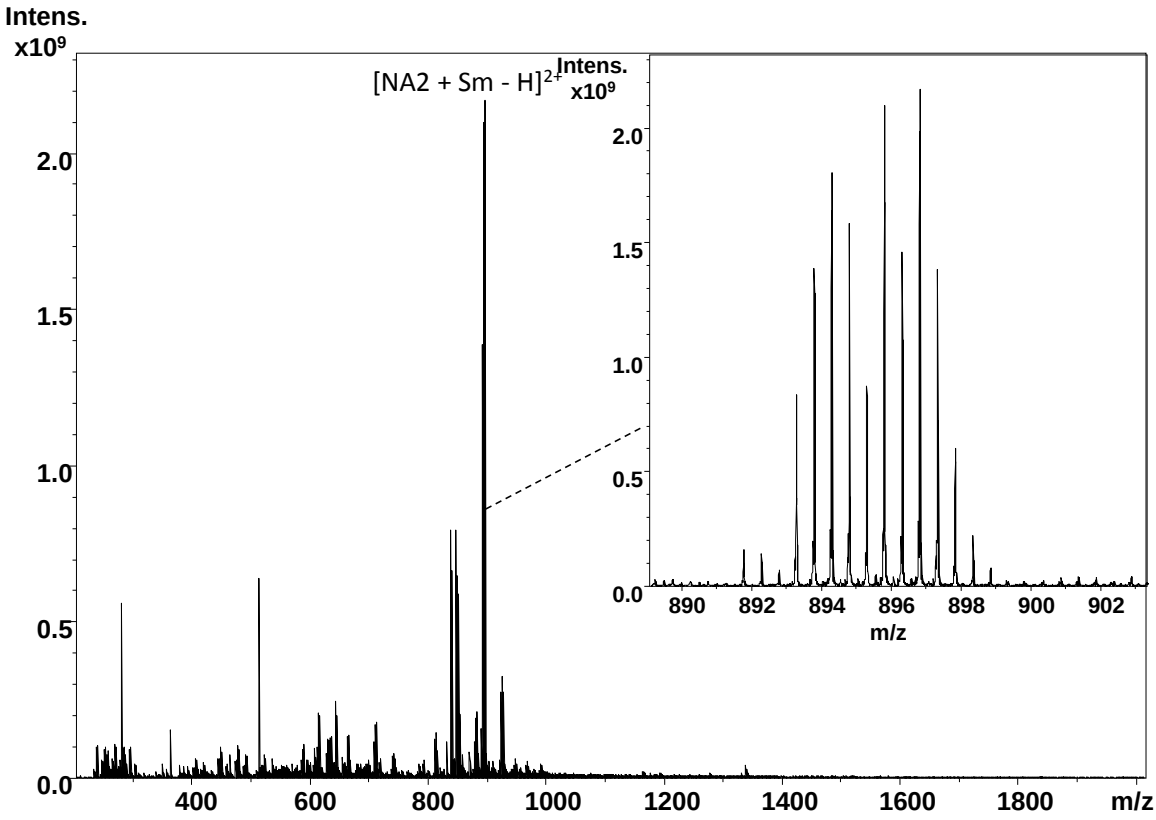

Figure 3.8 ESI-FT-ICR mass spectrum of a 5 μM NA2 solution with 20 μM $Sm(OAc)_3$ (64 scans). The most abundant ions correspond to $[NA2 + Sm - H]^{2+}$ (calculated average *m/z* = 895.43), as shown in the inset. $[NA2 + Sm]^{3+}$ (calculated average *m/z* = 597.29) was not observed.

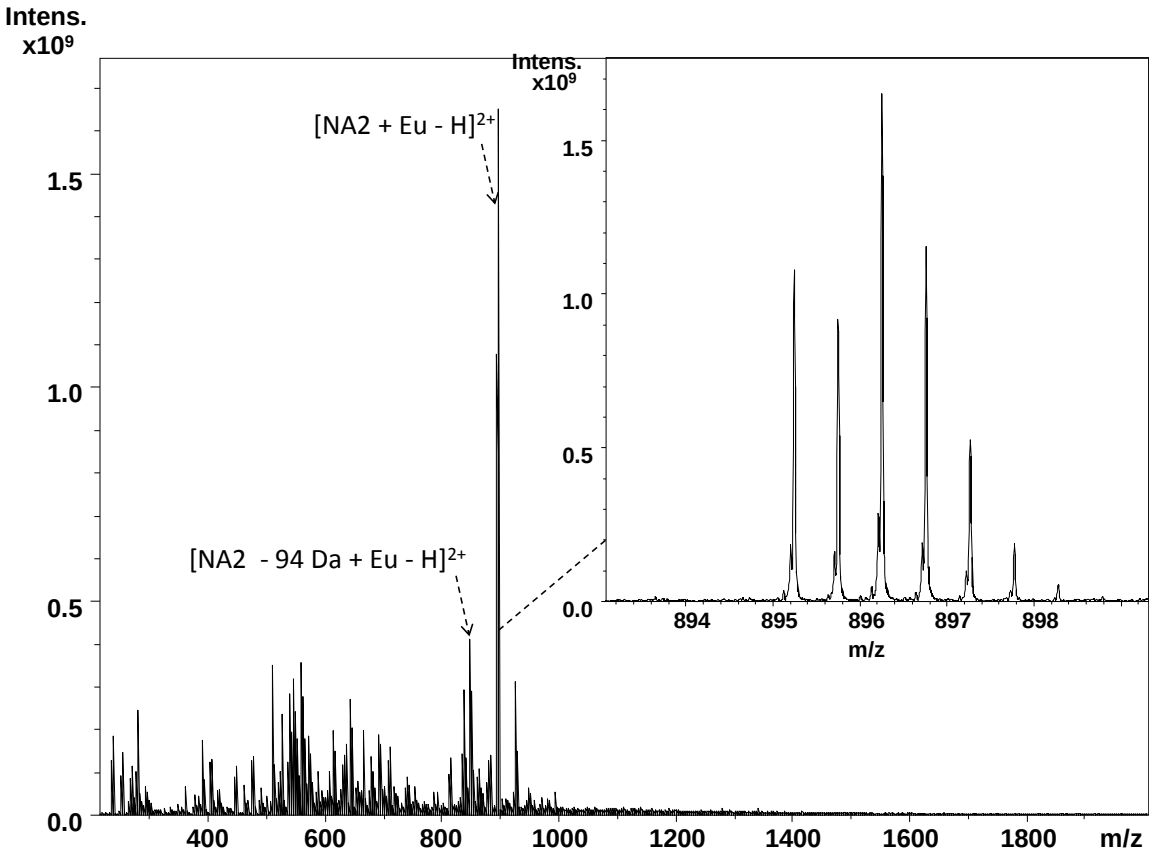

Figure 3.9 ESI-FT-ICR mass spectrum of 5 μM NA2 solution with 20 μM $Eu(OAc)_3$ (64 scans). The most abundant ions correspond to $[NA2 + Eu - H]^{2+}$ (calculated average m/z = 896.23), as shown in the inset. $[NA2 + Eu]^{3+}$ (calculated average m/z = 597.82) was not observed.

As illustrated in Figure 3.7, Sm has a highly complex isotopic distribution, rendering data interpretation challenging and also potentially diluting available signal. Eu has a less complex isotopic distribution but still causes widening of MS signals. Also, the high occurrence of one or two hydrogen transfers in ECD may be masked by the Eu isotopic distribution. Therefore, only Ce was further investigated as another trivalent metal, in addition to La and Al, for ECD and ETD-based structural characterization of underivatized glycans.

3.3.5 ECD and ETD of Doubly Charged Ce-Adducted Glycans

ECD and ETD of doubly charged Ce-adducted NA2, $[NA2 + Ce - H]^{2+}$, are shown in Figure 3.10. Although not as efficient as La in inducing ECD/ETD fragmentation from $[glycan + metal (III) - H]^{2+}$, Ce adduction still resulted in unique fragments compared with divalent metal-adducted NA2, including $^{0,4}X_1$ ($^{0,4}X_0$) ($^{0,4}X_{4\alpha}$) ($^{0,4}X_{5\alpha}$) ($^{1,3}X_{5\alpha}$) ($^{2,4}X_{5\alpha}$) ($^{0,4}X_{3\alpha}$) ($^{2,4}X_{3\alpha}$) and $^{0,4}X_1$ ($^{0,4}X_0$) ($^{0,4}X_{4\alpha}$) ($^{0,4}X_{5\alpha}$) ($^{1,3}X_{5\alpha}$) ($^{2,4}X_{5\alpha}$) ($^{0,4}X_{3\alpha}$) ($^{2,4}X_{3\alpha}$).

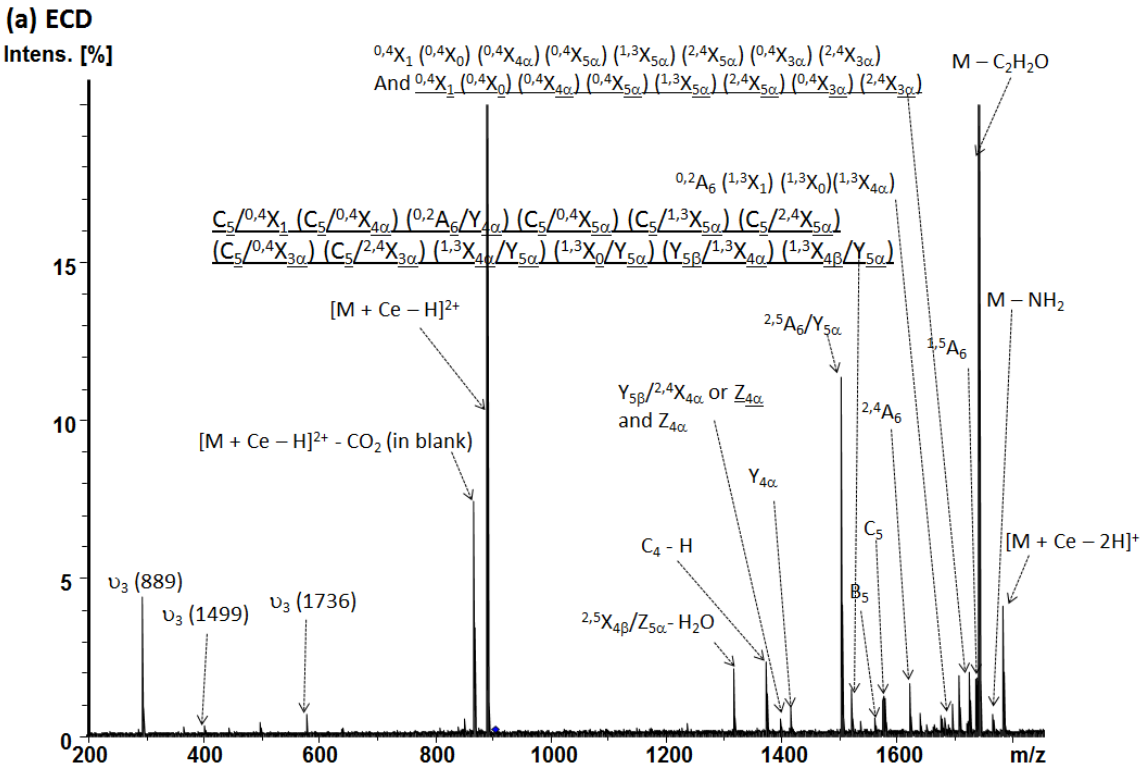
(a) ECD
Intens. [%]
$^{0,4}X_1$ ($^{0,4}X_0$) ($^{0,4}X_{4\alpha}$) ($^{0,4}X_{5\alpha}$) ($^{1,3}X_{5\alpha}$) ($^{2,4}X_{5\alpha}$) ($^{0,4}X_{3\alpha}$) ($^{2,4}X_{3\alpha}$)
And $^{0,4}X_1$ ($^{0,4}X_0$) ($^{0,4}X_{4\alpha}$) ($^{0,4}X_{5\alpha}$) ($^{1,3}X_{5\alpha}$) ($^{2,4}X_{5\alpha}$) ($^{0,4}X_{3\alpha}$) ($^{2,4}X_{3\alpha}$)
M – C_2H_2O
$^{0,2}A_6$ ($^{1,3}X_1$) ($^{1,3}X_0$)($^{1,3}X_{4\alpha}$)
$C_5/^{0,4}X_1$ ($C_5/^{0,4}X_{4\alpha}$) ($^{0,2}A_6/Y_{4\alpha}$) ($C_5/^{0,4}X_{5\alpha}$) ($C_5/^{1,3}X_{5\alpha}$) ($C_5/^{2,4}X_{5\alpha}$)
($C_5/^{0,4}X_{3\alpha}$) ($C_5/^{2,4}X_{3\alpha}$) ($^{1,3}X_{4\alpha}/Y_{5\alpha}$) ($^{1,3}X_0/Y_{5\alpha}$) ($Y_{5\beta}/^{1,3}X_{4\alpha}$) ($^{1,3}X_{4\beta}/Y_{5\alpha}$)
M – NH_2
[M + Ce – H]$^{2+}$
$^{2,5}A_6/Y_{5\alpha}$
$^{1,5}A_6$
$Y_{5\beta}/^{2,4}X_{4\alpha}$ or $Z_{4\alpha}$
and $Z_{4\alpha}$
$^{2,4}A_6$
[M + Ce – H]$^{2+}$ - CO_2 (in blank)
$Y_{4\alpha}$
C_5
C_4 - H
[M + Ce – 2H]$^+$
υ_3 (889)
υ_3 (1499)
υ_3 (1736)
$^{2,5}X_{4\beta}/Z_{5\alpha}$ - H_2O
B_5
0
5
10
15
200
400
600
800
1000
1200
1400
1600
m/z

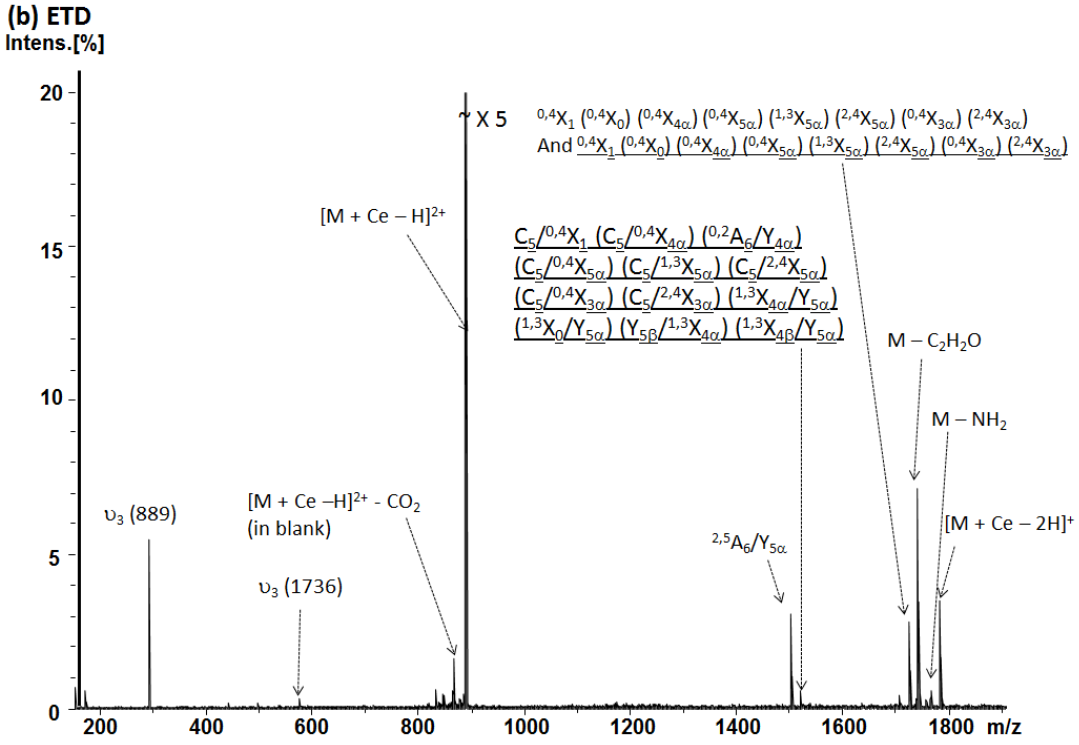
(b) ETD
Intens.[%]
~ X 5
$^{0,4}X_1$ ($^{0,4}X_0$) ($^{0,4}X_{4\alpha}$) ($^{0,4}X_{5\alpha}$) ($^{1,3}X_{5\alpha}$) ($^{2,4}X_{5\alpha}$) ($^{0,4}X_{3\alpha}$) ($^{2,4}X_{3\alpha}$)
And $^{0,4}X_1$ ($^{0,4}X_0$) ($^{0,4}X_{4\alpha}$) ($^{0,4}X_{5\alpha}$) ($^{1,3}X_{5\alpha}$) ($^{2,4}X_{5\alpha}$) ($^{0,4}X_{3\alpha}$) ($^{2,4}X_{3\alpha}$)
[M + Ce – H]$^{2+}$
$C_5/^{0,4}X_1$ ($C_5/^{0,4}X_{4\alpha}$) ($^{0,2}A_6/Y_{4\alpha}$)
($C_5/^{0,4}X_{5\alpha}$) ($C_5/^{1,3}X_{5\alpha}$) ($C_5/^{2,4}X_{5\alpha}$)
($C_5/^{0,4}X_{3\alpha}$) ($C_5/^{2,4}X_{3\alpha}$) ($^{1,3}X_{4\alpha}/Y_{5\alpha}$)
($^{1,3}X_0/Y_{5\alpha}$) ($Y_{5\beta}/^{1,3}X_{4\alpha}$) ($^{1,3}X_{4\beta}/Y_{5\alpha}$)
M – C_2H_2O
M – NH_2
[M + Ce – 2H]$^+$
υ_3 (889)
[M + Ce –H]$^{2+}$ - CO_2
(in blank)
$^{2,5}A_6/Y_{5\alpha}$
υ_3 (1736)
0
5
10
15
20
200
400
600
800
1000
1200
1400
1600
1800
m/z

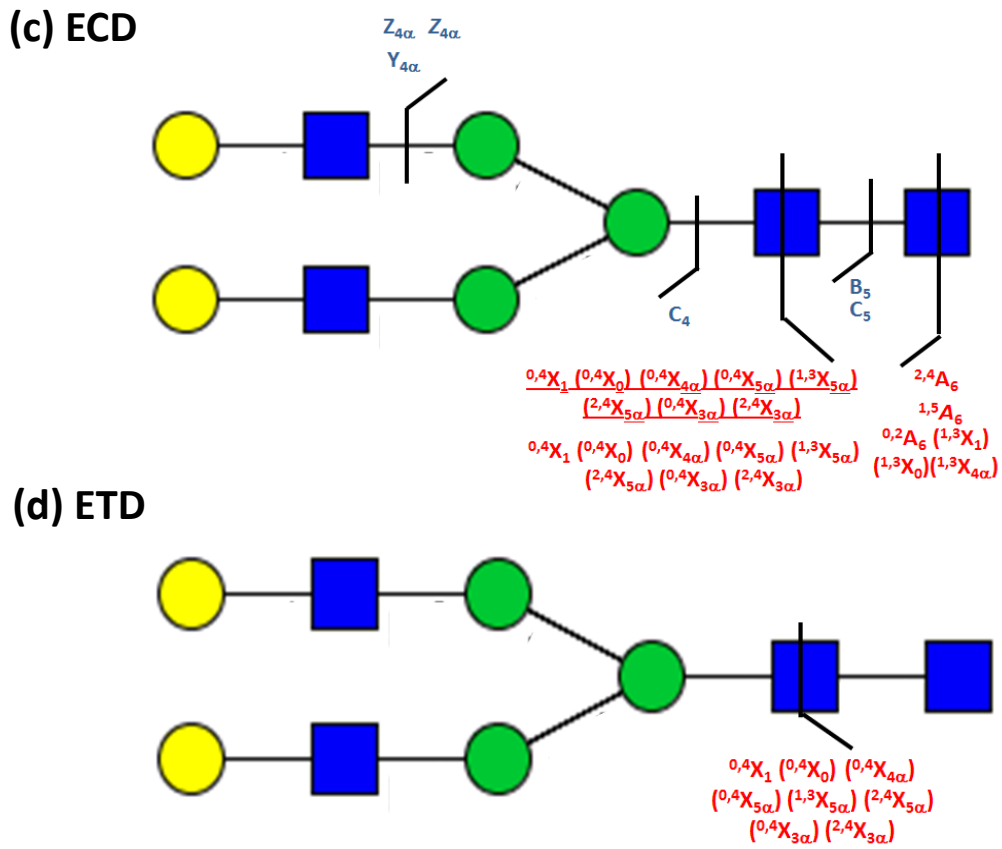

Figure 3.10 FT-ICR tandem mass spectra of doubly charged Ce-adducted NA2, $[NA2 + Ce - H]^{2+}$. (a) ECD (64 scans, 200 ms electron irradiation with a bias voltage of – 1.3 V); (b) ETD (64 scans, 600 ms reagent accumulation time and 100 ms reaction time). Underlined fragments are radical ions containing one additional, or one less, hydrogen atom than the corresponding even-electron fragment. Fragmentation patterns from ECD (c) and ETD (d). ν_3 = third harmonics.

Doubly charged Ce-adducted LNDFH was also generated by ESI with a higher abundance compared with NA2. This may be due to size effect. Ce is relatively a smaller metal ion, and LNDFH is smaller than NA2 as well. ECD and ETD fragmentation patterns for $[LNDFH + Ce – H]^{2+}$ are summarized in Table 3.4. The same number of cross-ring fragments were observed from ECD and ETD but ECD generated more glycosidic fragments than ETD.

Table 3.4 Product ions from ECD and ETD of doubly charged Ce-adducted LNDFH, $[LNDFH + Ce - H]^{2+}$. Underlined fragments are radical ions containing one additional, or one less, hydrogen atom than the corresponding even-electron fragment. Fragments in bold are unique to either ECD or ETD of the same precursor ions.

$[LNDFH + Ce - H]^{2+}$			
ECD		ETD	
Glycosidic (8)	Crossring (9)	Glycosidic (3)	Crossring (9)
$\underline{B_{3\alpha}}$ $\underline{Z_{3\alpha}}$ $\underline{C_{3\alpha}}$ $\underline{Y_{3\alpha}}$ $Z_{3\beta}$ (Z_4) - H_2O B_4 C_4 $Y_{3\beta}$ (Y_4)	$\underline{^{1,3}A_3}$ $\underline{^{0,2}X_2}$ $^{2,4}A_3$ - H_2O $\underline{^{2,4}A_3}$ $^{1,3}A_4$ $(^{2,4}A_4)$ $^{1,4}A_{4\alpha}$ $^{1,3}X_{3\alpha}$ $^{0,2}A_5$ $(^{0,2}X_{3\alpha})$ $^{0,4}X_2$ $(^{0,2}A_5)$ $(^{0,4}X_0)$ $(^{1,3}X_0)$ $(^{0,4}X_{3\alpha})$ $(^{2,4}X_{3\alpha})$ $(^{0,4}X_1)$	$\underline{C_{3\alpha}}$ $\underline{Y_{3\alpha}}$ $\underline{C_4}$	$^{1,3}A_4$ $(^{2,4}A_4)$ $\underline{^{1,4}A_{4\alpha}}$ $^{3,5}X_2$ $\underline{^{1,3}X_{3\alpha}}$ $^{0,2}A_5$ $(^{0,2}X_{3\alpha})$ $\underline{^{3,5}A_5}$ $^{3,5}X_{3\alpha}$ $(^{3,5}X_1)$ $\underline{^{0,4}X_2}$ $(^{0,2}A_5)$ $(^{0,4}X_0)$ $(^{1,3}X_0)$ $(^{0,4}X_{3\alpha})$ $(^{2,4}X_{3\alpha})$ $(^{0,4}X_1)$ $^{3,5}X_{3\beta}$ $(^{3,5}X_4)$

3.3.6 Isomer Differentiation by Trivalent Metal-Assisted ECD/ETD: The Case of LSTa, LSTb, and LSTc

We have previously shown (Chapter 2) that divalent metal adduction combined with ECD or ETD allows differentiation of the isomeric glycans LSTa, LSTb, and LSTc. ECD of Mg-adducted species was particularly powerful with much fewer fragments observed from ETD of the same species. The improved ECD and ETD shown above for trivalent metal adduction, even for doubly charged deprotonated precursors ions, suggests that improved isomer differentiation may be feasible via this approach, particularly by ETD. ECD and ETD fragmentation patterns of doubly charged deprotonated LSTa, $[LSTa + La - H]^{2+}$ and $[LSTa + Ce - H]^{2+}$, are shown in Figure 3.11. Similar to divalent metals, ECD produced more isomer-specific cross-ring fragments than ETD for the La-

adducted species: $^{2,5}A_2$, $^{1,4}A_2$, $^{1,5}A_2$, $\underline{^{1,3}A_3}$, $^{1,4}A_3$, $\underline{^{2,4}A3}$, $^{1,5}A_3$, $^{0,4}X_2$, $^{1,5}A_3$, and ($^{1,5}A_3 - H_2O$) versus $^{2,4}A_3$ and $^{0,2}A_3$ for ETD of the same species. ECD and ETD of $[LSTa + Ce - H]^{2+}$ both generated only one isomer-specific cross-ring fragment, $^{0,4}X_2$ in ECD, and the corresponding radical ions with one hydrogen atom less in ETD.

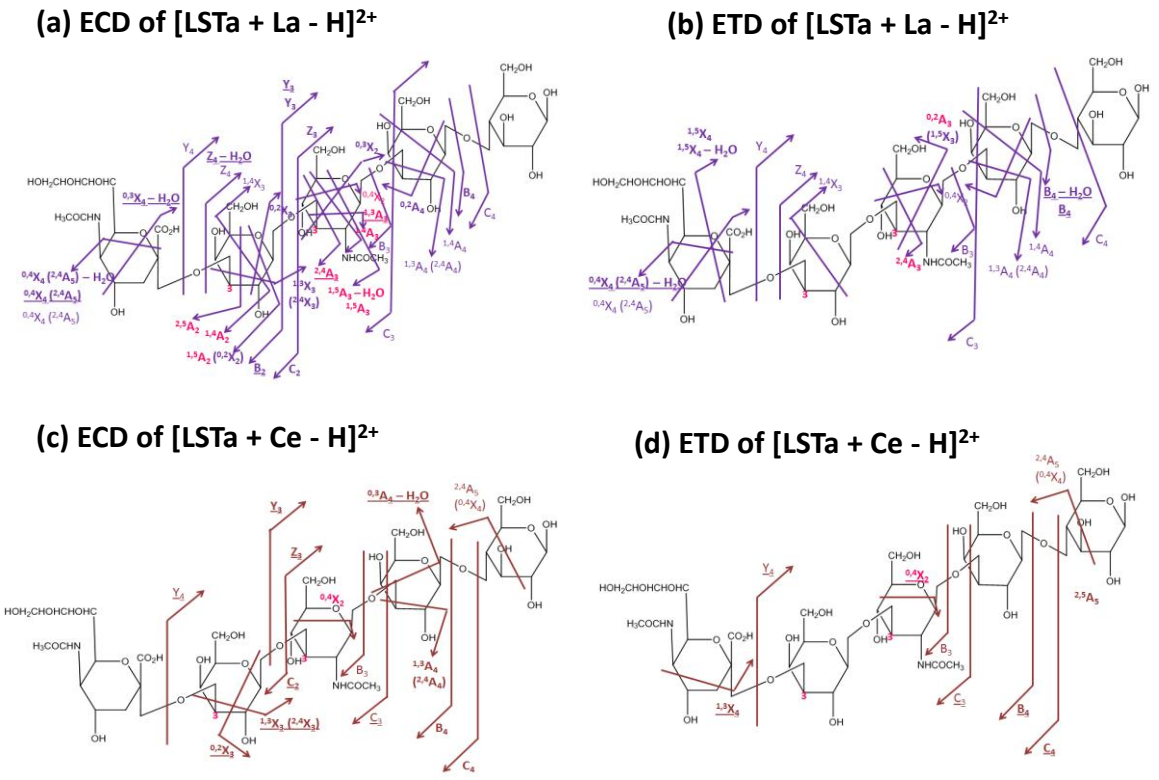

Figure 3.11 Fragmentation patterns from ECD and ETD of trivalent metal (La and Ce)-adducted doubly charged, deprotonated LSTa. (a) ECD of $[LSTa + La - H]^{2+}$; (b) ETD of $[LSTa + La - H]^{2+}$; (c) ECD of $[LSTa + Ce - H]^{2+}$; (d) ETD of $[LSTa + Ce - H]^{2+}$.

For LSTb, the isomer-diagnostic cross-ring fragments $^{0,4}X_2$, $^{3,5}A_2$, $^{2,5}A_2$, $^{0,3}X_2$ were identified in ECD of $[LSTb + La - H]^{2+}$, $^{3,5}X_{3\beta}$, $^{2,4}X_2$, $^{3,5}X_2$, $^{0,3}X_2$ were observed in ETD of $[LSTb + La - H]^{2+}$, $^{0,3}X_2$ and $\underline{^{0,4}X_2}$ were observed in ECD of $[LSTb + Ce - H]^{2+}$, and $^{0,3}X_2$ were observed in ETD of $[LSTb + Ce - H]^{2+}$ (see Figure 3.12).

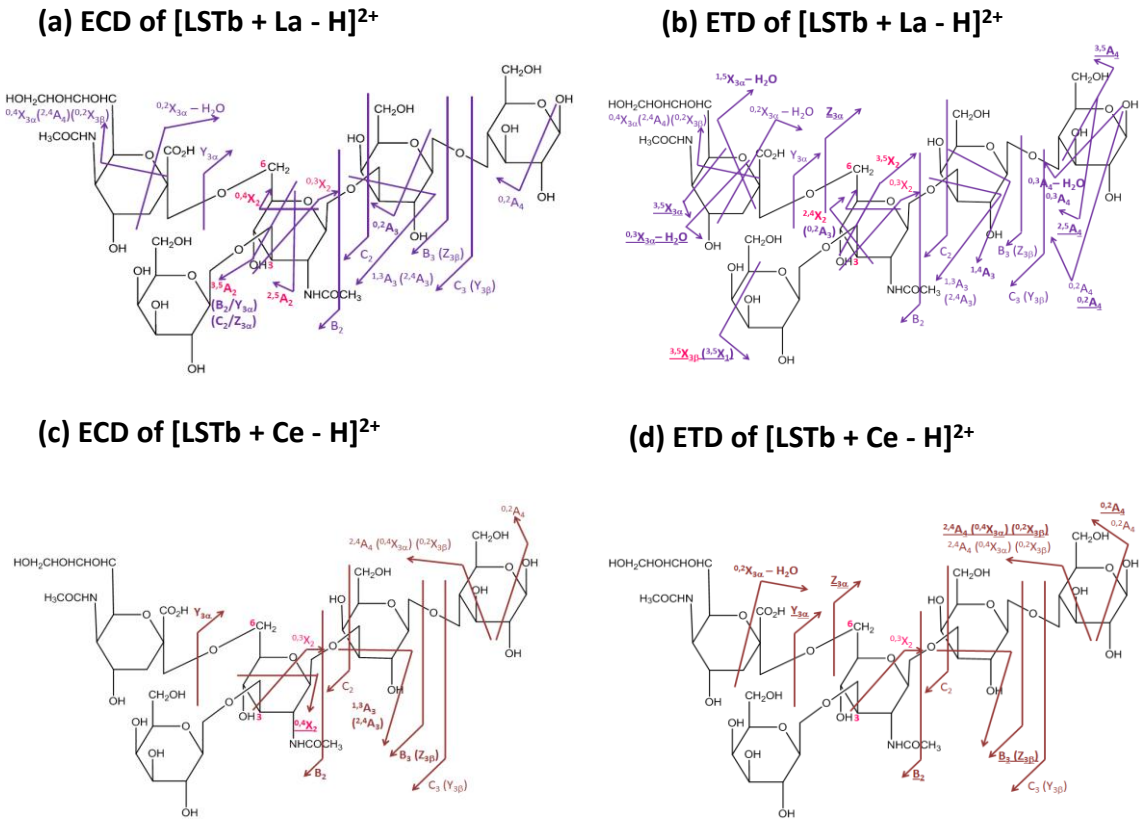

Figure 3.12 Fragmentation patterns from ECD and ETD of trivalent metal (La and Ce)-adducted doubly charged, deprotonated LSTb. (a) ECD of $[LSTb + La - H]^{2+}$; (b) ETD of $[LSTb + La - H]^{2+}$; (c) ECD of $[LSTb + Ce - H]^{2+}$; (d) ETD of $[LSTb + Ce - H]^{2+}$.

For LSTc, as shown in Figure 3.13, La adduction yielded the isomer-diagnostic cross-ring fragments $^{0,2}A_3$, 3,5A3, $^{0,3}A_3$, $^{1,5}A_3$, $^{0,4}X_2$, $^{2,4}A_3$, $^{2,5}A_2$, and $^{2,5}A_3$ from ECD, whereas the additional $\underline{^{0,4}X_2}$, ($^{1,4}X_3 - H_2O$), ($^{1,3}X_2 - H_2O$), and $\underline{^{1,3}X_2}$ diagnostic ions were generated by ETD of the same precursor ions, $[LSTc + La - H]^{2+}$. Ce adduction generated $^{0,2}A_3$, $\underline{^{3,5}A_3}$, $^{2,4}A_3$, and $^{0,4}X_2$ from ECD and $\underline{^{3,5}A_2}$, ($\underline{^{1,4}X_3 - H_2O}$), $\underline{^{0,4}X_2}$, $^{1,3}X_2$, [$^{1,3}X_2$ ($^{2,4}X_4$) – H_2O] from ETD.

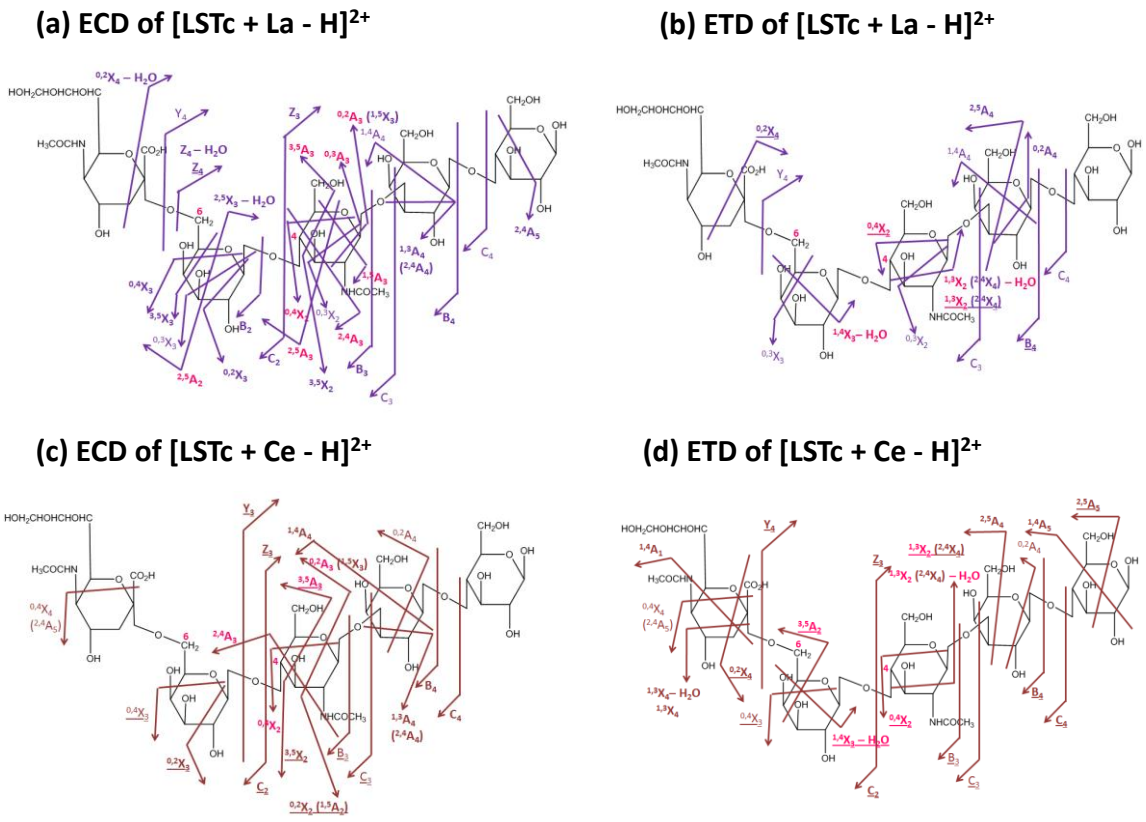

Figure 3.13 Fragmentation patterns from ECD and ETD of trivalent metal (La and Ce)-adducted doubly charged, deprotonated LSTc. (a) ECD of $[LSTc + La - H]^{2+}$; (b) ETD of $[LSTc + La - H]^{2+}$; (c) ECD of $[LSTc + Ce - H]^{2+}$; (d) ETD of $[LSTc + Ce - H]^{2+}$.

Isomer-diagnostic fragments from ECD and ETD of Mg, Co, Ca, La, and Ce-adducted LSTa/LTSb/LSTc are summarized in Table 3.5 (divalent metal data from Chapter 2). In general, trivalent metal adduction yielded more critical cross-ring cleavages for isomer differentiation. La adduction, in particular, demonstrated advantageous fragmentation in both ECD and ETD although ECD typically generated more diagnostic cross-ring cleavages than ETD.

Table 3.5 Summary of diagnostic cross-ring fragments for isomer differentiation generated from metal-assisted ECD and ETD of underivatized LSTa, LSTb, and LSTc. Underlined fragments are radical ions containing one additional, or one less, hydrogen atom than the corresponding even-electron fragment. Fragments in bold are unique to either ECD or ETD of the same precursor ions.

Metal	MS/MS	LSTa	LSTb	LSTc
Mg	ECD	$^{1,5}A_2$, $^{2,4}A_3 - H_2O$, $^{2,4}A_3$, $^{0,4}X_2$	$^{0,2}X_{3\beta}$, $^{2,4}X_2$, $^{3,5}X_2$, $^{0,3}X_2$, $^{0,4}X_2$, $^{1,4}A_2 - H_2O$, $^{1,4}A_2$, $^{0,3}A_2$, $^{3,5}A_2$	$\underline{^{2,4}A_3 - H_2O}$, $^{3,5}A_2$, $^{0,2}A_2$, $^{2,4}A_3$, $^{2,5}A_3 - H_2O$, $\underline{^{1,3}X_2}$, $^{0,3}A_3$, $^{0,4}X_2$, $^{0,2}A_3$
	ETD	$^{0,4}X_2$	$^{3,5}X_2$, $^{0,3}X_2$, $^{0,4}X_2$, $^{1,4}X_2 - H_2O\ (H)^+$, $^{2,5}X_{3\beta}$, $^{0,2}X_{3\beta}$, $^{0,2}X_{3\beta} - H_2O\ (H)^+$	$^{0,4}X_2$
Co	ECD	$^{0,4}X_2 - H_2O$, $^{0,4}X_2$, $^{1,5}A_2$, $\underline{^{2,4}A_3}$	$^{3,5}X_2$, $^{0,4}X_2$, $^{3,5}A_2$, $\underline{^{3,5}A_2}$, $^{1,4}A_2$	$\underline{^{3,5}A_2}$, $^{0,2}A_3$, $^{0,2}A_2$, $^{0,4}X_2$, $^{2,4}A_3$, $\underline{^{2,4}A_3} - H_2O$, $^{1,4}A_3$
	ETD		$^{0,4}X_2$	$^{1,3}X_2 - H_2O$, $^{3,5}A_2\ (H^+)$, $^{3,5}A_2$
Ca	ECD	$^{0,4}X_2 - H_2O$, $^{0,4}X_2$, $^{1,5}A_2$	$^{0,4}X_2$, $^{0,3}X_2$, $^{1,4}X_2 - H_2O$	$^{3,5}A_3$, $\underline{^{0,2}A_3}$, $^{0,2}A_3$, $\underline{^{1,3}X_2}$, $^{1,5}A_3$, $^{0,3}A_3 - H_2O$, $^{0,3}A_3$, $^{0,4}X_2$, $^{2,4}A_3$, $^{2,5}A_3$
	ETD			
La	ECD	$^{2,5}A_2$, $^{1,4}A_2$, $^{1,5}A_2$, $\underline{^{1,3}A_3}$, $^{1,4}A_3$, $\underline{^{2,4}A_3}$, $^{1,5}A_3$, $^{0,4}X_2$, $^{1,5}A_3$, $^{1,5}A_3 - H_2O$	$^{0,4}X_2$, $^{3,5}A_2$, $^{2,5}A_2$, $^{0,3}X_2$	$^{0,2}A_3$, $^{3,5}A_3$, $^{0,3}A_3$, $^{1,5}A_3$, $^{0,4}X_2$, $^{2,4}A_3$, $^{2,5}A_2$, $^{2,5}A_3$
	ETD	$^{2,4}A_3$, $^{0,2}A_3$	$\underline{^{3,5}X_{3\beta}}$, $^{2,4}X_2$, $^{3,5}X_2$, $^{0,3}X_2$	$\underline{^{0,4}X_2}$, $^{1,4}X_3 - H_2O$, $^{1,3}X_2 - H_2O$, $\underline{^{1,3}X_2}$
Ce	ECD	$^{0,4}X_2$	$^{0,3}X_2$, $\underline{^{0,4}X_2}$	$^{0,2}A_3$, $\underline{^{3,5}A_3}$, $^{2,4}A_3$, $^{0,4}X_2$
	ETD	$\underline{^{0,4}X_2}$	$^{0,3}X_2$	$\underline{^{3,5}A_2}$, $\underline{^{1,4}X_3 - H_2O}$, $\underline{^{0,4}X_2}$, $\underline{^{1,3}X_2}$, $^{1,3}X_2\ (^{2,4}X_4) - H_2O$

3.4 Discussion

A summary of ECD and ETD fragmentation outcomes for divalent (Chapter 2) and trivalent metal-adducted NA2 is shown in Table 3.6. Triply charged trivalent metal-adducted NA2 showed significantly enhanced fragmentation in both ECD and ETD compared with the same but doubly charged, deprotonated species, and with doubly charged species from divalent metal adduction with a much more dramatic charge state dependence in ETD than in ECD. Higher charge states have higher electron affinity and typically have more unfolded gas-phase structures due to Coulomb repulsion. The more unfolded gas-phase structures for triply charged ions eliminate the difference in fragmentation efficiency observed between ECD and ETD of doubly charged ions

(Chapter 2), presumably due to limited intramolecular non-covalent interactions and thus additional activation to disrupt such interactions is not required.

The presence of trivalent metals (particularly La and Al) was beneficial also for overall doubly charged precursor ions For example, for La-adducted deprotonated NA2, although at the same charge state as Mg- or Ca-adducted NA2, ECD/ETD of [NA2 + La – H]2+ yielded five cross-ring fragments that were not observed in either ECD or ETD of $[NA2 + Mg]^{2+}$, $[NA2 + Ca]^{2+}$, or $[NA2 + Co]^{2+}$.

Table 3.6 Summary of ECD and ETD fragmentation outcomes for Mg (II)-, Ca (II)-, Ce (III)-, Al (III)-, and La (III)-adducted NA2.

Charge Carrier	Charge State	ECD	ETD
Mg	2	6 glycosidic, 13 cross-ring	3 glycosidic, 6 cross-ring
Ca	2	4 glycosidic, 5 cross-ring	1 glycosidic, 1 cross-ring
Ce – H	2	6 glycosidic, 5 cross-ring	0 glycosidic, 1 cross-ring
La – H	2	4 glycosidic, 11 cross-ring	0 glycosidic, 0 cross-ring
Al	3	16 glycosidic, 5 cross-ring	19 glycosidic, 14 cross-ring
La	3	16 glycosidic, 13 cross-ring	12 glycosidic, 18 cross-ring

ECD and ETD fragmentation efficiencies for all metal-NA2 complexes were calculated and are summarized in Table 3.7. As expected, triply charged precursor ions result in higher fragmentation efficiencies than doubly charged precursor ions, even for the same metal charge carrier.

Table 3.7 Fragmentation efficiencies of NA2-metal complexes.

Charge Carrier	Charge State	ECD	ETD
Mg	2	16%	2%
Ca	2	6%	4%
Ce – H	2	10%	3%
La – H	2	13%	1%
Al	3	36%	22%
La	3	20%	30%

As discussed in Chapter 2 and the previous literature,[20-22, 31] electron-metal recombination energy likely affects ECD and ETD outcome because it determines the energy release upon electron capture or transfer, thus contributing to further excitation and fragmentation. For trivalent metals, the third ionization energy (IE3) is of interest rather than IE2, which has been examined for divalent metals.[31-33] However, triply-charged Al (IE3 = 28.45 eV)-adducted NA2 showed the highest fragmentation efficiency in ECD (36%) whereas triply-charged La (IE3 = 19.18 eV)-adducted NA2 fragmented most efficiently in ETD (30% fragmentation efficiency), thus indicating a more complex mechanism.

Gas-phase structures of precursor ions have been previously proposed to greatly influence ECD outcome. In particular, it has been proposed that a diversity of structures is necessary for extensive sequence coverage in peptides/proteins.[33-35] To further explore this hypothesis, we performed traveling wave ion mobility mass spectrometry of several metal-glycan complexes (see Figure 3.14). Multiple drift times were observed for triply-charged La-adducted NA2 and two major drift times for the corresponding doubly-

charged species. Triply charged aluminum complexes were not observed in these experiments (performed with a different instrument than ECD/ETD). For divalent metals, NA2 complexes with the divalent metals Ca, Co, and Mg showed only one drift time. For divalent metal-adducted LNDFH, Co and Mg complexes also showed two drift times while the Ca complex only showed one drift time. These data corroborate previous suggestions that both metal-electron recombination energy and gas-phase structures of metal complexes determine ECD/ETD outcomes.

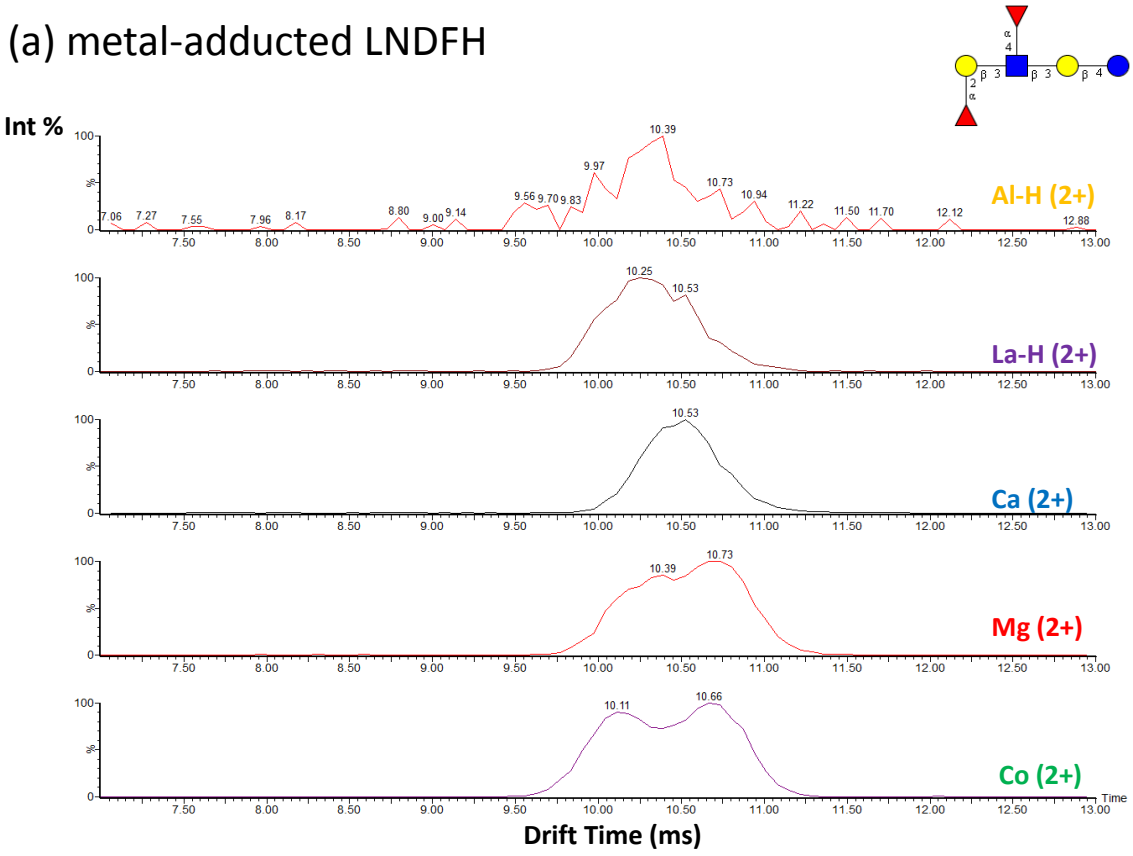

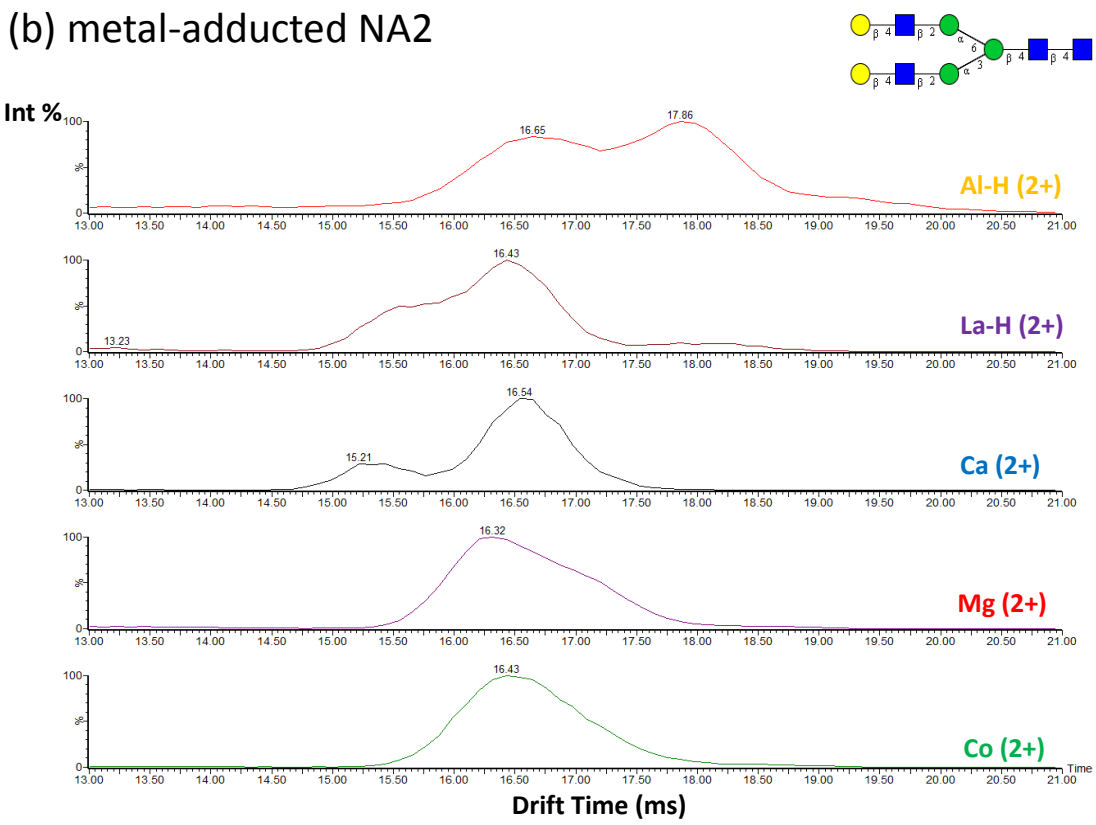

Figure 3.14 Drift times of divalent metal (Co, Mg, Ca) and trivalent metal (La, Al) adducted LNDFH and NA2. (a) metal-adducted LNDFH; (b) metal-adducted NA2.

3.5 Conclusions

In this chapter, trivalent metals were used for the first time to generate triply charged glycan complexes, resulting in improved ECD and ETD compared with doubly charged precursor ions from divalent metal adduction, or with doubly charged deprotonated precursor ions with the same trivalent metal charge carrier. The latter precursor ion type also showed unique fragmentation pathways compared with doubly charged divalent metal-adducted glycans, thus providing complementary structural information.

The mechanism of metal assisted ECD/ETD likely involves both the electron-metal recombination energy (which is related to the ionization energy of the metal ion) and the gas-phase structural diversity of glycan-metal complexes. Metals with a higher IE will release more energy and thus assist in generating more varieties of fragments. More structural populations of glycan-metal complexes presumably enable more fragmentation channels.

ECD/ETD of trivalent metal-adducted underivatized glycans is valuable for isomer differentiation. Even at the same charge state, trivalent metal adduction produces more cross-ring fragments than divalent metal adduction. In particular, for doubly charged precursors ions La and Ce adduction generated many more critical fragments than divalent metals. The superior advantage of trivalent metal in improving fragmentation efficiency and generating more fragments may be attributed to both the metal ionization energy and multiple populations of gas-phase structures.

3.6 Bibliography

(1) Brockhausen, I.; Schutzbach, J.; Kuhns, W. Glycoproteins and Their Relationship to Human Disease. *Acta Anato.* **1998**, *161*, 36-78.

(2) Dall'Olio, F.; Malagolini, N.; Trinchera, M.; Chiricolo, M. Mechanisms of Cancer-Associated Glycosylation Changes. *Frontiers in Bioscience-Landmark* **2012**, *17*, 670-699.

(3) Rasmussen, S.; Rapraeger, A. Altered Structure of the Hybrid Cell-Surface Proteoglycan of Mammary Epithelial-Cells in Response to Transforming Growth Factor-Beta. *J. Cell Biol.* **1988**, *107*, 1959-1967.

(4) Nagae, M.; Yamaguchi, Y. Function and 3D Structure of the N-Glycans on Glycoproteins. *Int. J. Mol. Sci.* **2012**, *13*, 8398-8429.

(5) Dwek, M. V.; Brooks, S. A. Harnessing Changes in Cellular Glycosylation in New Cancer Treatment Strategies. *Curr. Cancer Drug Tar.* **2004**, *4*, 425-442.

(6) Fuster, M. M.; Esko, J. D. The Sweet and Sour of Cancer: Glycans as Novel Therapeutic Targets. *Nat. Rev. Cancer* **2005**, *5*, 526-542.

(7) Lepenies, B.; Seeberger, P. H. The Promise of Glycomics, Glycan Arrays and Carbohydrate-Based Vaccines. *Immunopharm. Immunot.* **2010**, *32*, 196-207.

(8) Bernardes, G. J. L.; Castagner, B.; Seeberger, P. H. Combined Approaches to the Synthesis and Study of Glycoproteins. *ACS Chem. Biol.* **2009**, *4*, 703-713.

(9) Seeberger, P. H.; Werz, D. B. Synthesis and Medical Applications of Oligosaccharides. *Nature* **2007**, *446*, 1046-1051.

(10) Zaia, J. Mass Spectrometry and Glycomics. *OMICS* **2010**, *14*, 401-418.

(11) Zhou, W.; Hakansson, K. Structural Characterization of Carbohydrates by Fourier Transform Tandem Mass Spectrometry. *Curr. Proteomics* **2011**, *8*, 297-308.

(12) Zaia, J. Mass Spectrometry of Oligosaccharides. *Mass Spectrom. Rev.* **2004**, *23*, 161-227.

(13) Zhao, C.; Xie, B.; Chan, S. Y.; Costello, C. E.; O'Connor, P. B. Collisionally Activated Dissociation and Electron Capture Dissociation Provide Complementary Structural Information for Branched Permethylated Oligosaccharides. *J. Am. Soc. Mass. Spectrom.* **2008**, *19*, 138-150.

(14) Han, L.; Costello, C. Electron Transfer Dissociation of Milk Oligosaccharides. *J. Am. Soc. Mass. Spectrom.* **2011**, *22*, 997-1013.

(15) Halim, A.; Ruetschi, U.; Larson, G.; Nilsson, J. LC-MS/MS Characterization of O-Glycosylation Sites and Glycan Structures of Human Cerebrospinal Fluid Glycoproteins. *J. Proteome Res.* **2013**, *12*, 573-584.

(16) Kalli, A.; Hakansson, K. Electron Capture Dissociation of Highly Charged Proteolytic Peptides from Lys N, Lys C and Glu C Digestion. *Mol. Biosyst.* **2010**, *6*, 1668-1681.

(17) Liu, J.; McLuckey, S. A. Electron Transfer Dissociation: Effects of Cation Charge State on Product Partitioning in Ion/Ion Electron Transfer to Multiply Protonated Polypeptides. *Int. J. Mass spectrom.* **2012**, *330*, 174-181.

(18) Zubarev, R. A.; Haselmann, K. F.; Budnik, B.; Kjeldsen, F.; Jensen, F. Towards An Understanding of the Mechanism of Electron-Capture Dissociation: A Historical Perspective and Modern Ideas. *Eur. J. Mass Spectrom.* **2002**, *8*, 337-349.

(19) Good, D. M.; Wirtala, M.; McAlister, G. C.; Coon, J. J. Performance Characteristics of Electron Transfer Dissociation Mass Spectrometry. *Mol. Cell. Proteomics* **2007**, *6*, 1942-1951.

(20) Iavarone, A. T.; Paech, K.; Williams, E. R. Effects of Charge State and Cationizing Agent on the Electron Capture Dissociation of a Peptide. *Anal. Chem.* **2004**, *76*, 2231-2238.

(21) Chen, X.; Chan, W. Y. K.; Wong, P. S.; Yeung, H. S.; Chan, T. W. D. Formation of Peptide Radical Cations ($M^{+\cdot}$) in Electron Capture Dissociation of Peptides Adducted with Group IIB Metal Ions. *J. Am. Soc. Mass. Spectrom.* **2011**, *22*, 233-244.

(22) Liu, H.; Håkansson, K. Electron Capture Dissociation of Divalent Metal-Adducted Sulfated Oligosaccharides. *Int. J. Mass spectrom.* **2011**, *305*, 170-177.

(23) Liu, H.; Håkansson, K. Electron Capture Dissociation of Tyrosine *O*-Sulfated Peptides Complexed with Divalent Metal Cations. *Anal. Chem.* **2006**, *78*, 7570-7576.

(24) Adamson, J. T.; Håkansson, K. Electron Capture Dissociation of Oligosaccharides Ionized with Alkali, Alkaline Earth, and Transition Metals. *Anal. Chem.* **2007**, *79*, 2901-2910.

(25) Eva Fung, Y. M.; Liu, H.; Chan, T. W. D. Electron Capture Dissociation of Peptides Metalated with Alkaline-Earth Metal Ions. *J. Am. Soc. Mass. Spectrom.* **2006**, *17*, 757-771.

(26) Zhou, W.; Hakansson, K. Electron Capture Dissociation of Divalent Metal-adducted Sulfonated *N*-Glycans Released from Bovine Thyroid Stimulating Hormone. *J. Am. Soc. Mass. Spectrom.* **2013**, Accepted.

(27) Flick, T. G.; Williams, E. R. Supercharging with Trivalent Metal Ions in Native Mass Spectrometry. *J. Am. Soc. Mass. Spectrom.* **2012**, *23*, 1885-1895.

(28) Flick, T. G.; Donald, W. A.; Williams, E. R. Electron Capture Dissociation of Trivalent Metal Ion-Peptide Complexes. *J. Am. Soc. Mass. Spectrom.* **2013**, *24*, 193-201.

(29) Liu, H. C.; Hakansson, K.; Lee, J. Y.; Sherman, D. H. Collision-Activated Dissociation, Infrared Multiphoton Dissociation, and Electron Capture Dissociation of the Bacillus Anthracis Siderophore Petrobactin and Its Metal Ion Complexes. *J. Am. Soc. Mass. Spectrom.* **2007**, *18*, 842-849.

(30) Ceroni, A.; Maass, K.; Geyer, H.; Geyer, R.; Dell, A.; Haslam, S. M. GlycoWorkbench: A Tool for the Computer-Assisted Annotation of Mass Spectra of Glycans. *J. Proteome Res.* **2008**, *7*, 1650-1659.

(31) Chen, X.; Fung, Y.; Chan, W.; Wong, P.; Yeung, H.; Chan, T. W. Transition Metal Ions: Charge Carriers that Mediate the Electron Capture Dissociation Pathways of Peptides. *J. Am. Soc. Mass. Spectrom.* **2011**, *22*, 2232-2245.

(32) Leib, R. D.; Donald, W. A.; Bush, M. F.; O'Brien, J. T.; Williams, E. R. Internal Energy Deposition in Electron Capture Dissociation Measured Using Hydrated Divalent Metal Ions as Nanocalorimeters. *J. Am. Chem. Soc.* **2007**, *129*, 4894-4895.

(33) Liu, H.; Håkansson, K. Divalent Metal Ion-Peptide Interactions Probed by Electron Capture Dissociation of Trications. *J. Am. Soc. Mass. Spectrom.* **2006**, *17*, 1731-1741.

(34) Mihalca, R.; Kleinnijenhuis, A. J.; McDonnell, L. A.; Heck, A. J. R.; Heeren, R. M. A. Electron Capture Dissociation at Low Temperatures Reveals Selective Dissociations. *J. Am. Soc. Mass. Spectrom.* **2004**, *15*, 1869-1873.

(35) Robinson, E. W.; Leib, R. D.; Williams, E. R. The Role of Conformation on Electron Capture Dissociation of Ubiquitin. *J. Am. Soc. Mass. Spectrom.* **2006**, *17*, 1470-1480.

Chapter 4 Electron Induced Dissociation (EID) of Singly Protonated Glycans With and Without Aromatic Labels

4.1 Introduction

Glycosylation is one of the most ubiquitous forms of protein post-translational modification (PTM) and plays important roles in many key biological processes such as protein folding, self/nonself recognition, metastasis, cell adhesion, receptor activation, signal transmission, molecular trafficking and clearance.[1, 2] Glycans covalently attached to proteins are often significantly changed with onset of cancer and inflammation in various ways such as increased glycan branching, increased or decreased levels of glycosylation, elevated levels of sialic acids, or altered sulfonation.[3] Although the causes are not well understood, these disease-related alterations are thought to affect growth, adhesion, differentiation, transformation, progression, metastasis, and immune surveillance of cancer cells.[2, 4, 5] Therefore, detailed glycan structural information will facilitate further understanding of cellular function as well as disease.

On the other hand, the structural complexity of glycans is much larger than that of proteins due to the nature and order of constituent monosaccharides, position of glycosidic linkages, degree of branching, stereochemistry, isomers, modifications (sulfonation, phosphorylation, acylation, etc), and conjugation to proteins and other biomolecules. All these challenges have resulted in carbohydrates being less explored than other major classes of biomolecules such as proteins and nucleic acids. ^{1}H- and ^{13}C-

nuclear magnetic resonance (NMR) spectroscopy[6, 7] and X-ray crystallography[8, 9] have been used to elucidate structural information for glycans and their complexes. However, the requirement of relatively large amounts of sample or formation of crystals, respectively, has limited the application of these techniques. Chromatography is known for its high reproducibility and sensitivity (particularly when coupled with fluorescence detection) but standards are required and thus it is difficult to identify unknown structures.[10] Mass spectrometry (MS) is more sensitive than NMR spectroscopy and X-ray crystallography, and more selective than chromatography.[10, 11] Fourier transform ion cyclotron resonance (FT-ICR) MS is well known for its high mass accuracy and high resolution, and its compatibility with many tandem mass spectrometry (MS/MS) fragmentation techniques,[12] thus potentially it can be a powerful analytical platform for structural characterization of glycans.

MS ionization methods for biomolecules include fast atom bombardment (FAB), matrix-assisted laser desorption/ionization (MALDI), and electrospray ionization (ESI). FAB is much more energetic and less sensitive than MALDI and ESI, and is therefore currently used infrequently for glycan analysis.[13] At present, MALDI is the most used ionization method for MS analysis of glycans. Advantages of MALDI include convenience, high sensitivity, and tolerance to buffers and detergents. Sialic acid stabilization is an important problem and can be solved by chemical derivatization, such as permethylation.[11] However, this approach is challenging for low sample amounts (such as cell subpopulations, e.g., cancer stem cells) due to incomplete reactions, side reactions, and losses in the derivatization and the following clean-up process. On the other hand, ESI is an extremely soft ionization method in which sample solution is

sprayed through a needle supplied with an appropriate electrical potential (3-6 kV) to form singly or multiply charged gas-phase ions. In addition, because of its liquid-based nature, ESI is directly compatible with liquid chromatography in contrast to MALDI.

Following ionization, gas-phase fragmentation of glycans via MS/MS can generate extensive structural information through specific bond cleavages and unique fragmentation pathways. Most glycan tandem mass spectra are still generated by collision activated dissociation (CAD) in which selected precursor ions are activated by inelastic collisions with inert gas. CAD has the advantages of high fragmentation efficiency and wide availability.[12,14] In CAD, vibrational energy is increased and distributed over all vibrational degrees of freedom, thus preferentially cleaving the weakest chemical bonds. Infrared multiphoton dissociation (IRMPD) is also used in glycan structural analysis, although not as widely as CAD.[12, 15, 16] These two "slow heating" techniques generally result in predominant glycosidic bond cleavages (B, Y, C, Z-type fragments as defined by Domon and Costello[17]) for protonated glycans;[17, 18] however, in order to gain more detailed structural information such as glycan branch positions and specific linkages, cross-ring cleavages (A and X-type fragments[17]) are highly needed. Two available CAD based strategies to increase cross-ring cleavages are high energy CAD[19, 20] and metal ligation of oligosaccharides combined with CAD.[21, 22] However, high energy CAD involves extensive ion scattering (causing signal loss) and generally produces complex spectra in which glycosidic cleavages can be much more prevalent than cross-ring cleavages.[23] Negative ion mode MS/MS can be advantageous for acidic (e.g., sialylated, sulfonated, or phosphorylated) carbohydrates due to higher ionization efficiency for such species. In addition, negative ion mode CAD has been

reported to generate less in-source fragmentation,[24] and less internal but more diagnostic cleavages with the use of appropriate adducts such as nitrate and chloride.[25-28]

Our group has shown that electron capture dissociation (ECD) of metal-adducted underivatized oligosaccharides produces complementary fragmentation patterns compared with CAD and IRMPD of the same species, thus demonstrating utility of ECD for glycan structural analysis.[29] O'Connor and co-workers have also shown that "hot" ECD of permethylated glycans is highly complementary to CAD of the same species.[30] Other activation methods, including postsource decay (PSD),[31] electron detachment dissociation (EDD),[32-34] electron transfer dissociation (ETD),[35] and ultraviolet photodissociation (UVPD) at 157 nm,[36] 193 nm,[37] or 355 nm,[38] have all been reported for structural determination of glycans.

However, in spite of all these exciting achievements, challenges and limitations still remain in the area of mass spectrometry-based structural characterization of glycans. For example, desirable cross-ring cleavages that are crucial for identification of branching and linkage are elusive with conventional MS/MS techniques such as positive ion mode CAD. Migration/rearrangement of monosaccharide residues has also been reported in CAD MS/MS of glycans, thus yielding false structural information.[39, 40] On the other hand, more structurally informative activation methods such as ECD, EDD and ETD require multiply charged precursor ions, but glycans are typically more difficult to multiply ionize than, e.g., peptides due to lack of acidic or basic sites. Data interpretation for these ion-electron or ion-ion activation methods is also complex and tedious. In addition, the low fragmentation efficiency in ECD, EDD and ETD can pose a problem. Therefore, alternative MS/MS activation techniques are still in high need for generating

more informative fragments, particularly for singly charged glycan cations, which are frequently the most abundant species observed in both ESI and MALDI of glycans.

Electron induced dissociation (EID) has been shown to generate complementary fragmentation patterns compared with CAD for, e.g., metabolite anions,[41] peptide cations[42-44] and anions,[45] amino acids,[42] polycationic chitooligosaccharides,[46] glycosaminoglycans (GAGs),[47] polyketides,[48] biomolecule-metal complexes,[49, 50] and organic cations.[51] EID involves irradiation of singly (or multiply) charged cations or anions with >10 eV electrons and was first applied to oligosaccharides by Aberth and Burlingame in 1990.[52] More recently, Budnik et al applied EID with 10-13 eV electrons to several chitooligosaccharides in the forms $[M + 2H]^{2+}$, $[M + Na]^{+}$, and $[M + H]^{+}$. Diverse product ions, including several ^{1,5}X-type fragments, were observed following EID without ionization or electron capture.[46] Amster and co-workers performed EID of singly deprotonated GAGs to differentiate fragmentation pathways involving radical-driven dissociation and electronic/vibrational excitation in EDD of the same molecules.[47] EID is generally believed to involve both vibrational and electronic excitation without ionization (which would form neutral for anions). Costello, Lin and co-workers[53] have proposed an alternative mechanism, involving ionization followed by recapture of a low energy electron, i.e., electronic excitation dissociation (EED),[54] for activation of metal-adducted permethylated glycans following irradiation with >10 eV electrons. Here, EID is applied to singly protonated non-permethylated glycan cations with and without aromatic labels to yield valuable structural information. Some mechanistic insight into EID is also gained from investigating the effect of common fluorescent labels.

4.2 Experimental Section

4.2.1 Sample Preparation

Lacto-N-difucohexaose I (LNDFH I), lacto-N-fucopentaose (LNFP I), p-Lacto-N-hexaose (pLNH), lacto-N-hexaose (LNH), LS-tetrasaccharide B (LSTb), and an asialo galactosylated, biantennary glycan (NA2) (all from V-Labs, Inc., Covington, LA) were either used without fluorescent labeling or labeled with 9-aminofluorene (9FL), 2-amino benzamide (2AB), or 2-anthranilic acid (2AA) (all labels from Sigma-Aldrich, St. Louis, MO, see structures in Scheme 1.1) according to protocols adapted from previous literature[55, 56] as briefly outlined below. All chemicals for the labeling reactions were purchased from Sigma-Aldrich (St. Louis, MO).

4.2.2 9FL Labeling of Glycans

400 nmol 9-aminofluorene hydrochloride was dissolved in 200 μL deionized water, to which 400 nmol $NaHCO_3$ was added followed by incubation at room temperature for ten minutes. The resulting suspension was dried under vacuum and re-dissolved in 100 μL methanol. 0.05 mmol $NaCNBH_3$ and 5 μL glacial acetic acid were then added into the solution and this reagent was immediately added to the glycan solution (200 nmol glycan in 50 μL deionized water) followed by incubation in a water bath at 80 ℃ for 2 hours. The cooled solution was dried under vacuum and redissolved in 100 μL deionized water for subsequent desalting.

4.2.3 2AA Labeling of Glycans

Two nmol oligosaccharide was dissolved in 60 μL 2-AA labeling reagent (30 mg 2AA, 20 mg sodium cyanoborohydride, 20 mg boric acid, and 40 mg sodium acetate dissolved in 1 mL MeOH) and incubated in a water bath at 80 ℃ for 1 hour.

4.2.4 2AB Labeling of Glycans

Two nmol oligosaccharide was dissolved in 60 μL 2-AB labeling reagent (0.35 M 2AB, 1 M sodium cyanoborohydride in 30% glacial acetic acid, 70% DMSO (v/v)) and incubated in a water bath at 65 ℃ for 2 hours.

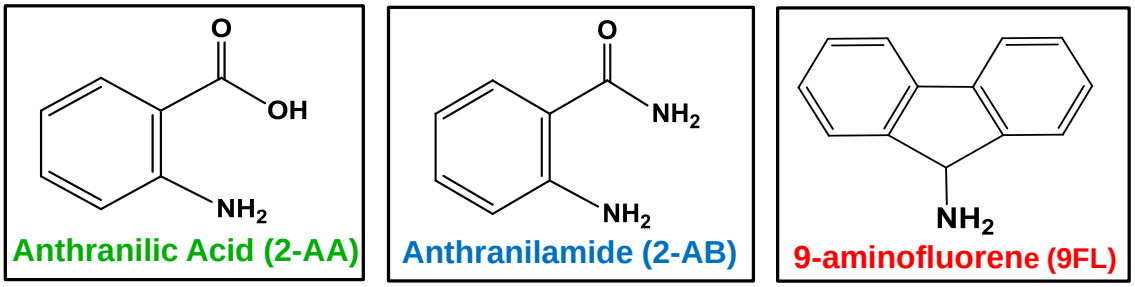

Scheme 4.1 Structures of 2-anthranilic acid (2AA), 2-amino benzamide (2AB), and 9-aminofluorene (9FL).

4.2.5 Desalting of Labeled Glycans

After derivatization, labeled glycans were cleaned up with SPE graphitized carbon column (Alltech). Columns were first equilibrated with 80% ACN, 0.1% formic acid (3 mL), and then washed stepwise with H_2O (3 mL). Sample solution was then slowly loaded onto the equilibrated and washed cartridge. After washing with 3-5 mL H_2O, 9FL- or 2AB- or 2AA- labeled glycans were eluted with 40% ACN, 0.1% formic acid, and 60% ACN, 0.1% formic acid stepwise, and then dried down under SpeedVac.

2AB- or 2AA-labeled glycans mostly elute with 40% ACN, 0.1% formic acid. 9FL-labeled glycans mostly elute with 60% ACN, 0.1% formic acid.

4.2.6 Fourier Transform Ion Cyclotron Resonance Mass Spectrometry

After desalting with SPE graphitized carbon columns (Alltech, Nicholasville, KY), labeled glycans were dried under vacuum and reconstituted in spray solution (50:50 methanol:H_2O, 0.5% formic acid) for analysis in positive ion mode. Singly protonated glycans, $[M + H]^+$, were generated by external electrospray ionization (ESI) at 70 μL/h (Apollo II dual-stage ion funnel ion source, Bruker Daltonics, Billerica, MA). All experiments were performed on a 7 Tesla quadrupole-FT-ICR mass spectrometer (APEX-Q, Bruker Daltonics, Billerica, MA). A heating current of 1.8 A was applied to the cathode. EID was performed inside the ICR cell with a cathode bias voltage of - 11 to - 21 V for 0.3 - 0.5 s. CAD was performed in the collision cell at a collision voltage of - 5.5 to - 35 V. Mass spectra were acquired with 512k data points and summed over 64 or 100 scans for EID and 32 or 64 scans for CAD (depending on the abundance of the precursor ion and the S/N ratio of the product ions).

4.2.7 Data Analysis

Data processing was performed with Data Analysis software (Bruker Daltonics, Billerica, MA). Calibration was performed internally based on the observed and calculated *m/z* ratios of the precursor ion and one expected product ion. Data were analyzed manually with the aid of GlycoWorkbench software.[57] Product ions were not assigned unless the S/N ratio was at least 3. Fragmentation efficiency was calculated according to:

$$\frac{\sum I\,(fi)}{Pi\,(before)} \qquad (1)$$

in which I (fi) is the summed product ion abundance (charge state normalization is unnecessary as all fragments are singly charged) and Pi (before) is the precursor ion abundance in a separate spectrum prior to dissociation.

4.3 Results and Discussion

The standard symbolic representation of monosaccharides established in Glycobiology[58] is used below.

4.3.1 CAD vs. EID of 9FL-Derivatized Glycans

Figure 4.1 shows CAD and EID spectra of 9FL-derivatized LNDFH, a branched neutral glycan with two fucose residues. As expected, CAD (see Figure 4.1 a) only produced glycosidic fragments, mostly Y-type but also two B/Y-type internal fragments from vibrational excitation. Despite yielding high sequence coverage, these Y-type fragments only provide information about the presence of monosaccharides but unfortunately do not provide any information about branching or linkage. Fucose migration peaks (ions at *m/z* 492 and *m/z* 654 as previously reported[55] and *m/z* 1003,

assigned as Y_1, Y_2, and Y_3 fragments with an additional fucose attached to the reducing end, respectively) are observed in CAD at significant abundance, ranging from 0.3 to 10% (relative to all the other fragments). The mechanism of fucose migration in fluorescently modified protonated glycan cations has been proposed, based on both experimental observations and modeling, to involve a two-step proton-catalyzed process: First, protonation of the introduced amine group is followed by intramolecular proton transfer to the glycosidic bond, and subsequent cleavage of the activated glycosidic bond aided by nucleophilic sites, such as hydroxyl or amine groups. Second, fucose transfer is promoted to either the monosaccharide adjacent to the fluorescent tag, or to the tag itself.[55] The resulting structurally rearranged species introduce ambiguity.

EID of the same precursor ions yielded very different fragmentation behavior (see Figure 4.1 b). In addition to enhanced glycosidic fragmentation (B-, Z-, and Y-type) and more internal fragments (B/Z/Y, B/Y/Y, Z/Z, Y/Z, B/Y, and C/Z), four characteristic X-type cross-ring cleavages were produced, yielding additional sequence information. All three fucose migration peaks were significantly reduced in EID compared with CAD to a range of 0.3-0.8% (relative abundance among all fragments). Table 4.1 summarizes the differences between CAD and EID of 9FL-LNDFH. As illustrated in this Table, in addition to the extensive glycosidic fragments, 18 more fragments are observed in EID than in CAD of the same singly protonated 9FL-derivatized glycan cations, including both glycosidic and cross-ring cleavages. The EID fragmentation efficiency for 9FL-LNDFH was 76 (or 58% if not considering the abundant fragment corresponding to loss of the tag) whereas the CAD fragmentation efficiency under the conditions used was

46%. EID generates complementary structural information compared with CAD, which currently is the most widely used activation method in carbohydrate MS/MS.

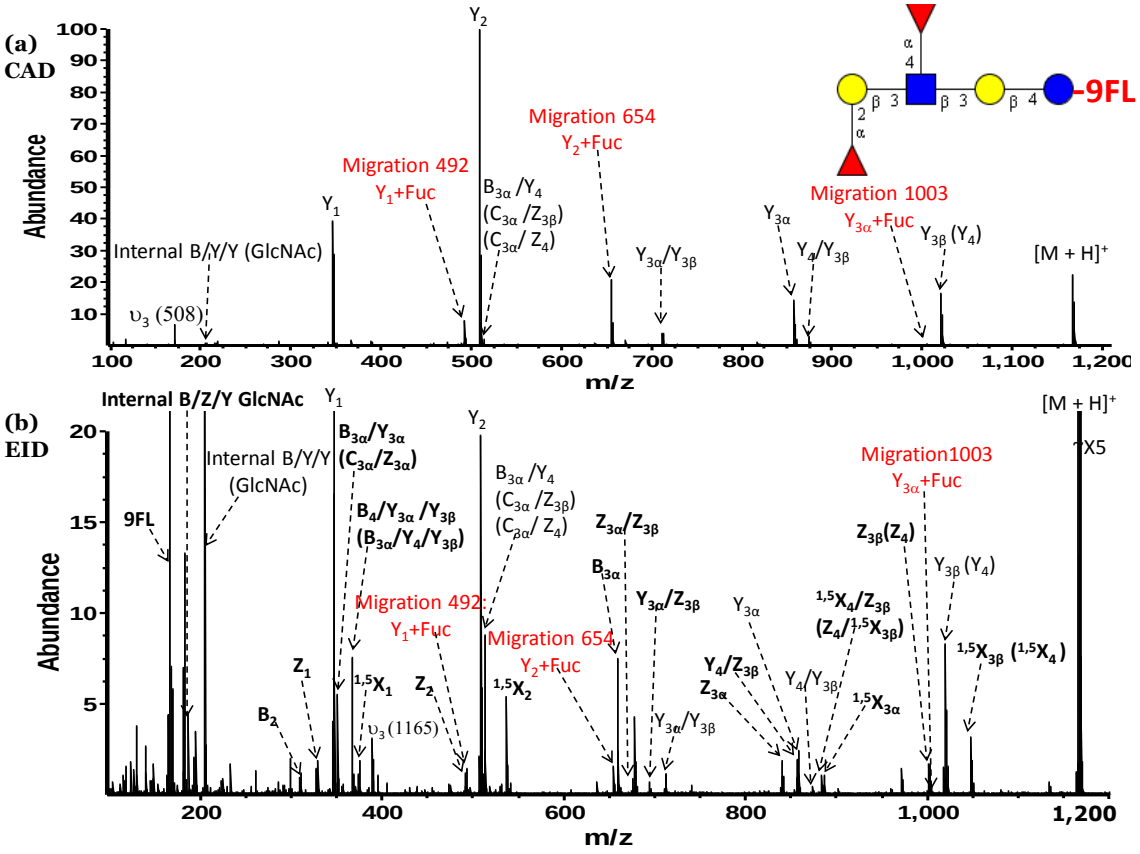

Figure 4.1 CAD and EID of 9-aminofluorene-labeled lacto-N-difucohexaose I (9FL-LNDFH): (a) CAD, (b) EID. For both spectra, precursor ions are labeled $[M + H]^+$. *: noise; ν_3: third harmonic peaks. Bold font indicates fragments that are unique to CAD or EID. Peaks highlighted in red are migration peaks that lead to false structure elucidation. Three migration peaks were observed for 9FL derivatized LNDFH, in both CAD and EID.

Table 4.1 Comparison of fragments observed in CAD and EID of 9FL-LNDFH. Percentage values in parentheses indicate relative abundance among all observed fragments. Fragments highlighted in bold on the right under "EID" are those unique to EID and are not observed in CAD. Fucose migration fragments (fucose represented by red triangles) and X-type cross-ring fragments are highlighted in red.

CAD	EID	
Internal B/Y/Y (GlcNAc) Y_1 Y_2 $B_4/Y_{3\alpha}$ ($B_{3\alpha}/Y_{3\beta}$) ($B_{3\alpha}/Y_4$) $Y_{3\alpha}/Y_{3\beta}$ $Y_{3\alpha}$ $Y_4/Y_{3\beta}$ $Y_{3\beta}(Y_4)$	Internal B/Y/Y (GlcNAc) Y_1 Y_2 $B_4/Y_{3\alpha}$ ($B_{3\alpha}/Y_{3\beta}$) ($B_{3\alpha}/Y_4$) $Y_{3\alpha}/Y_{3\beta}$ $Y_{3\alpha}$ $Y_4/Y_{3\beta}$ $Y_{3\beta}(Y_4)$	**9FL** **Internal B/Z/Y (GlcNAc)** **B_2** **Z_1** **$B_{3\alpha}/Y_{3\alpha}$ ($C_{3\alpha}/Z_{3\alpha}$)** **$B_4/Y_{3\alpha}$ /$Y_{3\beta}$** **$^{1,5}X_1$ (1.0%)** **Z_2** **$^{1,5}X_2$ (2.7%)** **$B_{3\alpha}$** **$Z_{3\alpha}/Z_{3\beta}$** **$Y_{3\alpha}/Z_{3\beta}$** **$Z_{3\alpha}$** **$Y_4/Z_{3\beta}$** **$^{1,5}X_4/Z_{3\beta}$** **$^{1,5}X_{3\alpha}$ (0.6%)** **$Z_{3\beta}(Z_4)$** **$^{1,5}X_{3\beta}$ ($^{1,5}X_4$)(1.6%)**
Y_1 +▲ : m/z 492 (3.8%) Y_2 +▲: m/z 654 (9.9%) $Y_{3\alpha}$ +▲: m/z 1003 (0.32%)	Y_1 +▲ : m/z 492 (0.7%) Y_2 +▲ : m/z 654(0.8%) $Y_{3\alpha}$ +▲: m/z 1003 (0.26%)	

Similar to 9FL-LNDFH, EID of 9FL-LNFP generates complementary structural information by producing characteristic glycosidic and cross-ring cleavages that can only be observed in EID. In addition to B, C, Z glycosidic cleavages that completely cover the glycan sequence, four ^{1,5}X-type cross-ring fragments confirms the sequence. Furthermore, fucose migration peaks are reduced in EID (see Figure 4.2), although not completely prevented. ^{1,5}X fragments have been reported frequently in high energy CAD. [59] Such similarity between EID and high energy CAD fragmentation outcomes indicates a similar mechanism of EID and that of high energy CAD, which is believed to involve electronic excitation.

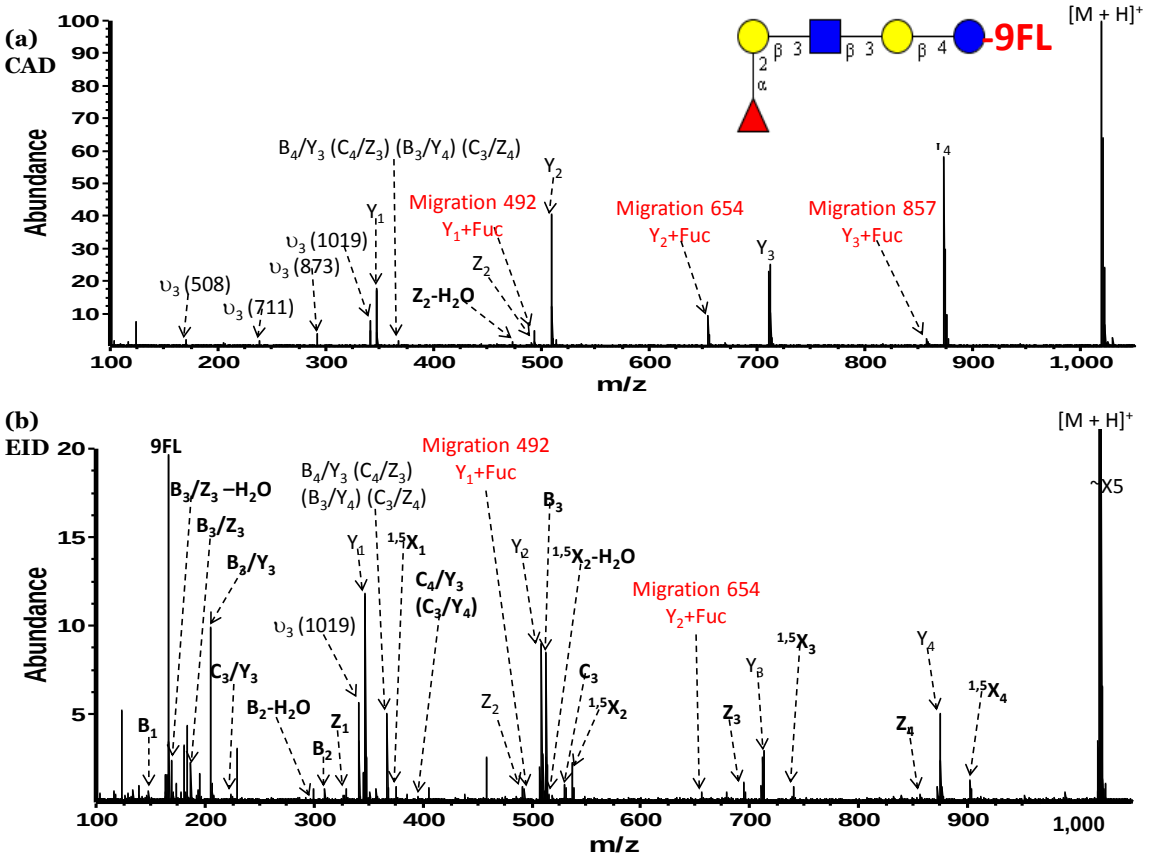

Figure 4.2 CAD and EID of 9-aminofluorene-labeled lacto-N-fucopentaose I (9FL-LNFP): (a) CAD, (b) EID. For both spectra, precursor ions are labeled $[M + H]^+$. *: noise; ν_3: third harmonic peaks. Bold font indicates fragments that are unique to CAD or EID. Peaks highlighted in red are migration peaks that lead to false structure elucidation. Three migration peaks were observed for 9FL derivatized LNDFH in CAD, while two of them were also observed in EID. Migration peaks were much less abundant in EID than in CAD.

Figure 4.3 compares CAD and EID of 9FL–LNH, a branched neutral glycan. In the CAD spectrum, all fragments correspond to glycosidic cleavages such as Y-, B-, Y/Z-, Y/Y-, and Z/Z-types while, in the EID spectrum, in addition to more glycosidic fragments such as B_{2x}/Y_{3x} (C_{2x}/Z_{3x}), B_{2x}/Z_{3x}, C_{2x}, B_3/Y_{2x}, C_3, and Z_{3x}, cross-ring fragments such as $^{1,5}X_1$, $^{1,5}X_{2x}$ and $^{1,5}X_{3x}$ are observed.

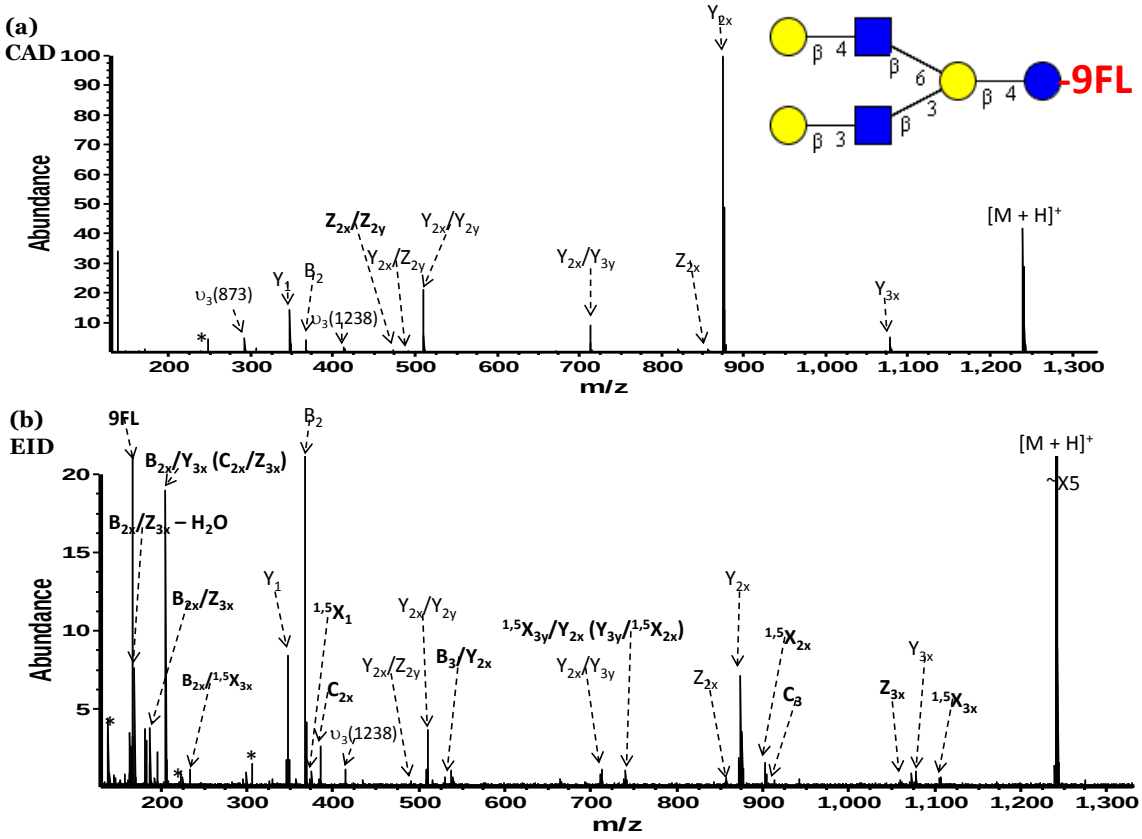

Figure 4.3 CAD and EID of 9-aminofluorene-labeled lacto-N-hexaose (9FL-LNH): (a) CAD, (b) EID. For both spectra, precursor ions are labeled $[M + H]^+$. *: noise; ν_3: third harmonic peaks. Bold font indicates fragments that are unique to CAD or EID.

Similar results were obtained in EID of acidic glycans, as shown in Figure 4.4 for LSTb, an acidic branched glycan with a sialic acid (Neu5Ac) at the non-reducing end. Due to this sialic acid, lower ionization efficiency was observed for LSTb in its native form compared with the neutral glycans discussed above. However, following 9FL derivatization, ionization efficiency improved, presumably due to the increased hydrophobicity. CAD of 9FL-derivatized LSTb only generated several low abundance Y-type product ions in addition to abundant Neu5Ac loss ($Y_{3\beta}$). Facile Neu5Ac loss prevented generation of more informative fragments. By contrast, in EID of the same singly protonated precursor ion, a higher variety of fragments was produced. All the Y-

type fragments detected in CAD could also be observed in EID. In addition, several Z-, B-type and internal fragments were unique to EID. A combination of $B_2/Y_{3\alpha}$, $B_2/Y_{3\beta}$, and B_2 indicates the branching site at the GlcNAc monosaccharide.

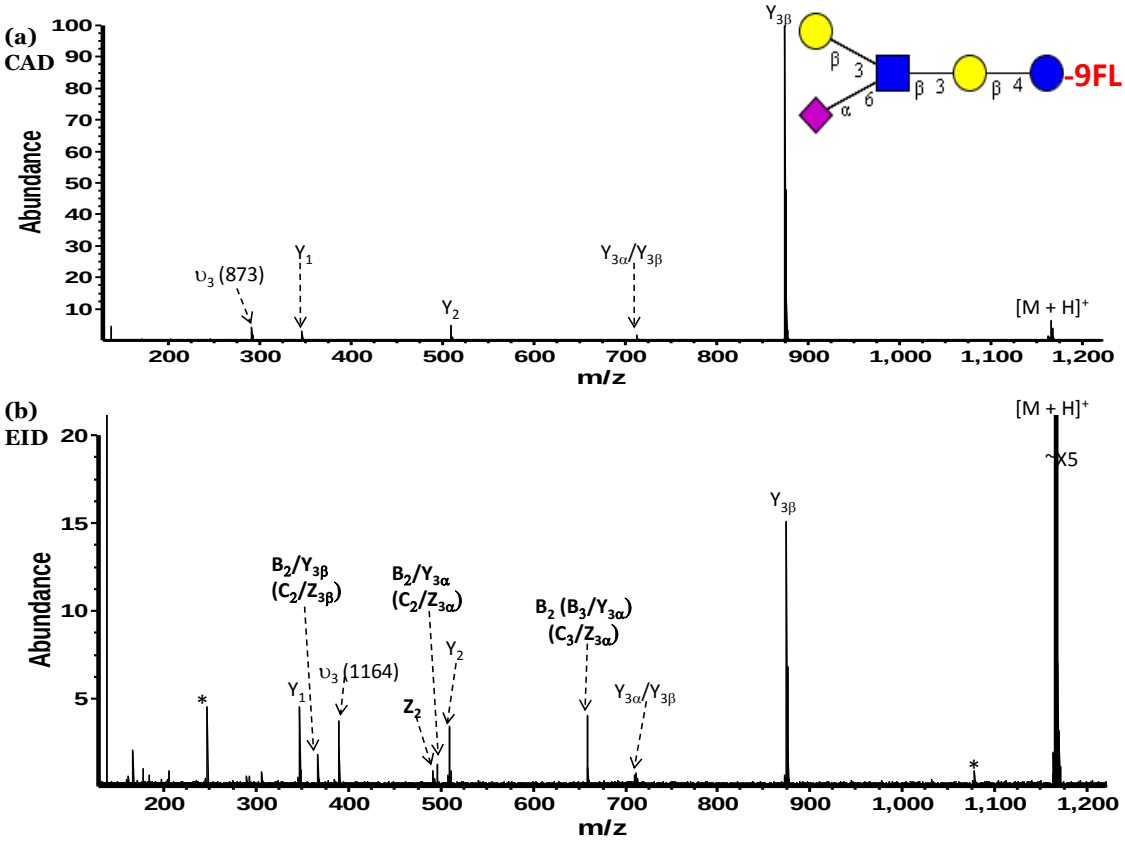

Figure 4.4 CAD and EID of 9-aminofluorene-labeled LS-tetrasaccharide B (9FL-LSTb): (a) CAD, (b) EID. For both spectra, precursor ions are labeled $[M + H]^+$. *: noise; ν_3: third harmonic peaks. Bold font indicates fragments that are unique to CAD or EID.

4.3.2 CAD vs. EID of Underivatized Glycans

EID was also applied to underivatized oligosaccharides, including LNDFH, LNFP, LNH, LSTb, and an N-linked glycan (NA2). CAD and EID spectra of underivatized glycans are compared in Figures 4.5-4.9.

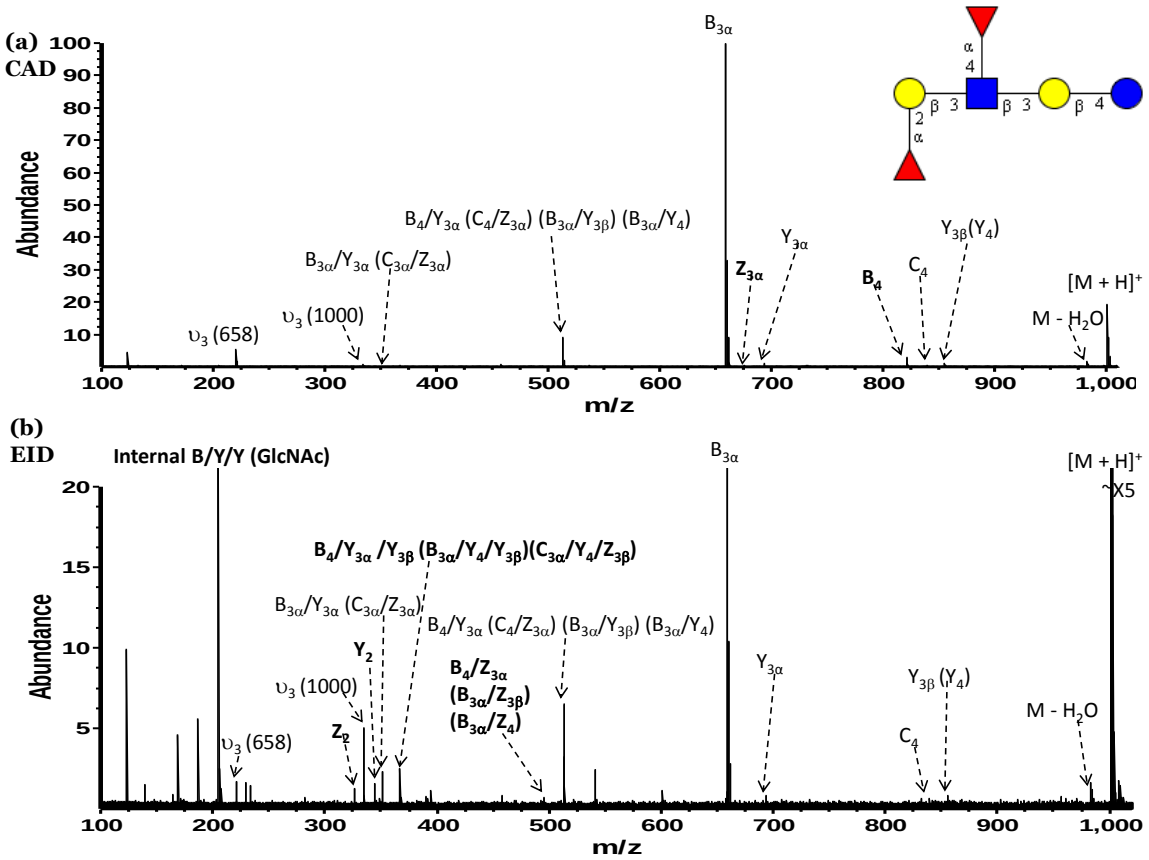

Figure 4.5 CAD and EID of lacto-N-difucohexaose I (LNDFH): (a) CAD, (b) EID. For both spectra, precursor ions are labeled $[M + H]^+$. *: noise; ν_3: third harmonic peaks. Bold font indicates fragments that are unique to CAD or EID.

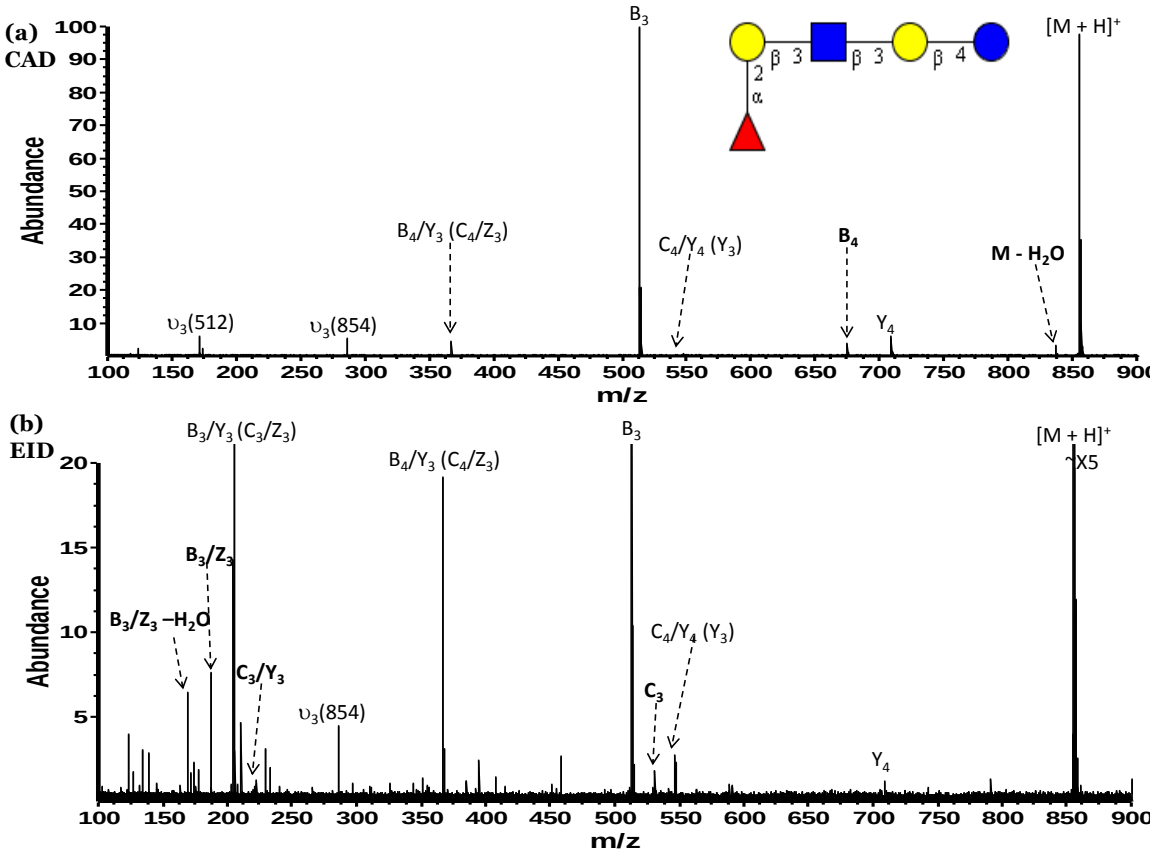

Figure 4.6 CAD and EID of lacto-N-fucopentaose I (LNFP): (a) CAD, (b) EID. For both spectra, precursor ions are labeled $[M + H]^+$. *: noise; ν_3: third harmonic peaks. Bold font indicates fragments that are unique to CAD or EID.

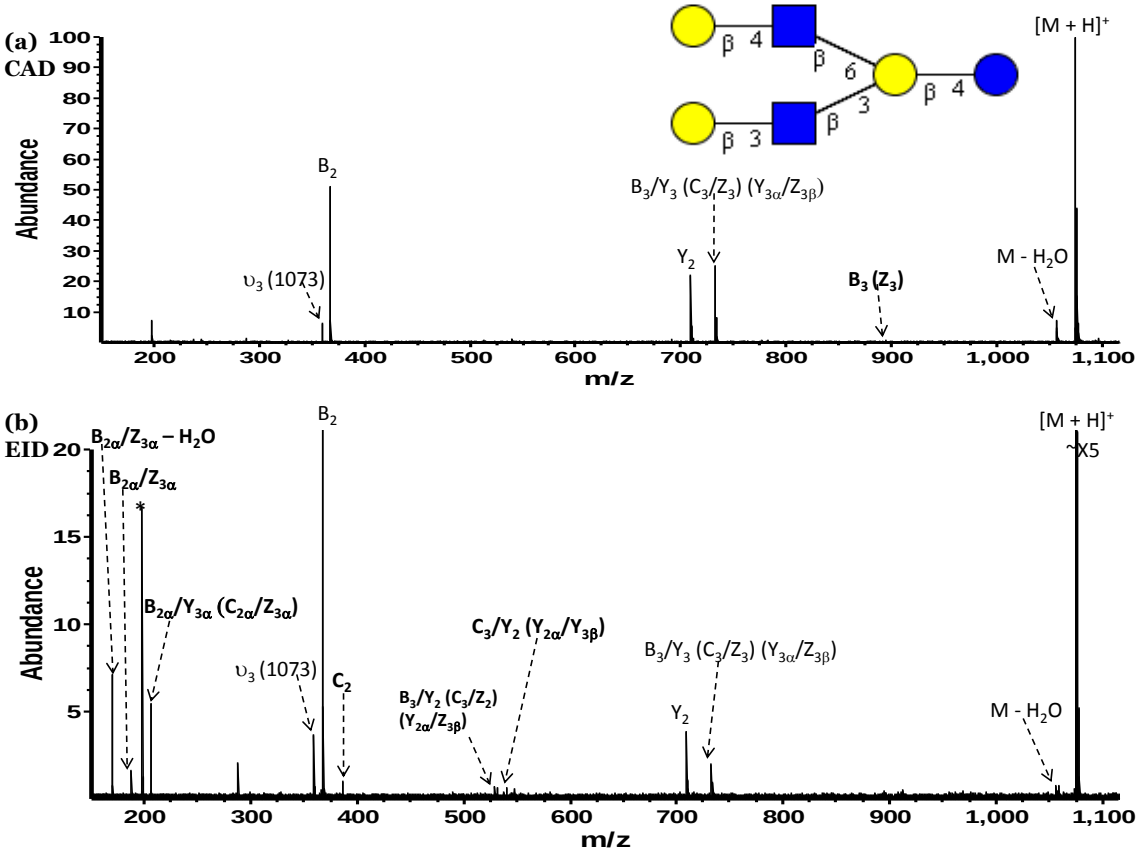

Figure 4.7 CAD and EID of lacto-N-hexaose (LNH): (a) CAD, (b) EID. For both spectra, precursor ions are labeled $[M + H]^+$. *: noise; ν_3: third harmonic peaks. Bold font indicates fragments that are unique to CAD or EID.

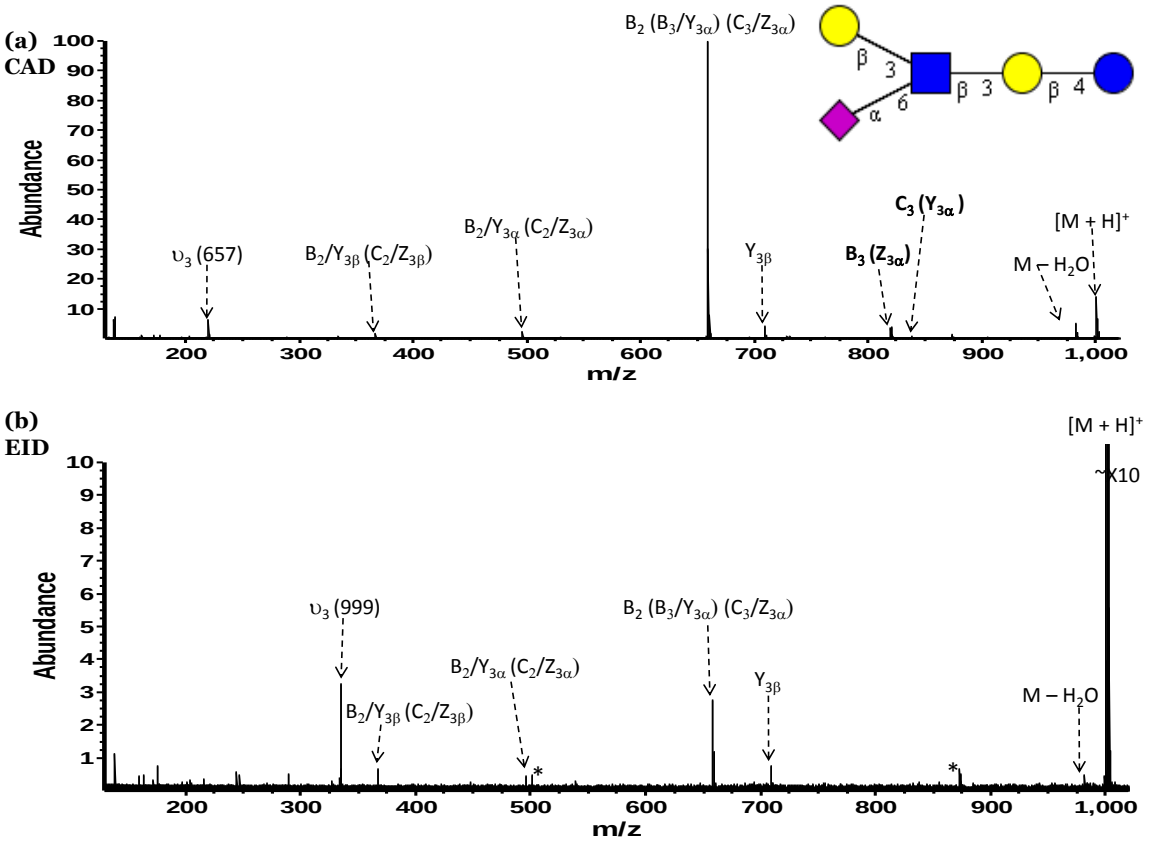

Figure 4.8 CAD and EID of LS-tetrasaccharide B (LSTb): (a) CAD, (b) EID. For both spectra, precursor ions are labeled $[M + H]^+$. *: noise; ν_3: third harmonic peaks. Bold font indicates fragments that are unique to CAD or EID.

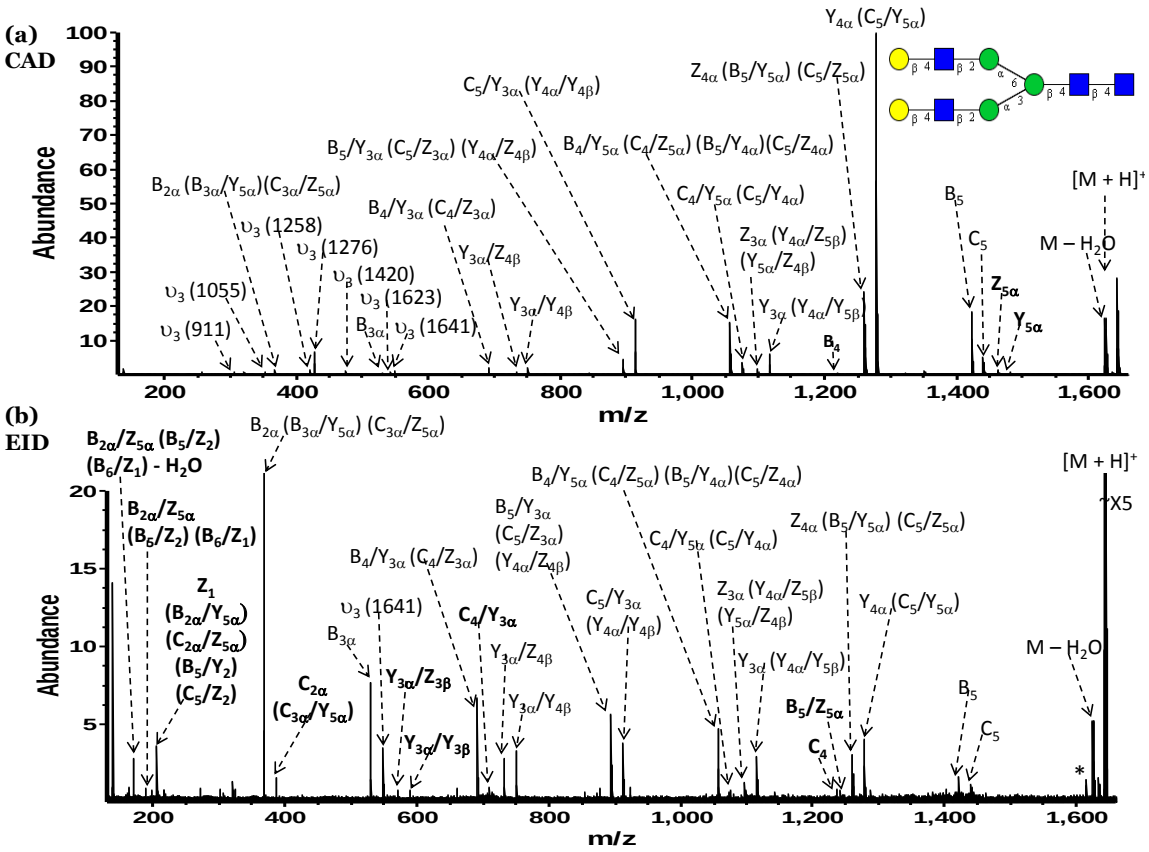

Figure 4.9 CAD and EID of an asialo, galactosylated, biantennary glycan (NA2): (a) CAD, (b) EID. For both spectra, precursor ions are labeled $[M + H]^+$. *: noise; υ_3: third harmonic peaks. Bold font indicates fragments that are unique to CAD or EID.

For CAD and EID of underivatized LNDFH (Figure 4.5) and LNFP (Figure 4.6), no migration peaks were observed in either CAD or EID. Without 9FL derivatization, CAD fragmentation efficiency for underivatized LNDFH was 104% whereas EID fragmentation efficiency was only 15%. Given that fucose migration peaks were observed in both CAD and EID (although to a lower extent in EID) of 9FL-derivatized glycans, reducing end derivatization appears to play a role in the phenomenon of gas-phase saccharide migration. For LNDFH, LNFP, and LNH (see Figure 4.7) EID provided complementary structural information by generating unique bond cleavages that could only be observed in EID but not in CAD. However, all of these additional

fragments were glycosidic cleavages from vibrational excitation, suggesting a critical effect of the aromatic tag in the EID activation process. For LSTb (see Figure 4.8), CAD produced more fragments than EID. However, because LSTb is an acidic glycan, low ionization efficiency in positive ion mode may be the reason for the low fragmentation efficiency (~5%) and limited structural information from EID alone. Although two additional fragments, B_3 ($Z_{3\alpha}$) and C_3 ($Y_{3\alpha}$), were generated only in CAD but not in EID of the same precursor ion, these two fragments did not add any structural information. For NA2 (see Figure 4.9), an N-linked glycan with a higher mass than previously examined oligosaccharides, EID also yielded more structural information compared with CAD, including nine additional fragments (two Z and C-type glycosidic cleavages and several B/Z-, Y/Z-, Y/Y-type internal cleavages).

Although EID of underivatized glycans did not yield cross-ring cleavages as in EID of 9FL derivatized glycans, EID still provides complementary fragmentation compared with CAD for underivatized glycans. This observation indicates a significant effect of the reducing end aromatic label in the EID process and thus we became interested in studying other fluorescent labels.

4.3.3 Effect of Different Fluorescent Tags in EID Fragmentation

In order to further study the effect of reducing end derivatization and potentially gain further insight into the EID mechanism, additional fluorescent tags were used for reducing end labeling prior to EID.

Figure 4.10 compares CAD and EID of 2AB-labeled NA2. The advantage of EID over CAD is quite obvious for this relatively larger glycan. CAD parameters were optimized with a decreased time-of-flight between the collision cell and the ICR cell (1.5

rather than 1.7 ms), higher collision cell RF amplitude (620 rather than 350 V), higher collision voltage (- 25 rather than - 14.5 V), and higher source ion accumulation time (7 rather than 2 s), to obtain the largest variety of fragments. However, only two B-type and three Y-type glycosidic fragments were generated, corresponding to poor sequence coverage and no branching information. The majority of the observed CAD product ions were Y/Y- and B/Y-type internal fragments which, in this case, do not add any structural information but congest the spectrum. Without the aforementioned CAD optimization, only two glycosidic fragments (B- and Y- type) were observed, even for complete precursor ion depletion at higher collision voltage. In contrast, EID of the singly protonated 2AB-derivatized NA2 cation produced extensive glycosidic fragments as well as three X-type cross-ring cleavages. $^{1,5}X_2$ and $^{1,5}X_{3\alpha}$ together provide valuable information about branching. To further compare EID with slow-heating MS/MS activation, IRMPD was also performed on the same precursor ions (see Figure 4.11 and Table 4.2). Compared with CAD, more fragments were observed in IRMPD, presumably due to increased secondary fragmentation. All fragments produced from IRMPD were also observed in EID. In addition, EID generated fourteen more cleavages, including cross-ring cleavages that could only be observed in EID. In summary, EID yielded important additional structural information by generating unique glycosidic cleavages and cross-ring cleavages, which further confirmed the composition and sequence, compared with the slow-heating MS/MS techniques CAD and IRMPD.

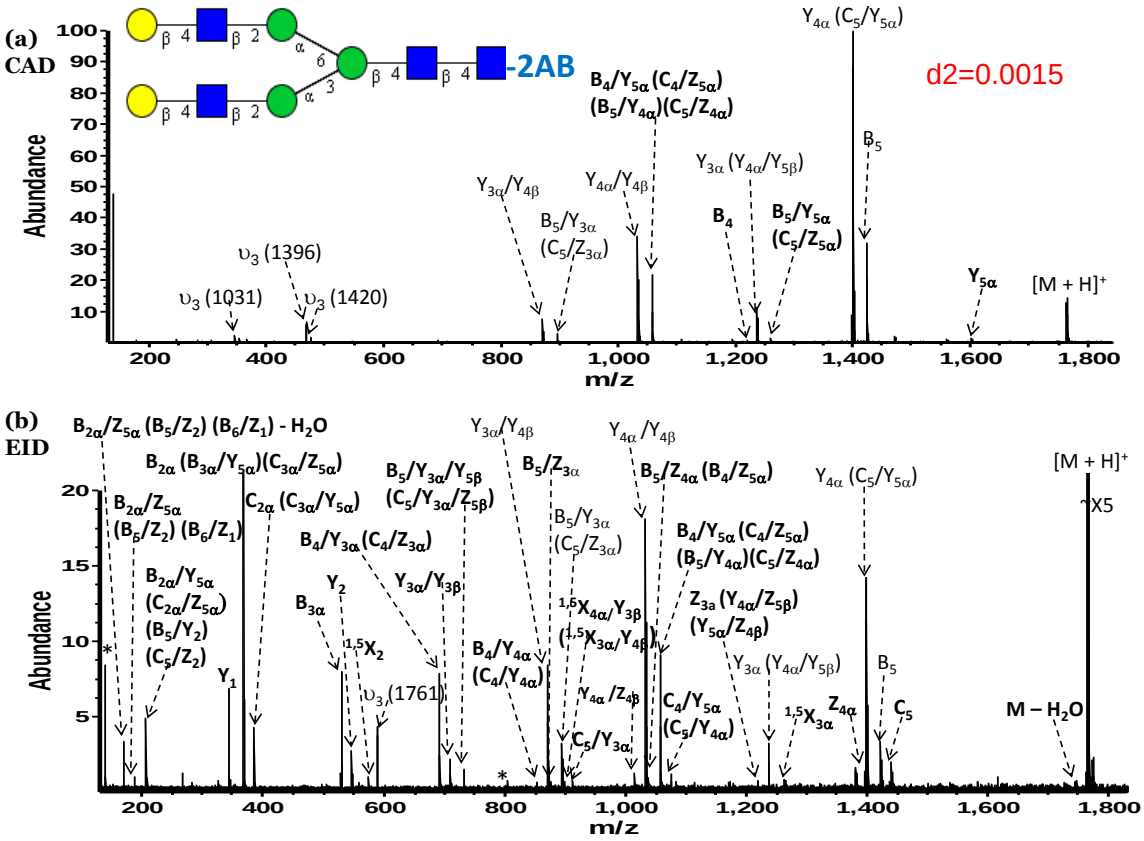

Figure 4.10 CAD and EID of a 2-amino benzamide-labeled asialo, galactosylated, biantennary glycan (2AB-NA2): (a) Improved CAD (d_2 = 1.5 ms), (b) EID. For both spectra, precursor ions are labeled [M + H]$^+$. *: noise; ν_3: third harmonic peaks. Bold font indicates fragments that are unique to CAD or EID.

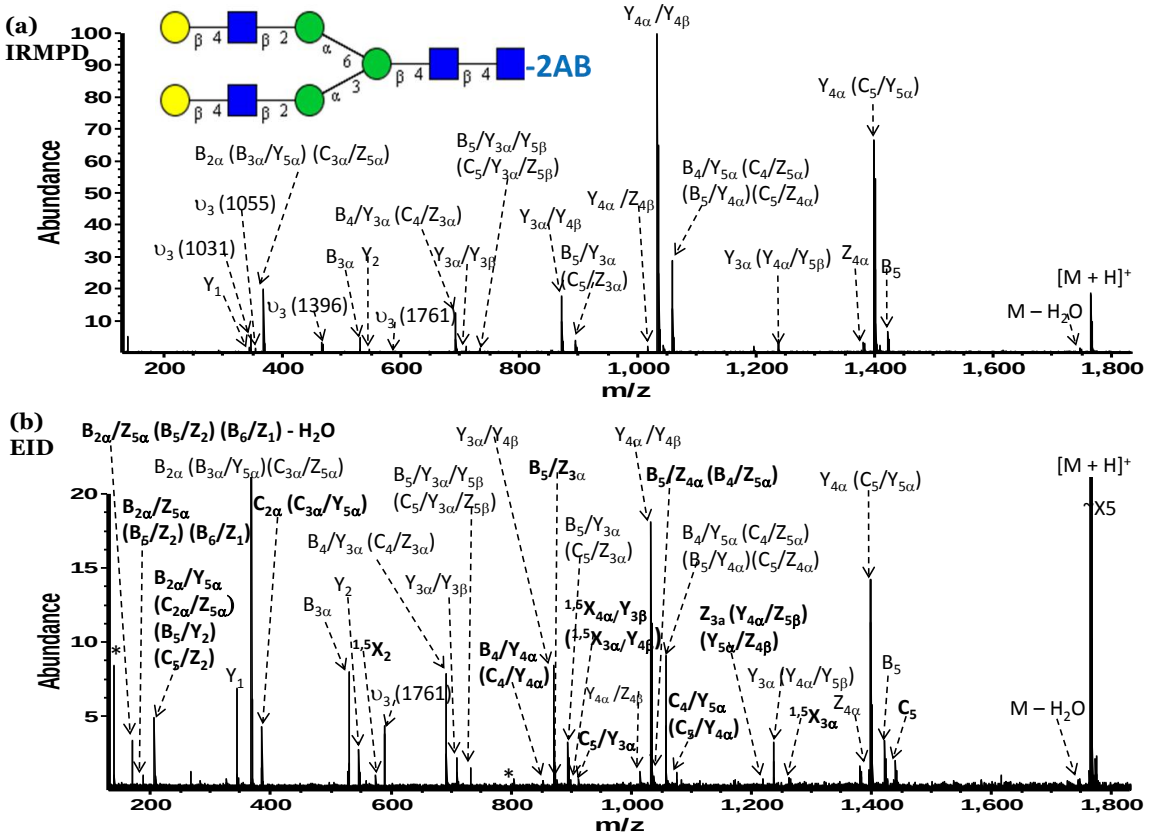

Figure 4.11 IRMPD and EID of a 2-amino benzamide-labeled asialo, galactosylated, biantennary glycan (2AB-NA2): (a) IRMPD, (b) EID. For both spectra, precursor ions are labeled $[M + H]^+$. *: noise; υ_3: third harmonic peaks. Bold font indicates fragments that are unique to IRMPD or EID.

Table 4.2 Comparison of fragments observed in IRMPD and EID of a 2-amino benzamide-labeled asialo, galactosylated, biantennary glycan (2AB-NA2). Fragments highlighted in bold on the right under "EID" are those unique to EID and are not observed in IRMPD.

IRMPD	EID	
Y_1	Y_1	**$B_{2\alpha}/Z_{5\alpha}$ (B_5/Z_2) (B_6/Z_1) - H_2O**
$B_{2\alpha}$ ($B_{3\alpha}/Y_{5\alpha}$) ($C_{3\alpha}/Z_{5\alpha}$)	$B_{2\alpha}$ ($B_{3\alpha}/Y_{5\alpha}$)($C_{3\alpha}/Z_{5\alpha}$)	**$B_{2\alpha}/Z_{5\alpha}$ (B_5/Z_2) (B_6/Z_1)**
$B_{3\alpha}$	$B_{3\alpha}$	**$B_{2\alpha}/Y_{5\alpha}$ ($C_{2\alpha}/Z_{5\alpha}$) (B_5/Y_2)**
$B_4/Y_{3\alpha}$ ($C_4/Z_{3\alpha}$)	$B_4/Y_{3\alpha}$ ($C_4/Z_{3\alpha}$)	**(C_5/Z_2)**
Y_2	Y_2	**$C_{2\alpha}$ ($C_{3\alpha}/Y_{5\alpha}$)**
$Y_{3\alpha}/Y_{3\beta}$	$Y_{3\alpha}/Y_{3\beta}$	**$^{1,5}X_2$**
$B_5/Y_{3\alpha}/Y_{5\beta}$ ($C_5/Y_{3\alpha}/Z_{5\beta}$)	$B_5/Y_{3\alpha}/Y_{5\beta}$ ($C_5/Y_{3\alpha}/Z_{5\beta}$)	**$B_4/Y_{4\alpha}$ ($C_4/Y_{4\alpha}$)**
$Y_{3\alpha}/Y_{4\beta}$	$Y_{3\alpha}/Y_{4\beta}$	**$B_5/Z_{3\alpha}$**
$B_5/Y_{3\alpha}$ ($C_5/Z_{3\alpha}$)	$B_5/Y_{3\alpha}$ ($C_5/Z_{3\alpha}$)	**$^{1,5}X_{4\alpha}/Y_{3\beta}$ ($^{1,5}X_{3\alpha}/Y_{4\beta}$)**
$Y_{4\alpha}$ /$Z_{4\beta}$	$Y_{4\alpha}$ /$Z_{4\beta}$	**$C_5/Y_{3\alpha}$**
$Y_{4\alpha}$ /$Y_{4\beta}$	$Y_{4\alpha}$ /$Y_{4\beta}$	**$B_5/Z_{4\alpha}$ ($B_4/Z_{5\alpha}$)**
$B_4/Y_{5\alpha}$ ($C_4/Z_{5\alpha}$)	$B_4/Y_{5\alpha}$ ($C_4/Z_{5\alpha}$)	**$Z_{3\alpha}$ ($Y_{4\alpha}/Z_{5\beta}$)($Y_{5\alpha}/Z_{4\beta}$)**
($B_5/Y_{4\alpha}$)($C_5/Z_{4\alpha}$)	($B_5/Y_{4\alpha}$)($C_5/Z_{4\alpha}$)	**$C_4/Y_{5\alpha}$ ($C_5/Y_{4\alpha}$)**
$Y_{3\alpha}$ ($Y_{4\alpha}/Y_{5\beta}$)	$Y_{3\alpha}$ ($Y_{4\alpha}/Y_{5\beta}$)	**$^{1,5}X_{3\alpha}$**
$Y_{4\alpha}$($C_5/Y_{5\alpha}$)	$Y_{4\alpha}$($C_5/Y_{5\alpha}$)	**C_5**
$Z_{4\alpha}$	$Z_{4\alpha}$	
B_5	B_5	
$M - H_2O$	$M - H_2O$	

Table 4.3 summarizes EID results for LNDFH labeled with different fluorescent tags (2AA, 2AB, and 9FL). CAD and EID spectra of 2AA-LNDFH and 2AB-LNDFH are shown in Figures 4.12-4.13. Overall, EID generated more fragments from 2AA to 2AB to 9FL. Fucose migration peaks were decreased from 2AA to 2AB to 9FL as well. We hypothesize that 9FL labeling results in richer EID product ion spectra due to its more conjugated structure compared with 2AA and 2AB, thereby facilitating electronic excitation in EID. The differences observed between the 2AA and 2AB labels with similar structures, may be related to the corresponding ionization efficiency: 2AA, which is more acidic than 2AB, is more difficult to ionize in positive ion mode. CAD and EID fragmentation efficiencies for 2AB and 2AA derivatized LNDFH were 35 and 14%, respectively. By contrast, 2AA-LNDFH showed a fragmentation efficiency of 28% in

CAD and 20% in EID. Labeling with 9FL increased EID fragmentation efficiency the most compared with CAD.

Table 4.3 Effects of different fluorescent tags (2AA, 2AB, 9FL) in EID of reducing end-labeled LNDFH. Percentage values in parentheses indicate relative abundance among all observed fragments. Fragments in bold in the sub-column on the right under "9FL"are unique to EID of 9FL-derivatized LNDFH. Cross-ring cleavages and fucose migration peaks are highlighted in red. Red triangle = fucose.

2AA 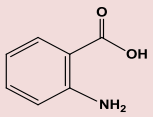	2AB 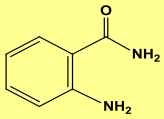	9FL 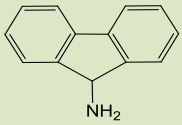	
Internal B/Y/Y (GlcNAc) Y_1 Y_2 $B_4/Y_{3\alpha}$ ($B_{3\alpha}/Y_{3\beta}$) ($B_{3\alpha}/Y_4$) $B_{3\alpha}$ $B_4/Y_{3\alpha}/Y_{3\beta}$ $Y_{3\alpha}$ $Y_{3\beta}$ (Y_4) $B_{3\alpha}/Y_{3\alpha}$ ($C_{3\alpha}/Z_{3\alpha}$)	Internal B/Y/Y (GlcNAc) Y_1 Y_2 $B_4/Y_{3\alpha}$ ($B_{3\alpha}/Y_{3\beta}$) ($B_{3\alpha}/Y_4$) $B_{3\alpha}$ $B_4/Y_{3\alpha}$ /$Y_{3\beta}$ $Y_{3\alpha}$ $Y_{3\beta}$ (Y_4) $B_{3\alpha}/Y_{3\alpha}$ ($C_{3\alpha}/Z_{3\alpha}$)	Internal B/Y/Y (GlcNAc) Y_1 Y_2 $B_4/Y_{3\alpha}$ ($B_{3\alpha}/Y_{3\beta}$) ($B_{3\alpha}/Y_4$) $B_{3\alpha}$ $B_4/Y_{3\alpha}$ /$Y_{3\beta}$ $Y_{3\alpha}$ $Y_{3\beta}$(Y_4) $B_{3\alpha}/Y_{3\alpha}$ ($C_{3\alpha}/Z_{3\alpha}$)	**tag** **Internal B/Z/Y (GlcNAc)** **B_2** **Z_1** **$Y_4/Y_{3\beta}$** **Z_2** **$Z_{3\alpha}/Z_{3\beta}$** **$Y_{3\alpha}/Z_{3\beta}$** **$Y_4/Z_{3\beta}$** **$^{1,5}X_4/Z_{3\beta}$** **$^{1,5}X_1$ (1.0%)** **$^{1,5}X_{3\alpha}$ (0.6%)**
$Z_{3\alpha}$ $Z_{3\beta}$ (Z_4)	$Y_{3\alpha}/Y_{3\beta}$	$Z_{3\alpha}$ $Z_{3\beta}$ (Z_4) $Y_{3\alpha}/Y_{3\beta}$	
$^{1,5}X_{3\beta}$ ($^{1,5}X_4$) (1.4%)	**$^{1,5}X_2$ (2.7%)** **$^{1,5}X_{3\beta}$ ($^{1,5}X_4$) (0.7%)**	**$^{1,5}X_2$ (2.7%)** **$^{1,5}X_{3\beta}$ ($^{1,5}X_4$) (1.6%)**	
Y_2 + ▲ :m/z 610 (2.4%) $Y_{3\alpha}$ + ▲: m/z 959 (N/A)	Y_1 + ▲: m/z 447 (2.2%) Y_2 + ▲: m/z 609 (4.3%) $Y_{3\alpha}$ + ▲: m/z 958 (N/A)	Y_1 + ▲: m/z 492 (0.7%) Y_2 + ▲: m/z 654 (0.8%) $Y_{3\alpha}$ + ▲: m/z 1003 (0.26%)	

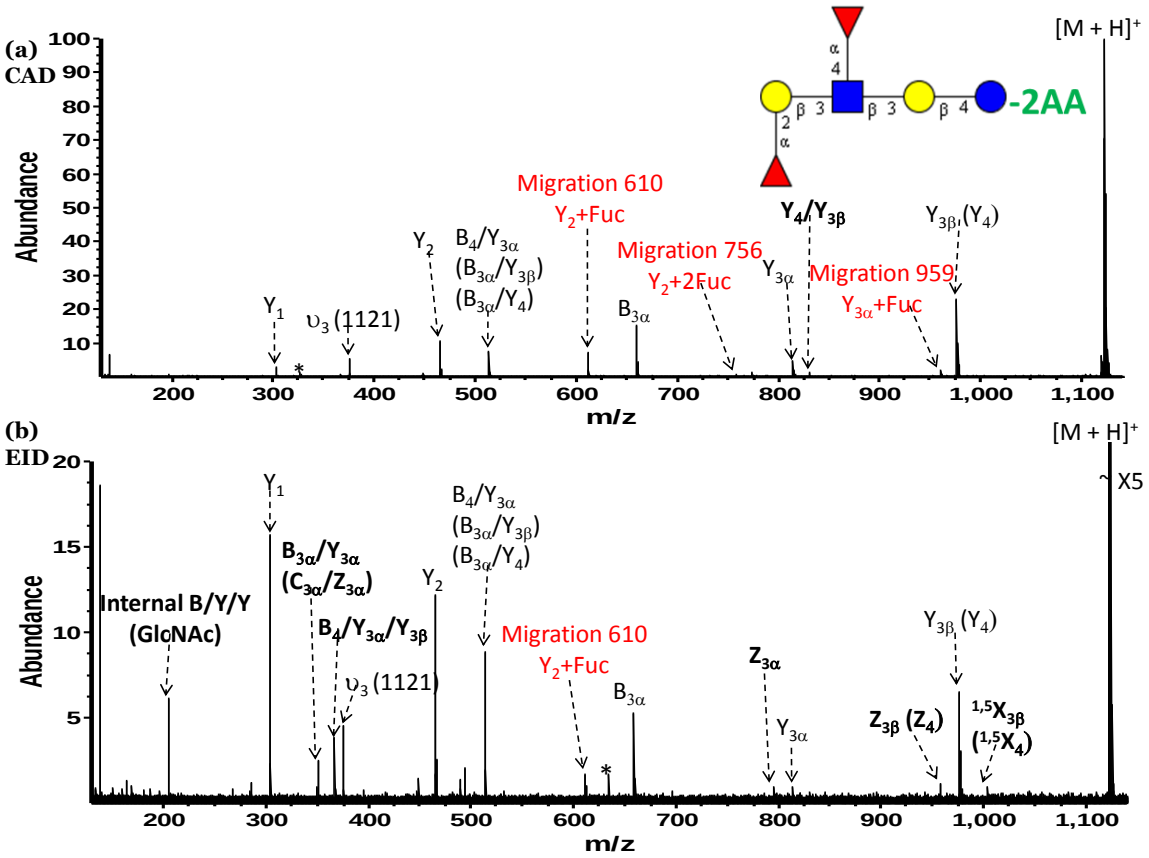

Figure 4.12 CAD and EID of a 2-anthranilic acid-labeled lacto-N-difucohexaose I (2AA-LNDFH): (a) CAD, (b) EID. For both spectra, precursor ions are labeled $[M + H]^+$. *: noise; ν_3: third harmonic peaks. Bold font indicates fragments that are unique to CAD or EID.

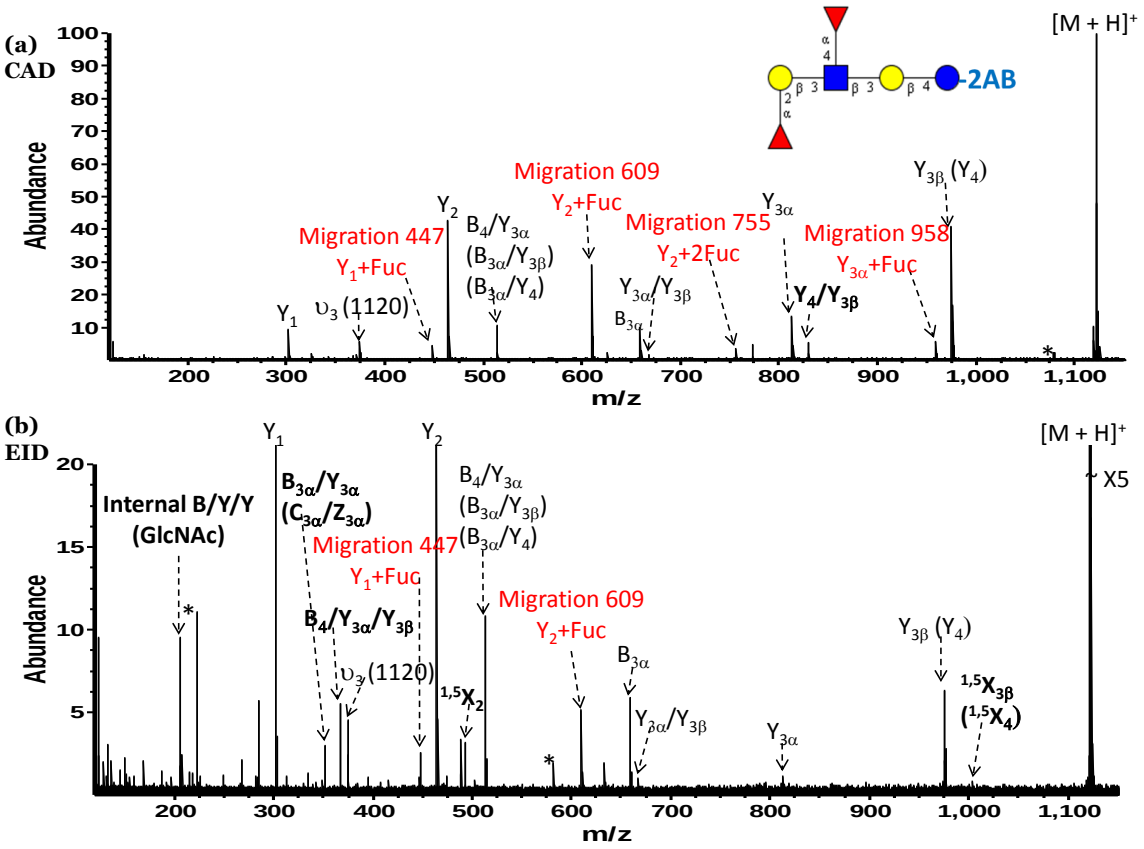

Figure 4.13 CAD and EID of a 2-amino benzamide-labeled lacto-N-difucohexaose I (2AB-LNDFH): (a) CAD, (b) EID. For both spectra, precursor ions are labeled $[M + H]^+$. *: noise; ν_3: third harmonic peaks. Bold font indicates fragments that are unique to CAD or EID.

EID of underivatized NA2 was also compared with EID of 2AB-labeled NA2, as shown in Table 4.4. EID of 2AB-labeled NA2 produced many more fragments compared to that of underivatized NA2, including three glycosidic, eleven internal cleavages, and two X-type cross-ring cleavages that could not be observed in EID of underivatized NA2.

Table 4.4 Comparison of fragments observed in EID of unlabeled and 2-amino benzamide-labeled NA2 (2AB-NA2). Fragments in bold in the sub-columns on the right under "underivatized" and "2AB" are unique fragments that were only observed in EID of "underivatized" or "2AB"-derivatized NA2. Cross-ring cleavages are highlighted in red.

underivatized		**2AB** 	
$B_{2\alpha}$ ($B_{3\alpha}/Y_{5\alpha}$)($C_{3\alpha}/Z_{5\alpha}$) $B_{3\alpha}$ $B_4/Y_{3\alpha}$ ($C_4/Z_{3\alpha}$) $Y_{3\alpha}/Y_{4\beta}$ $B_4/Y_{5\alpha}$ ($C_4/Z_{5\alpha}$) ($B_5/Y_{4\alpha}$)($C_5/Z_{4\alpha}$) $C_4/Y_{5\alpha}$ ($C_5/Y_{4\alpha}$) $Y_{3\alpha}$ ($Y_{4\alpha}/Y_{5\beta}$) $Z_{4\alpha}$ (B_5/Y_5) (C_5/Z_5) $Y_{4\alpha}$ ($C_5/Y_{5\alpha}$) B_5 C_5 $B_5/Y_{3\alpha}$ ($C_5/Z_{3\alpha}$) ($Y_{4\alpha}/Z_{4\beta}$) $C_5/Y_{3\alpha}$ ($Y_{4\alpha}/Y_{4\beta}$) $Z_{3\alpha}$ ($Y_{4\alpha}/Z_{5\beta}$) ($Y_{4\alpha}/Z_{5\beta}$) M – H_2O	**$Y_{3\alpha}/Z_{4\beta}$**	$B_{2\alpha}$ ($B_{3\alpha}/Y_{5\alpha}$)($C_{3\alpha}/Z_{5\alpha}$) $B_{3\alpha}$ $B_4/Y_{3\alpha}$ ($C_4/Z_{3\alpha}$) $Y_{3\alpha}/Y_{4\beta}$ $B_4/Y_{5\alpha}$ ($C_4/Z_{5\alpha}$) ($B_5/Y_{4\alpha}$)($C_5/Z_{4\alpha}$) $C_4/Y_{5\alpha}$ ($C_5/Y_{4\alpha}$) $Y_{3\alpha}$ ($Y_{4\alpha}/Y_{5\beta}$) $Z_{4\alpha}$ $Y_{4\alpha}$ B_5 C_5 $B_5/Y_{3\alpha}$($C_5/Z_{3\alpha}$) $C_5/Y_{3\alpha}$ $Z_{3\alpha}$ ($Y_{5\alpha}/Z_{4\beta}$) ($Y_{4\alpha}/Z_{5\beta}$) M – H_2O	**$B_{2\alpha}/Z_{5\alpha}$ (B_5/Z_2) (B_6/Z_1) - H_2O** **$B_{2\alpha}/Z_{5\alpha}$ (B_5/Z_2) (B_6/Z_1)** **$B_{2\alpha}/Y_{5\alpha}$ ($C_{2\alpha}/Z_{5\alpha}$) (B_5/Y_2) (C_5/Z_2)** **$C_{2\alpha}$ ($C_{3\alpha}/Y_{5\alpha}$)** **Y_1** **Y_2** **$^{1,5}X_2$** **$Y_{3\alpha}/Y_{3\beta}$** **$B_5/Y_{3\alpha}/Y_{5\beta}$ ($C_5/Y_{3\alpha}/Z_{5\beta}$)** **$B_4/Y_{4\alpha}$ ($C_4/Y_{4\alpha}$)** **$B_5/Z_{3\alpha}$** **$Y_{4\alpha}/Y_{4\beta}$** **$Y_{4\alpha}/Z_{4\beta}$** **$^{1,5}X_{4\alpha}/Y_{3\beta}$ ($^{1,5}X_{3\alpha}/Y_{4\beta}$)** **$B_5/Z_{4\alpha}$ ($B_4/Z_{5\alpha}$)** **$^{1,5}X_{3\alpha}$**

4.4 Conclusions

EID was applied towards singly protonated non-permethylated glycan cations for structural characterization. Results show that EID produces complementary structural information compared with CAD. Fragmentation in EID is enhanced, including more abundant B-, C-, Y-, and Z-type glycosidic cleavages, internal cleavages, as well as characteristic cross-ring cleavages that can only be observed in EID but not in CAD, nor in IRMPD. Such cross-ring fragments either confirm glycan sequence or are essential for determination of branching. ^{1,5}X-type cross-ring cleavages are more common than other X-type product ions in EID, similar to high-energy CAD.[59] This observation indicates similarity between the mechanism of EID and that of high-energy CAD, involving

electronic excitation. Fucose-migration fragments[55] are significantly less abundant in EID compared with CAD, presumably because EID is more prompt (10^{-14}~10^{-15} sec) than CAD. EID of fluorescently labeled glycans produces more fragments than that of underivatized glycans, and 9FL produces more fragments than 2AB or 2AA labeling, presumably because a more conjugated structure facilitates electronic excitation. Although this work involved ESI, EID should also be suitable for MALDI-generated glycan cations because it does not require multiply charged precursor ions.

4.5 Bibliography

(1) Bertozzi, C. R.; Kiessling, L. L. Chemical Glycobiology. *Science* **2001**, *291*, 2357-2364.

(2) Dennis, J. W.; Granovsky, M.; Warren, C. E. Glycoprotein Glycosylation and Cancer Progression. *BBA - Gen. Subjects* **1999**, *1473*, 21-34.

(3) Brooks, S. A. Altered Glycosylation of Proteins in Cancer: What is the Potential for New Anti-tumor Strategies. *Anti-Cancer Agent. Me.* **2008**, *8*, 2-21.

(4) Wu, Y. M.; Nowack, D. D.; Omenn, G. S.; Haab, B. B. Mucin Glycosylation Is Altered by Pro-Inflammatory Signaling in Pancreatic-Cancer Cells. *J. Proteome Res.* **2009**, *8*, 1876-1886.

(5) Laidler, P.; Lityńska, A. Tumor Cell *N*-Glycans in Metastasis. *Acta Biochim. Pol.* **1997**, *44*, 343-357.

(6) Kajihara, Y.; Sato, H. Structural Analysis of Oligosaccharides by Nuclear Magnetic Resonance Method. *Trends Glycosci. Glyc.* **2003**, *15*, 197-220.

(7) Duus, J. O.; Gotfredsen, C. H.; Bock, K. Carbohydrate Structural Determination by NMR Spectroscopy: Modern Methods and Limitations. *Chem. Rev.* **2000**, *100*, 4589-4614.

(8) Lutteke, T. Analysis and Validation of Carbohydrate Three-Dimensional Structures. *Acta Crystallogr. D* **2009**, *65*, 156-168.

(9) Lobsanov, Y. D.; Pletnev, V. Z.; Mokulskii, M. A. X-Ray Study of the Pea Lectin-Carbohydrate Complex at 2.4 A Resolution .2. Metal and Carbohydrate Binding-Sites-A Model of Lectin-Carbohydrate Interaction. *Bioorg. Khim* **1990**, *16*, 1599-1606.

(10) Davies, M. J.; Hounsell, E. F. Carbohydrate Chromatography: Towards Yoctomole Sensitivity. *Biomed. Chromatogr.* **1996**, *10*, 285-289.

(11) Zaia, J. Mass Spectrometry and the Emerging Field of Glycomics. *Chem. Biol.* **2008**, *15*, 881-892.

(12) Park, Y.; Lebrilla, C. B. Application of Fourier Transform Ion Cyclotron Resonance Mass Spectrometry to Oligosaccharides. *Mass Spectrom. Rev.* **2005**, *24*, 232-264.

(13) Bielik, A. M.; Zaia, J. Historical Overview of Glycoanalysis. *MIMB* **2010**, *600*, 9-30.

(14) Es-Safi, N. E.; Kerhoas, L.; Einhorn, J.; Ducrot, P. H. Application of ESI/MS, CID/MS and Tandem MS/MS to the Fragmentation Study of Eriodictyol 7-*O*-Glucosyl-(1 -> 2)-Glucoside and Luteolin 7-*O*-Glucosyl-(1 -> 2)-Glucoside. *Int. J. Mass spectrom.* **2005**, *247*, 93-100.

(15) Seipert, R. R.; Dodds, E. D.; Clowers, B. H.; Beecroft, S. M.; German, J. B.; Lebrilla, C. B. Factors that Influence Fragmentation Behavior of N-Linked Glycopeptide Ions. *Anal. Chem.* **2008**, *80*, 3684-3692.

(16) Adamson, J. T.; Hakansson, K. Infrared Multiphoton Dissociation and Electron Capture Dissociation of High-Mannose Type Glycopeptides. *J. Proteome Res.* **2006**, *5*, 493-501.

(17) Domon, B.; Costello, C. E. A Systematic Nomenclature for Carbohydrate Fragmentations in FAB-MS/MS Spectra of Glycoconjugates. *Glycoconjugate J.* **1988**, *5*, 397-409.

(18) Wuhrer, M.; Catalina, M. I.; Deelder, A. M.; Hokke, C. H. Glycoproteomics Based on Tandem Mass Spectrometry of Glycopeptides. *J. Chromatogr. B* **2007**, *849*, 115-128.

(19) Gillece-Castro, B. L.; Burlingame, A. L. In *Mass Spectrometry*; Academic Press, 1990; Vol. Volume 193, pp 689-712.

(20) Yu, S.-Y.; Wu, S.-W.; Khoo, K.-H. Distinctive characteristics of MALDI-Q/TOF and TOF/TOF tandem mass spectrometry for sequencing of permethylated complex type N-glycans. *Glycoconjugate J.* **2006**, *23*, 355-369.

(21) Kohler, M.; Leary, J. A. Gas Phase Reactions of Doubly Charged Alkaline Earth and Transition Metal(II)-Ligand Complexes Generated by Electrospray Ionization. *Int. J. Mass Spectrom. Ion Processes* **1997**, *162*, 17-34.

(22) Srikanth, R.; Reddy, P. N.; Srinivas, R.; Sharma, G. V. M.; Reddy, K. R.; Krishna, P. R. Mass Spectral Study of Alkali-Cationized Boc-Carbo-B3-Peptides

by Electrospray Tandem Mass Spectrometry. *Rapid Commun. Mass Spectrom.* **2004**, *18*, 3041-3050.

(23) Morelle, W.; Slomianny, M. C.; Diemer, H.; Schaeffer, C.; Dorsselaer, A. v.; Michalski, J. C. Fragmentation Characteristics of Permethylated Oligosaccharides Using a Matrix-Assisted Laser Desorption/Ionization Two-Stage Time-of-Flight (TOF/TOF) Tandem Mass Spectrometer. *Rapid Commun. Mass Spectrom.* **2004**, *18*, 2637-2649.

(24) Zhou, W.; Hakansson, K. Structural Characterization of Carbohydrates by Fourier Transform Tandem Mass Spectrometry. *Curr. Proteomics* **2011**, *8*, 297-308.

(25) Harvey, D. Fragmentation of Negative Ions from Carbohydrates: Part 1. Use of Nitrate and Other Anionic Adducts for the Production of Negative Ion Electrospray Spectra from N-Linked Carbohydrates. *J. Am. Soc. Mass. Spectrom.* **2005**, *16*, 622-630.

(26) Zhu, J.; Cole, R. B. Ranking of Gas-Phase Acidities and Chloride Affinities of Monosaccharides and Linkage Specificity in Collision-Induced Decompositions of Negative Ion Electrospray-Generated Chloride Adducts of Oligosaccharides. *J. Am. Soc. Mass. Spectrom.* **2001**, *12*, 1193-1204.

(27) Cai, Y.; Jiang, Y.; Cole, R. B. Anionic Adducts of Oligosaccharides by Matrix-Assisted Laser Desorption/Ionization Time-of-Flight Mass Spectrometry. *Anal. Chem.* **2003**, *75*, 1638-1644.

(28) Jiang, Y.; Cole, R. B. Oligosaccharide Analysis Using Anion Attachment in Negative Mode Electrospray Mass Spectrometry. *J. Am. Soc. Mass. Spectrom.* **2005**, *16*, 60-70.

(29) Adamson, J. T.; Håkansson, K. Electron Capture Dissociation of Oligosaccharides Ionized with Alkali, Alkaline Earth, and Transition Metals. *Anal. Chem.* **2007**, *79*, 2901-2910.

(30) Zhao, C.; Xie, B.; Chan, S. Y.; Costello, C. E.; O'Connor, P. B. Collisionally Activated Dissociation and Electron Capture Dissociation Provide Complementary Structural Information for Branched Permethylated Oligosaccharides. *J. Am. Soc. Mass. Spectrom.* **2008**, *19*, 138-150.

(31) Harvey, D. J. Analysis of Carbohydrates and Glycoconjugates by Matrix-Assisted Laser Desorption/Ionization Mass Spectrometry: An Update For 2003-2004. *Mass Spectrom. Rev.* **2009**, *28*, 273-361.

(32) Adamson, J. T.; Håkansson, K. Electron Detachment Dissociation of Neutral and Sialylated Oligosaccharides. *J. Am. Soc. Mass. Spectrom.* **2007**, *18*, 2162-2172.

(33) Wolff, J.; Laremore, T.; Busch, A.; Linhardt, R.; Amster, I. Electron Detachment Dissociation of Dermatan Sulfate Oligosaccharides. *J. Am. Soc. Mass. Spectrom.* **2008**, *19*, 294-304.

(34) Wolff, J. J.; Chi, L.; Linhardt, R. J.; Amster, I. J. Distinguishing Glucuronic from Iduronic Acid in Glycosaminoglycan Tetrasaccharides by Using Electron Detachment Dissociation. *Anal. Chem.* **2007**, *79*, 2015-2022.

(35) Han, L.; Costello, C. Electron Transfer Dissociation of Milk Oligosaccharides. *J. Am. Soc. Mass. Spectrom.* **2011**, *22*, 997-1013.

(36) Devakumar, A.; Thompson, M. S.; Reilly, J. P. Fragmentation of Oligosaccharide Ions with 157 nm Vacuum Ultraviolet Light. *Rapid Commun. Mass Spectrom.* **2005**, *19*, 2313-2320.

(37) Ko, B. J.; Brodbelt, J. S. 193 nm Ultraviolet Photodissociation of Deprotonated Sialylated Oligosaccharides. *Anal. Chem.* **2011**, *83*, 8192-8200.

(38) Wilson, J. J.; Brodbelt, J. S. Ultraviolet Photodissociation at 355 nm of Fluorescently Labeled Oligosaccharides. *Anal. Chem.* **2008**, *80*, 5186-5196.

(39) Wuhrer, M.; Koeleman, C. A. M.; Deelder, A. M. Hexose Rearrangements upon Fragmentation of *N*-Glycopeptides and Reductively Aminated *N*-Glycans. *Anal. Chem.* **2009**, *81*, 4422-4432.

(40) Ková; ccaron; ik, V.; Hirsch, J.; P.; Heerma, W.; Thomas-Oates, J.; Haverkamp, J. Oligosaccharide Characterization Using Collision-Induced Dissociation Fast Atom Bombardment Mass Spectrometry: Evidence for Internal Monosaccharide Residue Loss. *J. Mass Spectrom.* **1995**, *30*, 949-958.

(41) Yoo, H. J.; Liu, H.; Håkansson, K. Infrared Multiphoton Dissociation and Electron-Induced Dissociation as Alternative MS/MS Strategies for Metabolite Identification. *Anal. Chem.* **2007**, *79*, 7858-7866.

(42) Lioe, H.; O'Hair, R. Comparison of Collision-Induced Dissociation and Electron-Induced Dissociation of Singly Protonated Aromatic Amino Acids, Cystine and Related Simple Peptides Using a Hybrid Linear Ion Trap–FT-ICR Mass Spectrometer. *Anal. Bioanal. Chem.* **2007**, *389*, 1429-1437.

(43) Ly, T.; Yin, S.; Loo, J. A.; Julian, R. R. Electron-Induced Dissociation of Protonated Peptides Yields Backbone Fragmentation Consistent with a Hydrogen-Deficient Radical. *Rapid Commun. Mass Spectrom.* **2009**, *23*, 2099-2101.

(44) Kalli, A.; Hess, S. Fragmentation of Singly, Doubly, and Triply Charged Hydrogen Deficient Peptide Radical Cations in Infrared Multiphoton Dissociation and Electron Induced Dissociation. *J. Am. Soc. Mass. Spectrom.* **2012**, *23*, 244-263.

(45) Kalli, A.; Grigorean, G.; Håkansson, K. Electron Induced Dissociation of Singly Deprotonated Peptides. *J. Am. Soc. Mass. Spectrom.* **2011**, *22*, 2209-2221.

(46) Budnik, B. A.; Haselmann, K. F.; Elkin, Y. N.; Gorbach, V. I.; Zubarev, R. A. Applications of Electron−Ion Dissociation Reactions for Analysis of Polycationic Chitooligosaccharides in Fourier Transform Mass Spectrometry. *Anal. Chem.* **2003**, *75*, 5994-6001.

(47) Wolff, J. J.; Laremore, T. N.; Aslam, H.; Linhardt, R. J.; Amster, I. J. Electron-Induced Dissociation of Glycosaminoglycan Tetrasaccharides. *J. Am. Soc. Mass. Spectrom.* **2008**, *19*, 1449-1458.

(48) Wills, R. H.; Tosin, M.; O'Connor, P. B. Structural Characterization of Polyketides Using High Mass Accuracy Tandem Mass Spectrometry. *Anal. Chem.* **2012**, *84*, 8863-8870.

(49) Kaczorowska, M. A.; Cooper, H. J. Electron Induced Dissociation (EID) Tandem Mass Spectrometry of Octaethylporphyrin and Its Iron(III) Complex. *Chem. Commun.* **2011**, *47*, 418-420.

(50) Kaczorowska, M. A.; Cooper, H. J. Electron Induced Dissociation: A Mass Spectrometry Technique for the Structural Analysis of Trinuclear Oxo-Centred Carboxylate-Bridged Iron Complexes. *J. Am. Soc. Mass. Spectrom.* **2010**, *21*, 1398-1403.

(51) Mosely, J. A.; Smith, M. J. P.; Prakash, A. S.; Sims, M.; Bristow, A. W. T. Electron-Induced Dissociation of Singly Charged Organic Cations as a Tool for Structural Characterization of Pharmaceutical Type Molecules. *Anal. Chem.* **2011**, *83*, 4068-4075.

(52) Aberth, W.; Burlingame, A. L. *Electron Collision-Induced Dissociation (EL CID) Applied to Mass-Spectrometry*; Elsevier Science Publ B V: Amsterdam, 1990.

(53) Yu, X.; Huang, Y.; Lin, C.; Costello, C. E. Energy-Dependent Electron Activated Dissociation of Metal-Adducted Permethylated Oligosaccharides. *Anal. Chem.* **2012**, *84*, 7487-7494.

(54) Nielsen, M. L.; Budnik, B. A.; Haselmann, K. F.; Olsen, J. V.; Zubarev, R. A. Intramolecular Hydrogen Atom Transfer in Hydrogen-Deficient Polypeptide Radical Cations. *Chem. Phys. Lett.* **2000**, *330*, 558-562.

(55) Franz, A. H.; Lebrilla, C. B. Evidence for Long-Range Glycosyl Transfer Reactions in the Gas Phase. *J. Am. Soc. Mass. Spectrom.* **2002**, *13*, 325-337.

(56) Thaysen-Andersen, M.; Mysling, S.; Højrup, P. Site-Specific Glycoprofiling of N-Linked Glycopeptides Using MALDI-TOF MS: Strong Correlation between Signal Strength and Glycoform Quantities. *Anal. Chem.* **2009**, *81*, 3933-3943.

(57) Ceroni, A.; Maass, K.; Geyer, H.; Geyer, R.; Dell, A.; Haslam, S. M. GlycoWorkbench: A Tool for the Computer-Assisted Annotation of Mass Spectra of Glycans. *J. Proteome Res.* **2008**, *7*, 1650-1659.

(58) Varki, A.; Cummings, R. D.; Esko, J. D.; Freeze, H. H.; Stanley, P.; Bertozzi, C. R.; Hart, G. W.; Etzler, M. E. *Essentials of Glycobiology, 2nd edition*; Cold Spring Harbor (NY): Cold Spring Harbor Laboratory Press, 2009.

(59) Harvey, D. J.; Bateman, R. H.; Green, M. R. High-Energy Collision-Induced Fragmentation of Complex Oligosaccharides Ionized by Matrix-assisted Laser Desorption/Ionization Mass Spectrometry. *J. Mass Spectrom.* **1997**, *32*, 167-187.

Chapter 5 Electron Induced Dissociation (EID) of Singly Deprotonated Glycans With and Without Aromatic Labels

5.1 Introduction

Glycans constitute one of the three major classes of biomolecules with the other two being proteins and nucleic acids. For most living organisms, carbohydrates are not only the major structural support, but also the major energy source. In addition, carbohydrates and glycoconjugates are involved in a number of biological processes, including host-pathogen interactions, cell communication, proliferation and differentiation as well as initiation of immune response.[1-4] In order to fully understand the key roles glycans play in various cellular processes, knowledge of only the sequence of these compounds is far from sufficient. The linkage, degree of branching, and stereochemistry should also be determined.

Traditionally, nuclear magnetic resonance (NMR) spectroscopy, X-ray crystallography, and gas chromatography/mass spectrometry (GC/MS) have all been utilized for structural characterization of glycans.[5] However, these analytical approaches are not capable of achieving the high sensitivity required in glycoproteomics. On the other hand, electrospray ionization and matrix-assisted laser desorption/ionization (MALDI) tandem mass spectrometry have emerged as promising tools for structural elucidation. Modern mass spectrometers provide not only high sensitivity and high

selectivity, but also superior precision and resolution, all of which are particularly valuable for structural characterization of carbohydrates and carbohydrate conjugates, due to the highly complex nature and limited quantity of these molecules.

Two types of bond cleavages occur in carbohydrate MS/MS:[6] Glycosidic cleavages between neighboring monosaccharide residues, resulting in B, C, Y, and Z-type ions and cross-ring cleavages, occuring within one monosaccharide residue. Glycosidic cleavages provide valuable information about glycan composition but cross-ring cleavages are necessary for determining linkage and branching. However, such A- and X-type cross-ring fragments are more elusive as higher energy is required to cleave two chemical bonds.

Electron capture dissociation (ECD)[7-9], electron transfer dissociation (ETD)[10, 11] and electron detachment dissociation (EDD)[12, 13] have demonstrated significant advantages in generating cross-ring cleavages. Such ion-electron or ion-ion reactions provide complementary structural information to vibrational activation such as collision activation dissociation (CAD) and infrared multiphoton dissociation (IRMPD). ECD,ETD, and EDD all involve charge reduction and, therefore, these techniques require multiply charged precursor ions. This requirement can be challenging in carbohydrate analysis, because oligosaccharides frequently do not contain acidic or basic sites.

Electron induced dissociation (EID) is an MS/MS activation technique compatible with singly charged precursor ions.[14-22] In this technique, singly charged cations or anions are irradiated with >10 eV electrons to generate vibrational and electronic excitation without charge neutralization. Chapter 4 demonstrated positive ion mode EID of singly protonated glycans, generating enhanced fragmentation with less

fucose migration and additional cross-ring cleavages compared with CAD of the same species. Aromatic labels are found to have an essential effect in influencing EID fragmentation. More conjugated structure facilitates electronic excitation and therefore yield additional cleavages. In this Chapter, glycan EID is extended to negative ion mode. Negative mode MS/MS techniques have previously shown advantages such as lack of fucose migration, and more cross-ring cleavages.[23, 24] In addition, acidic analytes, such as glycans containing sialic acids, ionize more readily in negative ion mode. Sialic acids have been shown to play a significant role in cancer progression and metastasis with many cancer-related glycans containing sialic acids.[25]

5.2 Experimental Section

5.2.1 Sample Preparation

Lacto-N-difucohexaose I (LNDFH I), lacto-N-fucopentaose (LNFP I), lacto-N-hexaose (LNH), LS-tetrasaccharide A (LSTa), LS-tetrasaccharide B (LSTb), LS-tetrasaccharide C (LSTc), and an asialo biantennary glycan (NA2) (all from V-Labs, Inc., Covington, LA) were either used in their underivatized state, or labeled with 9-aminofluorene (9FL), 2-amino benzamide (2AB), or 2-anthranilic acid (2AA) (all labels from Sigma-Aldrich, St. Louis, MO) according to protocols adapted from previous literature, as briefly outlined below.[26-28] All chemicals for the labeling reactions were purchased from Sigma-Aldrich.

5.2.2 9FL Glycan Labeling

400 nmol 9-aminofluorene hydrochloride was dissolved in 200 μL deionized water to which 400 nmol $NaHCO_3$ was added followed by incubation at room

temperature for ten minutes. The resulting suspension was dried under vacuum and re-dissolved in 100 μL methanol. 0.05 mmol $NaCNBH_3$ and 5 μL glacial acetic acid were then added to the solution and this reagent was immediately added to the glycan solution (200 nmol glycan in 50 μL deionized water) followed by incubation in a water bath at 80 ℃ for 2 hours. The cooled solution was dried under vacuum and redissolved in 100 μL deionized water for subsequent desalting.

5.2.3 2AA Glycan Labeling

Two nmol oligosaccharide was dissolved in 60 μL 2-AA labeling reagent (30 mg 2AA, 20 mg sodium cyanoborohydride, 20 mg boric acid, and 40 mg sodium acetate dissolved in 1 mL MeOH) and incubated in a water bath at 80 ℃ for 1 hour.

5.2.4 2AB Glycan Labeling

Two nmol oligosaccharide was dissolved in 60 μL 2-AB labeling reagent (0.35 M 2AB and 1 M sodium cyanoborohydride in 30% glacial acetic acid and 70% DMSO (v/v)) and incubated in a water bath at 65 ℃ for 2 hours.

5.2.5 Desalting of Labeled Glycans

After derivatization, labeled glycans were cleaned up with an SPE graphitized carbon column (Alltech, Nicholasville, KY). Columns were first equilibrated with 80% ACN/0.1% formic acid (3 mL) and then washed stepwise with H_2O (3 mL). Sample solution was slowly loaded onto the equilibrated and washed cartridge. After washing with 3-5 mL H_2O, 9FL-, 2AB-, or 2AA-labeled glycans were stepwise eluted with 40% can/0.1% formic acid followed by 60% can/0.1% formic acid and dried down in a

vacuum concentrator. 2AB- and 2AA-labeled glycans mostly eluted with 40% ACN/0.1% formic acid whereas 9FL-labeled glycans mostly eluted with 60% ACN,/0.1% formic acid.

5.2.6 Fourier Transform Ion Cyclotron Resonance Mass Spectrometry

Underivatized and dried labeled glycans were dissolved in electrospray solution (50:50 methanol:H_2O, 0.1% ammonium hydroxide) for analysis in negative ion mode. Singly deprotonated unlabeled or labeled glycans, $[M - H]^-$, were generated by electrospray ionization (ESI) at 70 μL/h (Apollo II dual-stage ion funnel ion source, Bruker Daltonics, Billerica, MA). All experiments were performed with a 7 Tesla quadrupole-FT-ICR mass spectrometer (APEX-Q, Bruker Daltonics). EID was performed inside the ICR cell with a cathode heating current of 1.8 A, and a cathode bias voltage of - 12 to - 19 V for 2 - 4 s. CAD was performed in the collision cell at a collision voltage of - 5.5 to - 35 V. Mass spectra were acquired with 512k data points and summed over 64 scans or 100 scans.

5.2.7 Data Analysis

Data processing was performed with Data Analysis software (Bruker Daltonics). Calibration was performed internally by using the two most confident ions (one is the precursor ion, the other is a product ion). Data were analyzed manually with the aid of GlycoWorkbench software.[29] Product ions were not assigned unless the S/N ratio was at least 3.

5.3 Results and Discussion

The standard symbolic representation of monosaccharides established in Glycobiology[30] is used in the Figures below.

5.3.1 CAD and EID of Unlabeled and 9FL-Labeled Deprotonated LNDFH

Negative ion mode CAD and EID of unlabeled LNDFH are shown in Figure 5.1. CAD was optimized to generate the highest variety of fragments. The optimized collision voltage for underivatized LNDFH was 12.5 V compared with – 5.5 V in positive ion mode. The higher energy required to effectible dissociate the anion is likely due to the absence of a mobile proton in negative ion mode. Another difference from positive ion CAD is that C-type glycosidic cleavages are dominant, as expected from previous negative ion CAD of glycans.[31-34] Specifically, C_2, $C_{3\alpha,}$ and C_4 products are highly abundant. A more exciting difference compared with positive ion CAD is that several cross-ring cleavages are obtained in negative ion CAD, in accordance with previous literature. [35]

EID of deprotonated LNDFH required longer electron irradiation time than positive ion EID, 3 s rather than ~0.5 s (see Chapter 4). This behavior was not unexpected based on the longer irradiation times required in EDD (~1 s) vs. ECD (<100 ms) and the expected lower EID cross-section in negative ion mode. Negative ion EID resulted in significantly different fragmentation behavior compared with positive ion EID. For LNDFH, several A- and X- type cross-ring cleavages, providing valuable structural information, are observed in negative ion EID of the unlabeled oligosaccharide, adding whereas no cross-ring cleavages were observed in positive ion EID of unlabeled LNDFH and only ^{1,5}X-type cross-ring cleavages were detected for fluorescently labeled

LNDFH (Chapter 4).

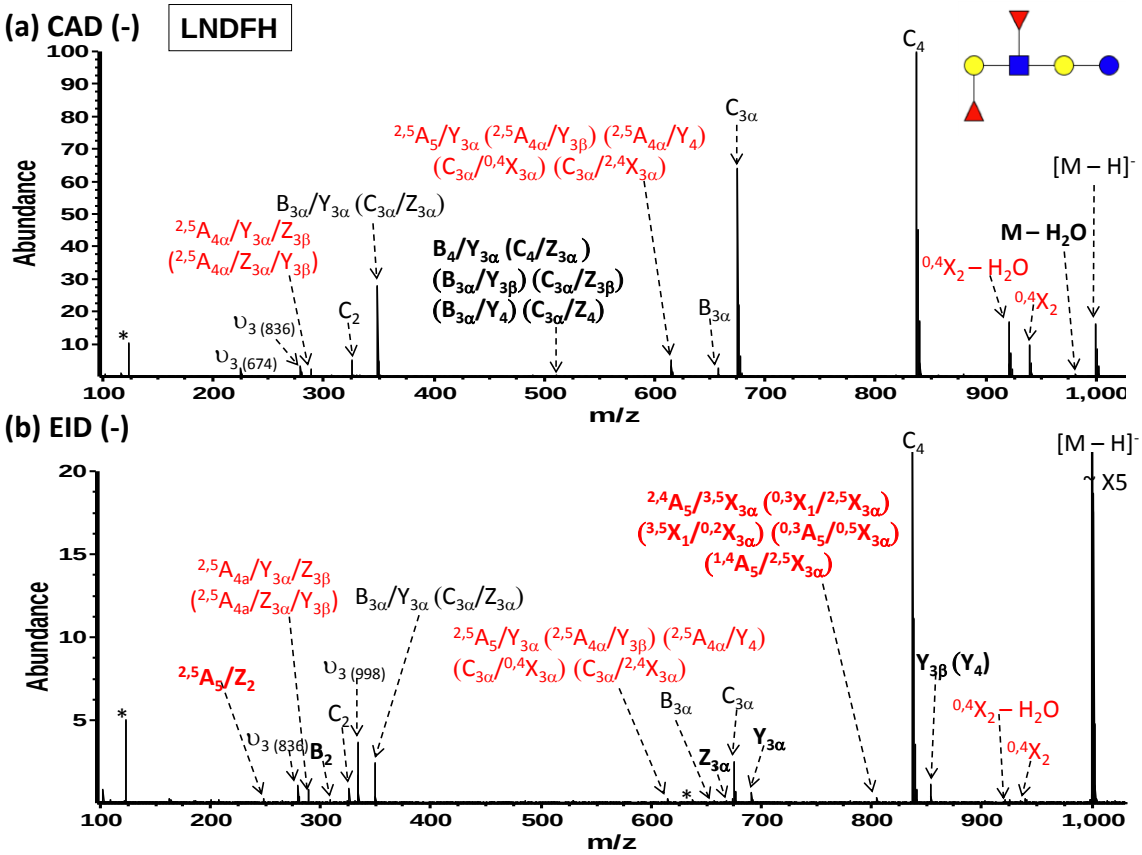

Figure 5.1 Negative ion MS/MS spectra of underivatized LNDFH. (a) CAD (100 scans, collision voltage 12.5 V); (b) EID (100 scans, 3 s electron irradiation with a cathode bias voltage of - 12 V). Fragments highlighted in red correspond to cross-ring cleavages and fragments highlighted in bold are unique to either negative ion CAD or EID. *: noise; υ: harmonic peaks.

A summary of negative ion CAD and EID of underivatized LNDFH is shown in Table 5.1. Nine fragments, including B- and C-type products, several internal fragments, and one $^{0,4}X_2$ cross-ring fragment are shared between these two negative mode MS/MS techniques. One internal fragment and one water loss ion are unique to CAD, whereas four glycosidic cleavages (B_2, $Z_{3\alpha}$, $Y_{3\alpha}$, and $Y_{3\beta}$ (or Y_4)) and two internal fragments, including cross-ring cleavages, are unique to EID. The additional product ions observed

from EID provide more detailed composition, sequence, and branching/linkage information.

Table 5.1 Product ions observed in negative ion CAD and EID of deprotonated underivatized LNDFH. Fragments highlighted in bold on the right under "CAD" and "EID" are unique to either technique.

CAD (-)		EID (-)	
$^{2,5}A_{4\alpha}/Y_{3\alpha}/Z_{3\beta}$ ($^{2,5}A_{4\alpha}/Z_{3\alpha}/Y_{3\beta}$) C_2 $B_{3\alpha}/Y_{3\alpha}$ ($C_{3\alpha}/Z_{3\alpha}$) $^{2,5}A_5/Y_{3\alpha}$ ($^{2,5}A_{4\alpha}/Y_{3\beta}$) ($^{2,5}A_{4\alpha}/Y_4$) ($C_{3\alpha}/^{0,4}X_{3\alpha}$) ($C_{3\alpha}/^{2,4}X_{3\alpha}$) $B_{3\alpha}$ $C_{3\alpha}$ C_4 $^{0,4}X_2 - H_2O$ $^{0,4}X_2$	**$B_4/Y_{3\alpha}$ ($C_4/Z_{3\alpha}$)** **($B_{3\alpha}/Y_{3\beta}$)** **($C_{3\alpha}/Z_{3\beta}$) ($B_{3\alpha}/Y_4$)** **($C_{3\alpha}/Z_4$)** **M – H_2O**	$^{2,5}A_{4\alpha}/Y_{3\alpha}/Z_{3\beta}$ ($^{2,5}A_{4\alpha}/Y_{3\beta}/Z_{3\alpha}$) C_2 $B_{3\alpha}/Y_{3\alpha}$ ($C_{3\alpha}/Z_{3\alpha}$) $^{2,5}A_5/Y_{3\alpha}$ ($^{2,5}A_{4\alpha}/Y_{3\beta}$) ($^{2,5}A_{4\alpha}/Y_4$) ($C_{3\alpha}/^{0,4}X_{3\alpha}$) ($C_{3\alpha}/^{2,4}X_{3\alpha}$) $B_{3\alpha}$ $C_{3\alpha}$ C_4 $^{0,4}X_2 - H_2O$ $^{0,4}X_2$	**$^{2,5}A_5/Z_2$** **B_2** **$^{2,4}A_5/^{3,5}X_{3\alpha}$** **($^{0,3}X_1/^{2,5}X_{3\alpha}$)** **($^{3,5}X_1/^{0,2}X_{3\alpha}$)** **($^{0,3}A_5/^{0,5}X_{3\alpha}$)** **($^{1,4}A_5/^{2,5}X_{3\alpha}$)** **$Z_{3\alpha}$** **$Y_{3\alpha}$** **$Y_{3\beta}$ (Y_4)**

CAD and EID of deprotonated 9FL-labeled LNDFH are shown in Figure 5.2. 9FL labeling enhanced both CAD and EID fragmentation in negative ion mode, similar to positive ion mode (Chapter 4). Negative ion CAD of 9FL-derivatized LNDFH (9FL-LNDFH) yielded more Y- and Z-type glycosidic cleavages as well as additional cross-ring fragments. Of particular interest are cleavages occurring on the second and third monosaccharide residue from the non-reducing end: $A_{3\alpha}$ and X_2 cross-ring fragments provide valuable branching information.

Similar to negative ion EID of unlabeled LNDFH, the most abundant product ion in negative ion EID of 9FL-LNDFH is a C_4 ion, corresponding to cleavage between the galactose (Gal) and Glu residues. 9FL labeling also resulted in additional EID fragments, including B_1, [$^{0,3}A_5$ ($^{1,4}A_5$) – H_2O], and [$^{0,2}A_5$ – H_2O]. 9FL is a conjugated structure with two aromatic rings. Such structure facilitates electronic excitation in EID.

Compared with negative ion CAD, negative ion EID of 9FL-LNDFH generated complementary and additional structural information: Sixteen product ions, including many glycosidic cleavages, cross-ring cleavages, and internal fragments could only be observed in EID (see Table 5.2).

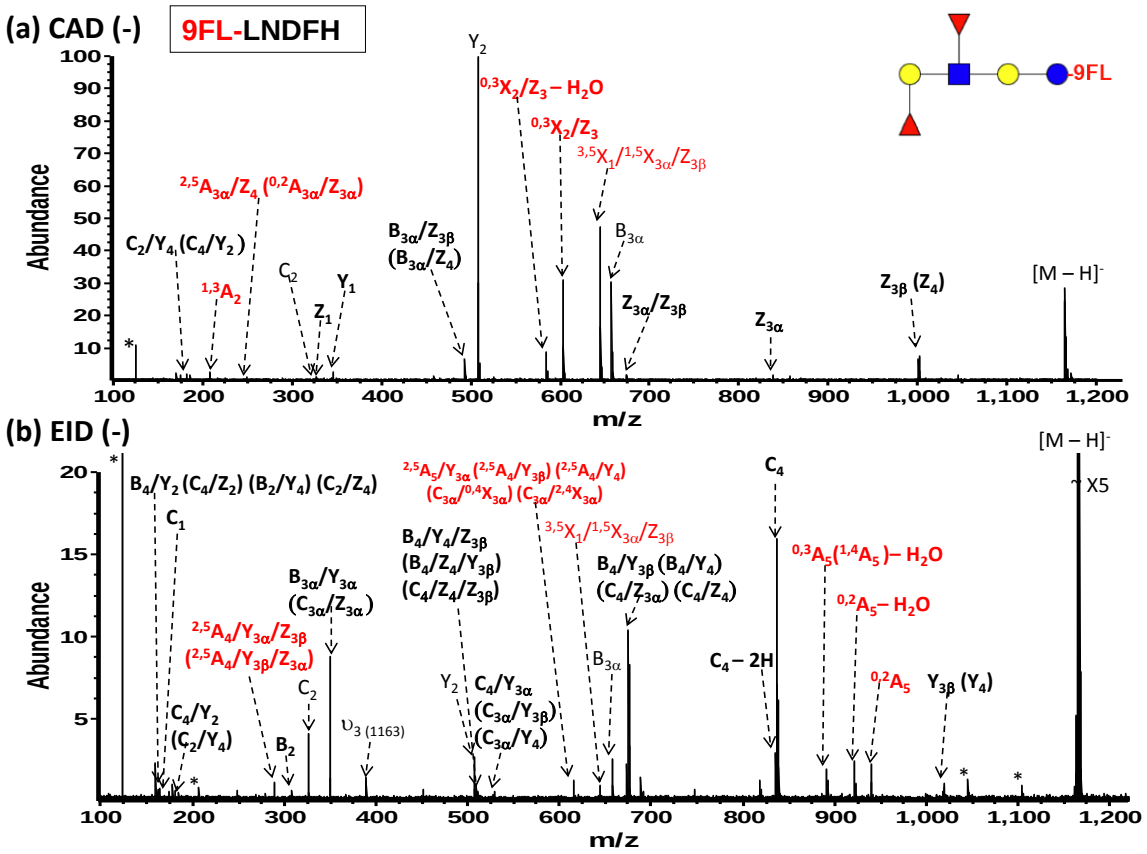

Figure 5.2 Negative ion MS/MS of 9FL-derivatized LNDFH (9FL-LNDFH). (a) CAD (100 scans, collision voltage 36.5 V); (b) EID (100 scans, 3 s electron irradiation with a cathode bias voltage of - 12 V). Fragments highlighted in red correspond to cross-ring cleavages and fragments highlighted in bold are unique to either CAD or EID. *: noise; υ: harmonic peaks.

Table 5.2 Products observed in negative ion CAD and EID of 9FL-LNDFH. Fragments highlighted in bold on the right under "CAD" and "EID" are unique to either technique

CAD (-)		EID (-)	
Y_2 C_2 $^{3,5}X_1/^{1,5}X_{3\alpha}/Z_{3\beta}$ $B_{3\alpha}$	**C_2/Y_4 (C_4/Y_2)** **$^{1,3}A_2$** **$^{2,5}A_{3\alpha}/Z_4(^{0,2}A_{3\alpha}/Z_{3\alpha})$** **$Z_1$** **$Y_1$** **$B_{3\alpha}/Z_{3\beta}$ ($B_{3\alpha}/Z_4$)** **$^{0,3}X_2/Z_3 - H_2O$** **$^{0,3}X_2/Z_3$** **$Z_{3\alpha}/Z_{3\beta}$** **$Z_{3\alpha}$** **$Z_{3\beta}$ (Z_4)**	Y_2 C_2 $^{3,5}X_1/^{1,5}X_{3\alpha}/Z_{3\beta}$ $B_{3\alpha}$	**C_2/Y_4 (C_4/Y_2)** **B_4/Y_2 (C_4/Z_2) (B_2/Y_4) (C_2/Z_4)** **C_1** **$^{2,5}A_{4\alpha}/Y_{3\alpha}/Z_{3\beta}$ ($^{2,5}A_{4\alpha}/Y_{3\beta}/Z_{3\alpha}$)** **$B_2$** **$B_{3\alpha}/Y_{3\alpha}$ ($C_{3\alpha}/Z_{3\alpha}$)** **$^{2,5}A_5/Y_{3\alpha}$ ($^{2,5}A_{4\alpha}/Y_{3\beta}$) ($^{2,5}A_{4\alpha}/Y_4$)** **$B_4/Y_4/Z_{3\beta}$ ($B_4/Z_4/Y_{3\beta}$)($C_4/Z_4/Z_{3\beta}$)** **$C_4/Y_{3\alpha}$ ($C_{3\alpha}/Y_{3\beta}$) ($C_{3\alpha}/Y_4$)** **$B_4/Y_{3\beta}$ (B_4/Y_4) ($C_4/Z_{3\alpha}$)(C_4/Z_4)** **$C_4 - 2H$** **C_4** **$^{0,3}A_5(^{1,4}A_5) - H_2O$** **$^{0,2}A_5 - H_2O$** **$^{0,2}A_5$** **$Y_{3\beta}(Y_4)$**

5.3.2 CAD and EID of Unlabeled and 9FL-Labeled Deprotonated LNFP

LNFP is a linear glycan with similar structure as LNDFH but without the fucose branch at the *N*-acetyl glucosamine (GlcNAc) residue. A series of C-type ions were resulted from negative ion CAD of unlabeled LNFP (see Figure 5.3a). Similar to unlabeled LNDFH, the most abundant peak in the CAD spectrum is a C_4 ion and the second most abundant peak is a C_3 ion. $^{1,3}A_2$ and $^{0,2}A_5$ cross-ring cleavages are also observed in CAD.

For unlabeled LNFP, unexpectedly, negative ion EID did not generate additional cross-ring cleavages compared with CAD (see Figure 5.3b and Table 5.3). However, two additional glycosidic cleavages, Y_3 and Y_4, and one additional internal fragment $C_4/Y_3(C_3/Y_4)$ are observed. These additional glycosidic fragments correspond to cleavage of the chemical bonds between the fucose and galactose residues, and the galactose and GlcNAc residues.

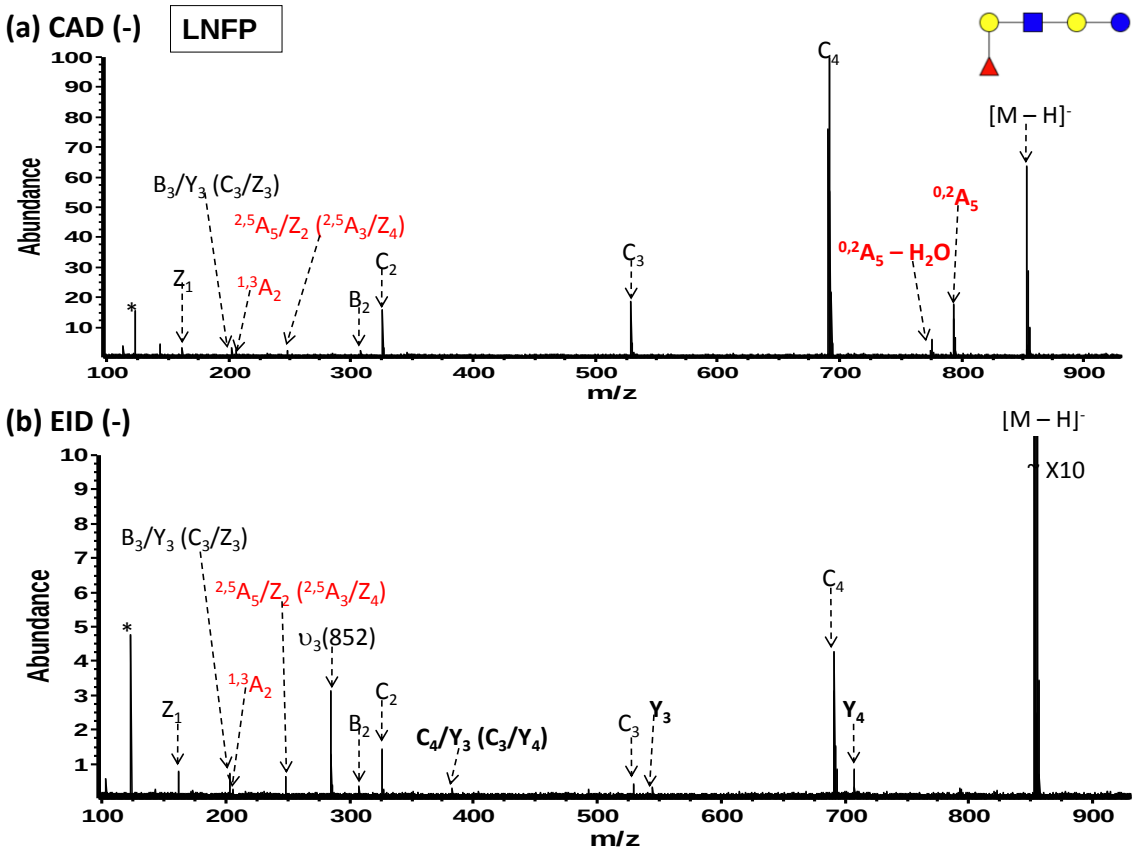

Figure 5.3 Negative ion MS/MS of LNFP. (a) CAD (64 scans, collision voltage 8.0 V); (b) EID (64 scans, 2 s electron irradiation with a cathode bias voltage of - 19 V). Fragments highlighted in red correspond to cross-ring cleavages and fragments highlighted in bold are unique to either CAD or EID. *: noise; υ: harmonic peaks.

Table 5.3 Products from negative ion CAD and EID of deprotonated LNFP. Fragments highlighted in bold on the right under "CAD" and "EID" are unique to either technique.

CAD (-)		EID (-)	
B_3/Y_3 (C_3/Z_3) Z_1 $^{1,3}A_2$ $^{2,5}A_5/Z_2$ ($^{2,5}A_3/Z_4$) B_2 C_2 C_3 C_4	**$^{0,2}A_5 - H_2O$** **$^{0,2}A_5$**	B_3/Y_3 (C_3/Z_3) Z_1 $^{1,3}A_2$ $^{2,5}A_5/Z_2$ ($^{2,5}A_3/Z_4$) B_2 C_2 C_3 C_4	**Y_4** **C_4/Y_3 (C_3/Y_4)** **Y_3 (C_4/Y_4)**

Deprotonated 9FL-derivatized LNFP underwent extensive fragmentation in negative ion CAD and EID (see Figure 5.4). 9FL labeling resulted in more X-type cross-ring cleavages from negative ion CAD, as shown in Figure 5.4a, but no A-type cross-ring cleavages. Also, more Y- and Z-type glycosidic cleavages were observed in negative ion CAD of 9FL-labeled LNDFH compared with unlabeled LNFP. EID of deprotonated 9FL-labeled LNFP induced a higher variety of cross-ring cleavages compared with unlabeled LNFP, including $^{1,4}A_4$, $^{0,3}A_5$($^{1,4}A_5$) and $^{0,2}A_5$.

Product ions from CAD and EID of singly deprotonated 9FL-labeled LNFP are summarized in Table 5.4. Although CAD generated eight unique fragments, not much structural information is gained compared with the unlabeled species. Z_2 and Z_4 provide the same structural information as Y_2 and Y_4 although the presence of both product ion types may increase sequence confidence. ($Z_3 - H_2O$) is less desired than Z_3, which was observed in EID. Overall, EID of the labeled species generated 22 unique fragments, including a variety of glycosidic fragments, cross-ring fragments, and internal fragments . Six A-type cross-ring fragments added important structural information compared with CAD.

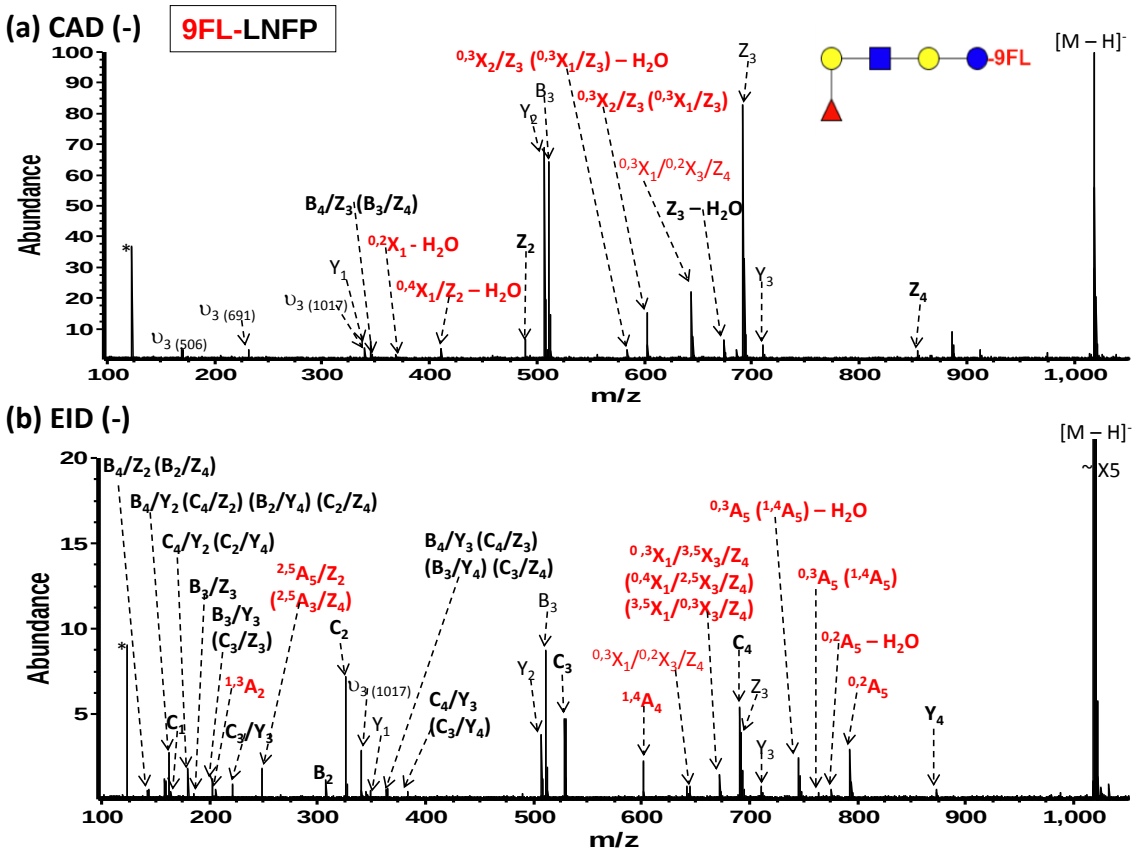

Figure 5.4 Negative ion MS/MS of 9FL-derivatized LNFP (9FL-LNFP). (a) CAD (100 scans, collision voltage 28.0 V); (b) EID (100 scans, 5 s electron irradiation with a cathode bias voltage of - 14 V). Fragments highlighted in red correspond to cross-ring cleavages and fragments highlighted in bold are unique to either CAD or EID. *: noise; υ: harmonic peaks.

Table 5.4 Products from negative ion CAD and EID of 9FL-derivatized LNFP (9FL-LNFP). Fragments highlighted in bold on the right under "CAD" and "EID" are unique to either technique.

CAD (-)		EID (-)	
B_3 Y_2 Z_3 Y_1 Y_3 $^{0,3}X_1/^{0,2}X_3/Z_4$	**Z_2** **$Z_3 - H_2O$** **Z_4** **B_4/Z_3 (B_3/Z_4)** **$^{0,2}X_1 - H_2O$** **$^{0,4}X_1/Z_2 - H_2O$** **$^{0,3}X_2/Z_3$ ($^{0,3}X_1/Z_3$) – H_2O** **$^{0,3}X_2/Z_3$ ($^{0,3}X_1/Z_3$)**	B_3 Y_2 Z_3 Y_1 Y_3 $^{0,3}X_1/^{0,2}X_3/Z_4$	**B_4/Z_2 (B_2/Z_4)** **B_4/Y_2 (C_4/Z_2) (B_2/Y_4) (C_2/Z_4)** **C_4/Y_2 (C_2/Y_4)** **B_3/Z_3** **B_3/Y_3 (C_3/Z_3)** **C_1** **$^{2,5}A_5/Z_2$ ($^{2,5}A_3/Z_4$)** **C_2** **C_3/Y_3** **$^{1,3}A_2$** **B_2** **B_4/Y_3 (C_4/Z_3) (B_3/Y_4) (C_3/Z_4)** **C_4/Y_3 (C_3/Y_4)** **C_3** **$^{0,3}X_1/^{3,5}X_3/Z_4$ ($^{0,4}X_1/^{2,5}X_3/Z_4$) ($^{3,5}X_1/^{0,3}X_3/Z_4$)** **$^{1,4}A_4$** **$^{0,3}A_5$ ($^{1,4}A_5$) – H_2O** **$^{0,3}A_5$ ($^{1,4}A_5$)** **$^{0,2}A_5 - H_2O$** **$^{0,2}A_5$** **Y_4** **C_4**

5.3.3 CAD and EID of Unlabeled Deprotonated NA2

For NA2, the simplest *N*-glycan, EID again demonstrated its preponderance for generating structurally informative fragmentation patterns (see Figure 5.5 and Table 5.5). Negative ion CAD of unlabeled deprotonated NA2 only generated five fragments, all of which could be observed in negative ion EID. In addition, negative ion EID generated 15 unique product ions, providing important complementary structural information. A series of C-ions aids identification of composition and sequence. $^{0,2}A_4$, $^{2,4}A_5$, and $^{0,2}A_5$ ions carry particularly valuable linkage information regarding the branching mannose residue and the neighboring GlcNAc residue.

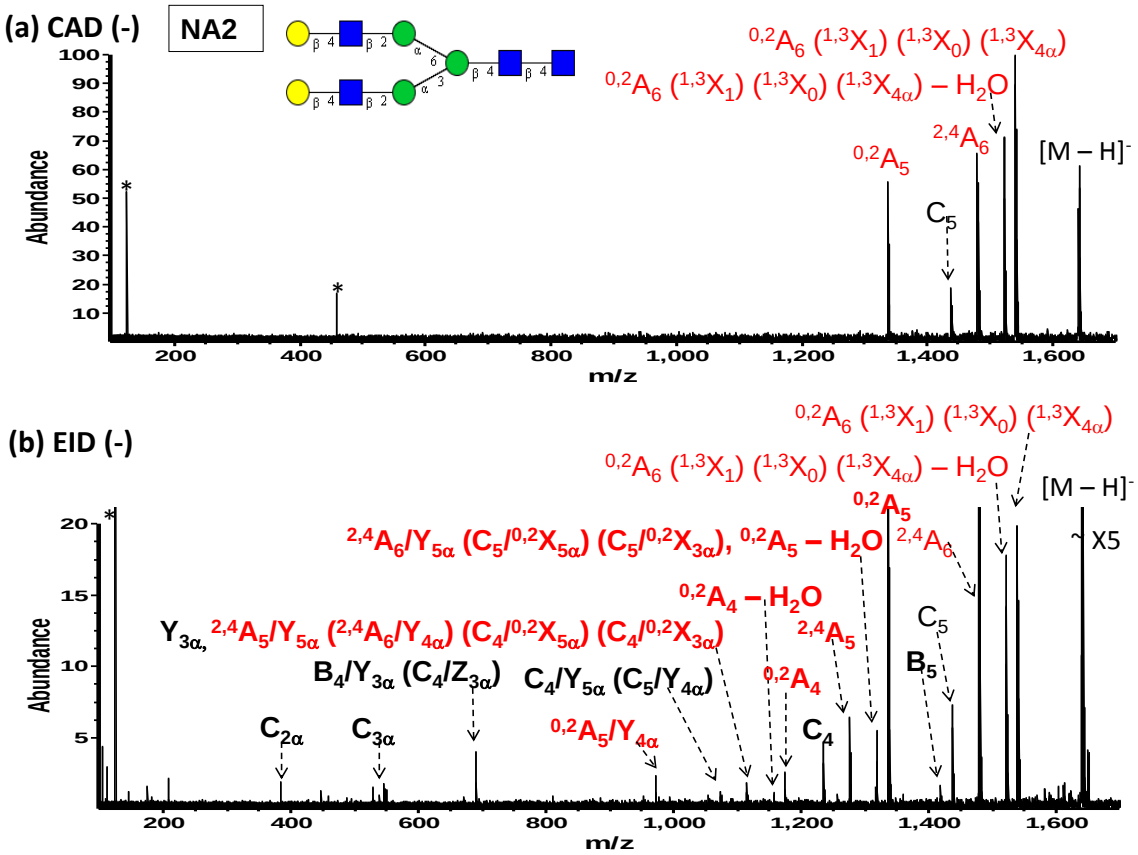

Figure 5.5 Negative ion MS/MS of deprotonated NA2. (a) CAD (100 scans, collision voltage 18 V); (b) EID (100 scans, 3 s electron irradiation with a cathode bias voltage of - 12 V). Fragments highlighted in red correspond to cross-ring cleavages and fragments highlighted in bold are unique to either CAD or EID. *: noise; υ: harmonic peaks.

Table 5.5 Products from negative ion CAD and EID of deprotonated NA2. Fragments highlighted in bold on the right are unique to EID.

CAD (-)	EID (-)	
$^{0,2}A_5$ C_5 $^{2,4}A_6$ $^{0,2}A_6$ ($^{1,3}X_1$) ($^{1,3}X_0$) ($^{1,3}X_{4\alpha}$) – H_2O $^{0,2}A_6$ ($^{1,3}X_1$) ($^{1,3}X_0$) ($^{1,3}X_{4\alpha}$)	$^{0,2}A_5$ C_5 $^{2,4}A_6$ $^{0,2}A_6$ ($^{1,3}X_1$) ($^{1,3}X_0$) ($^{1,3}X_{4\alpha}$) – H_2O $^{0,2}A_6$ ($^{1,3}X_1$) ($^{1,3}X_0$) ($^{1,3}X_{4\alpha}$)	**$C_{2\alpha}$** **$C_{3\alpha}$** **$B_4/Y_{3\alpha}$ ($C_4/Z_{3\alpha}$)** **$^{0,2}A_5/Y_{4\alpha}$** **$C_4/Y_{5\alpha}$ ($C_5/Y_{4\alpha}$)** **$Y_{3\alpha}$** **$^{2,4}A_5/Y_{5\alpha}$ ($^{2,4}A_6/Y_{4\alpha}$) ($C_4/^{0,2}X_{5\alpha}$) ($C_4/^{0,2}X_{3\alpha}$)** **$^{0,2}A_4$ – H_2O** **$^{0,2}A_4$** **C_4** **$^{2,4}A_5$** **$^{2,4}A_6/Y_{5\alpha}$ ($C_5/^{0,2}X_{5\alpha}$) ($C_5/^{0,2}X_{3\alpha}$)** **$^{0,2}A_5$ – H_2O** **$^{0,2}A_5$** **B_5**

5.3.4 Effect of Different Fluorescent Tags (2AA and 2AB) on Negative Ion CAD and EID Fragmentation

Tags seem to have an effect on CAD negative mode although without a clear mechanism being proposed. For example, 9FL derivatization showed a favor for more B- and Y-type fragments for negative mode CAD of all the glycans studied in this chapter. Similar to our previous positive ion EID experiments (Chapter 4), other fluorescent tags than 9FL were examined for potentially enhancing EID fragmentation patterns. Compared with 9FL, both 2AB and 2AA only contain one aromatic ring and therefore produce less fragments than 9FL in EID, because less conjugated structures cannot facilitate electronic excitation as well as the more conjugated structures. Such Compared with both 9FL and 2AB, 2AA is more acidic, which may aid ionization in negative mode.

2AB-labeled LNDFH fragmented extensively in both negative ion CAD and EID, see Figure 5.6 and Table 5.6). A wide variety of B-, Y-, and Z-type glycosidic cleavages,

and five cross-ring cleavages were generated from CAD. Negative ion EID yielded a series of C-type ions, two additional Y-type ions, and one more cross-ring/internal cleavage compared with negative ion CAD.

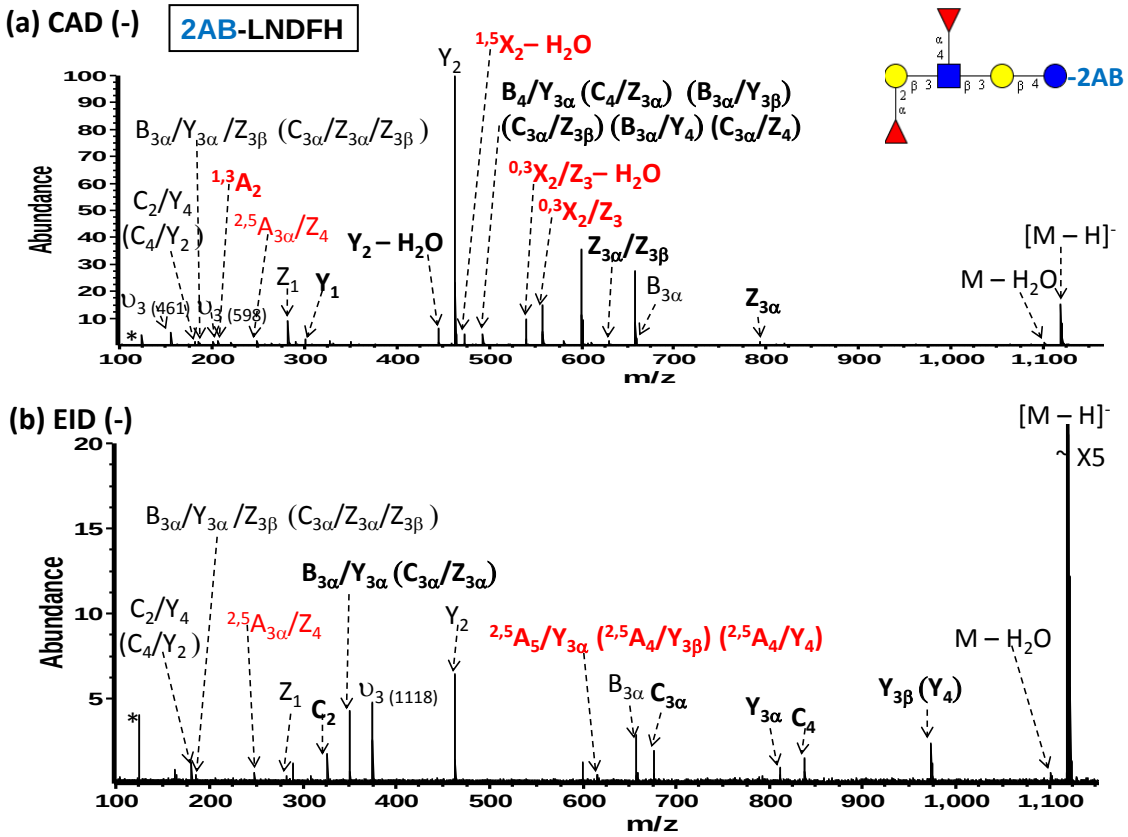

Figure 5.6 Negative ion MS/MS of 2AB-derivatized LNDFH (2AB-LNDFH). (a) CAD (100 scans, collision voltage 34 V); (b) EID (100 scans, 3 s electron irradiation with a cathode bias voltage of - 14 V). Fragments highlighted in red correspond to cross-ring cleavages and fragments highlighted in bold are unique to either CAD or EID. *: noise; υ: harmonic peaks.

Table 5.6 Products from negative ion CAD and EID of 2AB-derivatized LNDFH (2AB-LNDFH). Fragments highlighted in bold on the right under "CAD" and "EID" are unique toeither technique.

CAD (-)		EID (-)	
C_2/Y_4 (C_4/Y_2) $B_{3\alpha}/Y_{3\alpha}/Z_{3\beta}$ ($C_{3\alpha}/Z_{3\alpha}/Z_{3\beta}$) $^{2,5}A_{3\alpha}/Z_4$ Z_1 Y_2 $B_{3\alpha}$ $M - H_2O$	**$^{1,3}A_2$** **Y_1** **$Y_2 - H_2O$** **$^{1,5}X_2 - H_2O$** **$B_4/Y_{3\alpha}$ ($C_4/Z_{3\alpha}$) ($B_{3\alpha}/Y_{3\beta}$)** **($C_{3\alpha}/Z_{3\beta}$) ($B_{3\alpha}/Y_4$)** **($C_{3\alpha}/Z_4$)** **$^{0,3}X_2/Z_3 - H_2O$** **$^{0,3}X_2/Z_3$** **$Z_{3\alpha}/Z_{3\beta}$** **$Z_{3\alpha}$**	C_2/Y_4 (C_4/Y_2) $B_{3\alpha}/Y_{3\alpha}/Z_{3\beta}$ ($C_{3\alpha}/Z_{3\alpha}/Z_{3\beta}$) $^{2,5}A_{3\alpha}/Z_4$ Z_1 Y_2 $B_{3\alpha}$ $M - H_2O$	**$B_{3\alpha}/Y_{3\alpha}$ ($C_{3\alpha}/Z_{3\alpha}$)** **$^{2,5}A_5/Y_{3\alpha}$ ($^{2,5}A_{4\alpha}/Y_{3\beta}$)** **($^{2,5}A_{4\alpha}/Y_4$)** **$C_{3\alpha}$** **$Y_{3\alpha}$** **$C_2$** **$C_4$** **$Y_{3\beta}$ (Y_4)**

2AA-labeled LNDFH showed a straightforward fragmentation pattern in CAD than 2AB-labeled LNDFH, by generating a full series of Z and Y products and less internal fragments (see Figure 5.7a). Most of the fragments are Y- and Z-type product ions but one cross-ring cleavage is also observed. By contrast, negative ion EID resulted in 14 unique product ions that could not be observed in CAD (see Figure 5.7b and Table 5.7). The acidity of 2AA compared with 2AB may contribute to the improved fragmentation because of an enhanced ionization and increased S/N ratio.

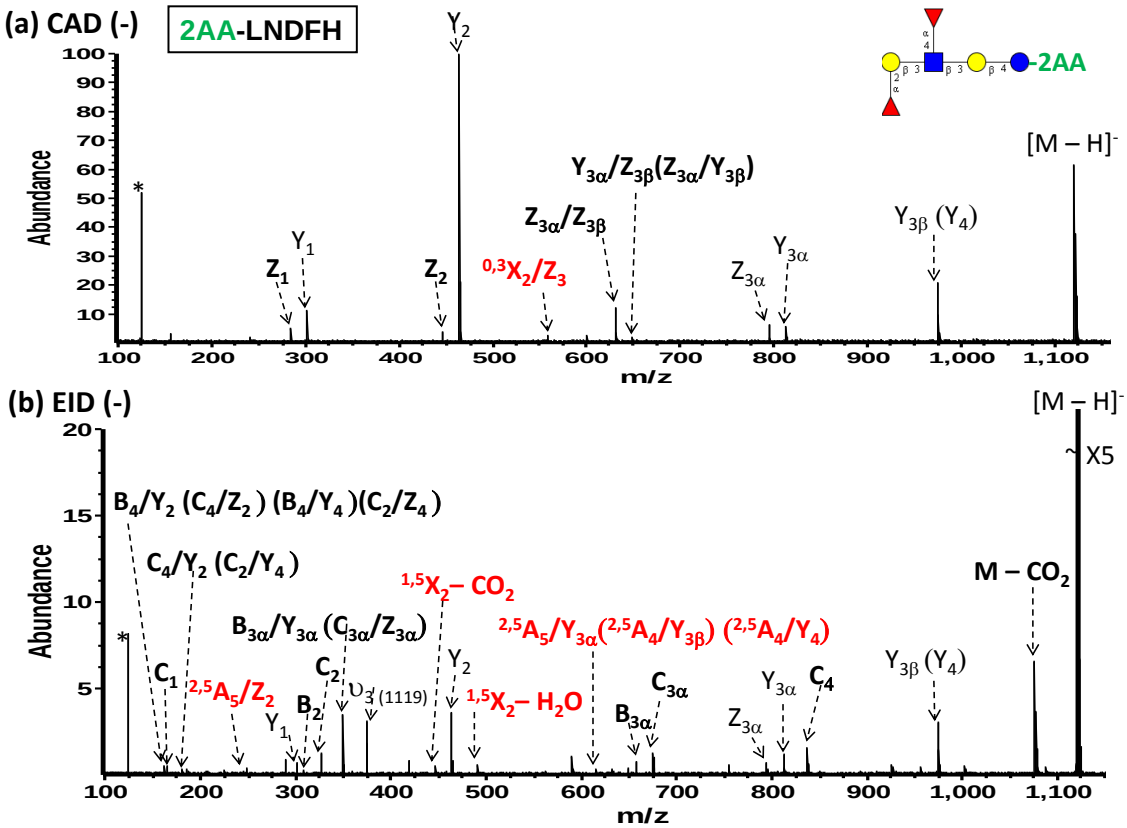

Figure 5.7 Negative ion MS/MS of 2AA-derivatized LNDFH (2AA-LNDFH). (a) CAD (100 scans, collision voltage 46 V); (b) EID (100 scans, 3.5 s electron irradiation with a cathode bias voltage of -13 V). Fragments highlighted in red correspond to cross-ring cleavages and fragments highlighted in bold are unique to either CAD or EID. *: noise; υ: harmonic peaks.

Table 5.7 Products from negative ion CAD and EID of 2AA-derivatized deprotonated LNDFH (2AA-LNDFH). Fragments highlighted in bold on the right under "CAD" and "EID" are unique to either technique.

CAD (-)		EID (-)	
Y_1	**Z_1**	Y_1	**B_4/Y_2 (C_4/Z_2) (B_4/Y_4)(C_2/Z_4)**
Y_2	**Z_2**	Y_2	**C_4/Y_2 (C_2/Y_4)**
$Z_{3\alpha}$	**$^{0,3}X_2/Z_3$**	$Z_{3\alpha}$	**C_1**
$Y_{3\alpha}$	**$Z_{3\alpha}/Z_{3\beta}$**	$Y_{3\alpha}$	**$^{2,5}A_5/Z_2$**
$Y_{3\beta}$ (Y_4)	**$Y_{3\alpha}/Z_{3\beta}$($Z_{3\alpha}/Y_{3\beta}$)**	$Y_{3\beta}$ (Y_4)	**B_2**
			C_2
			$B_{3\alpha}/Y_{3\alpha}$ ($C_{3\alpha}/Z_{3\alpha}$)
			$^{1,5}X_2 - CO_2$
			$^{1,5}X_2 - H_2O$
			$^{2,5}A_5/Y_{3\alpha}$($^{2,5}A_{4\alpha}/Y_{3\beta}$) ($^{2,5}A_{4\alpha}/Y_4$)
			$B_{3\alpha}$
			$C_{3\alpha}$
			C_4
			$M - CO_2$

In summary, similar to positive ion EID (Chapter 4), the choice of chemical tag plays a critical role in optimizing EID fragmentation (see Table 5.8 for both positive and negative ion mode). 9FL has a more conjugated structure than 2AB or 2AA and therefore is hypothesized to have a larger influence on EID whereas the different acidity between 2AA and 2AB may also influence EID fragmentation behavior.

Table 5.8 Products from positive and negative ion EID of unlabeled, 2-AA-, 2AB-, and 9FL-labeled LNDFH. The first row displays fragments shared between positive and negative ion mode whereas the second row displays fragments unique to positive and negative ion mode, respectively. The third row displays fucose migration peaks, which were only observed in positive ion EID of labeled LNDFH. Percentage values in parentheses indicate relative abundance among all observed fragments.

unlabeled		2-AA		2-AB		9FL	
EID (+)	EID (-)	EID (+)	EID (-)	EID (+)	EID (-)	EID (+)	EID (-)
$B_{3\alpha}$ $Y_{3\alpha}$ $Y_{3\beta}$ (Y_4) $B_{3\alpha}/Y_{3\alpha}$ ($C_{3\alpha}/Z_{3\alpha}$) C_4	$B_{3\alpha}$ $Y_{3\alpha}$ $Y_{3\beta}$ (Y_4) $B_{3\alpha}/Y_{3\alpha}$ ($C_{3\alpha}/Z_{3\alpha}$) C_4	$B_{3\alpha}$ Y_1 Y_2 $Y_{3\alpha}$ $Y_{3\beta}$ (Y_4) $B_{3\alpha}/Y_{3\alpha}$ ($C_{3\alpha}/Z_{3\alpha}$) $Z_{3\alpha}$	$B_{3\alpha}$ Y_1 Y_2 $Y_{3\alpha}$ $Y_{3\beta}$ (Y_4) $B_{3\alpha}/Y_{3\alpha}$ ($C_{3\alpha}/Z_{3\alpha}$) $Z_{3\alpha}$	$B_{3\alpha}$ Y_2 $Y_{3\alpha}$ $Y_{3\beta}$ (Y_4) $B_{3\alpha}/Y_{3\alpha}$ ($C_{3\alpha}/Z_{3\alpha}$)	$B_{3\alpha}$ Y_2 $Y_{3\alpha}$ $Y_{3\beta}$ (Y_4) $B_{3\alpha}/Y_{3\alpha}$ ($C_{3\alpha}/Z_{3\alpha}$)	$B_{3\alpha}$ Y_2 $Y_{3\beta}$ (Y_4) $B_{3\alpha}/Y_{3\alpha}$ ($C_{3\alpha}/Z_{3\alpha}$) B_2	$B_{3\alpha}$ Y_2 $Y_{3\beta}$ (Y_4) $B_{3\alpha}/Y_{3\alpha}$ ($C_{3\alpha}/Z_{3\alpha}$) B_2
Y_2 **Z_2** **$B_4/Y_{3\alpha}$** **($B_{3\alpha}/Y_{3\beta}$)** **($B_{3\alpha}/Y_4$)** **$B_4/Z_{3\alpha}$** **($B_{3\alpha}/Z_{3\beta}$)** **($B_{3\alpha}/Z_4$)** **$B_{3\alpha}/Y_{3\alpha}/Y_{3\beta}$** **$B_4/Y_{3\alpha}/Y_{3\beta}$** **M - H_2O**	**B_2** **C_2** **$C_{3\alpha}$** **$Z_{3\alpha}$** $^{2,5}A_5/Y_{3\alpha}$ ($^{2,5}A_{4\alpha}/Y_{3\beta}$) ($^{2,5}A_{4\alpha}/Y_4$) $^{2,5}A_{4\alpha}/Y_{3\alpha}/Z_{3\beta}$ ($^{2,5}A_{4\alpha}/Y_{3\beta}/Z_{3\alpha}$) $^{2,5}A_5/Z_2$ $^{0,4}X_2 - H_2O$ $^{0,4}X_2$ $^{2,4}A_5/^{3,5}X_{3\alpha}$ ($^{0,3}X_1/^{2,5}X_{3\alpha}$) ($^{3,5}X_1/^{0,2}X_{3\alpha}$) ($^{0,3}A_5/^{0,5}X_{3\alpha}$) ($^{1,4}A_5/^{2,5}X_{3\alpha}$)	**$B_{3\alpha}/Y_{3\alpha}/Y_{3\beta}$** **$B_4/Y_{3\alpha}$ ($B_{3\alpha}/Y_{3\beta}$)** **($B_{3\alpha}/Y_4$)** **$B_4/Y_{3\alpha}/Y_{3\beta}$** **$Z_{3\beta}$ (Z_4)** $^{1,5}X_{3\beta}$ ($^{1,5}X_4$)	**B_2** **C_1** **C_2** **$C_{3\alpha}$** **C_4** **B_4/Y_2 (C_4/Z_2)** **(B_4/Y_4) (C_2/Z_4)** **C_4/Y_2 (C_2/Y_4)** **M – CO_2** $^{2,5}A_5/Y_{3\alpha}$ ($^{2,5}A_{4\alpha}/Y_{3\beta}$) ($^{2,5}A_{4\alpha}/Y_4$) $^{2,5}A_5/Z_2$ $^{1,5}X_2 - CO_2$ $^{1,5}X_2 - H_2O$	**Y_1** **$B_{3\alpha}/Y_{3\alpha}/Y_{3\beta}$** **$B_4/Y_{3\alpha}$ ($B_{3\alpha}/Y_{3\beta}$)** **($B_{3\alpha}/Y_4$)** **$B_4/Y_{3\alpha}/Y_{3\beta}$** **$Y_{3\alpha}/Y_{3\beta}$** $^{1,5}X_2$ $^{1,5}X_{3\beta}$($^{1,5}X_4$)	**C_2** **C_4** **$C_{3\alpha}$** **Z_1** **C_2/Y_4** **(C_4/Y_2)** **$B_{3\alpha}/Y_{3\alpha}/Z_{3\beta}$** **($C_{3\alpha}/Z_{3\alpha}/Z_{3\beta}$)** **M – H_2O** $^{2,5}A_5/Y_{3\alpha}$ ($^{2,5}A_{4\alpha}/Y_{3\beta}$) ($^{2,5}A_{4\alpha}/Y_4$) $^{2,5}A_{3\alpha}/Z_4$	**tag** **Z_1** **Z_2** **$Z_{3\alpha}$** **$Z_{3\beta}$ (Z_4)** **Y_1** **$Y_{3\alpha}$** **$B_4/Y_{3\alpha}$ ($B_{3\alpha}/Y_{3\beta}$) ($B_{3\alpha}/Y_4$)** **$Y_{3\alpha}/Y_{3\beta}$** **$Y_4/Y_{3\beta}$** **$Z_{3\alpha}/Z_{3\beta}$** **$Y_{3\alpha}/Z_{3\beta}$** **$Y_4/Z_{3\beta}$** **$B_{3\alpha}/Y_{3\alpha}/Y_{3\beta}$** **$B_4/Y_{3\alpha}/Y_{3\beta}$** **$B_{3\alpha}/Y_{3\alpha}/Z_{3\beta}$** $^{1,5}X_4/Z_{3\beta}$ $^{1,5}X_1$ $^{1,5}X_2$ $^{1,5}X_{3\beta}$ ($^{1,5}X_4$) $^{1,5}X_{3\alpha}$	**C_1** **C_2** **C_4** **C_4 – 2H** **$B_4/Y_{3\beta}$ (B_4/Y_4) ($C_4/Z_{3\alpha}$)(C_4/Z_4)** **C_2/Y_4 (C_4/Y_2)** **B_4/Y_2 (C_4/Z_2) (B_2/Y_4) (C_2/Z_4)** **$B_4/Y_4/Z_{3\beta}$ ($B_4/Z_4/Y_{3\beta}$)($C_4/Z_4/Z_{3\beta}$)** **$C_4/Y_{3\alpha}$ ($C_{3\alpha}/Y_{3\beta}$) ($C_{3\alpha}/Y_4$)** $^{2,5}A_5/Y_{3\alpha}$ ($^{2,5}A_{4\alpha}/Y_{3\beta}$)($^{2,5}A_{4\alpha}/Y_4$) $^{2,5}A_{4\alpha}/Y_{3\alpha}/Z_{3\beta}$ ($^{2,5}A_{4\alpha}/Y_{3\beta}/Z_{3\alpha}$) $^{0,3}A_5$ ($^{1,4}A_5$) – H_2O $^{0,2}A_5$ – H_2O $^{0,2}A_5$
		Y_2 + ▲ (2.4%)		Y_1 + ▲ (2.2%) Y_2 + ▲ (4.3%)		Y_1 + ▲ (0.7%) Y_2 + ▲ (0.8%) $Y_{3\alpha}$ + ▲ (0.26%)	

5.3.5 Isomer Differentiation by CAD or EID of Unlabeled or Labeled Deprotonated Glycans

5.3.5.1 Differentiation of the Isomers LNH and pLNH

LNH and pLNH are both composed of six monosaccharides, including three galactose, two GlcNAc, and one glucose residue. However, LNH is a branched glycan with branching occurring at the second monosaccharide from the reducing end (see Figure 5.8), whereas pLNH is linear. The cross-ring fragments A_3 and X_1 are particularly valuable for differentiating these two isomers. Positive mode CAD and EID were not able to generate such informative cross-ring cleavages. Only $^{1,5}X$-type fragments were observed in positive mode EID.

On the other hand, critical cross-ring cleavages were observed in both CAD and EID of singly deprotonated unlabeled LNH (Figure 5.8). Negative ion MS/MS generated a higher variety of fragments compared with positive ion CAD and EID, even with 9FL labeling in positive ion mode (Figure 5.9). In particular, the cross-ring fragments $^{0,4}X_1(^{1,3}X_1)(^{2.4}X_1)$, $^{0,3}A_3(^{1,4}A_3)$, $^{0,4}X_1(^{1,3}X_1)$, and $(^{2.4}X_1 - H_2O)$ (highlighted in pink in Table 5.9) were observed.

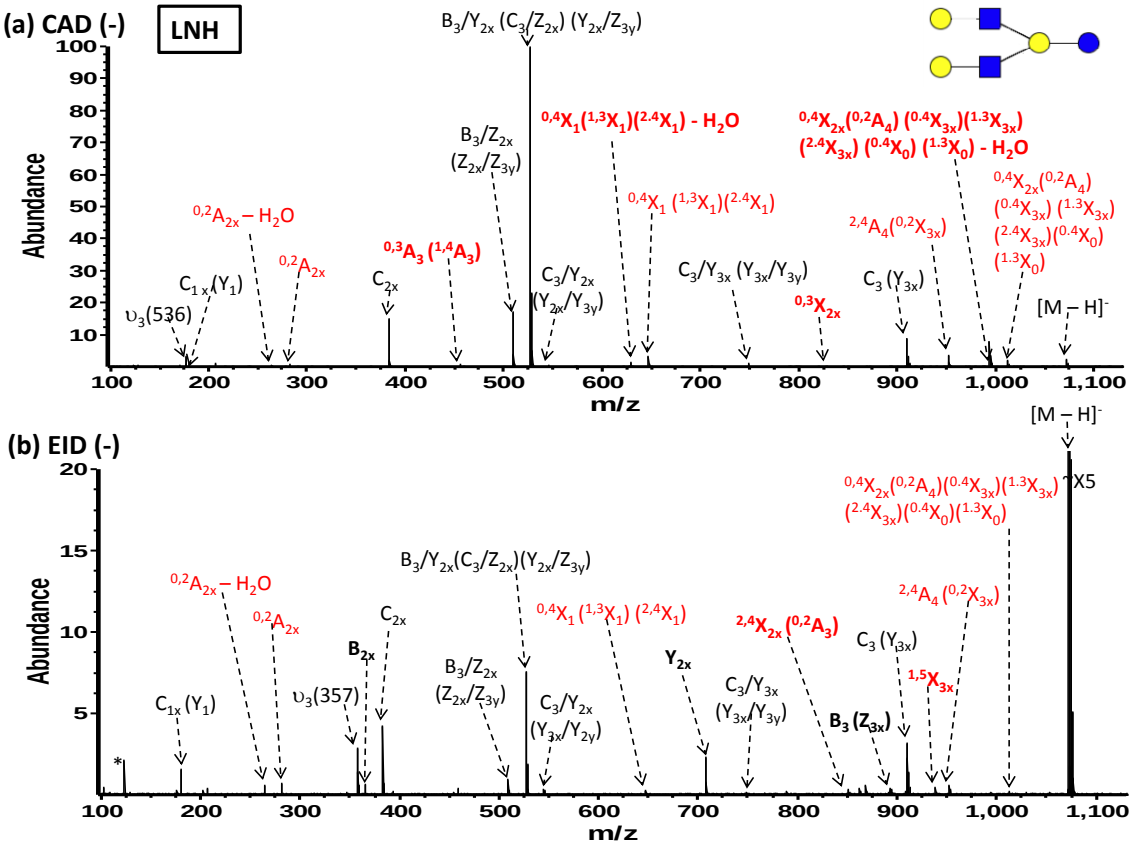

Figure 5.8 Negative ion MS/MS of singly deprotonated LNH. (a) CAD (100 scans, collision voltage 10 V); (b) EID (100 scans, 4 s electron irradiation with a cathode bias voltage of - 12 V). Fragments highlighted in bold are unique to either CAD or EID. *: noise; Δ: dimer. υ: harmonic peaks. Fragments in red correspond to cross-ring cleavages.

Table 5.9 Products from negative ion CAD and EID of singly deprotonated LNH. Fragments highlighted in bold are unique to either CAD or EID and fragments in pink are valuable for isomer differentiation. Underlined: H rearrangement.

CAD (-)		EID (-)	
C_{1x} (Y_1) $^{0,2}A_{2x} - H_2O$ $^{0,2}A_{2x}$ C_{2x} B_3/Z_{2x} (Z_{2x}/Z_{3y}) B_3/Y_{2x} (C_3/Z_{2x}) (Y_{2x}/Z_{3y}) C_3/Y_{2x} (Y_{2x}/Y_{3y}) C_3/Y_{3x} (Y_{3x}/Y_{3y}) $^{0,4}X_1(^{1,3}X_1)(^{2,4}X_1)$ C_3 (Y_{3x}) $^{2,4}A_4(^{0,2}X_{3x})$ $^{0,4}X_{2x}(^{0,2}A_4)$ ($^{0,4}X_{3x}$)($^{1,3}X_{3x}$) ($^{2,4}X_{3x}$) ($^{0,4}X_0$) ($^{1,3}X_0$)	**$^{0,3}A_3$ ($^{1,4}A_3$)** **$^{0,4}X_1(^{1,3}X_1)(^{2,4}X_1)$ - H_2O** **$^{0,3}X_{2x}$** **$^{0,4}X_{2x}(^{0,2}A_4)$** **($^{0,4}X_{3x}$)($^{1,3}X_{3x}$) ($^{2,4}X_{3x}$)** **($^{0,4}X_0$) ($^{1,3}X_0$) - H_2O**	C_{1x} (Y_1) $^{0,2}A_{2x} - H_2O$ $^{0,2}A_{2x}$ C_{2x} B_3/Z_{2x} (Z_{2x}/Z_{3y}) B_3/Y_{2x} (C_3/Z_{2x}) (Y_{2x}/Z_{3y}) C_3/Y_{2x} (Y_{3x}/Y_{2y}) C_3/Y_{3x}(Y_{3x}/Y_{3y}) $^{0,4}X_1$ ($^{1,3}X_1$) ($^{2,4}X_1$) C_3 (Y_{3x}) $^{2,4}A_4$ ($^{0,2}X_{3x}$) $^{0,4}X_{2x}(^{0,2}A_4)$ ($^{0,4}X_{3x}$)($^{1,3}X_{3x}$) ($^{2,4}X_{3x}$) ($^{0,4}X_0$) ($^{1,3}X_0$)	**B_{2x}** **$^{2,4}X_{2x}(^{0,2}A_3)$** **B_3 (Z_{3x})** **Y_{2x}** **$^{1,5}X_{3x}$**

9FL-derivatization of LNH (9FL-LNH) also resulted in several cross-ring fragments, highlighted in red in Figure 5.9. These fragments include $^{0,4}A_3(^{1,3}A_3)(^{2,4}A_3)$, $^{3,5}A_3$, $^{0,4}X_1(^{1,3}X_1)(^{2,4}X_1)$, and $^{0,3}A_3(^{1,4}A_3)$, which all contribute to isomer differentiation and are highlighted in pink in Table 5.10.

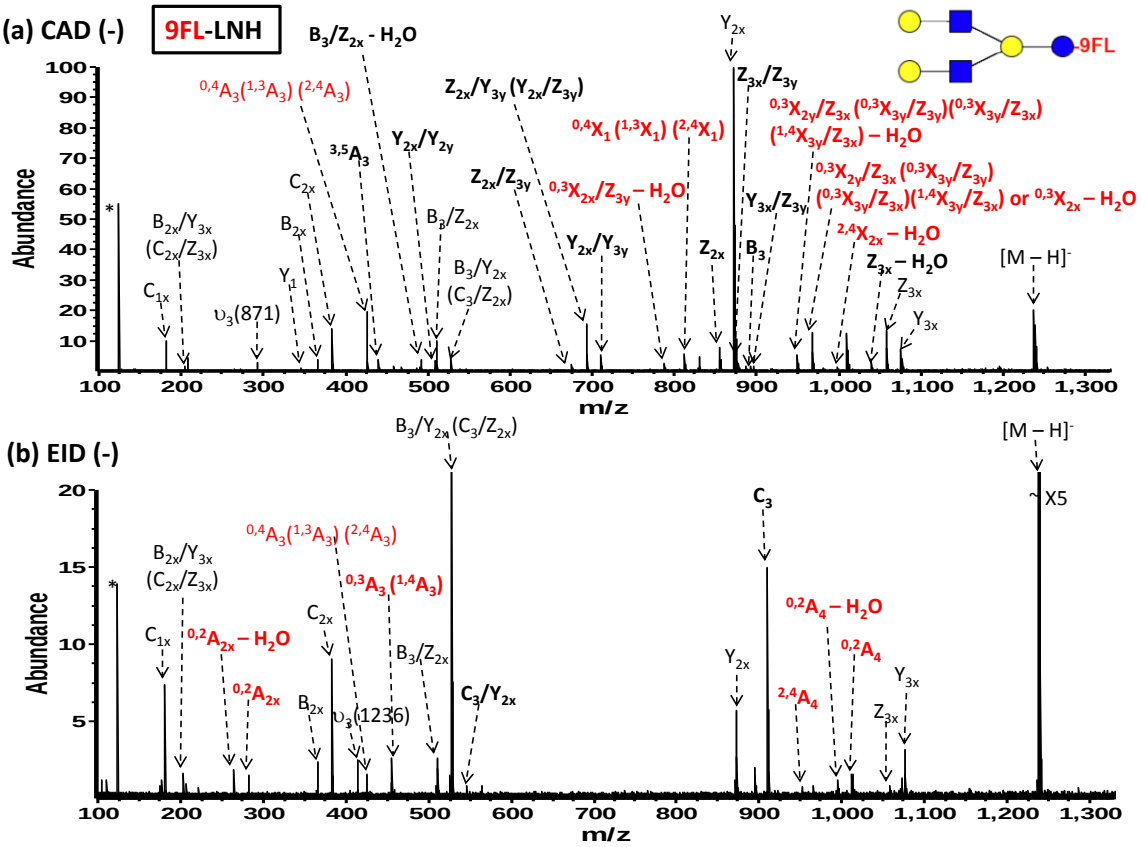

Figure 5.9 Negative ion MS/MS of singly deprotonated 9FL-LNH. (a) CAD (100 scans, collision voltage 37 V); (b) EID (100 scans, 3 s electron irradiation with a cathode bias voltage of - 14 V). Fragments highlighted in bold are unique to either CAD or EID. *: noise; Δ: dimer; underlined: H rearrangement. υ: harmonic peaks. Fragments in red correspond to cross-ring cleavages.

Table 5.10 Products from negative ion CAD and EID of singly deprotonated 9FL-LNH. Underlined: H rearrangement. Fragments highlighted in bold are unique to either CAD or EID and fragments in pink are valuable for isomer differentiation.

CAD (-)		EID (-)	
C_{1x}	$^{3,5}\underline{A_3}$	C_{1x}	$^{0,2}A_{2x} - H_2O$
B_{2x}/Y_{3x} (C_{2x}/Z_{3x})	Y_{2x}/Y_{2y}	B_{2x}/Y_{3x} (C_{2x}/Z_{3x})	$^{0,2}A_{2x}$
$\underline{^{0,4}A_3}$ ($\underline{^{1,3}A_3}$) ($\underline{^{2,4}A_3}$)	B_3/Z_{2x} - H_2O	$\underline{^{0,4}A_3}$ ($\underline{^{1,3}A_3}$) ($\underline{^{2,4}A_3}$)	$\underline{^{0,3}A_3}$ ($\underline{^{1,4}A_3}$)
C_{2x}	Z_{2x}/Z_{3y}	C_{2x}	C_3/Y_{2x}
B_{2x}	Z_{2x}/Y_{3y} (Y_{2x}/Z_{3y})	B_{2x}	C_3
B_3/Z_{2x}	$\underline{^{0,4}X_1}$ ($\underline{^{1,3}X_1}$) ($\underline{^{2,4}X_1}$)	B_3/Z_{2x}	$^{2,4}A_4$
B_3/Y_{2x} (C_3/Z_{2x})	$^{0,3}X_{2x}/Z_{3y} - H_2O$	B_3/Y_{2x} (C_3/Z_{2x})	$^{0,2}A_4 - H_2O$
Y_{2x}	Y_{2x}/Y_{3y}	Y_{2x}	$^{0,2}A_4$
Z_{3x}	Z_{2x}	Z_{3x}	
Y_{3x}	Z_{3x}/Z_{3y}	Y_{3x}	
	Y_{3x}/Z_{3y}		
	B_3		
	$^{0,3}X_{2y}/Z_{3x}$ ($^{0,3}X_{3y}/Z_{3y}$) ($^{0,3}X_{3y}/Z_{3x}$) ($^{1,4}X_{3y}/Z_{3x}$) - H_2O		
	$^{0,3}X_{2y}/Z_{3x}$ ($^{0,3}X_{3y}/Z_{3y}$) ($^{0,3}X_{3y}/Z_{3x}$) ($^{1,4}X_{3y}/Z_{3x}$) or $^{0,3}X_{2x}$-H_2O		
	$^{2,4}X_{2x}$ - H_2O		
	$Z_{3x} - H_2O$		

In summary, in order to differentiate LNH and pLNH, potential useful cross-ring cleavages should occur on the Gal monosaccharide (the second monosaccharide from the reducing end), which means X_1 or A_3 ions. In positive and negative mode CAD and EID of either singly protonated glycans or singly deprotonated glycans (with labeled or not), $^{1,5}X_1$, $^{0,4}X_1$ ($^{1,3}X_1$) ($^{2,4}X_1$), $^{3,5}A_3$, $^{0,4}A_3$ ($^{1,3}A_3$) ($^{2,4}A_3$), $^{0,3}A_3$ ($^{1,4}A_3$) were all the X_1 or A_3 ions observed (see Figure 5.10). However, $^{1,5}X_1$ which was yielded from positive mode EID does not contain the specific linkage and branching information, and therefore is not useful for isomer differentiation. On the other hand, $^{0,4}X_1$ ($^{1,3}X_1$) ($^{2,4}X_1$), $^{3,5}A_3$, $^{0,4}A_3$ ($^{1,3}A_3$) ($^{2,4}A_3$), $^{0,3}A_3$ ($^{1,4}A_3$) which were generated from negative mode CAD or EID, cleaves at certain particular sites on the particular monosaccharide. These cross-ring fragmenst are useful for isomer differentiation.

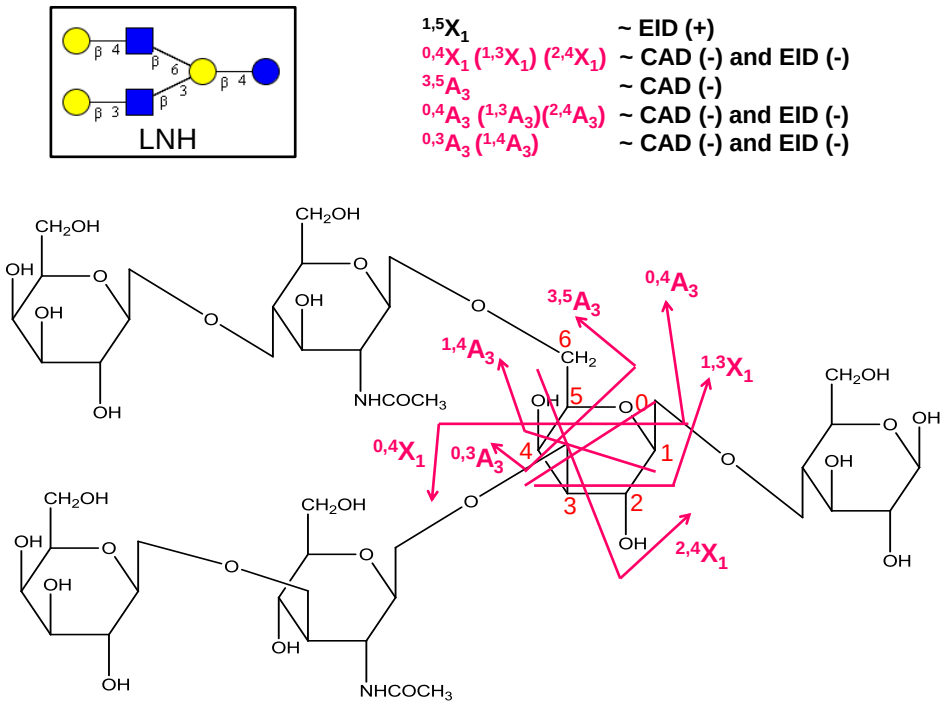

Figure 5.10 Summary of cross-ring cleavages generated from CAD and EID (positive or negative mode) of unlabeled or 9FL-labeled LNH. Fragments in pink are those useful for branching identification and isomer identification. Such useful fragments are also illustrated on the LNH glycan structure at the bottom.

5.3.5.2 LSTa, LSTb, LSTc

LSTa, LSTb, and LSTc are all composed of five monosaccharides (see Figure 5.11). LSTb is a branched glycan with two linkages at the 3 and 6 positions on the GlcNAc residue. For LSTb, isomer differentiating cross-ring cleavages correspond to A_2 and X_2 fragments. It is more difficult to differentiate LSTa and LSTc because both are linear glycans with the same composition and sequence. The only differences between these two glycans are the linkage between the sialic acid and the Gal, and the linkage between the Gal and the GlcNAc (see Figure 5.11). For differentiating LSTa and LSTc, critical cross-ring cleavages correspond to A_2, A_3, X_3, and X_2 products.

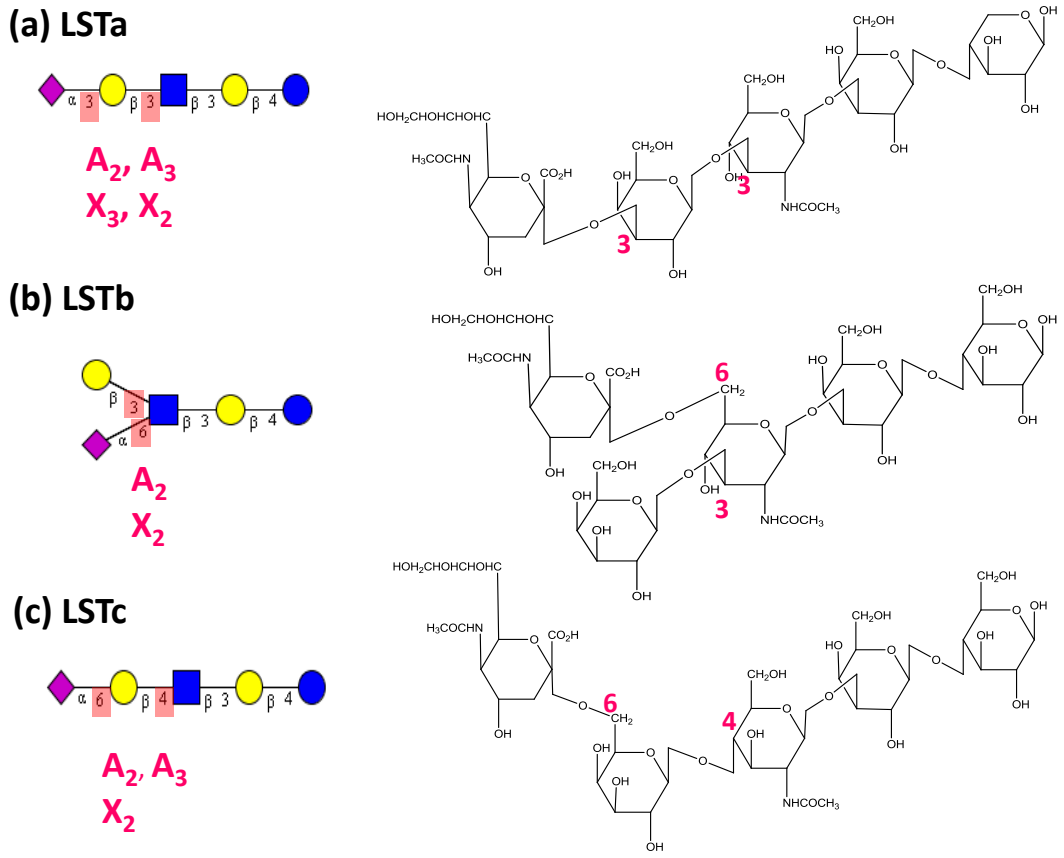

Figure 5.11 Structures of the isomers LSTa, (a) LSTb (b), and LSTc (c). Specific differences in branching or linkage are highlighted in pink and critical cross-ring cleavages are also indicated in pink.

Similar to LNH and pLNH, positive mode CAD and EID were not able to differentiate these three siomers. By contrast, egative mode CAD and EID produced superior fragmentation. Many cross-ring ions that were useful for isomer differentiation were produced and highlighted in pink in the tandem mass spectrometry spectra and the corresponding table (Figures 5.12 – 5.17, Tables 5.11 – 5.16)

For LSTa, $^{1,5}A_2$, $^{0,4}X_2$ ($^{0,4}X_3$), $^{1,3}A_3/Z_4$, $^{0,2}A_3$, $^{3,5}X_2/Y_4$ ($^{3,5}X_3/Y_4$) were observed in negative mode CAD or EID of unlabeled LSTa (see Figure 5.12 and Table 5.11). $^{1,3}A_3/Y_4$ and $^{0,4}X_2$ ($^{0,4}X_3$) were observed in negative mode EID of 9FL-LSTa (see Figure 5.13 and

Table 5.12). These cross-ring cleavages are able to differentiate LSTa because of the specific linkage information.

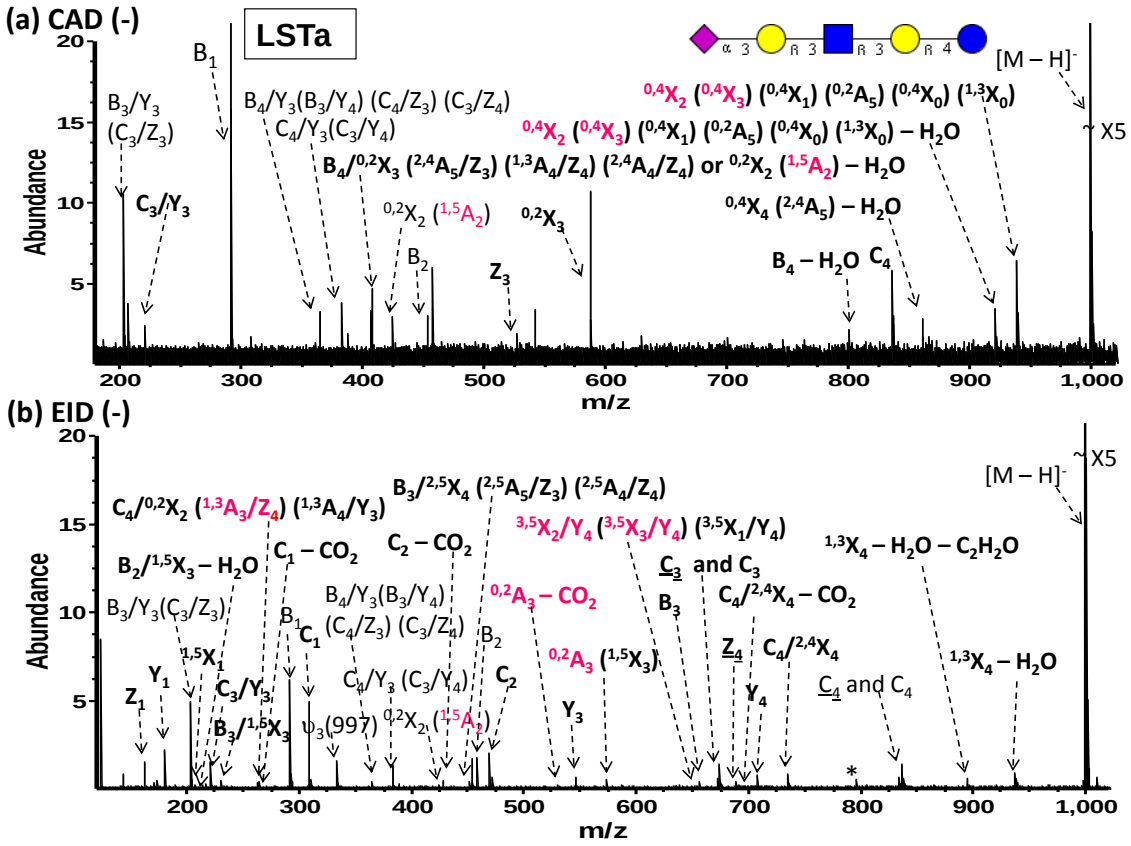

Figure 5.12 Negative mode CAD and EID mass spectra of singly deprotonated LSTa. (a) CAD (100 scans, collision voltage 35.0 V); (b) EID (100 scans, 3 sec electron irradiation with a cathode bias voltage of 15 V). *: noise; Δ: dimer; υ: harmonic peaks. Fragments highlighted in bold are unique to either CAD or EID. Fragments in pink are useful for isomer differentiation.

Table 5.11 Fragmentation summary of negative mode CAD and EID of singly deprotonated LSTa. (a) CAD (100 scans, collision voltage 35.0 V); (b) EID (100 scans, 3 sec electron irradiation with a cathode bias voltage of 15 V). *: noise; Δ: dimer; υ: harmonic peaks. Fragments highlighted in bold are unique to either CAD or EID. Fragments in pink are useful for isomer differentiation.

CAD (-)		EID (-)	
B_1	**Y_1**	B_1	**B_3/Y_3 (C_3/Z_3)**
B_4/Y_3 (B_3/Y_4)	**Z_2**	B_4/Y_3 (B_3/Y_4)	**$^{1,5}X_1$**
(C_4/Z_3) (C_3/Z_4)	**$^{0,3}X_2/Z_3$ ($^{0,3}X_1/Z_3$)**	(C_4/Z_3) (C_3/Z_4)	**C_3/Y_3**
Y_2	**$B_3 - CO_2$**	Y_2	**$B_3/^{1,5}X_3$**
Z_3	**$^{0,2}X_4$**	Z_3	**$C_4/^{0,2}X_2$ ($^{1,3}A_3/Y_4$) ($^{1,3}A_4/Y_3$) ($^{2,4}A_4/Y_3$) ($C_3/^{0,2}X_3$)**
Y_3		Y_3	**$C_1 - CO_2$**
Y_4		Y_4	**C_1**
			C_4/Y_3 (C_3/Y_4)
			$^{0,2}A_2$
			$^{1,5}A_2$
			$B_3/^{2,5}X_4$
			B_2
			$C_3/^{2,5}X_4$
			$^{0,2}A_3$
			B_3
			$^{1,3}A_4$ ($^{2,4}A_4$) – CO_2 or $\underline{C_3}$
			C_3
			$\underline{B_4}$
			$\underline{C_4}$
			C_4
			$^{1,5}X_4 - CO_2$
			$^{0,2}A_5 - H_2O$
			$^{0,2}A_5$
			$^{0,4}X_2$ ($^{0,4}X_3$) ($^{0,4}X_1$) ($^{0,4}X_0$) ($^{1,3}X_0$) - H_2O

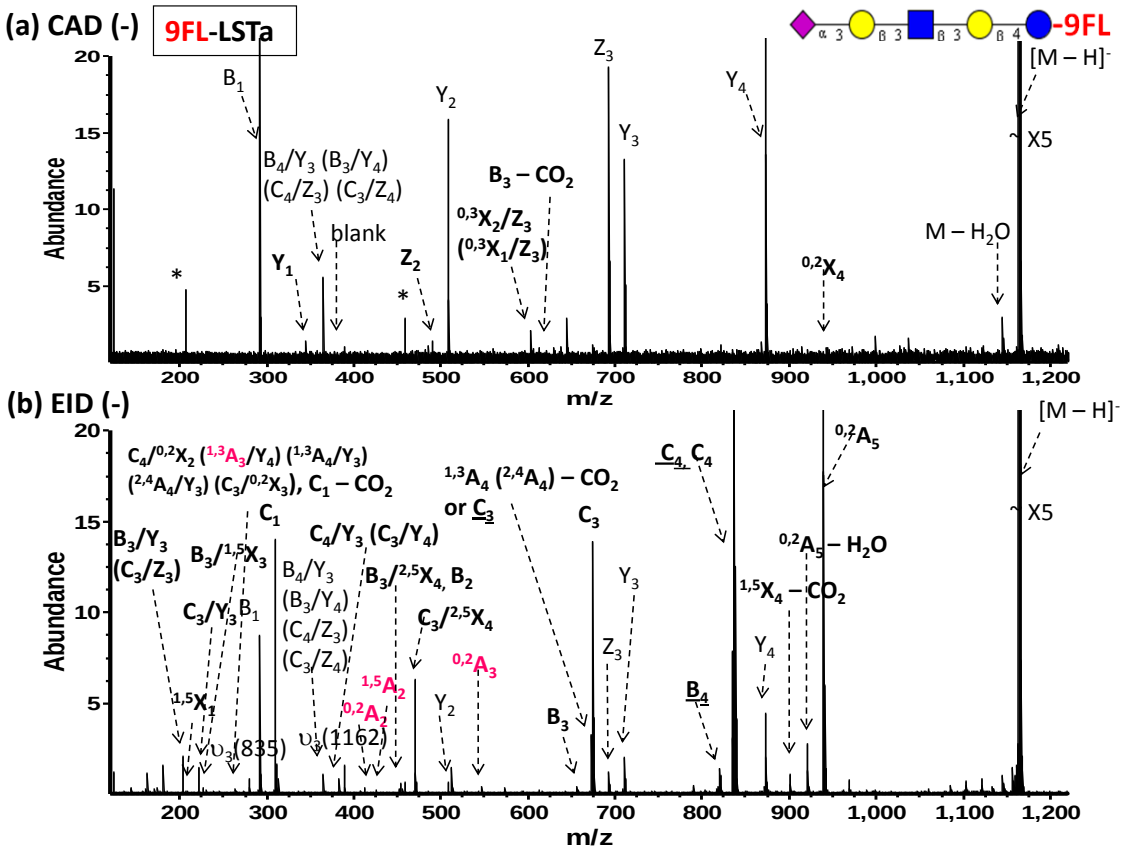

Figure 5.13 Negative mode CAD and EID mass spectra of singly protonated 9FL-LSTa. (a) CAD (100 scans, collision voltage 35.0 V); (b) EID (100 scans, 3 sec electron irradiation with a cathode bias voltage of 12 V). *: noise; Δ: dimer; υ: harmonic peaks. Fragments highlighted in bold are unique to either CAD or EID. Fragments in pink are useful for isomer differentiation.

Table 5.12 Fragmentation summary of negative mode CAD and EID of singly deprotonated 9FL-LSTa. (a) CAD (100 scans, collision voltage 35.0 V); (b) EID (100 scans, 3 sec electron irradiation with a cathode bias voltage of 12 V). *: noise; Δ: dimer; υ: harmonic peaks. Fragments highlighted in bold are unique to either CAD or EID. Fragments in pink are useful for isomer differentiation.

CAD (-)		EID (-)	
B_1	**Y_1**	B_1	**B_3/Y_3 (C_3/Z_3)**
B_4/Y_3 (B_3/Y_4)	**Z_2**	B_4/Y_3 (B_3/Y_4)	**$^{1,5}X_1$**
(C_4/Z_3) (C_3/Z_4)	**$^{0,3}X_2/Z_3$ ($^{0,3}X_1/Z_3$)**	(C_4/Z_3) (C_3/Z_4)	**C_3/Y_3**
Y_2	**$B_3 - CO_2$**	Y_2	**$B_3/^{1,5}X_3$**
Z_3	**$^{0,2}X_4$**	Z_3	**$C_4/^{0,2}X_2$ ($^{1,3}A_3/Y_4$) ($^{1,3}A_4/Y_3$) ($^{2,4}A_4/Y_3$) ($C_3/^{0,2}X_3$)**
Y_3		Y_3	**$C_1 - CO_2$**
Y_4		Y_4	**C_1**
			C_4/Y_3 (C_3/Y_4)
			$^{0,2}A_2$
			$^{1,5}A_2$
			$B_3/^{2,5}X_4$
			B_2
			$C_3/^{2,5}X_4$
			$^{0,2}A_3$
			B_3
			$^{1,3}A_4$ ($^{2,4}A_4$) – CO_2 or $\underline{C_3}$
			C_3
			$\underline{B_4}$
			$\underline{C_4}$
			C_4
			$^{1,5}X_4 - CO_2$
			$^{0,2}A_5 - H_2O$
			$^{0,2}A_5$
			$^{0,4}X_2$ ($^{0,4}X_3$) ($^{0,4}X_1$) ($^{0,4}X_0$) ($^{1,3}X_0$) - H_2O

For LSTb, the only branched glycan among these three, negative mode MS/MS also yielded many cross-ring cleavages (see Figure 5.14 and Table 5.13, Figure 5.15 and Table 5.14). $^{0,4}A_2$ and $^{1,4}A_2$ which were generated in negative mode EID of unlabeled or 9FL-labeled LSTb, could be used for isomer differentiation.

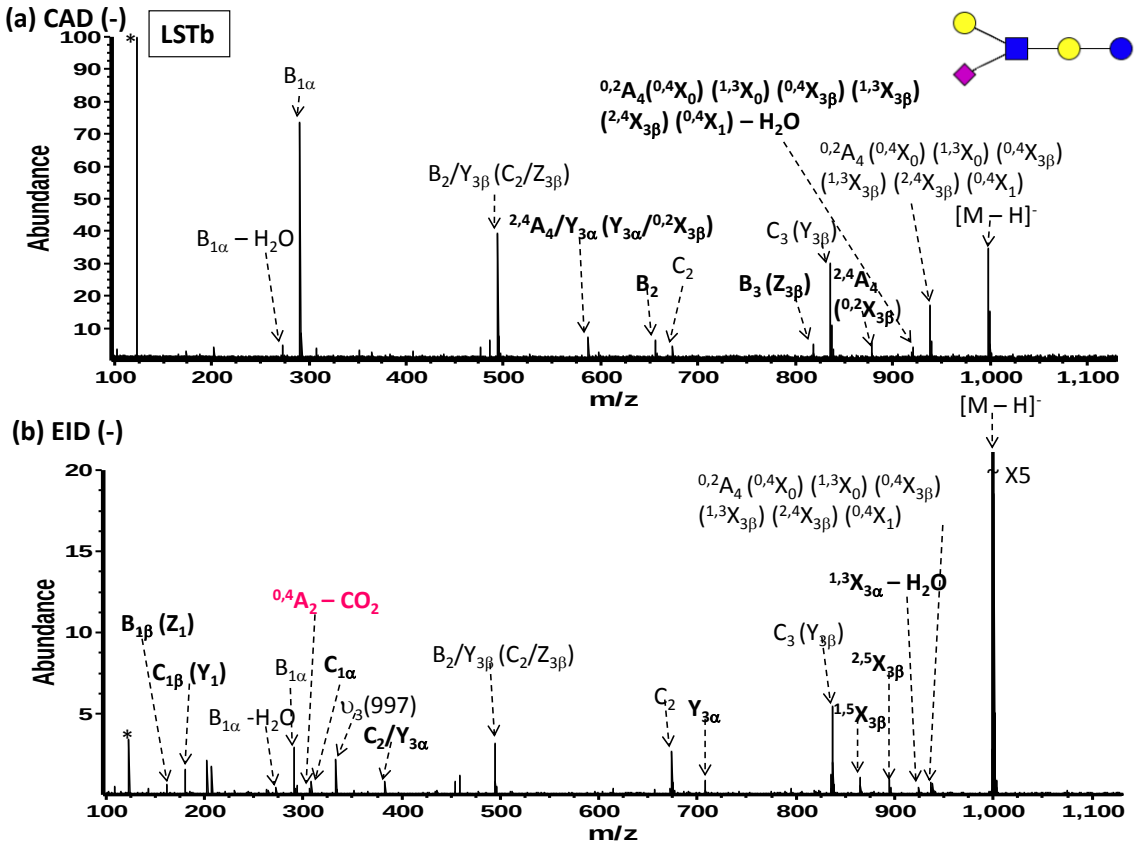

Figure 5.14 Negative mode CAD and EID mass spectra of singly deprotonated LSTb. (a) CAD (100 scans, collision voltage 40.5 V); (b) EID (100 scans, 3 sec electron irradiation with a cathode bias voltage of 14 V). Fragments highlighted in bold are unique to either CAD or EID. *: noise; Δ: dimer; υ: harmonic peaks. Fragments in pink are useful for isomer differentiation.

Table 5.13 Fragmentation summary of negative mode CAD and EID of singly deprotonated LSTb. (a) CAD (100 scans, collision voltage 40.5 V); (b) EID (100 scans, 3 sec electron irradiation with a cathode bias voltage of 14 V). Fragments highlighted in bold are unique to either CAD or EID. *: noise; Δ: dimer. Fragments in pink are useful for isomer differentiation.

CAD (-)		EID (-)	
$B_{1\alpha} - H_2O$	**$^{2,4}A_4/Y_{3\alpha}$ ($Y_{3\alpha}/^{0,2}X_{3\beta}$)**	$B_{1\alpha}$ -H_2O	**$B_{1\beta}$ (Z_1)**
$B_{1\alpha}$	**B_2**	$B_{1\alpha}$	**$C_{1\beta}$ (Y_1)**
C_2	**B_3 ($Z_{3\beta}$)**	C_2	**$^{0,4}A_2 - CO_2$**
C_3 ($Y_{3\beta}$)	**$^{2,4}A_4$ ($^{0,2}X_{3\beta}$)**	C_3 ($Y_{3\beta}$)	**$C_{1\alpha}$**
$B_2/Y_{3\beta}$ ($C_2/Z_{3\beta}$)	**$^{0,2}A_4$($^{0,4}X_0$) ($^{1,3}X_0$)**	B_2/Y_{3b} (C_2/Z_{3b})	**$C_2/Y_{3\alpha}$**
$^{0,2}A_4$ ($^{0,4}X_0$) ($^{1,3}X_0$)	**($^{0,4}X_{3\beta}$) ($^{1,3}X_{3\beta}$) ($^{2,4}X_{3\beta}$)**	$^{0,2}A_4$($^{0,4}X_0$) ($^{1,3}X_0$)	**$Y_{3\alpha}$**
($^{0,4}X_{3\beta}$) ($^{1,3}X_{3\beta}$)	**($^{0,4}X_1$) – H_2O**	($^{0,4}X_{3\beta}$) ($^{1,3}X_{3\beta}$)	**$^{2,5}X_{3\beta}$**
($^{2,4}X_{3\beta}$) ($^{0,4}X_1$)		($^{2,4}X_{3\beta}$) ($^{0,4}X_1$)	**$^{1,5}X_{3\beta}$**
			$^{1,3}X_{3\alpha} - H_2O$

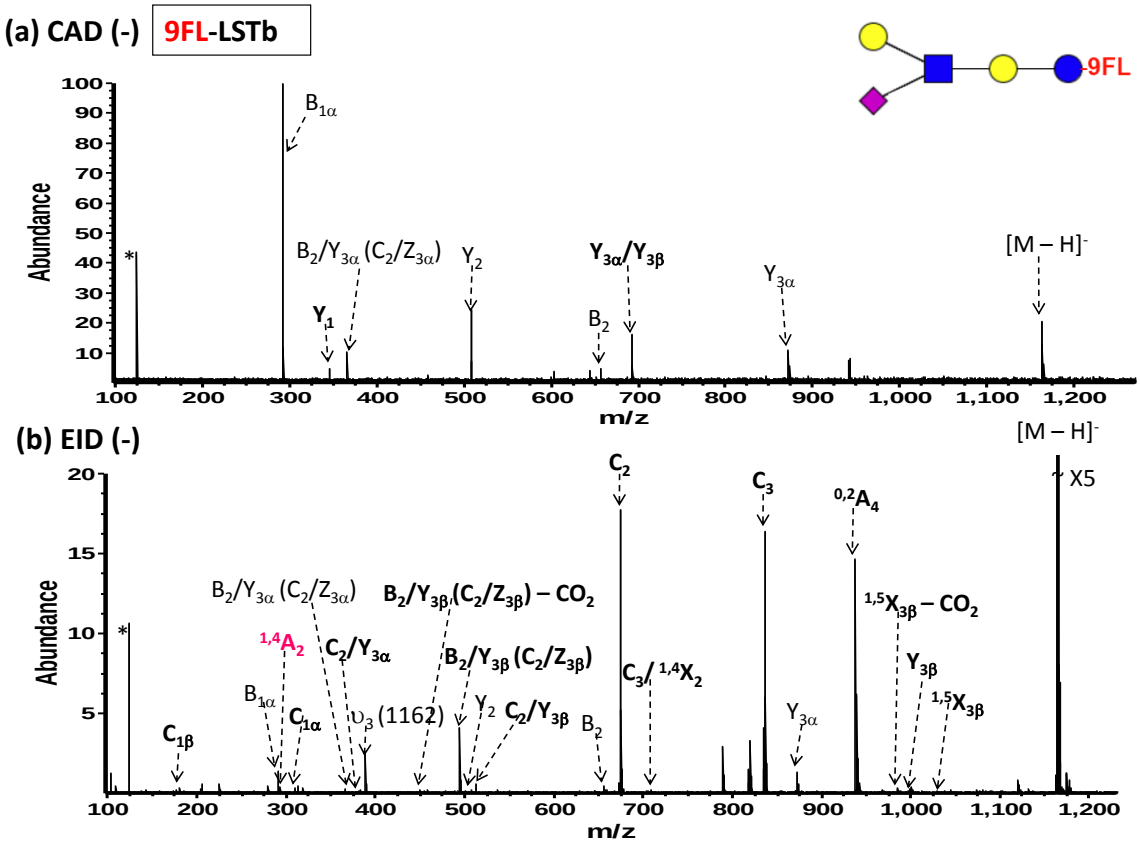

Figure 5.15 Negative mode CAD and EID mass spectra of singly deprotonated 9FL-LSTb. (a) CAD (100 scans, collision voltage 41.5 V); (b) EID (100 scans, 3 sec electron irradiation with a cathode bias voltage of 12 V). Fragments highlighted in bold are unique to either CAD or EID. *: noise; Δ: dimer; υ: harmonic peaks. Fragments in pink are useful for isomer differentiation.

Table 5.14 Fragmentation summary of negative mode CAD and EID of singly deprotonated 9FL-LSTb. (a) CAD (100 scans, collision voltage 41.5 V); (b) EID (100 scans, 3 sec electron irradiation with a cathode bias voltage of 12 V). Fragments highlighted in bold are unique to either CAD or EID. *: noise; Δ: dimer. Fragments in pink are useful for isomer differentiation.

CAD (-)		EID (-)	
$B_{1\alpha}$	**Y_1**	$B_{1\alpha}$	**$C_{1\beta}$**
$B_2/Y_{3\alpha}$ ($C_2/Z_{3\alpha}$)	**$Y_{3\alpha}/Y_{3\beta}$**	$B_2/Y_{3\alpha}$ ($C_2/Z_{3\alpha}$)	**$^{1,4}A_2$**
Y_2		Y_2	**$C_{1\alpha}$**
B_2		B_2	**$C_2/Y_{3\alpha}$**
$Y_{3\alpha}$		$Y_{3\alpha}$	**B_2/Y_{3b} (C_2/Z_{3b}) – CO_2**
			$B_2/Y_{3\beta}$ ($C_2/Z_{3\beta}$)
			$C_2/Y_{3\beta}$
			C_2
			$C_3/\,^{1,4}X_2$
			C_3
			$^{0,2}A_4$
			$^{1,5}X_{3\beta}$ – CO_2
			$Y_{3\beta}$
			$^{1,5}X_{3\beta}$

For LSTc, the other linear glycan besides LSTa, $^{3,5}A_2$, $^{0,2}A_2$, $^{0,2}A_3$, $^{0,4}X_2$, $^{2,4}A_3$, $^{1,5}A_2$ were generated in negative mode CAD or EID of unlabeled LSTc (see Figure 5.16 and Table 5.15). $^{3,5}A_2$, $^{0,2}A_2$, $^{0,3}A_3$, $^{0,2}A_3$ were observed in negative mode CAD or EID of 9FL-labeled LSTc (see Figure 5.17 and Table 5.16).

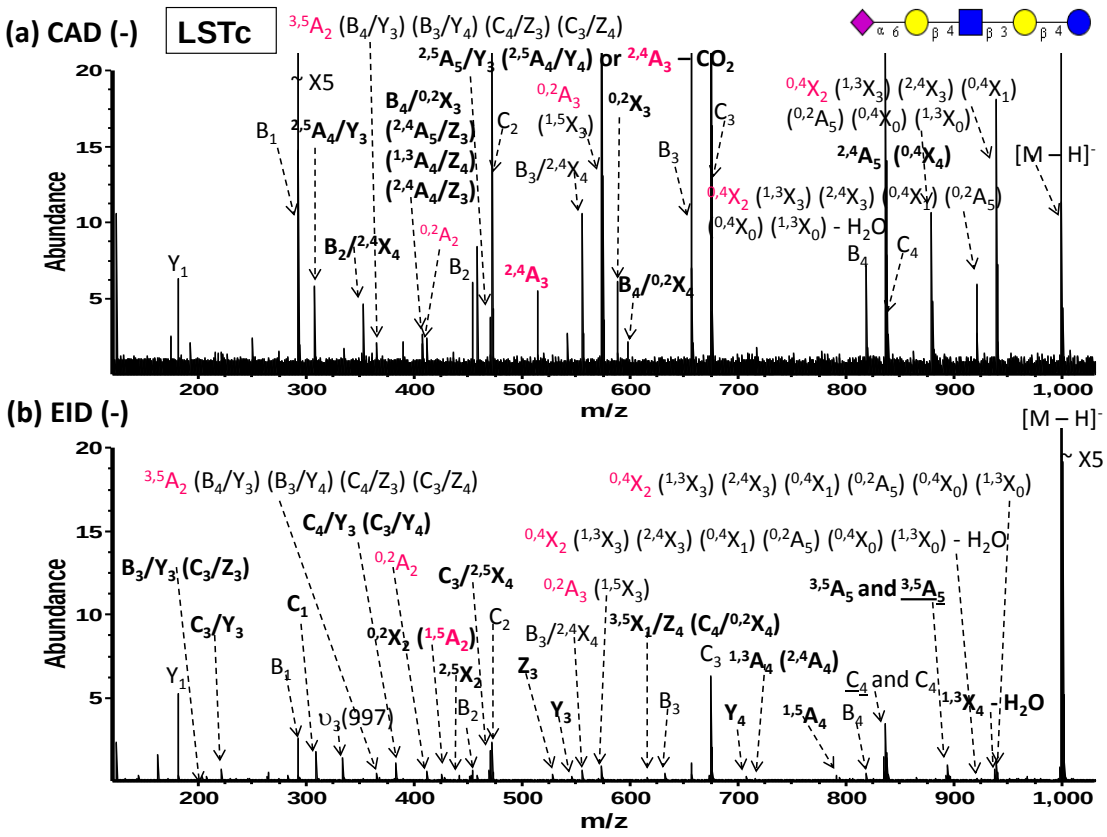

Figure 5.16 Negative mode CAD and EID mass spectra of singly deprotonated LSTc. (a) CAD (100 scans, collision voltage 10.0 V); (b) EID (100 scans, 1 sec electron irradiation with a cathode bias voltage of 15 V). Fragments highlighted in bold are unique to either CAD or EID. *: noise; Δ: dimer; υ: harmonic peaks. Fragments in pink are useful for isomer differentiation.

Table 5.15 Fragmentation summary of negative mode CAD and EID of singly deprotonated LSTc. (a) CAD (100 scans, collision voltage 10.0 V); (b) EID (100 scans, 1 sec electron irradiation with a cathode bias voltage of 15 V). Fragments highlighted in bold are unique to either CAD or EID. Fragments in pink are useful for isomer differentiation.

CAD (-)		EID (-)	
Y_1 B_1 $^{3,5}A_2$ (B_4/Y_3) (B_3/Y_4) (C_4/Z_3) (C_3/Z_4) $^{0,2}A_2$ B_2 C_2 $B_3/^{2,4}X_4$ $^{0,2}A_3$ ($^{1,5}X_3$) B_3 C_3 B_4 C_4 $^{0,4}X_2$ ($^{1,3}X_3$) ($^{2,4}X_3$) ($^{0,4}X_1$) ($^{0,2}A_5$) ($^{0,4}X_0$) ($^{1,3}X_0$) - H_2O $^{0,4}X_2$ ($^{1,3}X_3$) ($^{2,4}X_3$) ($^{0,4}X_1$) ($^{0,2}A_5$) ($^{0,4}X_0$) ($^{1,3}X_0$)	**$^{2,5}A_4/Y_3$** **$B_2/^{2,4}X_4$** **$B_4/^{0,2}X_3$ ($^{2,4}A_5/Z_3$)** **($^{1,3}A_4/Z_4$) ($^{2,4}A_4/Z_3$)** **$^{2,5}A_5/Y_3$ ($^{2,5}A_4/Y_4$) or** **$^{2,4}A_3$ – CO_2** **$^{2,4}A_3$** **$^{0,2}X_3$** **$B_4/^{0,2}X_4$** **$^{2,4}A_5$ ($^{0,4}X_4$)**	Y_1 B_1 $^{3,5}A_2$ (B_4/Y_3) (B_3/Y_4) (C_4/Z_3) (C_3/Z_4) $^{0,2}A_2$ B_2 C_2 $B_3/^{2,4}X_4$ $^{0,2}A_3$ ($^{1,5}X_3$) B_3 C_3 B_4 $\underline{C_4}$ and C_4 $^{0,4}X_2$ ($^{1,3}X_3$) ($^{2,4}X_3$) ($^{0,4}X_1$) ($^{0,2}A_5$) ($^{0,4}X_0$) ($^{1,3}X_0$) - H_2O $^{0,4}X_2$ ($^{1,3}X_3$) ($^{2,4}X_3$) ($^{0,4}X_1$) ($^{0,2}A_5$) ($^{0,4}X_0$) ($^{1,3}X_0$)	**B_3/Y_3 (C_3/Z_3)** **C_3/Y_3** **C_1** **C_4/Y_3 (C_3/Y_4)** **$^{0,2}X_2$ ($^{1,5}A_2$)** **$^{2,5}X_2$** **$C_3/^{2,5}X_4$** **Z_3** **Y_3** **$^{3,5}X_1/Z_4$ ($C_4/^{0,2}X_4$)** **Y_4** **$^{1,3}A_4$ ($^{2,4}A_4$)** **$^{1,5}A_4$** **$^{3,5}A_5$ and $^{3,5}\underline{A_5}$** **$^{1,3}X_4$ - H_2O**

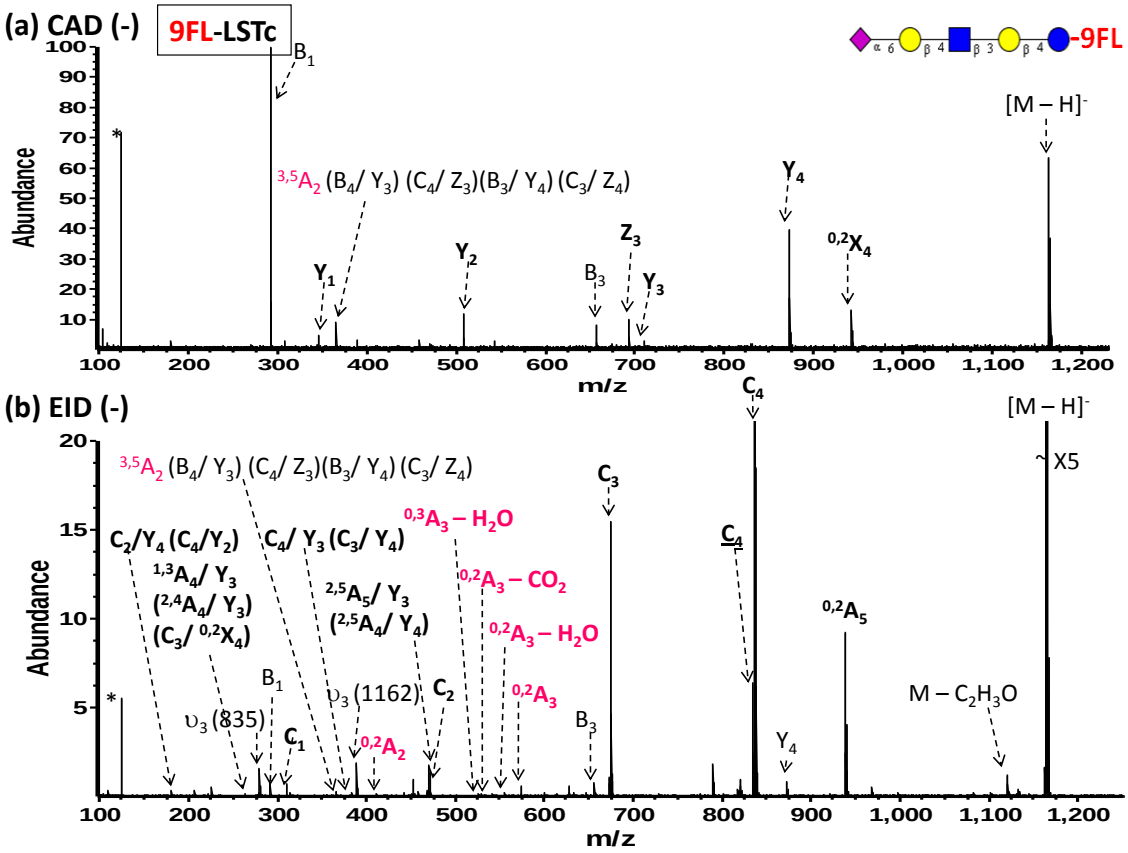

Figure 5.17 Negative mode CAD and EID mass spectra of singly deprotonated 9FL-LSTc. (a) CAD (100 scans, collision voltage 41.5 V); (b) EID (100 scans, 3 sec electron irradiation with a cathode bias voltage of 12 V). Fragments highlighted in bold are unique to either CAD or EID. *: noise; Δ: dimer; υ: harmonic peaks. Fragments in pink are useful for isomer differentiation.

Table 5.16 Fragmentation summary of negative mode CAD and EID of singly deprotonated 9FL-LSTc. (a) CAD (100 scans, collision voltage 41.5 V); (b) EID (100 scans, 3 sec electron irradiation with a cathode bias voltage of 12 V). Fragments highlighted in bold are unique to either CAD or EID. *: noise; Δ: dimer. Fragments in pink are useful for isomer differentiation.

CAD (-)		EID (-)	
B_1	**Y_1**	B_1	**C_2/Y_4 (C_4/Y_2)**
$^{3,5}A_2$ (B_4/ Y_3) (C_4/ Z_3)	**Y_2**	$^{3,5}A_2$ (B_4/ Y_3) (C_4/ Z_3)	**$^{1,3}A_4$/ Y_3 ($^{2,4}A_4$/ Y_3) (C_3/**
(B_3/ Y_4) (C_3/ Z_4)	**Z_3**	(B_3/ Y_4) (C_3/ Z_4)	**$^{0,2}X_4$)**
B_3	**Y_3**	B_3	**C_4/ Y_3 (C_3/ Y_4)**
Y_4	**$^{0,2}X_4$**	Y_4	**C_1**
			$^{0,2}A_2$
			$^{2,5}A_5$/ Y_3 ($^{2,5}A_4$/ Y_4)
			$^{0,3}A_3 - H_2O$
			C_2
			$^{0,2}A_3 - CO_2$
			$^{0,2}A_3 - H_2O$
			$^{0,2}A_3$
			C_3
			$\underline{C_4}$
			C_4
			$^{0,2}A_5$

In summary, similar to LNH and pLNH, positive mode CAD and EID, although generated many valuable fragments, were not able to produce specific cross-ring cleavages to help differentiate three isomers. Negative mode CAD and EID generated many more varieties of A-, and X-type cleavages. Among these additional fragments, many could be used for isomer differentiation.

5.4 Conclusions

In this chapter, EID was successfully applied to singly deprotonated glycans for structural characterization. Application of EID was extended to negative mode. Similar to positive ion mode, negative mode EID enhances fragmentation and provides complementary structural information compared to negative mode CAD.

As expected, fucose-migration fragments[26] are not observed in negative mode CAD or negative mode EID.

Also similar to positive mode EID, derivatization reactions and different tags have an effect in EID fragmentation. Negative mode EID of labeled glycans produces more fragments than that of unlabeled glycans and 9FL produces more fragments than 2AB or 2AA labels, presumably because a more conjugated structure facilitates electronic excitation upon electron irradiation.

Compared to positive ion mode EID, negative ion mode EID produces more cross-ring cleavages. While positive mode EID only generates ^{1,5}X-type ions, negative mode EID generates a variety of A- and X-type cross-ring cleavages. Negative mode MS/MS is more valuable for isomer differentiation than positive mode. While positive mode CAD and EID only generated glycosidic fragments or 1,5X-type cross-ring cleavages which do not add value to isomer differentiation, negative mode CAD and EID yielded many useful cross-ring fragments that cleave at critical positions.

5.5 Bibliography

(1) Gagneux, P.; Varki, A. Evolutionary Considerations in Relating Oligosaccharide Diversity to Biological Function. *Glycobiology* **1999**, *9*, 747-755.

(2) Kiessling, L. L.; Splain, R. A. In *Annual Review of Biochemistry, Vol 79*; Kornberg, R. D., Raetz, C. R. H., Rothman, J. E., Thorner, J. W., Eds.; Annual Reviews: Palo Alto, 2010; Vol. 79, pp 619-653.

(3) Gabius, H. J. Glycans: Bioactive Signals Decoded by Lectins. *Biochem. Soc. Trans.* **2008**, *36*, 1491-1496.

(4) Lepenies, B.; Seeberger, P. H. The Promise of Glycomics, Glycan Arrays and Carbohydrate-Based Vaccines. *Immunopharm. Immunot.* **2010**, *32*, 196-207.

(5) Harvey, D. J. Proteomic Analysis of Glycosylation: Structural Determination of N- and O-Linked Glycans by Mass Spectrometry. *Expert Rev. Proteomics* **2005**, *2*, 87-101.

(6) Domon, B.; Costello, C. E. A Systematic Nomenclature for Carbohydrate Fragmentations in FAB-MS/MS Spectra of Glycoconjugates. *Glycoconjugate J.* **1988**, *5*, 397-409.

(7) Adamson, J. T.; Hakansson, K. Infrared Multiphoton Dissociation and Electron Capture Dissociation of High-Mannose Type Glycopeptides. *J. Proteome Res.* **2006**, *5*, 493-501.

(8) Adamson, J. T.; Håkansson, K. Electron Capture Dissociation of Oligosaccharides Ionized with Alkali, Alkaline Earth, and Transition Metals. *Anal. Chem.* **2007**, *79*, 2901-2910.

(9) Zhao, C.; Xie, B.; Chan, S. Y.; Costello, C. E.; O'Connor, P. B. Collisionally Activated Dissociation and Electron Capture Dissociation Provide Complementary Structural Information for Branched Permethylated Oligosaccharides. *J. Am. Soc. Mass. Spectrom.* **2008**, *19*, 138-150.

(10) Han, L.; Costello, C. Electron Transfer Dissociation of Milk Oligosaccharides. *J. Am. Soc. Mass. Spectrom.* **2011**, *22*, 997-1013.

(11) Han, L. A.; Costello, C. E. Investigations of Structures and Fragmentation Pathways by Electron Transfer Dissociation of Permethylated Milk Sugars. *Glycobiology* **2010**, *20*, 1514-1515.

(12) Adamson, J. T.; Håkansson, K. Electron Detachment Dissociation of Neutral and Sialylated Oligosaccharides. *J. Am. Soc. Mass. Spectrom.* **2007**, *18*, 2162-2172.

(13) Wolff, J.; Laremore, T.; Busch, A.; Linhardt, R.; Amster, I. Electron Detachment Dissociation of Dermatan Sulfate Oligosaccharides. *J. Am. Soc. Mass. Spectrom.* **2008**, *19*, 294-304.

(14) Yoo, H. J.; Liu, H.; Håkansson, K. Infrared Multiphoton Dissociation and Electron-Induced Dissociation as Alternative MS/MS Strategies for Metabolite Identification. *Anal. Chem.* **2007**, *79*, 7858-7866.

(15) Lioe, H.; O'Hair, R. Comparison of Collision-Induced Dissociation and Electron-Induced Dissociation of Singly Protonated Aromatic Amino Acids, Cystine and Related Simple Peptides Using a Hybrid Linear Ion Trap–FT-ICR Mass Spectrometer. *Anal. Bioanal. Chem.* **2007**, *389*, 1429-1437.

(16) Ly, T.; Yin, S.; Loo, J. A.; Julian, R. R. Electron-Induced Dissociation of Protonated Peptides Yields Backbone Fragmentation Consistent with a Hydrogen-Deficient Radical. *Rapid Commun. Mass Spectrom.* **2009**, *23*, 2099-2101.

(17) Kalli, A.; Grigorean, G.; Håkansson, K. Electron Induced Dissociation of Singly Deprotonated Peptides. *J. Am. Soc. Mass. Spectrom.* **2011**, *22*, 2209-2221.

(18) Budnik, B. A.; Haselmann, K. F.; Elkin, Y. N.; Gorbach, V. I.; Zubarev, R. A. Applications of Electron−Ion Dissociation Reactions for Analysis of Polycationic Chitooligosaccharides in Fourier Transform Mass Spectrometry. *Anal. Chem.* **2003**, *75*, 5994-6001.

(19) Wills, R. H.; Tosin, M.; O'Connor, P. B. Structural Characterization of Polyketides Using High Mass Accuracy Tandem Mass Spectrometry. *Anal. Chem.* **2012**, *84*, 8863-8870.

(20) Kaczorowska, M. A.; Cooper, H. J. Electron Induced Dissociation (EID) Tandem Mass Spectrometry of Octaethylporphyrin and Its Iron(III) Complex. *Chem. Commun.* **2011**, *47*, 418-420.

(21) Kaczorowska, M. A.; Cooper, H. J. Electron Induced Dissociation: A Mass Spectrometry Technique for the Structural Analysis of Trinuclear Oxo-Centred Carboxylate-Bridged Iron Complexes. *J. Am. Soc. Mass. Spectrom.* **2010**, *21*, 1398-1403.

(22) Mosely, J. A.; Smith, M. J. P.; Prakash, A. S.; Sims, M.; Bristow, A. W. T. Electron-Induced Dissociation of Singly Charged Organic Cations as a Tool for Structural Characterization of Pharmaceutical Type Molecules. *Anal. Chem.* **2011**, *83*, 4068-4075.

(23) Zhou, W.; Hakansson, K. Structural Characterization of Carbohydrates by Fourier Transform Tandem Mass Spectrometry. *Curr. Proteomics* **2011**, *8*, 297-308.

(24) Zaia, J. Mass Spectrometry of Oligosaccharides. *Mass Spectrom. Rev.* **2004**, *23*, 161-227.

(25) Narayanan, S. Sialic-Acid as a Tumor-Marker. *Ann. Clin. Lab. Sci.* **1994**, *24*, 376-384.

(26) Franz, A. H.; Lebrilla, C. B. Evidence for Long-Range Glycosyl Transfer Reactions in the Gas Phase. *J. Am. Soc. Mass. Spectrom.* **2002**, *13*, 325-337.

(27) Thaysen-Andersen, M.; Mysling, S.; Højrup, P. Site-Specific Glycoprofiling of N-Linked Glycopeptides Using MALDI-TOF MS: Strong Correlation between Signal Strength and Glycoform Quantities. *Anal. Chem.* **2009**, *81*, 3933-3943.

(28) Franz, A. H.; Molinski, T. F.; Lebrilla, C. B. MALDI-FTMS Characterization of Oligosaccharides Labeled with 9-Aminofluorene. *J. Am. Soc. Mass. Spectrom.* **2001**, *12*, 1254-1261.

(29) Ceroni, A.; Maass, K.; Geyer, H.; Geyer, R.; Dell, A.; Haslam, S. M. GlycoWorkbench: A Tool for the Computer-Assisted Annotation of Mass Spectra of Glycans. *J. Proteome Res.* **2008**, *7*, 1650-1659.

(30) Varki, A.; Cummings, R. D.; Esko, J. D.; Freeze, H. H.; Stanley, P.; Bertozzi, C. R.; Hart, G. W.; Etzler, M. E. *Essentials of Glycobiology, 2nd edition*; Cold Spring Harbor (NY): Cold Spring Harbor Laboratory Press, 2009.

(31) Harvey, D. Fragmentation of Negative Ions from Carbohydrates: Part 1. Use of Nitrate and Other Anionic Adducts for the Production of Negative Ion Electrospray Spectra from N-Linked Carbohydrates. *J. Am. Soc. Mass. Spectrom.* **2005**, *16*, 622-630.

(32) Carroll, J. A.; Ngoka, L.; Beggs, C. G.; Lebrilla, C. B. Liquid Secondary-Ion Mass-Spectrometry Fourier-Transform Mass-Spectrometry of Oligosaccharide Anions. *Anal. Chem.* **1993**, *65*, 1582-1587.

(33) Harvey, D. J. Fragmentation of Negative Ions from Carbohydrates: Part 2. Fragmentation of High-Mannose N-Linked Glycans. *J. Am. Soc. Mass. Spectrom.* **2005**, *16*, 631-646.

(34) Harvey, D. Fragmentation of Negative Ions from Carbohydrates: Part 3. Fragmentation of Hybrid and Complex N-Linked Glycans. *J. Am. Soc. Mass. Spectrom.* **2005**, *16*, 647-659.

(35) Yoon, E. Y. Comparison between Positive and Negative Ion Mode FAB CAD MS/MS Spectra of Linkage-Isomeric Oligosaccharides. *J. Biochem. Mol. Biol.* **1997**, *30*, 253-257.

Chapter 6 Conclusions and Prospects for Future Work

6.1 Purpose of Dissertation

Glycans are attached to cell surfaces and also to many macromolecules (e.g., proteins and lipids), thus modulating and mediating cell-cell, cell-matrix, and cell-molecule interactions.[1, 2] Glycosylation is one of the most ubiquitious forms of post-translational modification (PTM) and plays important roles in many key biological processes such as protein folding, self/nonself recognition, metastasis, cell adhesion, receptor activation, signal transmission, molecular trafficking and clearance.[2-4] Structures of glycan chains covalently attached to proteins are often significantly changed with onset of cancer and inflammation in various ways such as increased glycan branching, increased or decreased levels of glycosylation, elevated levels of sialic acids, or altered sulfonation.[5] Although causes are not well understood, these cancer-related alterations are thought to affect growth, adhesion, differentiation, transformation, progression, metastasis, and immune surveillance of cancer cells.[4, 6, 7] Therefore, detailed and correct structural information of glycans would facilitate further understanding of cellular functions as well as disease. The work presented in this thesis was based on a collaborative effort with Prof. Simeone's group in the University of Michigan Medical School. They have recently identified pancreatic cancer stem cells on the basis of three glycoprotein surface markers; CD44, CD24, and epithelial-specific antigen (ESA) using a xenograft model in which primary human pancreatic cancer was grown in

immunocompromised mice.[8] The CD44+CD24+ESA+ subpopulation (0.2-0.8% of pancreatic cancer cells) showed 100-fold increased tumorigenic potential compared to "non-stem" cancer cells and showed stem cell properties such as self-renewal and differentiation. An improved understanding of these cancer stem cells, particularly structural information of related glycans, can not only improve understanding of the disease but also provide a means of cancer early detection, or identification of cancer vaccine candidates.

However, glycan structural complexity is much larger than that of proteins because of the nature and order of constituent monosaccharides, position of glycosidic linkages, degree of branching, stereochemistry, isomers, modifications (sulfonation, phosphorylation, acylation, etc), and conjugation to proteins and other biomolecules. All these challenges make carbohydrates the least explored among three major classes of biomolecules (carbohydrates, proteins and nucleic acids). As mentioned in Chapter 1, currently utilized analytical methods for structural characterization of glycans include ^{1}H- and ^{13}C- nuclear magnetic resonance (NMR) spectroscopy, [9-12] X-ray crystallography,[13, 14] and chromatography.[15] Mass spectrometry (MS) is more sensitive than NMR spectroscopy and X-ray crystallography and more selective than chromatography,[15, 16] so potentially it can be a very powerful tool for glycan structural characterization.

Mass spectrometry generates structural information through tandem mass spectrometry (MS/MS) techniques via specific bond cleavages and unique fragmentation pathways. Glycosidic cleavages provide information about sequence and composition and can also be helpful for branching and linkage determination. However, in order to elucidate more detailed structural information, A- and X- type cross-ring cleavages are

highly needed. The most widely used MS/MS technique, collision activated dissociation (CAD), typically yields glycosidic cleavages and very few cross-ring cleavages.[17-21] Cross-ring cleavages are desired, e.g., for identification ofcarbohydrate isomers. The first aim of this thesis was to develop and systematically characterize alternative MS/MS activation methods, including gas-phase ion-electron and ion-ion reactions for MS/MS-based structural characterization of glycans.

Fucose migration has been widely reported in positive ion mode MS/MS, leading to false structural information.[22-25] This thesis also aims to investigate gas-phase fucose migration/rearrangement in carbohydrate MS/MS, to develop methods that avoid this phenomenon, and to study the migration mechanism in the gas phase.

6.2 Summary of Results

ECD and ETD can serve as alternative MS/MS techniques but both techniques require multiply charged precursor ions. Chapter 2 demonstrated that divalent metal adduction can be an effective way to increase charge states. Divalent metal-assisted ECD and ETD of multiply charged glycan cations generate extensive glycosidic and cross-ring cleavages, providing rich structural information. Divalent metals not only increase charge states to enable ECD/ETD but also have a significant effect on fragmentation. Among the three metals investigated in this work, Ca formed metal-glycan complexes most readily, while Mg complexes generated superior ECD and ETD fragmentation. Divalent metal-assisted ECD and ETD were directly compared. For magnesium adduction, extensive glycosidic and cross-ring cleavages, many of which are unique to either ECD or ETD of underivatized glycans compared with CAD of the same precursor ions, or with ETD of reduced and permethylated glycans, are generated in both ECD and

ETD. However, the number of structurally informative fragments as well as the fragmentation efficiency is higher in ECD. This discrepancy between ECD and ETD, likely related to the different pressures during these reactions, is even more significant for cobalt and calcium adduction.

With specific salts, triply charged metal-glycan complexes were generated by ESI for the first time. Chapter 3 demonstrated that triply charged precursor ions generate more structural information than doubly charged precursor ions. Higher charge state facilitates ECD/ETD fragmentation. With trivalent metal adduction, even doubly charged precursor ions [metal (III) + glycan – H]$^{2+}$ resulted in distinctive ECD/ETD fragmentation behavior compared with divalent metal-adducted doubly charged precursor ions [metal (II) + glycan]$^{2+}$. Chapter 3 also further investigated the mechanism of metal-assisted ECD/ETD. Metals with higher ionization energy can release more energy during the electron capture or transfer process. Thus, more energy is potentially available for the following excitation and fragmentation events. Preliminary ion mobility experiments showed multiple drift times for triply-charged La-adducted NA2 and two major drift times for the corresponding doubly-charged species, whereas complexes with the divalent metals Ca, Co, and Mg mostly showed only one drift time. These data corroborate the previous suggestions that both metal-electron recombination energy and gas-phase structures and structural diversity of metal complexes determine ECD/ETD outcome.

In many cases, the most abundant ions observed in ESI-MS are singly charged. Therefore, MS/MS techniques compatible with singly charged precursor ions are of high interest to pursue. In Chapter 4, positive ion mode electron induced dissociation (EID) was applied towards singly protonated glycans for structural characterization. EID

yielded complementary fragmentation patterns for glycans compared with CAD. ^{1,5}X-type cleavages were more common than other X-type product ions in EID, similar to high-energy CAD. Such similarity suggests a similarity between the mechanism of EID and that of high-energy CAD. Fucose-migration fragments were much less abundant in EID compared with CAD. The mechanism of positive ion mode EID was also studied by derivatizing various standard glycans with different aromatic labels (2-amino benzamide (2AB), 2-anthranilic acid (2AA), and 9-aminofluorene (9FL)). EID of tagged glycans produced more fragments than that of untagged glycans and 9FL labeling produced more fragments than 2-AB- or 2-AA-labeled glycans, presumably because a more conjugated structure facilitates electronic excitation.

Many cancer related glycans contain sialic acids and such acidic glycans ionize more easily in negative ion mode.[32, 33] In addition, negative ion MS/MS has advantages such as lack of fucose migration and generation of more cross-ring cleavages. Chapter 5 further extended EID to negative ion mode for glycan structural analysis. A longer electron irradiation time and a slightly higher voltage are needed to obtain optimized EID conditions for singly deprotonated glycan anions. As expected, fucose migration was not observed in neither negative mode CAD, nor negative mode EID. Compared with positive ion mode EID, negative ion EID produced a higher variety of A- and X-type cross-ring cleavages, and provided a high level of valuable information regarding branching and linkage. Similar to positive ion mode EID, aromatically tagged glycans produced more fragments than untagged glycans. 9FL induced superior EID fragmentation patterns among all three investigated tags (2AB, 2AA, and 9FL), presumably because 9FL has more aromatic rings than 2AB or 2AA. Furthermore, in

negative ion mode, 2AA appears to result in improved EID fragmentation compared with 2AB, probably because 2AA has a more acidic structure than 2AB which improves ionization.

With all these novel MS/MS techniques, glycan isomers can be differentiated. Two isomer sets: (1) LNH and pLNH; (2) LSTa, LSTb, and LSTc were investigated in Chapters 2-5. A combination of negative ion mode CAD, EID, and metal-assisted ECD/ETD is valuable for isomer differentiation by generating critical cleavages at the specific linkage sites.

Overall, all chapters demonstrate that mass spectrometry is a powerful tool for structural characterization of glycans. Ion-electron and ion-ion reactions provide complementary structural information compared with conventional MS/MS methods.

6.3 Prospects for Future Work

6.3.1 Fucose Migration in Carbohydrate MS/MS

Franz and Lebrilla proposed two possible mechanisms for long-range fucose migration observed in their experiments: ion-dipole mechanism and proton-catalyzed mechanism.[25] While both mechanisms are feasible, neither of them involves aromatic labels (2AB, 2AA, or 9FL). Wuhrer and colleagues performed ion trap CAD of an *N*-glycan released from worms in native form (with underivatized reducing end), observed migration peaks (*m/z* 658, 1347, 1493, 1714) and thus claimed that rearrangements observed for this *N*-glycan do not depend on reducing end derivatization.[22] However, possible existence of isomers in their sample complicates this interpretation. The mechanism of fucose migration or rearrangement is still under debate. The data presented in Chapters 4 and 5 appear to suggest a relationship between aromatic

derivatization and migration phenomena. EID of underivatized glycans did not yield migration peaks, while EID of 2AB-, 2AA- or 9FL-labeled glycans show fucose migration peaks. Whether migration is due to mobile protons or reducing end derivatization is not understood.

Furthermore, how to ensure that fucose migration does not occur in MS/MS of protonated precursor ions is still unclear. Two possible directions are modification of analyte molecules and change of activation methods. Permethylation is considered as an effective way to prevent rearrangements[22, 34, 35] but this approach has not been completely verified. Wuhrer et al. suggested a time-independent nature of migration phenomena, because they observed migration peaks in both ion trap (ms time scale) and MALDI-TOF/TOF MS/MS (μs time scale).[22] However, these two spectra did show differences in relative abundance of the migration peaks. Further, it is possible that the time required for migration is shorter than μs. The data presented in this thesis show that EID (10^{-14}~10^{-15} s time scale) effectively reduced fucose migration peaks compared with CAD. Future work may include experiments on permethylated species and exploration of more "prompt" dissociation methods, such as υUVPD (less than 10^{-16} s).

Since the Reilly group published their first paper on fragmentation of singly charged peptide ions by photodissociation at 157 nm,[36] UVPD (including 157 nm υUVPD) has been extended to glycan cations and glycopeptides, providing valuable structural information.[37-40] However, this relatively new dissociation method has had limited application towards glycans and characterization of glycan anions or *O*-glycans have not been reported. The first task would be implementation of this dissociation technique on our Apex Q-FT-ICR mass spectrometer. This should be quite

straightforward because there is access to the ICR cell flange from the rear. An ultrahigh vacuum compatible CaF_2 window was recently installed at the rear cell flange to allow 157 nm photons from an F_2 excimer laser to interact with trapped ions. Initial experiments will include laser alignment and determination of the required number of laser pulses for efficient υUVPD and whether pre-activation of precursor ions (e.g, IR irradiation) is required. Most peptide literature on υUVPD involves MALDI rather than ESI. MALDI produces hotter ions that may get excited to higher energy levels upon absorption of 157 nm photon (7.9 eV) and thus may yield more informative fragments. Further experiments include examination of factors that impact υUVPD of glycans. For peptides, research has already shown that both photodissociation wavelength and mass analyzer can have an effect.[41]

6.3.2 8-Aminopyrene-1,3,6-Trisulfonate (APTS) Derivatization and Ion-Electron Reactions

8-Aminopyrene-1,3,6-trisulfonate (APTS) is a recently developed fluorescent tag for derivatization of glycans.[42] APTS has a more conjugated structure than 9FL, because APTS contains four aromatic rings (see Figure 6.1). APTS derivatization was successfully applied to LNDFH according to a literature protocol.[42] To briefly summarize, dried oligosaccharides were mixed with 2 mL derivatization reagent (0.02 M APTS in 25% acetic acid), followed by adding 10 mL H_2O. The mixed solution was incubated in a water bath at 75 °C for six hours. Products were purified with a column made of Sephadex G-25 (Sigma). Higher amounts of APTS and longer incubation time were also attempted to obtain optimized reaction conditions, but did not result in higher reaction efficiency.

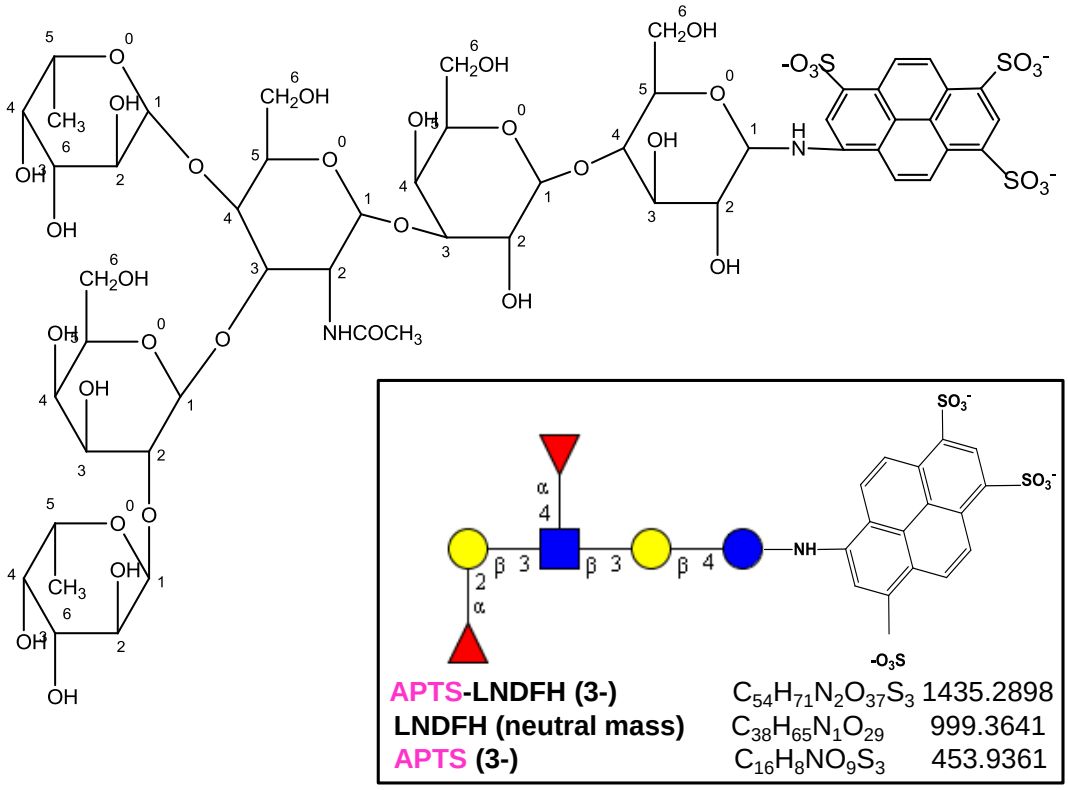

Figure 6.1 Structure of APTS-labeled LNDFH. Chemical reaction occurs between the amine group on APTS and the reducing end of the glycan. Different from 9FL, 2AB, or 2AA derivatization, the APTS-labeled glycan has a closed ring reducing end.

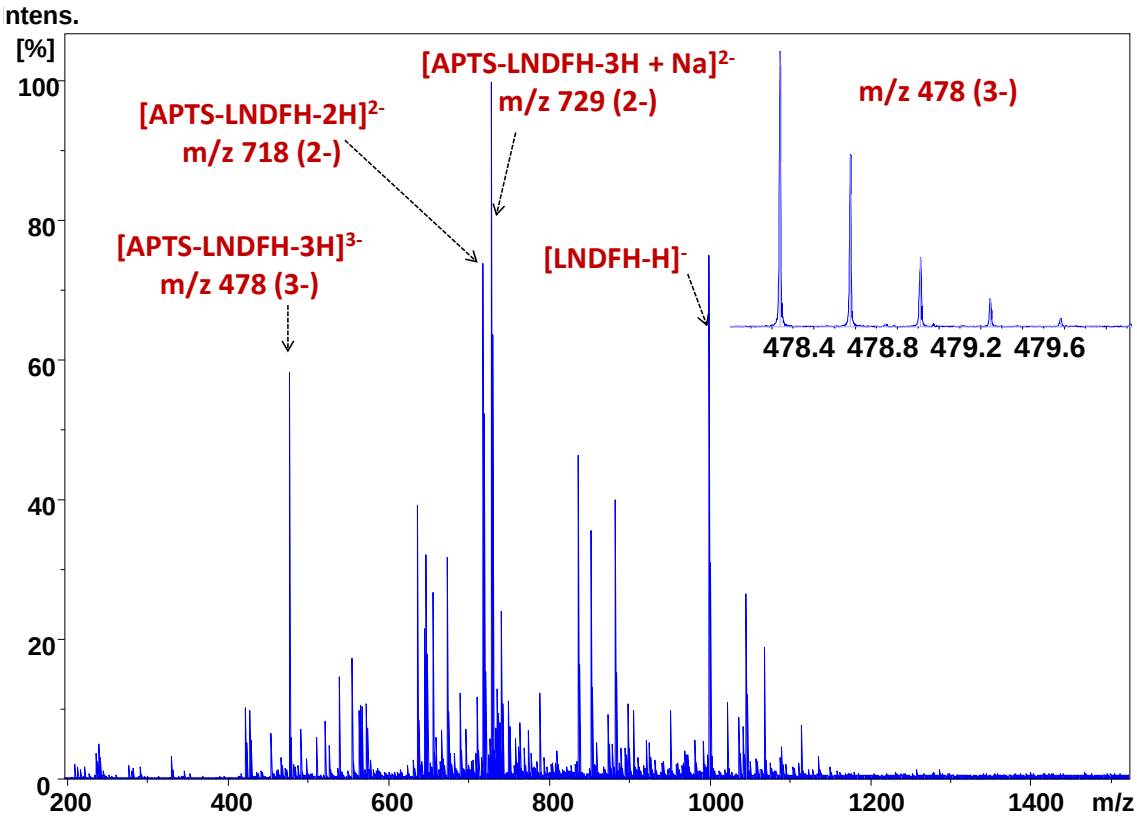

Figure 6.2 Negative ion mode FT-ICR MS of LNDFH APTS derivatization products.

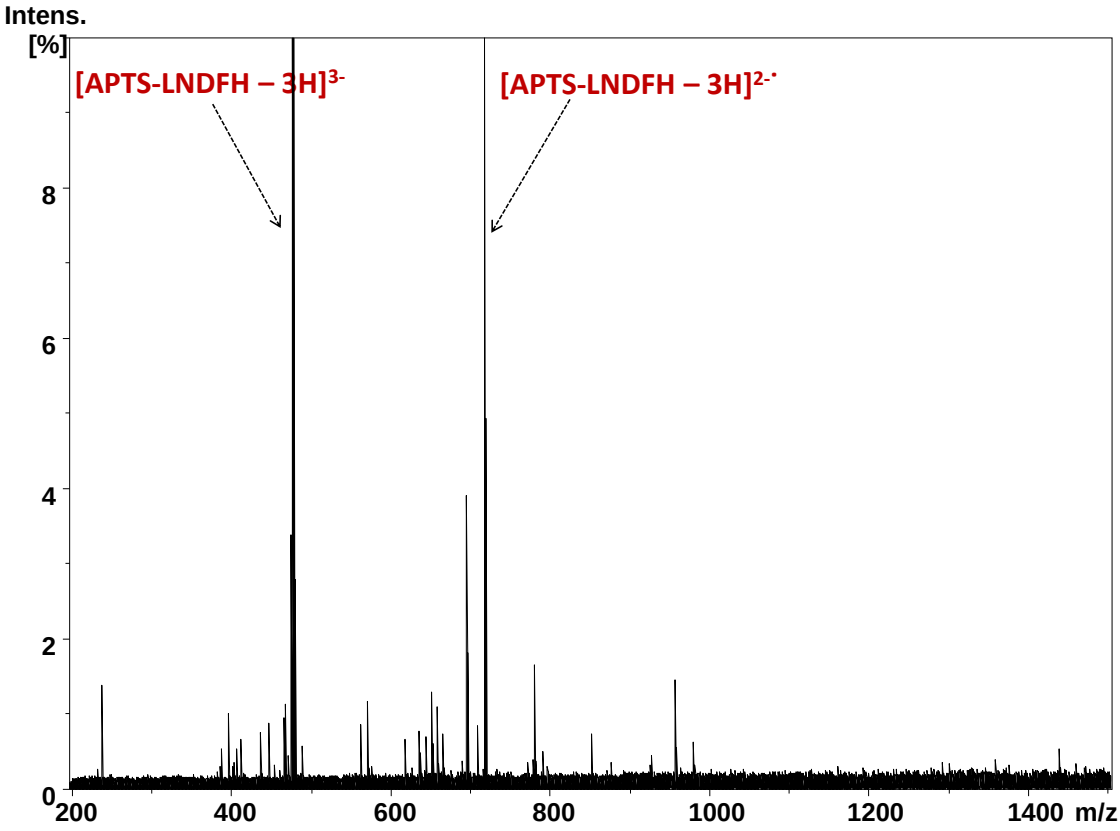

Figure 6.3 EID (5.5 s electron irradiation with a cathode bias voltage of 17.9 V) of triply deprotonated APTS-LNDFH at *m/z* 478. The spectrum shows EDD-type dissociation.

APTS-labeled LNDFH did (as expected) not ionize well in positive ion mode due to the three sulfonate groups on APTS. However in negative ion mode, triply charged anions (with three deprotonated sites) are the most abundant species (see Figure 6.2). Singly deprotonated species were not observed. Electron irradiation at typical EID conditions showed electron detachment dissociation (EDD) type dissociation as shown in Figure 6.3. In order to further study the mechanism of EID, proton transfer reaction (PTR) is one approach that can be implemented to generate abundant singly deprotonated precursor ions. APTS derivatization may also aid EDD, which requires multiply charged anions.

6.3.3 Nano-Scale Liquid Chromatography

Complete separation of glycans and glycopeptides is still challenging due to their structural complexity and various isomers. LC/MS, the combination of liquid chromatography and mass spectrometry, is widely used for glycan separation, detection and further analysis. Although glycans are hydrophilic in nature, derivatization methods, including permethylation and fluorescent labeling, can be utilized to allow informative-rich analysis and sensitive detection (as low as femtomol).[43] When nano-scale LC is coupled with nanoESI, LC/MS can be an even more powerful tool, operating at nL/min flow rates, thus requiring very low sample amounts. Targeted cells such as CD24+CD44+ESA+ only constitute 0.2-0.8% of sorted cancer cells from a xenograft tumor, so nano-scale LC is required to allow detailed analysis of 30,000 sorted cells.

Hydrophilic interaction liquid chromatography (HILIC)[44-46] and graphitized carbon chromatography[47, 48] of native glycans have begun to emerge for glycan analysis. Previous work in our group showed particularly promising results utilizing graphitized carbon chromatography for separating glycan isomers. Therefore, future work includes further investigation of nano-scale graphitized carbon chromatography. A pre-column (Thermo HYPER CARB, 50 mm * 0.075 mm, 5 um) and an analytical column (Thermo HYPER CARB, 100 mm * 0.075 mm, 5 um) have been purchased and set up. Both on-line and off-line nano-LC-FT-ICR MS (and MS/MS) will be optimized to facilitate highly sensitive detection and analysis. With the SolariX FT-ICR instrument, many possibly required fragmentation techniques (CAD, EID, ECD, ETD, and EDD) will be available for structural characterization (see Scheme 6.1 for *N*-glycan analysis).

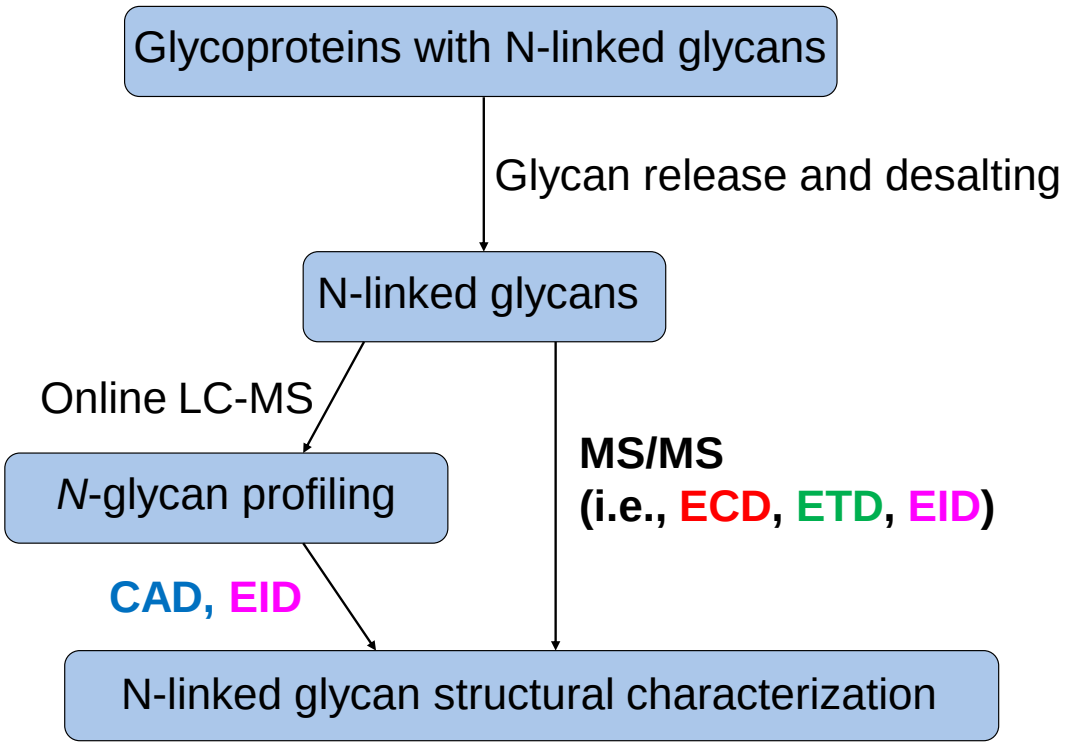

Scheme 6.1 Workflow of LC- and MS-based techniques for structural characterization of *N*-glycans.

Such LC-FT-ICR MS/MS (gas-phase ion-electron and ion-photon reactions) strategies can be further applied towards pancreatic cancer cell surfaces with the goal of identifying cancer vaccine candidates. Pancreatic cancer is a highly lethal disease because it is usually diagnosed at an advanced stage.[49]

Initial experiments will be conducted first with glycans from unsorted pancreatic cancer cells to investigate whether sufficient sensitivity can be achieved for sorted pancreatic cancer stem cells, which were recently identified as CD24+CD44+ESA+ by our collaborator Dr. Simeone at the University of Michigan Medical School.[8] Cell membrane fractions will be used to obtain surface glycans from the cells of interest according to a protocol reported by the Kakehi group.[50] *N*-glycans will be released

enzymatically with PNGaseF and *O*-glycans will be released chemically by β-elimination in alkaline borohydride. Each fraction will be analyzed by nano-LC-FT-ICR MS/MS. To obtain pancreatic cancer stem cells, pancreatic cancer cells will be sorted by flow cytometry by the Simeone group.[8]

In order to identify vaccine candidates, glycans on the surface of pancreatic cancer stem cells but not on the surface of pancreatic cancer cells are of particular interest. Therefore, LC/MS can be performed first to profile the different fractions, then more detailed structural characterization techniques will be conducted of glycans showing an abundance difference in LC/MS.

6.3.4 Glycoinformatics

Glycoinformatics is a relatively new field of bioinformatics and has already showed indispensable importance in the study of carbohydrates.[51-53] It broadly includes database, software, and algorithm development for research on carbohydrate structures, glycoconjugates, enzymatic carbohydrate synthesis and degradation, as well as carbohydrate interactions.[51, 54] High-throughput and automated techniques (mass spectrometry in particular) allow increasingly detailed structural analysis of complex glycans. Information concerning the primary structure (composition, sequence and linkages) can be derived from sufficient and informative fragments from various MS/MS techniques. Current available tools are not sufficient for rapid and detailed characterization. For example, GlycoWorkbench, an analytical tool used in this dissertation, is designed to semi-automatically annotate glycomics data. This tool can be used to annotate mass spectrometry (MS) and CAD MS/MS spectra of free oligosaccharides, N- and O-linked glycans, GAGs and glycolipids, as well as MS spectra

of glycoproteins.[55] Unique fragmentation patterns and complementary fragments (cross-ring cleavages in particular) from ion-electron and ion-ion reactions investigated in this dissertation will further develop such bioinformatics tools. A possible strategy will be a brief searching of glycosidic cleavages to obtain a brief idea of the sequence and composition, followed by more detailed interpretation of cross-ring cleavages. Sophisticated modeling and algorithm are needed after the first step, which is interpretation of glycosidic cleavages, to suggest some possible structures before more detailed interpretation of cross-ring cleavages.

6.4 Bibliography

(1) Muramatsu, T. Development: Carbohydrate Recognition in Spermatogenesis. *Science* **2002**, *295*, 53-54.

(2) Bertozzi, C. R.; Kiessling, L. L. Chemical Glycobiology. *Science* **2001**, *291*, 2357-2364.

(3) Ohtsubo, K.; Marth, J. D. Glycosylation in Cellular Mechanisms of Health and Disease. *Cell* **2006**, *126*, 855-867.

(4) Dennis, J. W.; Granovsky, M.; Warren, C. E. Glycoprotein Glycosylation and Cancer Progression. *Biochimica et Biophysica Acta (BBA) - General Subjects* **1999**, *1473*, 21-34.

(5) Brooks, S. A.; Carter, T. M.; Royle, L.; Harvey, D. J.; Fry, S. A.; Kinch, C.; Dwek, R. A.; Rudd, P. M. Altered Glycosylation of Proteins in Cancer: What is the Potential for New Anti-Tumour Strategies. *Anti-Cancer Agent. Me.* **2008**, *8*, 2-21.

(6) Wu, Y. M.; Nowack, D. D.; Omenn, G. S.; Haab, B. B. Mucin Glycosylation Is Altered by Pro-Inflammatory Signaling in Pancreatic-Cancer Cells. *J. Proteome Res.* **2009**, *8*, 1876-1886.

(7) Laidler, P.; Lityńska, A. Tumor Cell N-Glycans in Metastasis. *Acta Biochim. Pol.* **1997**, *44*, 343-357.

(8) Li, C. W.; Heidt, D. G.; Dalerba, P.; Burant, C. F.; Zhang, L. J.; Adsay, V.; Wicha, M.; Clarke, M. F.; Simeone, D. M. Identification of Pancreatic Cancer Stem Cells. *Cancer Res.* **2007**, *67*, 1030-1037.

(9) Kajihara, Y.; Sato, H. Structural Analysis of Oligosaccharides by Nuclear Magnetic Resonance Method. *Trends Glycosci. Glyc.* **2003**, *15*, 197-220.

(10) Kogelberg, H.; Solis, D.; Jimenez-Barbero, J. New Structural Insights into Carbohydrate-Protein Interactions from NMR Spectroscopy. *Curr. Opin. Struc. Biol.* **2003**, *13*, 646-653.

(11) Vanhalbeek, H. NMR Developments in Structural Studies of Carbohydrates and Their Complexes. *Curr. Opin. Struc. Biol.* **1994**, *4*, 697-709.

(12) Duus, J. O.; Gotfredsen, C. H.; Bock, K. Carbohydrate Structural Determination by NMR Spectroscopy: Modern Methods and Limitations. *Chem. Rev.* **2000**, *100*, 4589-4614.

(13) Lutteke, T. Analysis and Validation of Carbohydrate Three-Dimensional Structures. *Acta Crystallogr. D* **2009**, *65*, 156-168.

(14) Lobsanov, Y. D.; Pletnev, V. Z.; Mokulskii, M. A. X-Ray Study of the Pea Lectin-Carbohydrate Complex at 2.4 A Resolution .2. Metal and Carbohydrate Binding-Sites-A Model of Lectin-Carbohydrate Interaction. *Bioorg. Khim* **1990**, *16*, 1599-1606.

(15) Davies, M. J.; Hounsell, E. F. Carbohydrate Chromatography: Towards Yoctomole Sensitivity. *Biomed. Chromatogr.* **1996**, *10*, 285-289.

(16) Zaia, J. Mass Spectrometry and the Emerging Field of Glycomics. *Chem. Biol.* **2008**, *15*, 881-892.

(17) Park, Y.; Lebrilla, C. B. Application of Fourier Transform Ion Cyclotron Resonance Mass Spectrometry to Oligosaccharides. *Mass Spectrom. Rev.* **2005**, *24*, 232-264.

(18) Harvey, D. J. Analysis of Carbohydrates and Glycoconjugates by Matrix-Assisted Laser Desorption/Ionization Mass Spectrometry: An Update For 2003-2004. *Mass Sectrometry Reviews* **2009**, *28*, 273-361.

(19) Penn, S. G.; Cancilla, M. T.; Lebrilla, C. B. Collision-Induced Dissociation of Branched Oligosaccharide Ions with Analysis and Calculation of Relative Dissociation Thresholds. *Anal. Chem.* **1996**, *68*, 2331-2339.

(20) Maslen, S.; Sadowski, P.; Adam, A.; Lilley, K.; Stephens, E. Differentiation of Isomeric N-Glycan Structures by Normal-Phase Liquid Chromatography-MALDI-TOF/TOF Tandem Mass Spectrometry. *Anal. Chem.* **2006**, *78*, 8491-8498.

(21) Es-Safi, N. E.; Kerhoas, L.; Einhorn, J.; Ducrot, P. H. Application of ESI/MS, CID/MS and Tandem MS/MS to the Fragmentation Study of Eriodictyol 7-O-Glucosyl-(1 -> 2)-Glucoside and Luteolin 7-O-Glucosyl-(1 -> 2)-Glucoside. *Int. J. Mass spectrom.* **2005**, *247*, 93-100.

(22) Wuhrer, M.; Koeleman, C. A. M.; Hokke, C. H.; Deelder, A. M. Mass Spectrometry of Proton Adducts of Fucosylated N-Glycans: Fucose Transfer Between Antennae Gives Rise to Misleading Fragments. *Rapid Commun. Mass Spectrom.* **2006**, *20*, 1747-1754.

(23) Broberg, A. High-Performance Liquid Chromatography/Electrospray Ionization Ion-Trap Mass Spectrometry for Analysis of Oligosaccharides Derivatized by

Reductive Amination and N,N-Dimethylation. *Carbohydr. Res.* **2007**, *342*, 1462-1469.

(24) Ernst, B.; Muller, D. R.; Richter, W. J. False Sugar Sequence Ions in Electrospray Tandem Mass Spectrometry of Underivatized Sialyl-Lewis-Type Oligosaccharides. *Int. J. Mass Spectrom. Ion Processes* **1997**, *160*, 283-290.

(25) Franz, A. H.; Lebrilla, C. B. Evidence for Long-Range Glycosyl Transfer Reactions in the Gas Phase. *J. Am. Soc. Mass. Spectrom.* **2002**, *13*, 325-337.

(26) Wuhrer, M.; Koeleman, C. A. M.; Deelder, A. M. In *Glycomics: Methods and Protocols*; Packer, N. H., Karlsson, N. G., Eds.; Humana Press Inc, 999 Riverview Dr, Ste 208, Totowa, NJ 07512-1165 USA, 2009; Vol. 534, pp 79-91.

(27) Huang, B. X.; Jiang, H.; Zhang, J. Q.; Xiang, J. H. Profiling the Plasma Proteome of Fenneropenaeus Chinensis with SDS-PAGE and LC-MS/MS. *Oceanologia et Limnologia Sinica* **2009**, *40*, 208-213.

(28) Schiel, J. E.; Au, J.; He, H. J.; Phinney, K. W. LC-MS/MS Biopharmaceutical Glycoanalysis: Identification of Desirable Reference Material Characteristics. *Anal. Bioanal. Chem.* **2012**, *403*, 2279-2289.

(29) Groleau, P. E.; Desharnais, P.; Cote, L.; Ayotte, C. Low LC-MS/MS Detection of Glycopeptides Released from Pmol Levels of Recombinant Erythropoietin Using Nanoflow HPLC-Chip Electrospray Ionization. *J. Mass Spectrom.* **2008**, *43*, 924-935.

(30) Lazar, I. M.; Lee, W.; Lazar, A. C. Glycoproteomics on the Rise: Established Methods, Advanced Techniques, Sophisticated Biological Applications. *Electrophoresis* **2013**, *34*, 113-125.

(31) Zhao, J.; Liu, Y. H.; Reichert, P.; Pflanz, S.; Pramanik, B. Glycosylation Analysis of Interleukin-23 Receptor: Elucidation of Glycosylation Sites and Characterization of Attached Glycan Structures. *J. Mass Spectrom.* **2010**, *45*, 1416-1425.

(32) Narayanan, S. Sialic-Acid as a Tumor-Marker. *Ann. Clin. Lab. Sci.* **1994**, *24*, 376-384.

(33) Varki, A. Glycan-Based Interactions Involving Vertebrate Sialic-Acid-Recognizing Proteins. *Nature* **2007**, *446*, 1023-1029.

(34) Franski, R.; Matlawska, I.; Bylka, W.; Sikorska, M.; Fiedorow, P.; Stobiecki, M. Differentiation of Interglycosidic Linkages in Permethylated Flavonoid Glycosides from Linked-Scan Mass Spectra (B/E). *J. Agric. Food. Chem.* **2002**, *50*, 976-982.

(35) Shi, S. D. H.; Hendrickson, C. L.; Marshall, A. G.; Siegel, M. M.; Kong, F.; Carter, G. T. Structural Validation of Saccharomicins by High Resolution and High Mass Accuracy Fourier Transform-Ion Cyclotron Resonance-Mass Spectrometry and Infrared Multiphoton Dissociation Tandem Mass Spectrometry. *J. Am. Soc. Mass. Spectrom.* **1999**, *10*, 1285-1290.

(36) Thompson, M. S.; Cui, W.; Reilly, J. P. Fragmentation of Singly Charged Peptide Ions by Photodissociation at λ=157 nm. *Angew. Chem. Int. Ed.* **2004**, *43*, 4791-4794.

(37) Zhang, L.; Reilly, J. P. Extracting Both Peptide Sequence and Glycan Structural Information by 157 nm Photodissociation of N-Linked Glycopeptides. *J. Proteome Res.* **2009**, *8*, 734-742.

(38) Wilson, J. J.; Brodbelt, J. S. Ultraviolet Photodissociation at 355 nm of Fluorescently Labeled Oligosaccharides. *Anal. Chem.* **2008**, *80*, 5186-5196.

(39) Devakumar, A.; Mechref, Y.; Kang, P.; Novotny, M. V.; Reilly, J. P. Identification of Isomeric N-Glycan Structures by Mass Spectrometry with 157 nm Laser-Induced Photofragmentation. *J. Am. Soc. Mass. Spectrom.* **2008**, *19*, 1027-1040.

(40) Devakumar, A.; Thompson, M. S.; Reilly, J. P. Fragmentation of Oligosaccharide Ions with 157 nm Vacuum Ultraviolet Light. *Rapid Commun. Mass Spectrom.* **2005**, *19*, 2313-2320.

(41) Thompson, M. S.; Cui, W.; Reilly, J. P. Factors That Impact the Vacuum Ultraviolet Photofragmentation of Peptide Ions. *J. Am. Soc. Mass. Spectrom.* **2007**, *18*, 1439-1452.

(42) Chen, S.-T.; Her, G.-R. Linkage and Branch Analysis of High-Mannose Oligosaccharides Using Closed-Ring Labeling of 8-Aminopyrene-1,3,6-Trisulfonate and P-Aminobenzoic Ethyl Ester and Negative Ion Trap Mass Spectrometry. *J. Am. Soc. Mass. Spectrom.* **2012**, *23*, 1408-1418.

(43) Wuhrer, M.; Deelder, A. M.; Hokke, C. H. Protein Glycosylation Analysis by Liquid Chromatography-Mass Spectrometry. *J. Chromatogr. B* **2005**, *825*, 124-133.

(44) Luo, Q. Z.; Rejtar, T.; Wu, S. L.; Karger, B. L. Hydrophilic Interaction 10 μm ID Porous Layer Open Tubular Columns for Ultratrace Glycan Analysis by Liquid Chromatography-Mass Spectrometry. *J. Chromatogr. A* **2009**, *1216*, 1223-1231.

(45) Scott, N. E.; Parker, B. L.; Connolly, A. M.; Paulech, J.; Edwards, A. V. G.; Crossett, B.; Falconer, L.; Kolarich, D.; Djordjevic, S. P.; Hojrup, P.; Packer, N. H.; Larsen, M. R.; Cordwell, S. J. Simultaneous Glycan-Peptide Characterization Using Hydrophilic Interaction Chromatography and Parallel Fragmentation by CID, Higher Energy Collisional Dissociation, and Electron Transfer Dissociation MS Applied to the N-Linked Glycoproteome of Campylobacter jejuni. *Mol. Cell. Proteomics* **2011**, *10*.

(46) Yamaguchi, Y.; Nishima, W.; Re, S.; Sugita, Y. Confident Identification of Isomeric N-Glycan Structures by Combined Ion Mobility Mass Spectrometry and Hydrophilic Interaction Liquid Chromatography. *Rapid Commun. Mass Spectrom.* **2012**, *26*, 2877-2884.

(47) Ruhaak, L. R.; Deelder, A. M.; Wuhrer, M. Oligosaccharide Analysis by Graphitized Carbon Liquid Chromatography-Mass Spectrometry. *Anal. Bioanal. Chem.* **2009**, *394*, 163-174.

(48) Fan, J. Q.; Kondo, A.; Kato, I.; Lee, Y. C. High-Performance Liquid-Chromatography of Glycopeptides and Oligosaccharides on Graphitized Carbon Columns. *Anal. Biochem.* **1994**, *219*, 224-229.

(49) Jemal, A.; Siegel, R.; Ward, E.; Murray, T.; Xu, J.; Smigal, C.; Thun, M. J. Cancer Statistics, 2006. *CA Cancer J Clin* **2006**, *56*, 106-130.

(50) Naka, R.; Kamoda, S.; Ishizuka, A.; Kinoshita, M.; Kakehi, K. Analysis of Total N-Glycans in Cell Membrane Fractions of Cancer Cells Using a Combination of Serotonin Affinity Chromatography and Normal Phase Chromatography. *J. Proteome Res.* **2006**, *5*, 88-97.

(51) Mamitsuka, H. Glycoinformatics: Data Mining-based Approaches. *Chimia* **2011**, *65*, 10-13.

(52) Artemenko, N. V.; McDonald, A. G.; Davey, G. P.; Rudd, P. M. Databases and Tools in Glycobiology. *Methods in molecular biology (Clifton, N.J.)* **2012**, *899*, 325-350.

(53) Frank, M.; Schloissnig, S. Bioinformatics and Molecular Modeling in Glycobiology. *Cellular and Molecular Life Sciences* **2010**, *67*, 2749-2772.

(54) Perez, S.; Mulloy, B. Prospects for Glycoinformatics. *Curr. Opin. Struc. Biol.* **2005**, *15*, 517-524.

(55) Damerell, D.; Ceroni, A.; Maass, K.; Ranzinger, R.; Dell, A.; Haslam, S. M. The GlycanBuilder and GlycoWorkbench Glycoinformatics Tools: Updates and New Developments. *Biol. Chem.* **2012**, *393*, 1357-1362.